

Exploring biocatalytic alternatives for challenging chemical reactions

Wu, Y.

DOI

[10.4233/uuid:ae1a632b-91ab-466c-b40c-c111ac2ffe2d](https://doi.org/10.4233/uuid:ae1a632b-91ab-466c-b40c-c111ac2ffe2d)

Publication date

2023

Document Version

Final published version

Citation (APA)

Wu, Y. (2023). *Exploring biocatalytic alternatives for challenging chemical reactions*. [Dissertation (TU Delft), Delft University of Technology]. <https://doi.org/10.4233/uuid:ae1a632b-91ab-466c-b40c-c111ac2ffe2d>

Important note

To cite this publication, please use the final published version (if applicable). Please check the document version above.

Copyright

Other than for strictly personal use, it is not permitted to download, forward or distribute the text or part of it, without the consent of the author(s) and/or copyright holder(s), unless the work is under an open content license such as Creative Commons.

Takedown policy

Please contact us and provide details if you believe this document breaches copyrights. We will remove access to the work immediately and investigate your claim.

Exploring biocatalytic alternatives for challenging chemical reactions

Dissertation

for the purpose of obtaining the degree of doctor
at Delft University of Technology
by the authority of the Rector Magnificus, prof.dr.ir. T.H.J.J. van der Hagen
chair of the Board for Doctorates
to be defended publicly on
Wednesday 20 September 2023 at 17:30 o'clock

by

Yinqi WU (吴殷琦)

Master of Engineering in Light Industry Technology and Engineering,
East China University of Science and Technology, China
Born in Wuxi, China

This dissertation has been approved by the promotor.

Composition of the doctoral committee:

Rector Magnificus,	chairperson
Prof.dr. F. Hollmann	Delft University of Technology, promotor
Dr. C.E. Paul	Delft University of Technology, copromotor

Independent members:

Prof.dr. U. Hanefeld	Delft University of Technology
Prof.dr.ir. M.W. Fraaije	University of Groningen
Prof.dr. O. Thum	Delft University of Technology
Dr. C. Roullier	University of Nantes
Dr. K. Haslinger	University of Groningen

Reserve member:

Prof.dr. E.A. Pidko	Delft University of Technology
---------------------	--------------------------------



Funding: This research is supported by the European Union (ERC, PeroxyZyme, No 101054658) and the China Scholarship Council.

Printed by: Proefschriftspecialist

Cover by: Yinqi Wu

ISBN: 978-94-6366-702-9

All rights reserved. No parts of this publication may be reproduced, stored in a retrieval system, or transmitted in any form or by any means, electronic, mechanical, photo-copying recording, or otherwise, without the prior written permission of the author.

Table of Contents

Summary	5
Samenvatting.....	9
Chapter 1: General introduction	13
Chapter 2: Peroxygenase-promoted enzymatic cascades for the valorisation of fatty acids	57
Chapter 3: An alginate-confined peroxygenase-CLEA for styrene epoxidation.....	93
Chapter 4: Intensification of photobiocatalytic decarboxylation of fatty acids for the production of biodiesel.....	129
Chapter 5: Stabilisation of the fatty acid decarboxylase from <i>Chlorella variabilis</i> by caprylic acid	153
Chapter 6: Conclusion and Outlook	171
Curriculum Vitae	183
Acknowledgements	185

Summary

Catalysts are often used in challenging chemical reactions to accelerate the reaction rate, increase reaction efficiency, reduce energy consumption, and minimise waste production. In biocatalysis, enzymes or whole cells are used as catalysts with the advantage of reactivity, selectivity and mild reaction condition over chemocatalysis. Nowadays, with the increasing variety of enzymes, biocatalysis exhibits more and more applicability potential as an alternative tool for chemical reactions.

This thesis focuses on two categories of challenging chemical reactions: oxyfunctionalisation and decarboxylation reactions, where two enzyme families have been investigated. Unspecific peroxygenases (UPOs) exhibit remarkable catalytic activity by facilitating the specific incorporation of oxygen atoms into both C-H and C=C bonds through hydroxylation and epoxidation reactions, respectively. This biocatalytic ability occurs under mild reaction conditions, rendering UPOs highly versatile and attractive for various synthetic applications. Fatty acid photodecarboxylases (FAPs) demonstrate the capacity to effectively catalyse the cleavage of carboxylic groups from substrates, leading to the formation of the corresponding alka(e)nes when subjected to illumination. This photoenzymatic reaction offers a sustainable and environmentally friendly pathway for the conversion of fatty acids into valuable hydrocarbon products by harnessing light as an energy source. In **chapter 1**, we show a critical and quantitative comparison between chemocatalysis and biocatalysis in oxyfunctionalisation reactions and an overview of decarboxylation reactions.

For oxyfunctionalisation reactions, this thesis is focusing on both classic hydroxylation and epoxidation reactions. For instance, further derivatisation fatty acids generally relies on pre-existing functional groups such as the carboxylate group or C=C-double bonds. However, the enzymatic conversions of saturated, non-activated fatty acids remain relatively underdeveloped, primarily owing to the inherent difficulty of C-H activation. In **chapter 2**, we demonstrate the application of a peroxygenase mutant *AaeUPO-Fett* for selective fatty acid hydroxylation. The primary products (i.e. hydroxy fatty acids) are interesting building blocks for lactone and polyester synthesis. Besides, when the produced ω -1 hydroxy fatty acid (esters) are transformed, further synthetic possibilities arise as demonstrated by the fatty acid

Summary

decarboxylation, Baeyer-Villiger oxidation and reductive amination reactions. Thereby, the utilisation of peroxygenase-promoted enzymatic cascades has emerged as a versatile toolbox for the conversion of recalcitrant saturated fatty acids into valuable products and essential building blocks.

In **chapter 3**, we aim to utilise biocatalysts in neat substrate conditions for a high reaction efficiency. Enzyme immobilisation and its optimisation have been employed to obtain an alginate-confined peroxygenase-CLEA (imm-AaeUPO). Therefore, we set out to use the imm-AaeUPO to catalyse the enantioselective epoxidation of *cis*- β -methylstyrene in a solvent-free reaction system. We obtained promising turnover numbers of 96 000 for the biocatalyst and epoxide product concentration of 48 mM. The current system outperforms comparable reaction systems using chemical catalysts and other established enzymatic systems, driving the preparative-scale applications of epoxidation reactions.

For the decarboxylation reaction, we mainly focus on the fatty acid decarboxylation catalysed by the light-dependent FAP from *Chlorella variabilis* NC64A (CvFAP). In **chapter 4**, we set out to utilise CvFAP for the production of alkanes as biofuel, while it is found that light-driven biocatalytic processes are notoriously hampered by poor penetration of light into the turbid reaction media. We then demonstrate that the rate of photobiocatalytic reactions, such as the decarboxylation of fatty acids, can be dramatically increased by using intensified internal illumination. The implementation of these wireless light emitters has led to a more than 22-fold acceleration of the product formation rate in palmitic acid decarboxylation. The notable improvement achieved underscores the potential of internal illumination wireless light emitters as a valuable tool in facilitating efficient and expedited photobiocatalytic reactions.

Chapter 5 of this thesis reveals that the photoinactivation of CvFAP poses a significant obstacle in its practical application. We demonstrate that the photostability of CvFAP can be effectively enhanced by the administration of medium-chain length carboxylic acids such as caprylic acid. The results highlight the importance of optimising reaction conditions and substrate affinity of enzymes to ensure the sustained stability and functionality of CvFAP, ultimately facilitating its successful application in various biotechnological and industrial processes.

Overall, this thesis contributes to the applications of biocatalysis in challenging chemical reactions (i.e. oxyfunctionalisation and decarboxylation), offering alternatives to chemocatalysis. In addition, the outcomes obtained in these

aforementioned chapters will not only reinforce the existing advantages of biocatalysis but also provide valuable insights into prospective avenues for future research in this field.

Summary

Samenvatting

Katalysatoren worden vaak gebruikt in uitdagende chemische reacties om de reactiesnelheid te versnellen, de reactie-efficiëntie te verhogen, energieverbruik te verminderen en afvalproductie te minimaliseren. In biokatalyse worden enzymen of hele cellen gebruikt als katalysatoren, met als voordeel dat ze reactief, selectief en mildere reactieomstandigheden bieden ten opzichte van chemokatalyse. Tegenwoordig vertoont biokatalyse, met de toenemende verscheidenheid aan enzymen, steeds meer potentieel in toepassingen als een alternatief hulpmiddel voor chemische reacties.

Dit proefschrift richt zich op twee categorieën van uitdagende chemische reacties: oxyfunctionalisatie en decarboxyleringsreacties, waarbij twee enzymfamilies zijn onderzocht. Onspecifieke peroxygenases (UPO's) vertonen opmerkelijke katalytische activiteit door de specifieke incorporatie van zuurstofatomen in zowel C-H als C=C-bindingen te vergemakkelijken via hydroxylatie- en epoxidatiereacties, respectievelijk. Dit biokatalytische vermogen treedt op onder milde reactieomstandigheden, waardoor UPO's zeer veelzijdig en aantrekkelijk zijn voor verschillende synthetische toepassingen. Fatty acid photodecarboxylases (FAP's) tonen het vermogen om effectief carboxylgroepen af te splitsen van substraten, resulterend in de vorming van de overeenkomstige alkanen/alkenen wanneer ze worden blootgesteld aan verlichting. Deze foto-enzymatische reactie biedt een duurzame en milieuvriendelijke route voor de omzetting van vetzuren in waardevolle koolwaterstofproducten door gebruik te maken van licht als energiebron. In **hoofdstuk 1** laten we een kritische en kwantitatieve vergelijking zien tussen chemokatalyse en biokatalyse in oxyfunctionalisatiereacties en een overzicht van decarboxyleringsreacties.

Voor oxyfunctionalisatiereacties richt dit proefschrift zich zowel op klassieke hydroxylatie-als epoxidatiereacties. Bijvoorbeeld, de verdere functionaliserende van vetzuren berust over het algemeen op reeds aanwezige functionele groepen zoals de carboxylaatgroep of C=C-dubbele bindingen. Echter, de enzymatische omzettingen van verzadigde, nietgeactiveerde vetzuren blijven relatief onderontwikkeld, voornamelijk door de inherente moeilijkheid van C-H-activatie. In **hoofdstuk 2** laten we de toepassing zien van een peroxygenasemutant AaeUPO-

Samenvatting

Fett voor selectieve vetzuurhydroxylatie. De primaire producten (d.w.z. hydroxy-vetzuren) zijn interessante bouwstenen voor de synthese van lactonen en polyester. Bovendien, wanneer de geproduceerde ω -1 hydroxy-vetzuren (esters) worden omgezet, ontstaan verdere synthetische mogelijkheden, zoals aangetoond door vetzuurdecarboxylering, Baeyer-Villiger-oxidatie en reductieve aminering. Daardoor is het gebruik van door peroxygenase-gepromote enzymatische cascades naar voren gekomen als een veelzijdige gereedschapskist voor de omzetting van lastige vetzuren in waardevolle producten en essentiële bouwstenen.

In **hoofdstuk 3** streven we naar het gebruik van biokatalysatoren in zuivere substraatcondities voor een hoge reactie-efficiëntie. Enzymimmobilisatie en de optimalisatie ervan zijn toegepast om een alginaat-beperkte peroxygenase-CLEA (imm-AaeUPO) te verkrijgen. We gebruiken vervolgens de imm-AaeUPO om de enantioselectieve epoxidatie van *cis*- β -methylstyreen in een oplosmiddelvrij reactiesysteem te katalyseren. Wij verkregen veelbelovende omzetsnelheden van 96 000 voor de biokatalysator en epoxideconcentraties van 48. Het huidige systeem presteert beter dan vergelijkbare reactiesystemen met chemische katalysatoren en andere gevestigde enzymatische systemen, wat de toepassing op preparatieve schaal van epoxidatiereacties stimuleert.

Voor de decarboxyleringsreactie richten we ons voornamelijk op de vetzuurdecarboxylering gekatalyseerd door de lichtafhankelijke FAP van *Chlorella variabilis* NC64A (CvFAP). In **hoofdstuk 4** zijn we begonnen met het gebruik van CvFAP voor de productie van alkanen als biobrandstof, waarbij bleek dat lichtgestuurde biokatalytische processen vaak worden belemmerd door de slechte doordringing van licht in het troebele reactiemedium. We laten vervolgens zien dat de snelheid van fotobiokatalytische reacties, zoals de decarboxylering van vetzuren, drastisch kan worden verhoogd door gebruik te maken van geïntensiveerde interne verlichting. De implementatie van deze draadloze lichtzenders heeft geleid tot een meer dan 22-voudige versnelling van de reactiesnelheid bij de decarboxylering van palmitinezuur. De opmerkelijke verbetering benadrukt het potentieel van intern verlichte, draadloze lichtzenders als waardevol instrument bij het bevorderen van efficiënte en versnelde fotobiokatalytische reacties.

Hoofdstuk 5 van deze scriptie onthult dat de fotoinactivatie van CvFAP een aanzienlijke hindernis vormt voor de praktische toepassing ervan. We tonen aan dat de fotostabiliteit van CvFAP effectief kan worden verbeterd door het toedienen van

middellang geketende carbonzuren, zoals caprylzuur. De resultaten benadrukken het belang van het optimaliseren van reactieomstandigheden en substraataffiniteit van het enzym om de langdurige stabiliteit en functionaliteit van CvFAP te waarborgen, wat uiteindelijk leidt tot succesvolle toepassing ervan in diverse biotechnologische en industriële processen.

In het algemeen draagt deze scriptie bij aan de toepassingen van biokatalyse in uitdagende chemische reacties, zoals oxyfunctionalisatie en decarboxylering, en biedt het alternatieven voor chemokatalyse. Bovendien zullen de resultaten die in deze voorgaande hoofdstukken zijn behaald niet alleen de bestaande voordelen van biokatalyse versterken, maar ook waardevolle inzichten bieden voor toekomstig onderzoek op dit gebied.

Samenvatting

Chapter 1: General introduction

Yinqi Wu, Caroline E. Paul, and Frank Hollmann

Based on “Mirror, mirror on the wall who is the greenest of them all? A critical comparison of chemo- and biocatalytic oxyfunctionalisation reactions.” (*Manuscript in preparation*)

1. Oxyfunctionalisation reactions

Two widely used types of catalysis, chemocatalysis and biocatalysis are critically compared in this chapter. Comparative analysis of the environmental impact of chemocatalytic and biocatalytic oxyfunctionalisation reactions based on published experimental data reveals that both methods produce comparable amounts of waste, with the majority stemming from the solvent used. However, it is emphasised that the synthesis of the catalysts themselves, including biocatalysts, should also be considered when assessing their environmental impact. The chapter underscores the complexity of assessing the environmental impact of catalysis and suggests that a comprehensive life cycle assessment approach is required to evaluate their environmental impact.

The chapter also discusses the relationship between solvent properties and the energy demands for chemical transformations and downstream processing, emphasising that the choice of solvent can significantly impact the environmental impact of a catalytic process. Additionally, the chapter highlights the importance of considering the recyclability of reagents and the secondary CO₂ emissions caused by the energy requirements of the reaction when evaluating the environmental impact of a catalytic process.

In conclusion, while both chemocatalysis and biocatalysis have environmental impact, the greenness of either method is dependent on several factors, including the type of waste generated, the recyclability of reagents, and the secondary CO₂ emissions caused by the energy requirements of the reaction. The chapter suggests that a comprehensive life cycle assessment approach is required to evaluate the environmental impact of catalysis, and highlights the importance of considering the synthesis of catalysts themselves.

1.1 Introduction

The addition of oxygen atoms into C-H or C-C bonds, as well as C=C bonds, known as catalytic oxyfunctionalisation reactions, is gaining importance in organic synthesis due to their potential for producing highly functionalised and complex molecules. However, these reactions present significant challenges that must be addressed to achieve high yields and selectivity.

One major challenge is controlling selectivity, as oxyfunctionalisation reactions can result in multiple products due to the presence of multiple reaction sites in the substrate. Another challenge is generating and controlling highly reactive oxygen species, which can lead to issues with catalyst stability, selectivity, and unwanted byproduct formation. Additionally, traditional oxidants used in these reactions are often toxic or environmentally hazardous.

As a result, most catalysis disciplines are actively developing catalytic oxyfunctionalisation catalysts, reactions, and processes. Homogeneous catalysis and biocatalysis are particularly active in this area, and interdisciplinary interactions could be beneficial. However, these fields do not interact as much as they could, with each often disavouring the other approach.

Arguments against biocatalysis often include the high specificity of enzymes, poor enzyme stability, dependence on costly cofactors, and poor scalability. In contrast, biocatalysis publications often disfavour chemocatalysis due to toxic catalysts and solvents and harsh reaction conditions.

To provide a balanced, objective overview, a comparison of chemo- and biocatalysts for their efficiency and environmental impact is needed. This approach aims to promote a more quantitative discussion and comparison of both fields and potentially start some productive controversies from which we can all learn.

1.2 Catalysts available

In the majority of chemical oxyfunctionalisation reactions, catalysis is required to decrease the activation enthalpies and increase selectivity. One common catalytic strategy is to activate molecular oxygen or hydrogen peroxide as higher-valent metal oxo species or as (hydro)peroxo species, as shown in Figure 1.1. Additionally, organic oxidants such as hydroperoxides and peracids are frequently utilised.

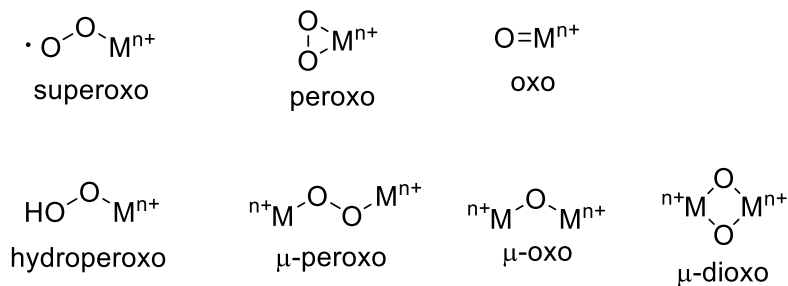
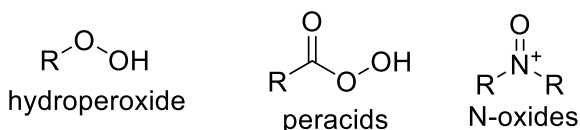
metal-based oxygen transfer catalystsorganic oxygen-transfer catalysts

Figure 1.1. Selection of (in)organic activated oxygen species for oxyfunctionalisation chemistry.

In oxyfunctionalisation reactions, catalysis is often required to lower the activation enthalpies and increase selectivity. One common catalytic strategy is to activate molecular oxygen or hydrogen peroxide as higher-valent metal oxo species or as (hydro)peroxo species, while organic oxidants such as hydroperoxides and peracids are also frequently used. Among the catalysts used, various metals such as elements of the platinum group (Ru, Rh, Pd, Os, Ir, and Pt) are prevalent for the activation of molecular oxygen (Figure 1.2). For already reduced oxygen species ((hydro)peroxide), salts of V,^[1-2] Mn,^[3-5] Fe,^[6-8] Ni,^[9-10] Co,^[11-12] Cu,^[13] or Pt^[14-15] are commonly used, while photocatalytic systems based on TiO₂^[16] or SiO₂^[17] are emerging. Organic catalysts such as BINAP,^[18] flavins^[19-21] or peptides^[22] have also been reported, and many of these catalytic systems are applied for different oxyfunctionalisation reactions.

Compared to the wide range of catalysts used in chemical oxyfunctionalisation, biocatalysis relies on a narrower selection of (bioavailable) metals such as Fe, Cu, V, and Mo, and organic catalysts such as flavins and pterins. The most widely known oxyfunctionalisation enzymes are Fe-dependent oxygenases. The heme-dependent P450 monooxygenases^[23-28] and peroxygenases^[29-33] catalyse a broad range of C-H functionalisation reactions and epoxidation reactions, while Baeyer-Villiger oxidations

are yet unknown. Non-heme Fe oxygenases exhibit an even broader repertoire including *cis*-dihydroxylations of arenes or halogenation of non-activated C-H-bonds, but also no BV-oxidations.^[34-36] Flavin-dependent monooxygenases catalyse Baeyer-Villiger oxidations, epoxidation reactions, and aromatic hydroxylations,^[37-39] and some flavin-dependent monooxygenases even catalyse aromaticity-breaking hydroxylations of arenes^[40] or hydroxylation of sp^3 -C-H bonds (which is generally reserved to metal-dependent enzymes).^[41] Flavin-dependent oxidases also catalyse the non-aerobic benzylic oxyfunctionalisation of *p*-alkyl substituted phenols.^[42-44] Other metals and cofactors such as W or Mo,^[45] V^[46-48] or Cu play a lesser role in biocatalytic oxyfunctionalisation chemistry, but lytic polysaccharide monooxygenases (LPMOs)^[49-51] for the valorisation of recalcitrant polysaccharides are currently experiencing increasing interest.

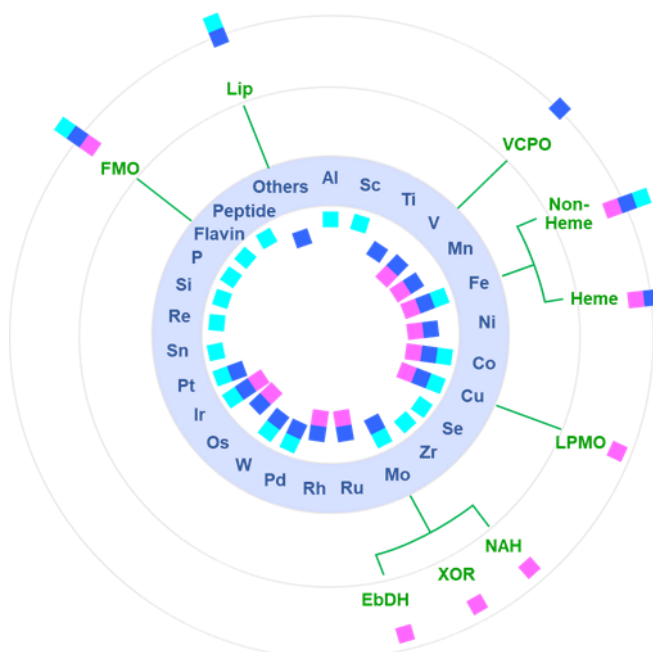


Figure 1.2. Classification of chemocatalysts (■) and biocatalysts (–) for hydroxylation (■), epoxidation (■) and Baeyer-Villiger oxidation reactions (■). FMO: flavin-containing monooxygenases, such as styrene monooxygenases; Heme: heme-dependent enzymes, such as cytochrome P450 monooxygenases; Non-heme: non-heme-dependent enzymes, such as ammonia monooxygenases.

Chapter 1

1.3 Productivities, catalyst loadings and catalyst performance

The term *productivity* is widely used and recognised as crucial, however, it is often ambiguously defined. For the purpose of this discussion, we adopt the definition of productivity as the rate of volumetric product formation (as defined by equation 1).

$$\text{Productivity [mM}\cdot\text{h}^{-1}] = \frac{\Delta n(\text{Product})}{\text{volume} \cdot \Delta \text{time}} \left[\frac{\text{mmol}}{\text{L}\cdot\text{h}} \right] \text{ (eq. 1)}$$

Undoubtedly, this parameter is of paramount importance, particularly in terms of the economic viability of any chemical process at an industrial scale, as it directly impacts operational expenditure (OPEX). Moreover, from an environmental standpoint, productivity plays a crucial role, as the duration of a reaction is directly proportional to energy consumption (including associated CO₂ emissions) resulting from activities such as stirring, pumping, or thermal control.

Figure 1.3a illustrates the notable disparity in productivity between biocatalytic and chemocatalytic oxyfunctionalisation reactions. Specifically, over two-thirds of biocatalytic reactions have a productivity level below 10 mM×h⁻¹, whereas only one-third of chemocatalytic reactions fall into this category. Moreover, a considerable portion (20%) of chemocatalytic reactions achieve a productivity of 0.1 M×h⁻¹ or higher, which is an exceptional achievement in biocatalysis.

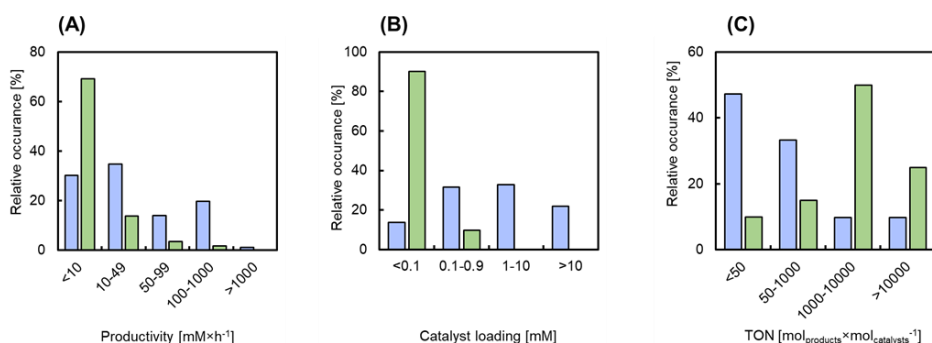


Figure 1.3. Comparison of productivities (A), catalyst loadings (B) and catalyst turnover numbers (C) in oxyfunctionalisation reactions catalysed by chemocatalysts (■) and biocatalysts (■). Results of a literature analysis covering 68 chemocatalytic and 58 biocatalytic oxyfunctionalisation reactions.

Part of the reason for this discrepancy can be attributed to the traditionally lower molar catalyst loading used in enzymes as compared to chemocatalysts (as shown in Figure 1.3b). Enzymes are usually employed at much lower concentrations, ranging from the lower micromolar to nanomolar range (approximately 90% of the

time), while chemical catalysts are typically used at concentrations of 1 mM or higher (over 50% of the time). This results in significantly higher catalyst turnover numbers (i.e. $\text{moles}_{\text{product}} \times \text{moles}_{\text{catalyst}}^{-1}$) for biocatalysts compared to chemocatalysts (as shown in Figure 1.3c).

Another parameter that is relevant in this context is catalyst performance, which refers to the extent of rate acceleration a catalyst provides compared to the non-catalysed reaction. While such comparisons are not commonly reported in the literature, we will use the turnover frequency (TF) of a catalyst as a metric for rate acceleration (equation 2).

$$\text{TF} [\text{h}^{-1}] = \frac{n_{\text{product}}}{n_{\text{catalyst}} \cdot \text{time}} \left[\frac{\text{mol}}{\text{mol} \cdot \text{h}} \right] \quad (\text{eq. 2})$$

As shown in Figure 1.4, typical TFs for chemocatalysts range below 100 h^{-1} whereas more than 70% of the enzyme catalysts exhibit TFs higher than 1000 h^{-1} .

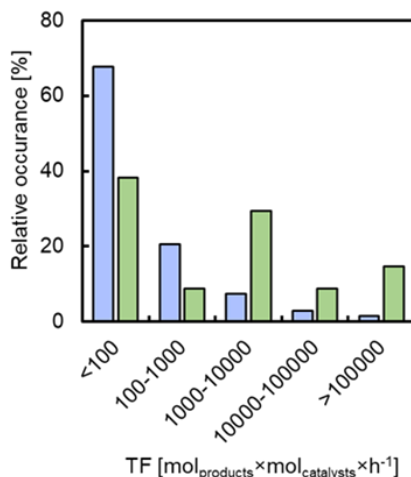


Figure 1.4. Comparison of turnover frequency of chemocatalysts (■) and biocatalysts (■) in oxyfunctionalisation reactions. Results of a literature analysis covering 68 chemocatalytic and 58 biocatalytic oxyfunctionalisation reactions.

In terms of productivity, it is evident that chemocatalysis currently outperforms biocatalysis. This can partly be attributed to the lower enzyme concentrations that are traditionally used. However, the high turnover frequencies (TFs) and turnover numbers (TNs) observed for enzymes suggest that their potential has not been fully explored yet.

Chapter 1

1.4 Reagent loadings and solvents

High product loadings are evidently crucial for the economic feasibility of chemical processes as they increase the efficiency of infrastructure and operational resources used. Additionally, downstream processing is generally easier, less time-consuming, and requires fewer resources and less energy when the product concentration is high. As mentioned earlier, these economic factors also translate into environmental impacts. In other words, the higher the product concentration, the lower the overall environmental footprint of a transformation. Thus, we compared the substrate loadings reported for both biocatalytic and chemocatalytic oxyfunctionalisation processes (Figure 1.5).

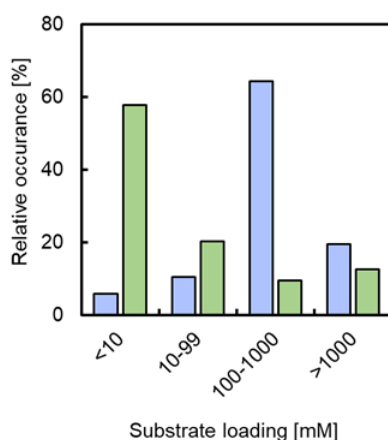


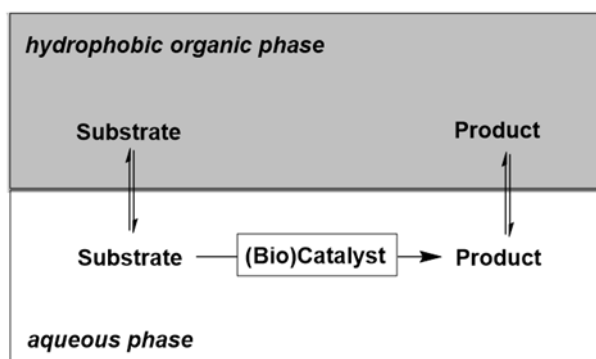
Figure 1.5. Comparison of substrate loadings in oxyfunctionalisation reactions catalysed by chemocatalysts (■) and biocatalysts (■).

A majority of oxyfunctionalisation biocatalysis occurs in dilute reaction media, with over 80% of the reactions being performed in solutions containing less than 100 mM of starting material. In contrast, over 80% of chemocatalytic processes are conducted with starting material concentrations of 100 mM or higher.

There is a clear cultural difference between researchers in the fields of chemocatalysis and biocatalysis when it comes to the choice of solvent for a reaction. Chemists tend to choose the most suitable solvent for the reaction, while biocatalysis researchers predominantly use water. This is understandable from a traditional perspective, as water is often referred to as the "solvent of life" and many enzymes are water-soluble. Moreover, water is perceived as a green solvent, being abundant and renewable in many regions of the world and non-toxic (at least prior to its use as solvent). However, due to its high polarity, water is a poor solvent for hydrophobic

reagents such as hydrocarbons, which partially explains the low substrate concentrations used in biocatalysis (Figure 1.5). In contrast, chemocatalysis often employs organic solvents such as alcohols (e.g. methanol, ethanol, isopropanol), alkanes, and aromatics (e.g. toluene, xylene), and even halogenated solvents such as CH_2Cl_2 or CHCl_3 , allowing for high substrate loadings. In the case of liquid starting materials, solvent-free reactions are not uncommon.

Today, biocatalysis for oxyfunctionalisation predominantly relies on aqueous reaction media, which presents challenges to scalability and greenness. However, it is worth noting that non-aqueous applications of hydrolases^[52] and lyases^[53] are quite common. Oxidoreductases, on the other hand, have been slower to adapt. Pioneering work by Klibanov and coworkers^[54-57] has recently regained attention from the biocatalysis community.^[58] To address the incompatibility of hydrophobic reagents and water-borne catalysts such as enzymes or whole cells, the two-liquid phase system (2LPS) approach has been developed (Scheme 1.1).^[59-63] This approach not only allows for high overall product concentrations but also enables control over the selectivity of the overall reaction. For example, hydrophobic aldehyde intermediates can be extracted into the hydrophobic organic phase, avoiding their over-oxidation.^[59, 64] Additionally, water-labile products such as epoxides can be stabilised using the 2LPS approach.^[65]



Scheme 1.1. The two-liquid phase concept. The hydrophobic organic phase allows for overall high reagent loadings and serves as substrate reservoir and product sink.

Micro aqueous reaction systems (MARS) can be considered an extension of the 2LPS approach, but with an even more extreme reduction of water content to the minimum required amount. While MARS have shown great potential in certain types of chemical reactions, they may not be suitable for biocatalysts that rely on diffusible,

Chapter 1

polar cofactors like the nicotinamide cofactors or stoichiometric cosubstrates with high polarity (such as glucose). Therefore, the application of MARS is largely restricted and may not be suitable for the commonly used P450 monooxygenase systems (except for peroxide shunt pathway applications that are cofactor-independent). However, the recently emerging peroxygenase enzymes have shown promising results in both 2LPS and MARS systems, highlighting their potential as versatile catalysts for green and sustainable chemical transformations.^[66-70]

1.5 Oxidants

Stoichiometric oxidants play a crucial role in oxyfunctionalisation reactions. In recent years, a wide range of oxidising agents, which also serve as an O-source, have replaced traditional oxidants such as chromate or permanganate (Table 1.1). The oxidant scope of chemocatalytic methods is broader than their biocatalytic counterparts. Chemocatalytic oxyfunctionalisation reactions utilise a diverse range of oxidants, including oxygen (as O₂ or O₃), peroxides (such as H₂O₂ or (in)organic hydroperoxides), peracids (e.g. *m*CPBA or peracetic acid), or halides (elementary, hypohalites, or hypervalent iodine species).^[71] In contrast, the oxidant of choice for biocatalytic oxyfunctionalisation reactions is traditionally molecular oxygen. However, hydrogen peroxide and organic hydroperoxides, such as tert-Butyl hydroperoxide, have recently gained popularity.^[72]

From an environmental perspective, oxidants that are safe to handle and produce harmless waste products are preferred. Oxygen-based oxidants such as O₂ and O₃ generate water or hydrogen peroxide as by-products and are often considered the ultimate green oxidants. H₂O₂ is also a popular choice in green oxidation.

Table 1.1. Selection of terminal oxidants frequently used.

Oxidant	Hydroxylation	Epoxidation	BV-oxidation
O ₂ chemo	Mn (1) ^[73]	Mn (2) ^[74]	SiO ₂ (3) ^[17]
O ₂ bio	P450s, ^[75] VAO-like oxidases ^[43]	FMOs, ^[76] P450s ^[25]	BVMOs ^[77]
H ₂ O ₂ chemo	Co/Fe (4), ^[78] Fe (5) ^[8]	Ti (6), ^[79] Mn (7), ^[80] Mn (8), ^[81]	Co (9), ^[12] Pd (10), ^[82] Sn (11), ^[83]
H ₂ O ₂ bio	Peroxygenases, ^[84] P450s ^[85]	Peroxygenases, ^[86] P450s ^[87]	Lipases/carboxylic acids ^[88]

<i>m</i> CPBA chemo	Fe (12) ^[89]	Ni (13) ^[90]	Sc (14) ^[91]
PhIO chemo	Fe (15) ^[92]	Mn (16) ^[93]	Fe (17) ^[94]
PhIO bio	CYP2A ^[95]		
PhI(OAc) ₂ chemo	Fe (18) ^[96]	Mn (19) ^[97]	

1: Mn^{II}-Met@MMNPs, 2: Fe₃O₄-[Mn(TCPP-Ind)Cl], 3: mSiO₂-500, 4: [Co^{III}₄ Fe^{III}₂ O(L¹⁰)₈] 4DMF•H₂O, 5: [((*R*)-(-)-N4Py*)Fe^{II}(CH₃CN)]²⁺, 6: proline-derived C₁-symmetric titanium(salan) complexes, 7: Mn^{III} complex immobilised via mesoporous silica SBA-15 by covalent bond, 8: MnO₂ NP/g-C₃N₄, 9: (*R,R*)-*N,N*-bis(3,5-di-*tert*-butylsalicylidene)-1,2-cyclohexanediamino-Co(II), 10: (PhCN)₂PdCl. 11: Sn–Y zeolite, 12: Fe^{III}₂(O)(L)(OBz)](ClO₄), 13: [Ni^{II}(L⁹)Cl], HL⁹=(2-[bis(pyridin-2-ylmethyl)amino]-*N*-(quinolin-8-yl)acetamide), 14: L-RaPr₂-*t*Bu-Sc(OTf)₃, 15: Vaulted Binaphthyl Metalloporphyrins, 16: [Mn^{III}(TDCPP)Cl], 17: [Fe^{II}(CH₃CN)(*N,N*-bis(2-pyridylmethyl)-*N*-bis(2-pyridyl)methyl-amine)(ClO₄)]ClO₄, 18: Fe^{III} porphyrin complex, 19: [Mn(^Rpeb)(OTf)₂] (peb=1-(1-ethyl-1*H*-benzo[d]imidazol-2-yl)-*N*-((1-((1-ethyl-1*H*-benzo[d]imidazol-2-yl)methyl) pyrrolidin-2-yl)methyl)-*N*-methylmethanamine)).

Although O₂ is a highly preferred oxidant in oxyfunctionalisation reactions, its low solubility in aqueous media presents challenges for biocatalysis. The amount of oxygen available may lie below the enzyme's K_M value, leading to sub-optimal enzyme activities. Enzyme engineering can generate mutants with higher O₂ affinity,^[98] but O₂ diffusion rate into the aqueous reaction mixture remains a limiting factor. Process engineering can address this issue.^[99-100] Enzyme stability under aeration reaction conditions is another consideration. Exposure to the gas-liquid interface can cause denaturation of enzymes, and oxidation of labile amino acids such as methionine and cysteine can impair enzyme activity or stability.^[98]

Despite these challenges, O₂ is still considered an attractive green oxidant, as it generates water or hydrogen peroxide as by-products, but proper risk management in terms of oxygen concentration and equipment construction is necessary to avoid explosion or fire. Chemical oxidants are also widely used in oxyfunctionalisation reactions, and the choice of oxidant should consider safety, environmental impact, and waste generation.

One challenge faced by heme- and non-heme monooxygenase reactions is uncoupling.^[101] Monooxygenases first activate molecular oxygen through a reductive process to produce an activated, enzyme-bound oxygen species that then performs oxygen insertion.^[34] The reducing equivalents required for this reaction are typically obtained from reduced nicotinamide cofactors and delivered to the monooxygenase

Chapter 1

through complex electron transport chains. However, a significant portion of the reducing equivalents provided by the sacrificial electron donor can also be wasted in a futile uncoupling reaction, which involves the direct aerobic oxidation of radical intermediates. This loss of reducing equivalents hinders the large-scale application of biocatalytic oxyfunctionalisation, as the cost contribution of the sacrificial electron donor exceeds the economically feasible range and results in additional consumption of feedstock.^[101] In addition, the reactive oxygen species formed in the uncoupling process can impair the stability of biocatalysts.

Peroxygenases, in contrast to monooxygenases, do not suffer from uncoupling issues, as they utilise already reduced oxygen in the form of H_2O_2 as a stoichiometric oxidant, resulting in highly simplified reaction schemes. This advantage makes peroxygenases an attractive option for industrial oxyfunctionalisation processes, as the cost contribution of a sacrificial electron donor, which is often necessary for monooxygenase-catalysed reactions, can be eliminated. However, like all heme-containing enzymes, peroxygenases are susceptible to irreversible heme degradation in the presence of high concentrations of H_2O_2 , but this can be easily controlled by adjusting the *in situ* H_2O_2 concentration.^[31, 102] Despite the somewhat limited substrate scope of peroxygenases, recent research efforts have successfully expanded the range of substrates that these enzymes can act on,^[103-110] demonstrating their potential for future applications.

In comparison to biocatalysis, chemocatalysis offers a wider range of oxidants for oxyfunctionalisation reactions. While biocatalytic reactions have shown promising results, issues such as coupling efficiency and oxidative inactivation must be addressed for the practical application of these reactions at a larger scale. However, the advantages of using environmentally friendly, easily handleable oxidants that generate innocuous waste products, such as peroxides, make biocatalytic oxyfunctionalisation reactions attractive for green chemistry applications. Peroxygenases have shown particular promise in this regard, as they rely on H_2O_2 as a stoichiometric oxidant, resulting in simplified reaction schemes with no uncoupling issues. Despite some limitations in their substrate scope, ongoing research is focused on expanding the applicability of peroxygenases and other biocatalysts for oxyfunctionalisation reactions.

1.6 Selectivity

The selectivity of catalytic oxyfunctionalisation reactions depends on two factors: (1) the reactivity of a position and (2) the positioning of the starting material relative to the catalytically active species. In chemocatalysis, steric repulsion between (chiral) ligands and substrates has traditionally been used to raise the energy of one of the (diastereomeric) transition states over the other. Alternatively, attractive noncovalent interactions are increasingly used to control enantioselectivity.^[111] However, as low-molecular-weight compounds, chiral ligands have limited possibilities to control substrate binding and require pre-existing polar groups to enable attractive interactions (Figure 1.6). In contrast, an enzyme active site offers various attractive and repulsive interactions with the starting material, providing the enzyme with more opportunities to control substrate binding relative to the catalytically active group (Figure 1.6).

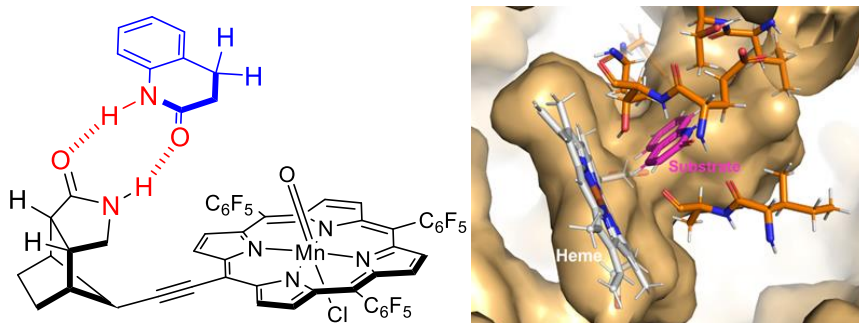


Figure 1.6. Comparison of binding interactions between chemo- (left) and biocatalyst (right) and starting materials.

The difference in control of binding interactions can be exemplified in the hydroxylation of non-functionalized alkanes. In chemical hydroxylation reactions, the reactivity of a given C-H bond and the steric hindrance around it determine the regioselectivity of the reaction. While these factors also play a role in enzymatic hydroxylations, they are complemented by the interaction of the starting material with the enzyme active site. This interaction favours the binding of the starting material to the hydroxylation catalyst in an orientation leading to a kinetically favourable product. An illustrative example is the oxyfunctionalisation of octane, which chemically typically yields a statistical mixture of regio- and stereoisomeric 1- to 4-octanols (Figure 1.7).^[112-114] However, the cytochrome P450 monooxygenase from *Mycobacterium* sp HXN-1500 produces 1-octanol in greater than 95% selectivity.^{[115-}

Chapter 1

^{116]} Similarly, alkane hydroxylases (i.e. non-heme Fe monooxygenases)^[117] generally exhibit a preference for terminal hydroxylation, while hydroxylases from different organisms exhibit other selectivities.^[118-120] While the majority of wild-type hydroxylases exhibit poor selectivity towards non-natural starting materials such as octane, modern enzyme design enables the modification and fine-tuning of hydroxylase selectivity towards these substrates. Recent studies have shown the success of enzyme design in modifying the selectivity of hydroxylases towards various substrates.^[23, 31, 104, 121-130]

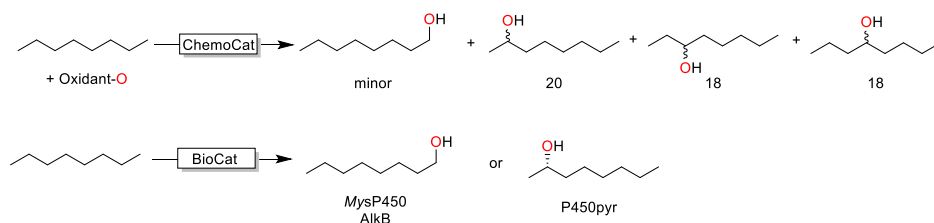


Figure 1.7. Comparison of the selectivity of chemo- and biocatalytic hydroxylation. For reasons of simplicity overoxidation products have been omitted.

Enzymes are also superior to chemical catalysts in terms of stereoselectivity (Figure 1.8). As mentioned earlier, enzymes have more control over the orientation of the substrate with respect to the catalytic site, and this is crucial for achieving high stereoselectivity. For instance, chiral transition metal catalysts typically give enantiomeric excess (*ee*) in the range of 40-80% for the stereoselective benzylic hydroxylation of ethyl benzene,^[5, 8, 131] and low reaction temperatures are often required to achieve high stereoselectivity, resulting in significant energy input for the transformations. In contrast, a wide range of highly (*R*)- or (*S*)-selective oxygenases are available, including heme-dependent monooxygenases^[132-133] and peroxygenases,^[86] which have been reported to achieve high selectivity. In addition, more "exotic enzymes" such as Mo-dependent dehydrogenases and flavin-dependent oxidases, which follow a desaturation-hydration mechanism, have also been reported to exhibit high stereoselectivity.^[43, 134-135]

Both chemical and enzymatic catalysts face the challenge of overoxidation in hydroxylation reactions, where the hydroxylated product is more reactive than the starting material and can be further converted. One approach to mitigate overoxidation is *in situ* removal of the alcohol product from the reaction mixture, which prevents further conversion.^[59, 136-137] Another strategy is medium engineering, where

the reaction conditions are adjusted to favour alcohol accumulation.^[96, 138] For enzyme catalysts, modulation of the hydrophobicity of the active site can also help to reduce the overoxidation rate.^[139]

Compared to hydroxylation, there are a broad range of highly enantioselective epoxidation catalysts available, including those reported by Jacobsen and Katsuki,^[140] Sharpless,^[141] Shi^[142] and more.^[74, 79] In addition, a variety of suitable oxidoreductases are also available. For example, flavin-dependent styrene monooxygenases are proven epoxidation catalysts,^[37, 143-147] but heme- and non-heme-dependent monooxygenases and peroxygenases can also catalyse a wide range of enantioselective epoxidation reactions. However, it should be noted that heme-dependent oxygenases may suffer from limited selectivity, as allylic hydroxylation frequently competes with epoxidation.^[30, 148-149]

Baeyer-Villiger oxidation reactions also face selectivity challenges, especially with unsymmetrically substituted ketones that can yield two ester isomers, normal (NP) and abnormal (AP). In chemical BV-oxidations, stereoelectronic effects dominate the migration tendency of carbonyl substituents within the Criegee intermediate, favouring the formation of NP and yielding a product mix that reflects the starting material's regioselectivity. However, when the substituents' carbocation stabilising tendencies are similar, such as in 3-methyl cyclohexanone, the product mixture can become more complex. In contrast, some enzymatic BV-oxidation catalysts, such as the BVMO from *Aspergillus flavus*, show excellent regioselectivity by favouring the migration of the less stabilizing substituent and yielding the AP. Moreover, protein engineering can further modulate the selectivity of BVMOs for either NP or AP, enabling the efficient synthesis of a specific isomer.^[91, 150-153]

Enantioselectivity has been extensively studied in both chemical and biocatalytic Baeyer-Villiger oxidations. In the case of chemical catalysis, a number of investigations have focused on the development of enantioselective catalysts.^[20, 22, 91, 154-155] Similarly, significant efforts have been devoted to the development of biocatalytic BV-oxidation processes with high enantioselectivity.^[150, 156-167] These investigations have led to the development of highly enantioselective catalysts in both chemical and biocatalytic BV-oxidations.

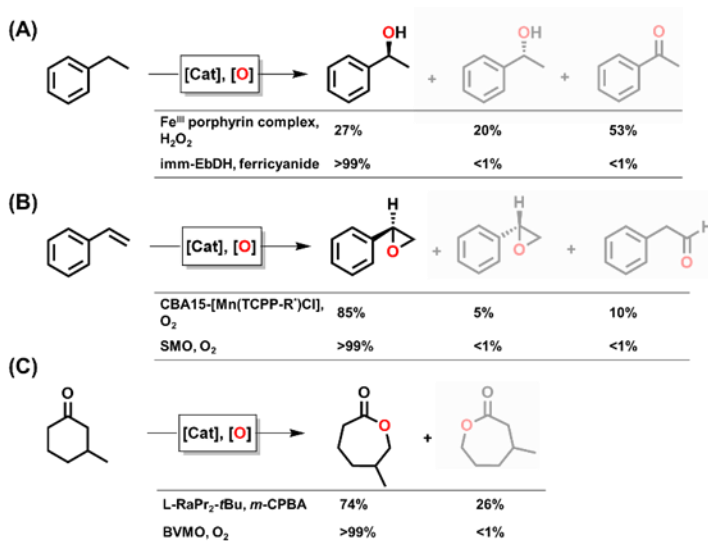


Figure 1.8. Representative examples of (non)selective hydroxylation (A),^[96, 168] epoxidation (B)^[74, 169] and Baeyer-Villiger (C)^[91, 151] oxidation reactions catalysed by chemocatalysts and biocatalysts.

Overall, it can be concluded that selectivity is a clear strength of biocatalysis, with enzymes able to offer high selectivity for a wide range of reactions. While some highly selective chemical catalysts have been developed in recent decades, biocatalysts remain unparalleled in terms of selectivity. Furthermore, enzyme selectivity can often be improved through protein engineering, making them even more attractive for use in industrial processes.

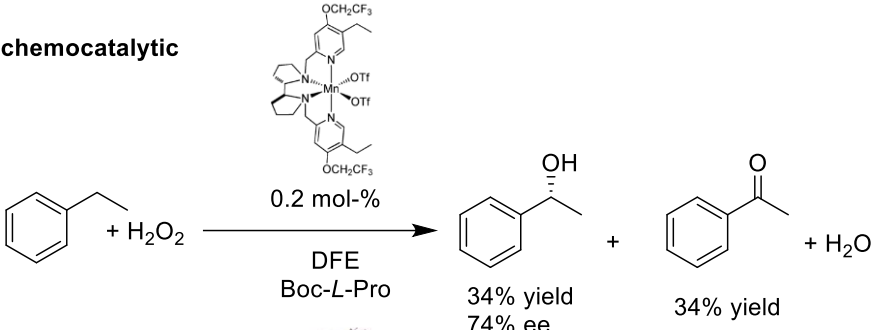
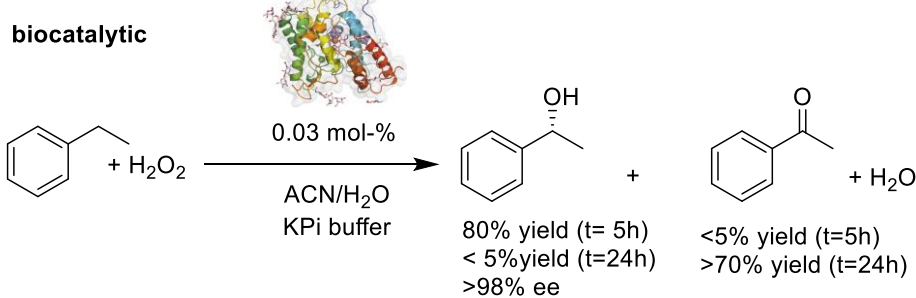
1.7 Environmental impact

The literature on biocatalysis often highlights the environmental benefits of using enzyme-catalysed reactions, such as the renewable nature of the catalysts, mild reaction conditions, high selectivity, and the use of water as a benign solvent.^[170] However, these claims are often oversimplified, and more quantitative comparisons are necessary to accurately assess potential environmental advantages.^[171] One useful tool for estimating the environmental impact of a reaction is Sheldon's E-factor (eq. 3), which calculates the ratio of the mass of wastes generated to the mass of product produced.^[172-173] By using this measure, a more precise assessment of the environmental impact of a reaction can be made.

$$E = \frac{\sum m_{\text{Waste}}}{m_{\text{Product}}} \left[\frac{\text{kg}}{\text{kg}} \right] \text{ (eq. 3)}$$

We conducted a comparative study between a chemocatalytic and a biocatalytic hydroxylation of ethyl benzene,^[4, 174] based on the experimental data published in the literature (Table 1.2). Surprisingly, we found that both methods produced comparable amounts of waste (28.1 and 36.5 kg_{waste}×kg_{product}⁻¹). Furthermore, in both cases, the majority of waste generated was due to the use of solvent (approximately 95%), and the contribution of the catalysts to waste generation was negligible (<0.1%). These findings suggest that simple claims of environmental superiority of biocatalysis may not always hold, and more quantitative analyses are necessary to assess the actual environmental impact of a reaction.

Table 1.2. E-factor comparison of a chemocatalytic and a biocatalytic oxyfunctionalisation of ethyl benzene.

chemocatalytic				
biocatalytic				
	chemocatalytic		biocatalytic	
	E-factor contribution		E-factor contribution	
	[g×g ⁻¹]	[%]	[g×g ⁻¹]	[%]
Catalyst	0.021	< 0.1	< 0.02	< 0.1
Additives ^[a]	0.76	2.7	1	2.7
Solvents ^[b]	27.0	95.9	34.5	94.5
Unreacted substrate & byproducts	0.37	1.3	1	2.7
Sum	28.1	100	36.5	100

Chapter 1

[a] Chemocatalytic: Boc-*L*-Proline, biocatalytic: KPi buffer; [b] chemocatalytic: difluoroethanol (DFE) including H₂O from H₂O₂ addition, biocatalytic: H₂O/ACN (1/1).

However, it should be noted that the simple E-factor does not take into account several important factors. Firstly, it does not consider the recyclability, energy costs and hazards of the reagents such as solvents, catalysts, and unreacted starting materials, unless explicitly reported. Secondly, the E-factor does not reflect the harmfulness of the wastes produced. For example, it is difficult to assess the environmental impact (e.g. toxicity, greenhouse gas potential, bioaccumulation, etc.) of difluoroethanol compared to H₂O/ACN, when considering solvent wastes. Thirdly, the E-factor does not include secondary CO₂ emissions caused by the energy requirements of the reaction. In this regard, the biocatalytic reaction, performed at ambient temperature, appears to be more environmentally friendly than its chemocatalytic counterpart, which requires temperature control at -30 °C.

In this context, it is important to emphasise the relationship between solvent properties and the resulting energy demands for the chemical transformation as well as downstream processing. It should be noted that distillation is a commonly used method for solvent recycling and purification, but it is an energy-intensive process. Unless powered by off-heat from other exothermic processes, it necessitates the consumption of primary energy and causes greenhouse gas emissions. Table 1.3 provides examples of the theoretical energy consumption for the distillation purification of some commonly used solvents. It also gives an indication of the energy consumption required for temperature adjustment during a reaction. The higher the specific heat capacity (C_p) and boiling point (b_p) of a solvent, the higher the energy required. Based on these numbers, water may not necessarily be among the 'greenest solvents'.

Table 1.3. Exemplary calculation of the energy consumption (and coupled CO₂ releases) for the distillation purification of some common solvents.

Solvent	C _p [J×g ⁻¹ ×K ⁻¹]	b _p [°C]	Energy consumption for distillation [kJ L ⁻¹] [a]	CO ₂ emission caused [g(CO ₂) L ⁻¹][b]
Water	4.18	100	334	27.8
Acetone	2.14	56	60	5
Ethanol	2.4	78	110	9.2
Acetonitrile	2.25	82	110	9.2
Chloroform	1.05	61	64	5.3
Toluene	1.51	110	117	9.8

[a] assuming ambient pressure and starting from 20 °C; [b] assuming a CO₂ intensity of 300 g(CO₂)×kWh⁻¹ (<https://www.eea.europa.eu/ims/greenhouse-gas-emission-intensity-of-1>)

Also, the viscosity of the reaction medium directly correlates with the energy demands for stirring and pumping.

Fourthly, it is essential to note that the E-factor does not account for the "prehistory" of the components used, i.e., the energy- and resource-consuming synthesis and waste generated during the production of the starting materials. For instance, an E-factor of 209000 kg_{waste}×kg_{AzeUPO}⁻¹ has been estimated for the biocatalyst.^[175] Taking this prehistory into account increases the catalyst E-factor contribution of the biocatalyst in Table 1.2 from <0.02 to 4180! A similar consideration for the chemocatalyst based on the synthesis information given in 4 suggest an E-factor of only ca. 34 kg_{waste}×kg_{Cat}⁻¹ for the Mn-catalyst, suggesting a much lower overall contribution to the final product. However, it is important to note that, in contrast to the enzyme calculation, no CO₂ emissions due to energy consumption have been taken into account.

Furthermore, it is important to keep in mind that also the starting materials used in the syntheses have a "prehistory" of energy and resource consumption as well as waste generation. Jessop proposed building synthesis trees for chemicals tracing back their synthesis to the original compounds (extracted from the ground, air, or sea).^[176] A comparison of the synthesis trees for the chemo- and the biocatalyst reveals the significantly more complex prehistory of the former, indicating a much higher E-factor prehistory. Therefore, a more detailed and comprehensive analysis is required to assess the true environmental impact of a reaction.

The synthesis tree also reveals that enzymes are not entirely renewable. Although enzymes are biocatalysts and have renewable sources such as microorganisms, the

Chapter 1

mineral components used for their growth media are often mined from finite resources. For example, phosphate is a well-known example of a non-renewable resource. Additionally, other fermentation components such as NH_3 or MeOH , which are synthesised using natural gas as feedstock, are still dependent on fossil resources. Thus, the sustainability of biocatalysis should also consider the renewable and non-renewable resources used in the synthesis of the fermentation components and the growth media.

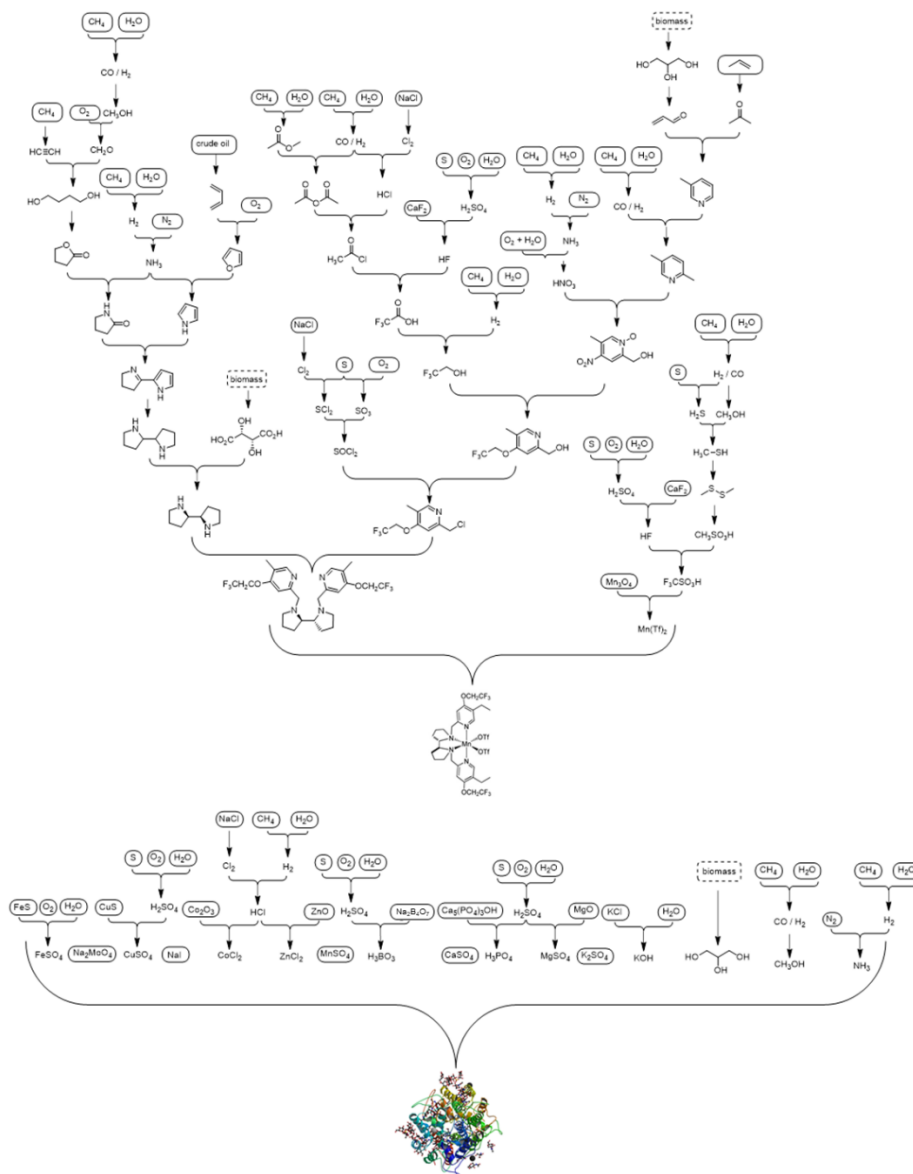


Figure 1.9. Synthesis trees for the catalysts are compared in Table 1.2. The trees were constructed using literature information^[4, 136] as well as publically available information such as Wikipedia. Compounds circled represent original compounds.

It is important to note that a high E-factor for the preparation of a given catalyst does not necessarily correspond to a large impact on the production of the final product. As the performance of the catalyst increases in terms of TTN (turnover number), its

Chapter 1

contribution to the overall E-factor decreases. This means that the cost contribution of the catalyst to the final product also decreases (Figure 1.10).

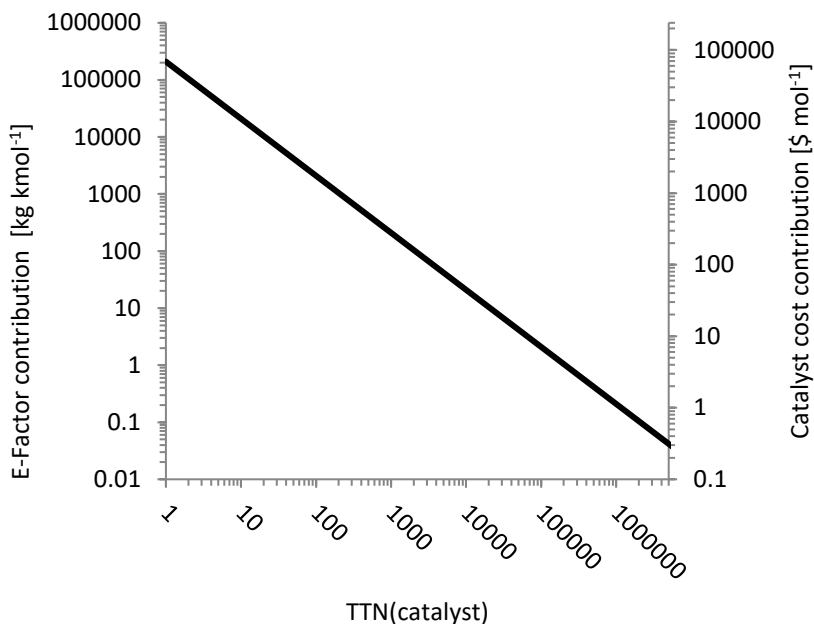


Figure 1.10. Model calculation for the E-factor contribution and cost contribution for a catalyst exhibiting a pre-history E-factor of 200000 g×g⁻¹ and costing 2000\$/kg⁻¹.

Overall, assessing the environmental impact of a catalyst is a complex task that cannot be trivialised, and simple arguments in favour or against a particular type of catalyst may not be appropriate. It requires a comprehensive evaluation of various factors, including the E⁽⁺⁾-factor, recyclability of reagents, harmfulness of wastes, energy requirements, and prehistory of the components used. In addition, it is essential to consider the relationship between solvent properties and the resulting energy demands for chemical transformation, as well as downstream processing. Therefore, a detailed analysis is necessary to make informed decisions regarding the use of a particular catalyst.

1.8 Conclusion

In conclusion, the environmental impact of a catalyst is a complex and multi-faceted issue that cannot be adequately captured by a single metric such as the E-factor. While the E-factor provides a useful starting point for assessing the environmental impact of a reaction, it has limitations, such as not accounting for the recyclability of

reagents, the toxicity of waste products, and the resource and energy requirements of the reaction. Therefore, it is important to use a combination of metrics and approaches to comprehensively evaluate the environmental impact of a catalyst.

It is difficult to make a definitive conclusion on which type of catalysis is greener based on the arguments above. Both chemocatalysis and biocatalysis have advantages and disadvantages in terms of environmental impact. Biocatalysis has the advantage of being more selective and operating at ambient temperatures, but it also has some drawbacks such as the current limitation to aqueous reaction media. On the other hand, chemocatalysis has the advantage of being more versatile and having a shorter reaction time, but it may require harsher reaction conditions, leading to higher energy consumption and waste generation. Additionally, the environmental impact of the starting materials, catalyst synthesis, solvent properties, and downstream processing should also be taken into account. Therefore, a case-by-case analysis is needed to determine which catalysis type is greener for a specific reaction.

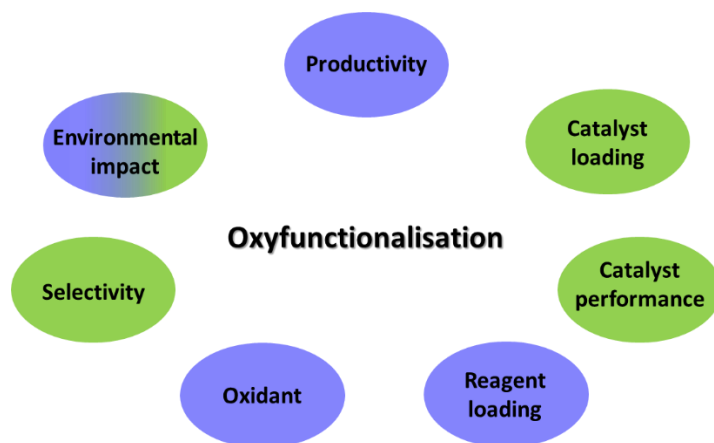


Figure 1.11. The advantage of chemocatalysis (●); the advantage of biocatalysis (●)

We have shown that the choice of solvent can have a significant impact on the environmental footprint of a reaction, not only due to the solvent's physical properties but also its sourcing and disposal. Furthermore, the energy requirements for purification and downstream processing of the reaction products should also be considered. We also highlighted the importance of considering the prehistory of each component used in the reaction, including the catalyst, which can have a significant impact on the overall environmental impact.

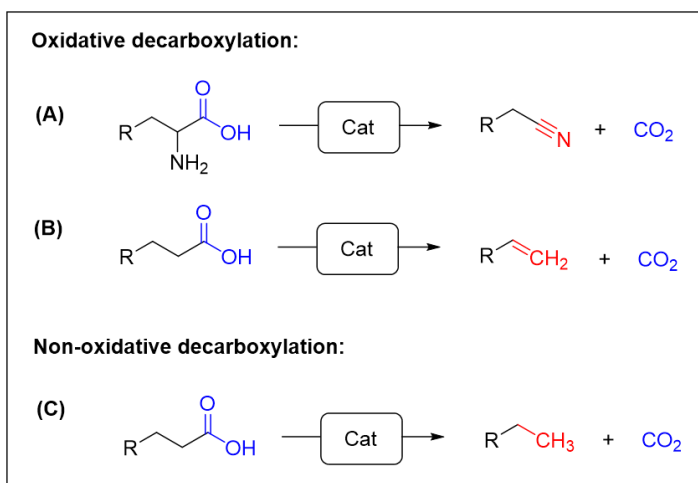
Chapter 1

Overall, assessing and minimising the environmental impact of catalysts is an important goal for achieving sustainable chemistry and mitigating the impact of chemical processes on the environment. By using a multi-faceted approach to evaluate catalysts and focusing on sustainable design principles, we can move towards a more sustainable future for the chemical industry.

2. Decarboxylation reactions

2.1 Different categories of decarboxylation reaction

Transformations of the carboxylate group are very well established enabling (trans)esterification, amidation and reduction reactions.^[52, 177] The conversion of carboxylic acids to their corresponding C₁-shorten decarboxylation products opens up the synthesis of a wide range of products such as building blocks for surfactants,^[178] herbicides,^[179] lubricants,^[180] and biofuels,^[181] which is however still less well-established. Currently, there are mainly two categories of decarboxylation reactions. In oxidative decarboxylation reactions, carboxylic acids are converted to the corresponding nitriles or terminal alkenes. In non-oxidative decarboxylation reactions, the carboxylate groups are cleaved without forming unsaturated bonds, producing alkanes, alcohols or amines (Scheme 1.2).



Scheme 1.2. Examples of (non-)oxidative decarboxylation reactions.

In organic synthesis for decarboxylation, different approaches have been reported (Table 1.4). On the one hand, it was reported that activated halogenated species could be used as oxidants in oxidative decarboxylation reactions, where the oxidants

were obtained via the addition of hypohalite,^[182] *in situ* generation heterogeneous catalytic system or electrochemical method.^[183-186] In the activated halogenated species-mediated decarboxylation reactions, issues of utilising the toxic organic solvent, a significant amount of excess reagents, selectivity and hampering product purification procedure remain. As alternatives, transition metal-catalysed decarboxylation is another promising approach in not only oxidative but also non-oxidative decarboxylation reactions. For instance, palladium,^[187-188] nickel,^[189] rhodium,^[190] iridium,^[191] iron,^[192] and silver/copper,^[193] have been investigated for the production of α -olefin.

On the other hand, biocatalysts have also been enjoying an increasing interest in decarboxylation reactions. Among peroxide-dependent haloperoxidases, vanadium-dependent haloperoxidase (VCPO) could catalyse the transformation of amino acids to nitriles,^[194-195] where activated halide is oxidised from halide and H_2O_2 . In the transformation of fatty acids to terminal alkenes, there are several enzyme classes reported for the oxidative decarboxylation reactions, including cytochrome P450 fatty acid peroxygenase (OleT_{JE}),^[196-197] oxidative decarboxylase UndA,^[198-199] a new family of membrane-bound fatty acid desaturase-like UndB,^[200] and soybean lipoyxygenase I.^[201-202] As for non-oxidative decarboxylation, when amino acids are used as substrates, the classical L-amino acid decarboxylases catalyse the cleavage of the carboxylic group with pyridoxal 5' phosphate (PLP) or a pyruvyl moiety as cofactor.^[203-205] Nowadays, decarboxylases, including glutamate decarboxylases (GAD),^[206] tyrosine decarboxylases (TDC),^[207] phenolic acid decarboxylases (PAD)^[208] and lysine decarboxylases (LDC)^[209] have been widely investigated. Another class of non-oxidative decarboxylase is fatty acid photodecarboxylases (FAP), catalysing the decarboxylation of fatty acids to alkanes under blue light illumination.^[181]

Table 1.4. Assortment of catalysts for decarboxylation reactions.

Substrate	Reaction type	Product	Catalyst	Ref.
	O		Ru(OH) _x /γ-Al ₂ O ₃	[210]
	O		VCPO	[194-195]
	O		Pd/C	[188]
	O		OleT _{JE} , UndA, UndB	[196-197] [198-199] [200]
	N		Pd/Al ₂ O ₃	[211]
	N		GAD	[206]
	N		Ni/ZrO ₂	[212]
	N		FAP	[181]

O: oxidative decarboxylation; N: non-oxidative decarboxylation

The catalytic performance and reaction conditions differ from chemocatalysis to biocatalysis. Dawes *et al.* summarised and made clear comparisons among different catalysis. For chemocatalysts, a high reaction temperature is commonly required to obtain high turnover frequency (TOF), while up to 10⁶ min⁻¹ TOF could be reached at ambient temperature in biotransformations (Figure 1.12).^[213] The advantages of biocatalysts in high reaction efficiency and mild reaction condition make biocatalysis economical and environmental as an alternative for decarboxylation reactions.

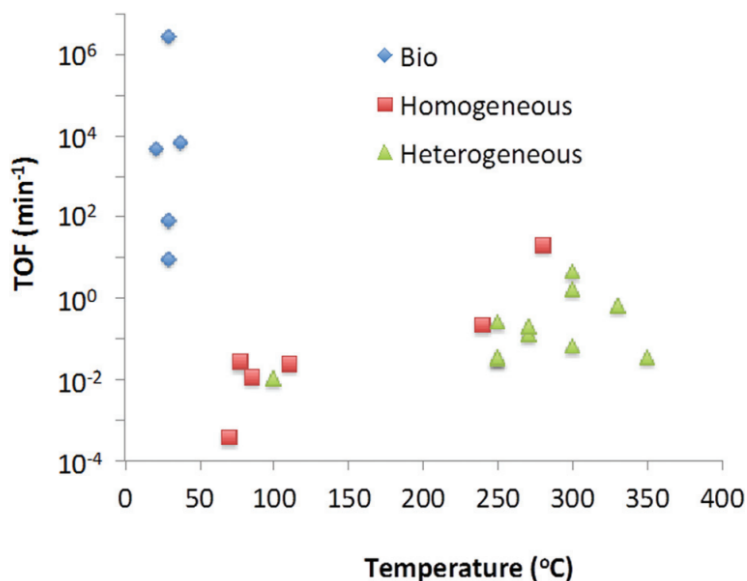
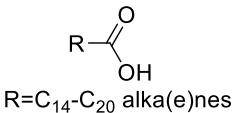
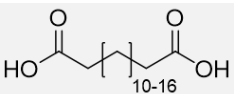
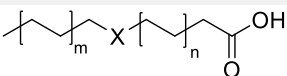
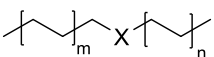
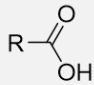
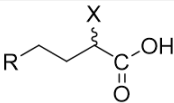
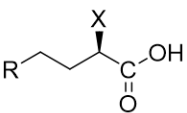

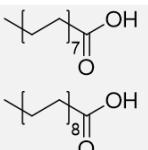
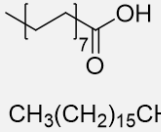
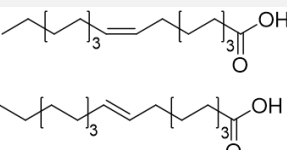
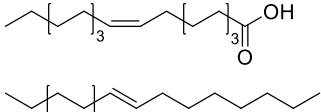
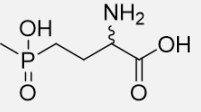
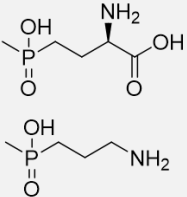


Figure 1.12. TOF as a function of temperature for different classes of catalysts.^[213]

2.2 Synthesis applications of FAPs

Among different types of decarboxylation reactions, non-oxidative fatty acid decarboxylation plays an important role in the production of a wide range of useful products (Table 1.5). The light-dependent fatty acid photodecarboxylase was discovered from *Chlorella variabilis* NC64A (CvFAP) in 2017.^[214] There have been some papers published about the novel photobiocatalyst. Natural (wild-type) CvFAP prefers to catalyse the decarboxylation of linear mid- to long-chain fatty acids forming corresponding alka(e)nes as biofuels.^[181] It was then demonstrated enzyme activity towards functionalised carboxylic acids,^[215-218] *trans*-fatty acids,^[219] dicarboxylic acids,^[220] and phosphinothricin,^[221] exploring synthesis potential of CvFAP for the production of alcohols, amines, esters and chiral phosphinothricin. Furthermore, substrate specificity could also be modified by two strategies. The so-called decoy molecule approach has been applied to improve enzyme activity towards short-chain fatty acids in the presence of C₉-C₁₅ alkanes.^[222] Besides, protein substrate tunnel engineering was also employed to regulate the substrate selectivity of the enzyme. It has been reported that several hot spots in the substrate entry channel, including T430, V453, G462, Y466, and S573,^[215, 219, 221, 223-225] are essential to regulate the substrate scope of the enzyme.

Table 1.5. Applications of CvFAP wild-type and its variants.

Enzyme	Substrate	Product	Ref.
CvFAP WT		R-H	[181]
CvFAP WT		R-H R=C ₁₂ -C ₁₈ alka(e)nes	[220]
CvFAP WT	 <p>X=-CHOH-, -CHNH₂-, -COO-, -CHOCH-</p>		[215-218]
CvFAP WT		R-H	[222]
CvFAP G462A/V	R=short chain alka(e)nes	R=short chain alka(e)nes	[224]
CvFAP G462Y	 <p>X=OH or NH₂; R=-(CH₂)₁₋₉CH₃, -S(CH₂)₀₋₁CH₃, -(CH₂)₁₋₃Cl</p>	 	[215]
CvFAP Y466F			[225]
CvFAP V453E			[219]
CvFAP T430R/G462F/S573G			[221]

2.3 Catalytic mechanism and photoinactivation of FAP

In the expansion of CvFAP applications, the catalytic mechanism of the enzyme has been enjoying increasing interest, due to its role in facilitating the rational design and optimisation of enzymatic reactions. CvFAP is a member of the glucose-methanolcholine oxidoreductase family with an N-terminal FAD-binding domain and a C-terminal substrate-binding domain. The crystal structure clearly showed that there is a long and hydrophobic substrate entry channel in the enzyme, where the highly conserved hydrophobic residues (A576, C432 and R451) interacted with the substrate determining the substrate preference.^[226-228] Furthermore, the light-initiating photodecarboxylation includes different states of FAD (Figure 1.13).^[227-229] It was proposed that the FAD cofactor was photoexcited to a FAD singlet excited state ($^1\text{FAD}^*$) upon the illumination of blue light. An electron was then transferred from the surrounding carboxylate group of the substrate to the $^1\text{FAD}^*$ forming an anionic semiquinone FAD ($\text{FAD}^{\bullet-}$) and alkyl radical and releasing CO_2 . The catalytic cycle of photodecarboxylation is completed by the transfer of a proton from C432 or R451 and an electron from $\text{FAD}^{\bullet-}$ to the alkyl radical to produce the alkane product. Although the last step of proton and electron transfer is still being debated, it is clear that the reserved residues C432 and R451 are crucial in the catalytic circle.

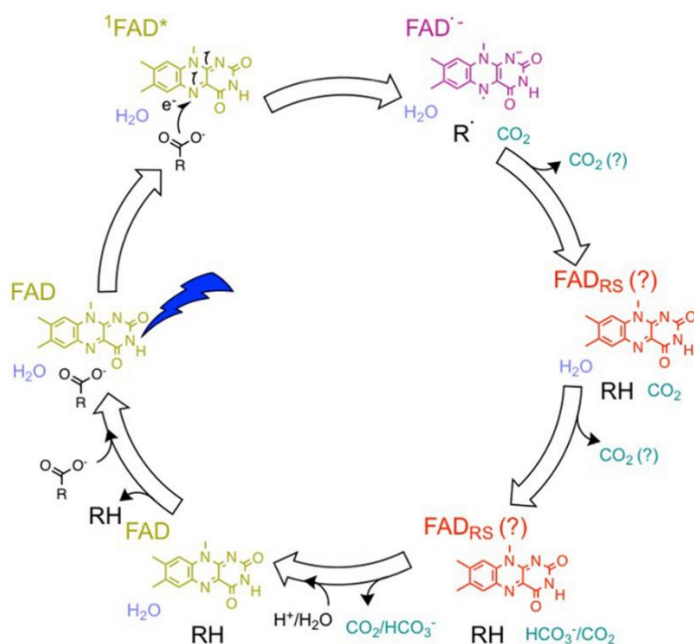


Figure 1.13. The consensus photocatalytic cycle of fatty acid photodecarboxylase.^[229]

Chapter 1

For wider applications of CvFAPs, photoinactivation is one of the major limitations. It was found that blue light illumination could lead to enzyme inactivation in the absence of reactive substrates.^[230] Especially, when purified enzymes were used as catalysts, FAPs completely lost activity within a very short time (< 1 h).^[231] It was proposed that in the absence of substrate, the generated 1FAD* from the first step might interact with enzyme residues forming the radical amino acids, which may result in the adduct formation and fragmentation of the protein.^[230] To circumvent this limitation, using the form of whole cell or cell-free extract would make the catalyst robust.^[224] Besides, further investigation of photoinactivation helps to better understand the photoinactivation mechanism, engineer the enzyme, and optimise the photobiocatalytic reactions for a robust reaction system.^[231]

3. Goal of the thesis

This thesis aims to explore biocatalytic alternatives for challenging chemical reactions. Specifically, we focus on the oxyfunctionalisation and decarboxylation reactions. In **chapter 1**, in order to compare the efficiency and greenness of chemocatalysis and biocatalysis in both oxyfunctionalisation and decarboxylation reactions, we evaluate the opportunities and limitations for *AaeUPO* and CvFAP. After the general introduction, the following four chapters focus on the applications of biocatalysis.

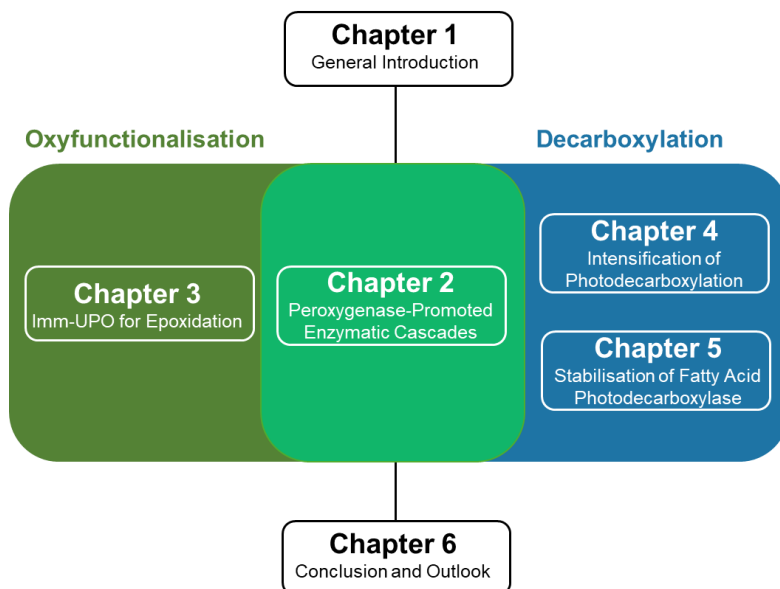
In **chapter 2**, we attempt to explore the synthetic potential of peroxygenase for selective fatty acid hydroxylation. The peroxygenase-promoted enzymatic cascade reactions for the valorisation of fatty acids have been established, in the combination of several classes of enzymes.

Since the non-aqueous phase reaction condition is one of the approaches to make biocatalysis more efficient and lower environmental factors, in **chapter 3**, we aim to immobilise peroxygenase in an alginate matrix for the epoxidation reaction in a solvent-free reaction system.

Light-driven biocatalytic processes are hampered by poor penetration of light into the turbid reaction media. To alleviate this shortcoming, in **chapter 4**, we aim at establishing a new photoreactor concept comprising internal illumination by means of wirelessly powered light emitters.

In **chapter 5**, the photostability of cell-free extract and purified enzyme of CvFAP is compared under light illumination. Here, we point out the effect of various additives on enzyme stabilisation.

Finally, in **chapter 6**, we provide a general conclusion and outlook for the biocatalytic alternatives researched in the chapters above.



Scheme 1.3. Overview of the thesis outline.

References

- [1] L. Hu, C. Wang, B. Yue, X. Chen, H. He, *Mater. Today Commun.* **2017**, *11*, 61-67.
- [2] M. Sutradhar, N. V. Shvydkiy, M. F. C. G. da Silva, M. V. Kirillova, Y. N. Kozlov, A. J. Pombeiro, G. B. Shul'pin, *Dalton Trans.* **2013**, *42*, 11791-11803.
- [3] A. Farokhi, H. Hosseini-Monfared, *New J. Chem.* **2016**, *40*, 5032-5043.
- [4] R. V. Ottenbacher, E. P. Talsi, T. V. Rybalova, K. P. Bryliakov, *ChemCatChem* **2018**, *10*, 5323-5330.
- [5] E. P. Talsi, D. G. Samsonenko, R. V. Ottenbacher, K. P. Bryliakov, *ChemCatChem* **2017**, *9*, 4580-4586.
- [6] X. Engelmann, D. D. Malik, T. Corona, K. Warm, E. R. Farquhar, M. Swart, W. Nam, K. Ray, *Angew. Chem.* **2019**, *131*, 4052-4056.
- [7] R. Turcas, D. Lakk-Bogáth, G. Speier, J. Kaizer, *Inorg. Chem. Commun.* **2018**, *92*, 141-144.
- [8] D. Lakk-Bogáth, B. Kripli, B. I. Meena, G. Speier, J. Kaizer, *Inorg. Chem. Commun.* **2019**, *104*, 165-170.
- [9] M. Sankaralingam, P. Vadivelu, E. Suresh, M. Palaniandavar, *Inorganica Chim. Acta* **2013**, *407*, 98-107.
- [10] S. Muthuramalingam, K. Anandababu, M. Velusamy, R. Mayilmurugan, *Catal. Sci. Technol.* **2019**, *9*, 5991-6001.
- [11] K. Anandababu, S. Muthuramalingam, M. Velusamy, R. Mayilmurugan, *Catal. Sci. Technol.* **2020**, *10*, 2540-2548.
- [12] G. Bianchini, A. Cavarzan, A. Scarso, G. Strukul, *Green Chem.* **2009**, *11*, 1517-1520.
- [13] S. Kumari, S. Muthuramalingam, A. K. Dhara, U. Singh, R. Mayilmurugan, K. Ghosh, *Dalton Trans.* **2020**, *49*, 13829-13839.
- [14] O. Tomita, R. Abe, B. Ohtani, *Chem. Lett.* **2011**, *40*, 1405-1407.
- [15] A. Cavarzan, G. Bianchini, P. Sgarbossa, L. Lefort, S. Gladiali, A. Scarso, G. Strukul, *Eur. J. Chem.* **2009**, *15*, 7930-7939.
- [16] Y. Shiraishi, N. Saito, T. Hirai, *J. Am. Chem. Soc.* **2005**, *127*, 12820-12822.
- [17] X. Zhang, H. Yang, G. Yang, S. Li, X. Wang, J. Ma, *ACS Sustain. Chem. Eng.* **2018**, *6*, 5868-5876.

- [18] K. Zhu, S. Hu, M. Liu, H. Peng, F. E. Chen, *Angew. Chem.* **2019**, *131*, 10028-10032.
- [19] P. P. Poudel, K. Arimitsu, K. Yamamoto, *Chem. Commun.* **2016**, *52*, 4163-4166.
- [20] S. I. Murahashi, S. Ono, Y. Imada, *Angew. Chem., Int. Ed.* **2002**, *41*, 2366-2368.
- [21] Y. Imada, H. Iida, S. Ono, Y. Masui, S. I. Murahashi, *Chem. Asian J.* **2006**, *1*, 136-147.
- [22] D. K. Romney, S. M. Colvin, S. J. Miller, *J. Am. Chem. Soc.* **2014**, *136*, 14019-14022.
- [23] H. Alwaseem, R. Fasan, *Protein Eng. Des. Sel.* **2021**, 207-242.
- [24] R. Fasan, *ACS Catal.* **2012**, *2*, 647-666.
- [25] V. B. Urlacher, M. Girhard, *Trends Biotechnol.* **2019**, *37*, 882-897.
- [26] R. Bernhardt, V. B. Urlacher, *Appl. Microbiol. Biotechnol.* **2014**, *98*, 6185-6203.
- [27] S. Schulz, M. Girhard, V. B. Urlacher, *ChemCatChem* **2012**, *4*, 1889-1895.
- [28] G. C. Schröder, M. S. Smit, D. J. Opperman, *Curr. Opin. Green Sustain. Chem.* **2022**, *39*, 100734.
- [29] X. Xu, T. Hilberath, F. Hollmann, *Curr. Opin. Green Sustain. Chem.* **2022**, *39*, 100745.
- [30] M. Hobisch, D. Holtmann, P. G. de Santos, M. Alcalde, F. Hollmann, S. Kara, *Biotechnol. Adv.* **2021**, *51*, 107615.
- [31] D. T. Monterrey, A. Ménes-Rubio, M. Keser, D. Gonzalez-Perez, M. Alcalde, *Curr. Opin. Green Sustain. Chem.* **2023**, *41*, 100786.
- [32] A. Beltrán-Nogal, I. Sánchez-Moreno, D. Méndez-Sánchez, P. G. de Santos, F. Hollmann, M. Alcalde, *Curr. Opin. Green Sustain. Chem.* **2022**, *73*, 102342.
- [33] M. Hofrichter, R. Ullrich, *Curr Opin Chem Biol.* **2014**, *19*, 116-125.
- [34] L. M. Blank, B. E. Ebert, K. Buehler, B. Bühler, *Antioxid. Redox Signal.* **2010**, *13*, 349-394.
- [35] C. Peters, R. M. Buller, *Catalysts* **2019**, *9*, 221.

Chapter 1

- [36] J. Dong, E. Fernández-Fueyo, F. Hollmann, C. E. Paul, M. Pesic, S. Schmidt, Y. Wang, S. Younes, W. Zhang, *Angew. Chem., Int. Ed.* **2018**, *57*, 9238-9261.
- [37] C. E. Paul, D. Eggerichs, A. H. Westphal, D. Tischler, W. J. van Berkel, *Biotechnol. Adv.* **2021**, *51*, 107712.
- [38] M. J. Fürst, A. Gran-Scheuch, F. S. Aalbers, M. W. Fraaije, *ACS Catal.* **2019**, *9*, 11207-11241.
- [39] E. Romero, J. R. n. Gómez Castellanos, G. Gadda, M. W. Fraaije, A. Mattevi, *Chem. Rev.* **2018**, *118*, 1742-1769.
- [40] S. A. Baker Dockrey, A. L. Lukowski, M. R. Becker, A. R. Narayan, *Nat. Chem.* **2018**, *10*, 119-125.
- [41] L. Feng, W. Wang, J. Cheng, Y. Ren, G. Zhao, C. Gao, Y. Tang, X. Liu, W. Han, X. Peng, *Proc. Natl. Acad. Sci.* **2007**, *104*, 5602-5607.
- [42] T. A. Ewing, G. Gygli, M. W. Fraaije, W. J. van Berkel, *The Enzymes* **2020**, *47*, 87-116.
- [43] N. G. Leferink, D. P. Heuts, M. W. Fraaije, W. J. van Berkel, *Arch. Biochem. Biophys.* **2008**, *474*, 292-301.
- [44] R. H. van den Heuvel, M. W. Fraaije, A. Mattevi, C. Laane, W. J. van Berkel, *J. Mol. Catal. B Enzym.* **2001**, *11*, 185-188.
- [45] L. E. Bevers, P.-L. Hagedoorn, W. R. Hagen, *Coord. Chem. Rev.* **2009**, *253*, 269-290.
- [46] M. Sutradhar, A. J. Pombeiro, J. A. L. da Silva, *Vanadium Catalysis*, Royal Society of Chemistry, **2020**.
- [47] R. Wever, B. E. Krenn, R. Renirie, *Meth. Enzymol.* **2018**, *605*, 141-201.
- [48] H. Michibata, *Vanadium: biochemical and molecular biological approaches*, Springer Science & Business Media, **2011**.
- [49] A. Karnaouri, K. Choroziyan, D. Zouraris, A. Karantonis, E. Topakas, U. Rova, P. Christakopoulos, *Bioresour. Technol.* **2022**, *345*, 126491.
- [50] V. G. Eijsink, D. Petrovic, Z. Forsberg, S. Mekasha, Å. K. Røhr, A. Várnai, B. Bissaro, G. Vaaje-Kolstad, *Biotechnol. Biofuels* **2019**, *12*, 58.
- [51] R. R. Singhanian, P. Dixit, A. K. Patel, B. S. Giri, C.-H. Kuo, C.-W. Chen, C. Di Dong, *Bioresour. Technol.* **2021**, *335*, 125261.

- [52] U. T. Bornscheuer, R. J. Kazlauskas, *Hydrolases in organic synthesis: regio- and stereoselective biotransformations*, John Wiley & Sons, **2006**.
- [53] M. Paravidino, M. J. Sorgedragar, R. V. Orru, U. Hanefeld, *Eur. J. Chem.* **2010**, *16*, 7596-7604.
- [54] J. S. Dordick, M. A. Marletta, A. M. Klibanov, Bioengineering, *Biotechnol. Bioeng.* **1987**, *30*, 31-36.
- [55] J. S. Dordick, M. A. Marletta, A. M. Klibanov, *Proc. Natl. Acad. Sci.* **1986**, *83*, 6255-6257.
- [56] A. Zaks, A. M. Klibanov, *Proc. Natl. Acad. Sci.* **1985**, *82*, 3192-3196.
- [57] A. Zaks, A. M. Klibanov, *Science* **1984**, *224*, 1249-1251.
- [58] M. M. van Schie, J.-D. Spöring, M. Bocola, P. D. de María, D. Rother, *Green Chem.* **2021**, *23*, 3191-3206.
- [59] B. Bühler, I. Bollhalder, B. Hauer, B. Witholt, A. Schmid, *Biotechnol. Bioeng.* **2003**, *81*, 683-694.
- [60] A. Schmid, I. Vereyken, M. Held, B. Witholt, *J. Mol. Catal. B Enzym.* **2001**, *11*, 455-462.
- [61] M. G. Wubbolts, O. Favre-Bulle, B. Witholt, *Biotechnol. Bioeng.* **1996**, *52*, 301-308.
- [62] M.-J. de Smet, H. Wynberg, B. Witholt, *Appl. Environ. Microbiol.* **1981**, *42*, 811-816.
- [63] J. B. Park, D. S. Clark, *Biotechnol. Bioeng.* **2006**, *94*, 189-192.
- [64] R. Gandolfi, N. Ferrara, F. Molinari, *Tetrahedron Lett.* **2001**, *42*, 513-514.
- [65] K. Hofstetter, J. Lutz, I. Lang, B. Witholt, A. Schmid, *Angew. Chem., Int. Ed.* **2004**, *43*, 2163-2166.
- [66] M. Hobisch, M. M. C. H. van Schie, J. Kim, K. Røjkjær Andersen, M. Alcalde, R. Kourist, C. B. Park, F. Hollmann, S. Kara, *ChemCatChem* **2020**, *12*, 4009-4013.
- [67] F. E. Nintzel, Y. Wu, M. Planchestainer, M. Held, M. Alcalde, F. Hollmann, *Chem. Commun.* **2021**, *57*, 5766-5769.
- [68] F. Perz, S. Bormann, R. Ulber, M. Alcalde, P. Bubenheim, F. Hollmann, D. Holtmann, A. Liese, *ChemCatChem*, *12*, 3666-3669.
- [69] M. C. Rauch, F. Tieves, C. E. Paul, I. W. Arends, M. Alcalde, F. Hollmann, *ChemCatChem* **2019**, *11*, 4519-4523.

Chapter 1

- [70] E. Churakova, I. W. Arends, F. Hollmann, *ChemCatChem* **2013**, *5*, 565-568.
- [71] N. Jiao, S. S. Stahl, *Green Oxidation in Organic Synthesis*, **2019**.
- [72] D. Holtmann, M. W. Fraaije, I. W. Arends, D. J. Opperman, F. Hollmann, *Chem. Commun.* **2014**, *50*, 13180-13200.
- [73] A. R. Faraji, F. Ashouri, Z. Hekmatian, S. Heydari, S. Mosazadeh, *Polyhedron* **2019**, *157*, 90-106.
- [74] A. Farokhi, K. Berijani, H. Hosseini-Monfared, *Catal. Lett.* **2018**, *148*, 2608-2618.
- [75] R. R. Chao, I. C. K. Lau, T. Coleman, L. R. Churchman, S. A. Child, J. H. Lee, J. B. Bruning, J. J. De Voss, S. G. Bell, *Eur. J. Chem.* **2021**, *27*, 14765-14777.
- [76] H. Toda, R. Imae, N. Itoh, *Adv. Synth. Catal.* **2014**, *356*, 3443-3450.
- [77] E. Beneventi, M. Niero, R. Motterle, M. Fraaije, E. Bergantino, *J. Mol. Catal. B Enzym.* **2013**, *98*, 145-154.
- [78] D. S. Nesterov, E. N. Chygorin, V. N. Kokozay, V. V. Bon, R. Boča, Y. N. Kozlov, L. S. Shul'pina, J. Jezierska, A. Ozarowski, A. J. Pombeiro, *Inorg. Chem.* **2012**, *51*, 9110-9122.
- [79] K. Matsumoto, T. Oguma, T. Katsuki, *Angew. Chem., Int. Ed.* **2009**, *48*, 7432-7435.
- [80] M. J. Calvete, M. Piñeiro, L. D. Dias, M. M. Pereira, *ChemCatChem* **2018**, *10*, 3615-3635.
- [81] Y. Zhang, H. Li, L. Zhang, R. Gao, W.-L. Dai, Engineering, *ACS Sustain. Chem. Eng.* **2019**, *7*, 17008-17019.
- [82] A. V. Malkov, F. Friscourt, M. Bell, M. E. Swarbrick, P. Kocovsky, *J. Org. Chem.* **2008**, *73*, 3996-4003.
- [83] Z. Zhu, H. Xu, J. Jiang, P. Wu, *J. Phys. Chem.* **2016**, *120*, 23613-23624.
- [84] J. B. Park, D. S. Clark, *Biotechnol. Bioeng.* **2006**, *93*, 1190-1195.
- [85] P. Zhao, F. Kong, Y. Jiang, X. Qin, X. Tian, Z. Cong, *J. Am. Chem. Soc.* **2023**, *145*, 5506-5511.
- [86] M. Kluge, R. Ullrich, K. Scheibner, M. Hofrichter, *Green Chem.* **2012**, *14*, 440-446.
- [87] P. Zhao, J. Chen, N. Ma, J. Chen, X. Qin, C. Liu, F. Yao, L. Yao, L. Jin, Z. Cong, *Chem. Sci.* **2021**, *12*, 6307-6314.

- [88] X.-P. Wang, P.-F. Zhou, Z.-G. Li, B. Yang, F. Hollmann, Y.-H. Wang, *Sci. Rep.* **2017**, *7*, 1-5.
- [89] T. Nagataki, Y. Tachi, S. J. J. o. M. C. A. C. Itoh, *J. Mol. Catal. A Chem.* **2005**, *225*, 103-109.
- [90] D. S. Nesterov, O. V. Nesterova, *Catalysts* **2021**, *11*, 1148.
- [91] W. Wu, W. Cao, L. Hu, Z. Su, X. Liu, X. Feng, *Chem. Sci.* **2019**, *10*, 7003-7008.
- [92] J. T. Groves, P. Viski, *J. Org. Chem.* **1990**, *55*, 3628-3634.
- [93] M. Guo, Y.-M. Lee, M. S. Seo, Y.-J. Kwon, X.-X. Li, T. Ohta, W.-S. Kim, R. Sarangi, S. Fukuzumi, W. Nam, *Inorg. Chem.* **2018**, *57*, 10232-10240.
- [94] D. Lakk-Bogáth, G. Speier, J. Kaizer, *New J. Chem.* **2015**, *39*, 8245-8248.
- [95] S. J. Strohmaier, J. M. Baek, J. J. De Voss, U. Jurva, S. Andersson, E. M. Gillam, *ChemCatChem* **2020**, *12*, 1750-1761.
- [96] P. Le Maux, H. F. Srour, G. Simonneaux, *Tetrahedron* **2012**, *68*, 5824-5828.
- [97] J. Tian, J. Lin, J. Zhang, C. Xia, W. Sun, *Adv. Synth. Catal.* **2022**, *364*, 593-600.
- [98] A. Al-Shameri, L. Schmermund, V. Sieber, *Curr. Opin. Green Sustain. Chem.* **2022**, *40*, 100733.
- [99] W. Johns, *Kirk-Othmer Encyclopedia of Chemical Technology* **2000**.
- [100] A. Lorente-Arevalo, M. Ladero, J. M. Bolivar, *Curr. Opin. Green Sustain. Chem.* **2021**, *32*, 100544.
- [101] D. Holtmann, F. Hollmann, *ChemBioChem* **2016**, *17*, 1391-1398.
- [102] B. O. Burek, S. Bormann, F. Hollmann, J. Z. Bloh, D. Holtmann, *Green Chem.* **2019**, *21*, 3232-3249.
- [103] A. Knorrscheidt, J. Soler, N. Hünecke, P. Püllmann, M. Garcia-Borràs, M. J. Weissenborn, *ACS Catal.* **2021**, *11*, 7327-7338.
- [104] P. Gomez de Santos, I. Mateljak, M. D. Hoang, S. J. Fleishman, F. Hollmann, M. Alcalde, *J. Am. Chem. Soc.* **2023**, *145*, 3443-3453.
- [105] P. Gómez de Santos, A. González-Benjumea, Á. Fernández García, Y. Wu, A. But, P. Molina-Espeja, D. M. Maté, D. González-Pérez, W. Zhang, J. Kiebig, *Angew. Chem., Int. Ed.* **2022**, *62*, e2022173.
- [106] M. Ramirez-Escudero, P. Molina-Espeja, P. Gomez de Santos, M. Hofrichter, J. Sanz-Aparicio, M. Alcalde, *ACS Chem. Biol.* **2018**, *13*, 3259-3268.

Chapter 1

- [107] M. Alcalde, *Directed enzyme evolution: Advances and applications*, Springer, **2017**.
- [108] P. Püllmann, M. J. Weissenborn, *ACS Synth. Biol.* **2021**, *10*, 1360-1372.
- [109] A. Knorrscheidt, J. Soler, N. Hünecke, P. Püllmann, M. Garcia-Borràs, M. J. Weissenborn, *Catal. Sci. Technol.* **2021**, *11*, 6058-6064.
- [110] A. Knorrscheidt, P. Püllmann, E. Schell, D. Homann, E. Freier, M. J. Weissenborn, *ChemCatChem* **2020**, *12*, 4788-4795.
- [111] A. Fanourakis, P. J. Docherty, P. Chuentragool, R. J. Phipps, *ACS Catal.* **2020**, *10*, 10672-10714.
- [112] L. Soobramoney, M. D. Bala, H. B. Friedrich, M. N. Pillay, *Polyhedron* **2019**, *163*, 63-70.
- [113] D. Naicker, H. B. Friedrich, B. Omondi, *RSC Adv.* **2015**, *5*, 63123-63129.
- [114] D. Naicker, S. Alapour, H. B. Friedrich, *J. Chem. Res.* **2021**, *45*, 282-289.
- [115] R. K. Gudiminchi, C. Randall, D. J. Opperman, O. A. Olaofe, S. T. Harrison, J. Albertyn, M. S. Smit, *Appl. Microbiol. Biotechnol.* **2012**, *96*, 1507-1516.
- [116] E. G. Funhoff, J. Salzmann, U. Bauer, B. Witholt, J. B. van Beilen, *Enzyme Microb.* **2007**, *40*, 806-812.
- [117] J. B. Van Beilen, E. G. Funhoff, *Appl. Microbiol. Biotechnol.* **2007**, *74*, 13-21.
- [118] A. Glieder, E. T. Farinas, F. H. Arnold, *Nat. Biotechnol.* **2002**, *20*, 1135-1139.
- [119] S. Peter, M. Kinne, X. Wang, R. Ullrich, G. Kayser, J. T. Groves, M. Hofrichter, *FEBS J.* **2011**, *278*, 3667-3675.
- [120] M. J. Maseme, A. Pennec, J. van Marwijk, D. J. Opperman, M. S. Smit, *Angew. Chem.* **2020**, *132*, 10445-10448.
- [121] M. W. Peters, P. Meinhold, A. Glieder, F. H. Arnold, *J. Am. Chem. Soc.* **2003**, *125*, 13442-13450.
- [122] P. Meinhold, M. W. Peters, A. Hartwick, A. R. Hernandez, F. H. Arnold, *Adv. Synth. Catal.* **2006**, *348*, 763-772.
- [123] C. G. Acevedo-Rocha, A. Li, L. D'Amore, S. Hoebenreich, J. Sanchis, P. Lubrano, M. P. Ferla, M. Garcia-Borràs, S. Osuna, M. T. Reetz, *Nat. Commun.* **2021**, *12*, 1621.
- [124] A. Li, C. G. Acevedo-Rocha, L. D'Amore, J. Chen, Y. Peng, M. Garcia-Borràs, C. Gao, J. Zhu, H. Rickerby, S. Osuna, *Angew. Chem.* **2020**, *132*, 12599-12605.

- [125] J. b. Wang, A. Ilie, M. T. Reetz, *Adv. Synth. Catal.* **2017**, *359*, 2056-2060.
- [126] A. Ilie, R. Lonsdale, R. Agudo, M. T. Reetz, *Tetrahedron Lett.* **2015**, *56*, 3435-3437.
- [127] A. Ilie, R. Agudo, G.-D. Roiban, M. T. Reetz, *Tetrahedron* **2015**, *71*, 470-475.
- [128] G. D. Roiban, R. Agudo, M. T. Reetz, *Angew. Chem., Int. Ed.* **2014**, *53*, 8659-8663.
- [129] R. Fasan, S. Jennifer Kan, H. Zhao, *ACS Catal.* **2019**, *9*, 9775-9788.
- [130] R. Singh, J. N. Kolev, P. A. Sutera, R. Fasan, *ACS Catal.* **2015**, *5*, 1685-1691.
- [131] R. Siedlecka, *Catalysts* **2023**, *13*, 121.
- [132] A. Li, S. Wu, J. P. Adams, R. Snajdrova, Z. Li, *Chem. Commun.* **2014**, *50*, 8771-8774.
- [133] Y. C. Yin, H. L. Yu, Z. J. Luan, R. J. Li, P. F. Ouyang, J. Liu, J. H. Xu, *ChemBioChem* **2014**, *15*, 2443-2449.
- [134] J. Heider, M. Szaleniec, K. Suenwoldt, M. Boll, *Microb. Physiol.* **2016**, *26*, 45-62.
- [135] Y. Guo, L. Alvigini, M. Trajkovic, L. Alonso-Cotchico, E. Monza, S. Savino, I. Marić, A. Mattevi, M. W. Fraaije, *Nat. Commun.* **2022**, *13*, 7195.
- [136] F. Tonin, F. Tieves, S. Willot, A. van Troost, R. van Oosten, S. Breestraat, S. van Pelt, M. Alcalde, F. Hollmann, *Org. Process Res. Dev.* **2021**, *25*, 1414-1418.
- [137] B. Bühler, A. Schmid, *J. Biotechnol.* **2004**, *113*, 183-210.
- [138] V. Dantignana, M. Milan, O. Cussó, A. Company, M. Bietti, M. Costas, *ACS Cent. Sci.* **2017**, *3*, 1350-1358.
- [139] S. Peter, A. Karich, R. Ullrich, G. Gröbe, K. Scheibner, M. Hofrichter, *J. Mol. Catal. B Enzym.* **2014**, *103*, 47-51.
- [140] E. N. Jacobsen, W. Zhang, A. R. Muci, J. R. Ecker, L. Deng, *J. Am. Chem. Soc.* **1991**, *113*, 7063-7064.
- [141] K. B. Sharpless, *Angew. Chem., Int. Ed.* **2002**, *41*, 2024-2032.
- [142] Z.-X. Wang, Y. Tu, M. Frohn, J.-R. Zhang, Y. Shi, *J. Am. Chem. Soc.* **1997**, *119*, 11224-11235.
- [143] A. Schmid, K. Hofstetter, H. J. Feiten, F. Hollmann, B. Witholt, *Adv. Synth. Catal.* **2001**, *343*, 732-737.

Chapter 1

- [144] S. Panke, M. Held, M. G. Wubbolts, B. Witholt, A. Schmid, *Biotechnol. Bioeng.* **2002**, *80*, 33-41.
- [145] S. Panke, B. Witholt, A. Schmid, M. G. Wubbolts, *Appl. Environ. Microbiol.* **1998**, *64*, 2032-2043.
- [146] H. Toda, R. Imae, T. Komio, N. Itoh, *Appl. Microbiol. Biotechnol.* **2012**, *96*, 407-418.
- [147] H. Toda, R. Imae, N. Itoh, *Tetrahedron: Asymmetry* **2012**, *23*, 1542-1549.
- [148] J. Li, W. Gu, Z. Wang, X. Zhou, Y. Chen, *ChemBioChem* **2023**, *24*, e202200719.
- [149] G.-D. Roiban, R. Agudo, M. T. Reetz, *Tetrahedron* **2013**, *69*, 5306-5311.
- [150] G. Li, M. Garcia-Borràs, M. J. Fürst, A. Ilie, M. W. Fraaije, K. Houk, M. T. Reetz, *J. Am. Chem. Soc.* **2018**, *140*, 10464-10472.
- [151] F. Ferroni, M. Smit, D. Opperman, *J. Mol. Catal. B Enzym.* **2014**, *107*, 47-54.
- [152] F. M. Ferroni, C. Tolmie, M. S. Smit, D. J. Opperman, *PLoS One* **2016**, *11*, e0160186.
- [153] K. Balke, S. Schmidt, M. Genz, U. T. Bornscheuer, *ACS Chem. Biol.* **2016**, *11*, 38-43.
- [154] L. Zhou, X. Liu, J. Ji, Y. Zhang, X. Hu, L. Lin, X. Feng, *J. Am. Chem. Soc.* **2012**, *134*, 17023-17026.
- [155] Y. Imada, H. Iida, S. I. Murahashi, T. Naota, *Angew. Chem., Int. Ed.* **2005**, *44*, 1704-1706.
- [156] G. Li, M. J. Fürst, H. R. Mansouri, A. K. Ressmann, A. Ilie, F. Rudroff, M. D. Mihovilovic, M. W. Fraaije, M. T. Reetz, *Org. Biomol. Chem.* **2017**, *15*, 9824-9829.
- [157] Z. G. Zhang, G. D. Roiban, J. P. Acevedo, I. Polyak, M. T. Reetz, *Adv. Synth. Catal.* **2013**, *355*, 99-106.
- [158] Z. G. Zhang, L. P. Parra, M. T. Reetz, *Eur. J. Chem.* **2012**, *18*, 10160-10172.
- [159] S. Wu, J. P. Acevedo, M. T. Reetz, *Proc. Natl. Acad. Sci.* **2010**, *107*, 2775-2780.
- [160] D. J. Opperman, M. T. Reetz, *ChemBioChem* **2010**, *11*, 2589-2596.
- [161] M. T. Reetz, S. Wu, *J. Am. Chem. Soc.* **2009**, *131*, 15424-15432.
- [162] M. Bocola, F. Schulz, F. Leca, A. Vogel, M. W. Fraaije, M. T. Reetz, *Adv. Synth. Catal.* **2005**, *347*, 979-986.

- [163] M. T. Reetz, B. Brunner, T. Schneider, F. Schulz, C. M. Clouthier, M. M. Kayser, *Angew. Chem.* **2004**, *116*, 4167-4170.
- [164] K. Balke, M. Bäumgen, U. T. Bornscheuer, *ChemBioChem* **2017**, *18*, 1627-1638.
- [165] J. Rehdorf, M. D. Mihovilovic, U. T. Bornscheuer, *Angew. Chem., Int. Ed.* **2010**, *26*, 4506-4508.
- [166] A. Kirschner, U. T. Bornscheuer, *Appl. Microbiol. Biotechnol.* **2008**, *81*, 465-472.
- [167] K. Geitner, A. Kirschner, J. Rehdorf, M. Schmidt, M. D. Mihovilovic, U. T. Bornscheuer, *Tetrahedron: Asymmetry* **2007**, *18*, 892-895.
- [168] M. Tataruch, J. Heider, J. Bryjak, P. Nowak, D. Knack, A. Czerniak, J. Liesiene, M. Szaleniec, *J. Biotechnol.* **2014**, *192*, 400-409.
- [169] M. L. Corrado, T. Knaus, F. G. Mutti, *ChemBioChem* **2018**, *19*, 679-686.
- [170] R. A. Sheldon, J. M. Woodley, *Chem. Rev.* **2018**, *118*, 801-838.
- [171] L. Zhou, X. Liu, J. Ji, Y. Zhang, W. Wu, Y. Liu, L. Lin, X. Feng, *Org. Lett.* **2014**, *16*, 3938-3941.
- [172] R. A. Sheldon, M. L. Bode, S. G. Akakios, *Curr. Opin. Green Sustain. Chem.* **2022**, *33*, 100569.
- [173] R. A. Sheldon, *Green Chem.* **2017**, *19*, 18-43.
- [174] T. Hilberath, A. van Troost, M. Alcalde, F. Hollmann, *Front. Catal.* **2022**, *2*, 882992.
- [175] F. Tieves, F. Tonin, E. Fernández-Fueyo, J. M. Robbins, B. Bommarius, A. S. Bommarius, M. Alcalde, F. Hollmann, *Tetrahedron* **2019**, *75*, 1311-1314.
- [176] P. G. Jessop, *Green Chem.* **2011**, *13*, 1391-1398.
- [177] K. Noweck, W. Grafahrend, *Chemistry* **2012**, *14*, 117.
- [178] A. Bhadani, A. Kafle, T. Ogura, M. Akamatsu, K. Sakai, H. Sakai, M. Abe, *Curr. Opin. Colloid Interface Sci.* **2020**, *45*, 124-135.
- [179] C. A. Brunharo, H. K. Takano, C. A. Mallory-Smith, F. E. Dayan, B. D. Hanson, *J. Agric. Food Chem.* **2019**, *67*, 8431-8440.
- [180] C. B. Davis, R. D. Hartnell, P. D. Madge, D. J. Owen, R. J. Thomson, A. K. Chong, R. L. Coppel, M. Von Itzstein, *Carbohydr. Res.* **2007**, *342*, 1773-1780.
- [181] M. M. E. Huijbers, W. Zhang, F. Tonin, F. Hollmann, *Angew. Chem., Int. Ed.* **2018**, *57*, 13648-13651.

Chapter 1

- [182] E. V. Bellale, S. N. Huddar, U. S. Mahajan, K. G. Akamanchi, *Pure Appl. Chem.* **2011**, *83*, 607-612.
- [183] X. Wang, J. Zhao, *Chem. Lett.* **2004**, *33*, 332-333.
- [184] K. Ogura, M. Kobayashi, M. Nakayama, Y. Miho, *J. Electroanal. Chem.* **1999**, *463*, 218-223.
- [185] J. J. Dai, Y. B. Huang, C. Fang, Q. X. Guo, Y. Fu, *ChemSusChem* **2012**, *5*, 617-620.
- [186] N. Kuleshova, A. Vvedenskii, E. Bobrinskaya, *Russ. J. Electrochem.* **2018**, *54*, 592-597.
- [187] A. John, L. T. Hogan, M. A. Hillmyer, W. B. Tolman, *Chem. Commun.* **2015**, *51*, 2731-2733.
- [188] A. Chatterjee, V. R. Jensen, *ACS Catal.* **2017**, *7*, 2543-2547.
- [189] A. John, M. O. Miranda, K. Ding, B. s. Dereli, M. A. Ortuño, A. M. LaPointe, G. W. Coates, C. J. Cramer, W. B. Tolman, *Organometallics* **2016**, *35*, 2391-2400.
- [190] J. A. Miller, J. A. Nelson, M. P. Byrne, *J. Org. Chem.* **1993**, *58*, 18-20.
- [191] J. Ternel, T. Lebarbé, E. Monflier, F. Hapiot, *ChemSusChem* **2015**, *8*, 1585-1592.
- [192] S. Maetani, T. Fukuyama, N. Suzuki, D. Ishihara, I. Ryu, *Chem. Commun.* **2012**, *48*, 2552-2554.
- [193] C. Walling, D. M. Camaioni, *J. Org. Chem.* **1978**, *43*, 3266-3271.
- [194] A. But, J. Le Nôtre, E. L. Scott, R. Wever, J. P. Sanders, *ChemSusChem* **2012**, *5*, 1199-1202.
- [195] M. Nieder, L. Hager, *Arch. Biochem. Biophys.* **1985**, *240*, 121-127.
- [196] C. H. Hsieh, X. Huang, J. A. Amaya, C. D. Rutland, C. L. Keys, J. T. Groves, R. N. Austin, T. M. Makris, *Biochemistry* **2017**, *56*, 3347-3357.
- [197] C. E. Wise, C. H. Hsieh, N. L. Poplin, T. M. Makris, *ACS Catal.* **2018**, *8*, 9342-9352.
- [198] O. M. Manley, R. Fan, Y. Guo, T. M. Makris, *J. Am. Chem. Soc.* **2019**, *141*, 8684-8688.
- [199] S. Zhang, Y. Liu, *Org. Biomol. Chem.* **2019**, *17*, 9808-9818.
- [200] Z. Rui, N. C. Harris, X. Zhu, W. Huang, W. Zhang, *ACS Catal.* **2015**, *5*, 7091-7094.
- [201] K. Liu, S. Li, *Curr. Opin. Biotechnol* **2020**, *62*, 7-14.

- [202] J. Blazeck, L. Liu, R. Knight, H. S. Alper, *J. Biotechnol.* **2013**, *165*, 184-194.
- [203] F. Jordan, H. Patel, *ACS Catal.* **2013**, *3*, 1601-1617.
- [204] F. De Schouwer, L. Claes, A. Vandekerkhove, J. Verduyckt, D. E. De Vos, *ChemSusChem* **2019**, *12*, 1272-1303.
- [205] M. D. Toney, *Biochim. Biophys. Acta - Proteins Proteom.* **2011**, *1814*, 1407-1418.
- [206] C. Ke, X. Yang, H. Rao, W. Zeng, M. Hu, Y. Tao, J. Huang, *Springerplus* **2016**, *5*, 591.
- [207] M. Jiang, G. Xu, J. Ni, K. Zhang, J. Dong, R. Han, Y. Ni, *Appl. Biochem. Biotechnol.* **2019**, *188*, 436-449.
- [208] Á. Gómez Baraibar, D. Reichert, C. Mügge, S. Seger, H. Gröger, R. Kourist, *Angew. Chem., Int. Ed.* **2016**, *55*, 14823-14827.
- [209] W. Ma, W. Cao, H. Zhang, K. Chen, Y. Li, P. Ouyang, *Biotechnol. Lett.* **2015**, *37*, 799-806.
- [210] L. Claes, J. Verduyckt, I. Stassen, B. Lagrain, D. E. De Vos, *Chem. Commun.* **2015**, *51*, 6528-6531.
- [211] F. De Schouwer, L. Claes, N. Claes, S. Bals, J. Degrevè, D. E. De Vos, *Green Chem.* **2015**, *17*, 2263-2270.
- [212] A. Kiméné, R. Wojcieszak, S. Paul, F. Dumeignil, *J. Chem. Technol. Biotechnol.* **2019**, *94*, 658-669.
- [213] G. J. S. Dawes, E. L. Scott, J. Le Nôtre, J. P. Sanders, J. H. Bitter, *Green Chem.* **2015**, *17*, 3231-3250.
- [214] D. Sorigué, B. Legeret, S. Cuiné, S. Blangy, S. Moulin, E. Billon, P. Richaud, S. Brugière, Y. Cauté, D. Nurizzo, *Science* **2017**, *357*, 903-907.
- [215] J. Xu, Y. Hu, J. Fan, M. Arkin, D. Li, Y. Peng, W. Xu, X. Lin, Q. Wu, *Angew. Chem.* **2019**, *131*, 8562-8566.
- [216] H. J. Cha, S. Y. Hwang, D. S. Lee, A. R. Kumar, Y. U. Kwon, M. Voß, E. Schuiten, U. T. Bornscheuer, F. Hollmann, D. K. Oh, *Angew. Chem.* **2020**, *132*, 7090-7094.
- [217] W. Zhang, J.-H. Lee, S. H. Younes, F. Tonin, P.-L. Hagedoorn, H. Pichler, Y. Baeg, J.-B. Park, R. Kourist, F. Hollmann, *Nat. Commun.* **2020**, *11*, 1-8.
- [218] R. Ge, P. Zhang, X. Dong, Y. Li, Z. Sun, Y. Zeng, B. Chen, W. Zhang, *ChemSusChem* **2022**, *15*, e2022012.

Chapter 1

- [219] Q. Wu, D. Li, T. Han, J. Xue, W. Xu, J. Xu, *Angew. Chem.* **2021**, *133*, 20863-20867.
- [220] Y. Y. Zeng, L. Liu, B. S. Chen, W. Zhang, *ChemistryOpen* **2021**, *10*, 553.
- [221] F. Cheng, H. Li, D.-Y. Wu, J.-M. Li, Y. Fan, Y.-P. Xue, Y.-G. Zheng, *Green Chem.* **2020**, *22*, 6815-6818.
- [222] W. Zhang, M. Ma, M. M. Huijbers, G. A. Filonenko, E. A. Pidko, M. van Schie, S. de Boer, B. O. Burek, J. Z. Bloh, W. J. van Berkel, *J. Am. Chem. Soc.* **2019**, *141*, 3116-3120.
- [223] J. Xu, J. Fan, Y. Lou, W. Xu, Z. Wang, D. Li, H. Zhou, X. Lin, Q. Wu, *Nat. Commun.* **2021**, *12*, 1-10.
- [224] M. Amer, E. Z. Wojcik, C. Sun, R. Hoeven, J. M. Hughes, M. Faulkner, I. S. Yunus, S. Tait, L. O. Johannissen, S. J. Hardman, *Energy Environ. Sci.* **2020**, *13*, 1818-1831.
- [225] P. Santner, L. K. Szabó, S. N. Chanquia, A. H. Merrild, F. Hollmann, S. Kara, B. E. Eser, *ChemCatChem* **2021**, *13*, 4038-4046.
- [226] V. A. Aleksenko, D. Anand, A. Remeeva, V. V. Nazarenko, V. Gordeliy, K.-E. Jaeger, U. Krauss, I. Gushchin, *Catalysts* **2020**, *10*, 1072.
- [227] D. J. Heyes, B. Lakavath, S. J. Hardman, M. Sakuma, T. M. Hedison, N. S. Scrutton, *ACS Catal.* **2020**, *10*, 6691-6696.
- [228] D. Sorigué, K. Hadjidemetriou, S. Blangy, G. Gotthard, A. Bonvalet, N. Coquelle, P. Samire, A. Aleksandrov, L. Antonucci, A. Benachir, *Science* **2021**, *372*, eabd5687.
- [229] T. M. Hedison, D. J. Heyes, N. S. Scrutton, *Curr Opin Chem Biol.* **2022**, *2*, 100017.
- [230] B. Lakavath, T. M. Hedison, D. J. Heyes, M. Shanmugam, M. Sakuma, R. Hoeven, V. Tilakaratna, N. S. Scrutton, *Anal. Biochem.* **2020**, *600*, 113749.
- [231] Y. Wu, C. E. Paul, F. Hollmann, *ChemBioChem* **2021**, *22*, 2420-2423.

Chapter 2: Peroxygenase-promoted enzymatic cascades for the valorisation of fatty acids

Yinqi Wu, Caroline E. Paul, Thomas Hilberath, Ewald P.J. Jongkind, Wuyuan Zhang, Miguel Alcalde, and Frank Hollmann

Based on *ChemCatChem*. 2023, e202300411.

Summary

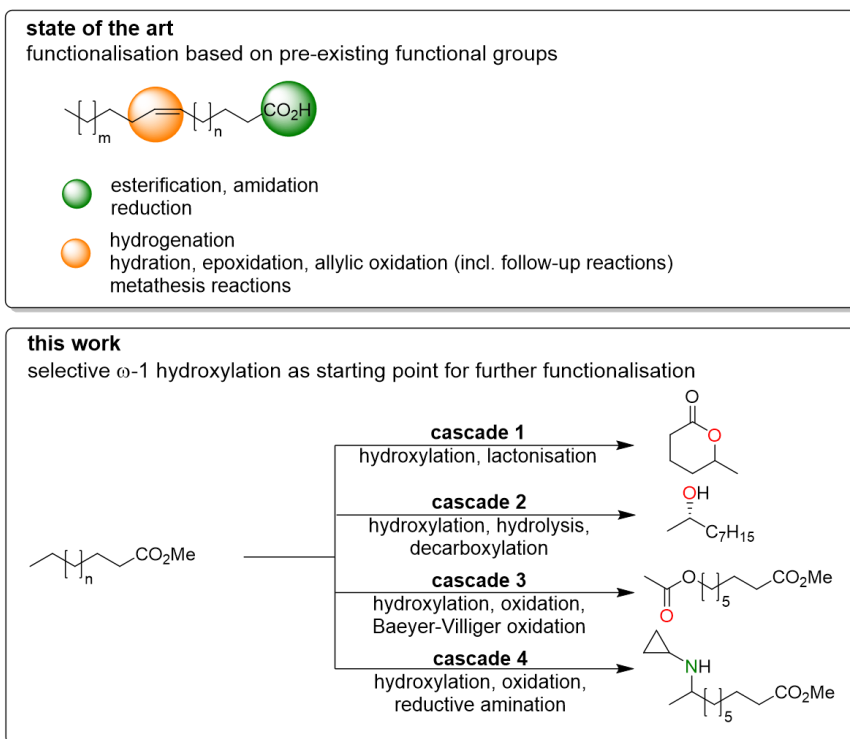
Utilisation of fatty acids generally relies on pre-existing functional groups such as the carboxylate group or C=C-double bonds. Addition of new functionalities into the hydrocarbon part opens up new possibilities for fatty acid valorisation. In this contribution, we demonstrate the synthetic potential of a peroxygenase mutant *AaeUPO-Fett* for selective fatty acid oxyfunctionalisation. The ω -1 hydroxy fatty acid (esters) produced are further transformed into lactones, alcohols, esters and amines via multi-enzyme cascades thereby paving the way for new fatty acid valorization pathways.

1. Introduction

En route to a circular economy, renewable feedstock is increasingly recognised as starting materials for the synthesis of intermediates and consumer products.^[1] Fatty acids as well as their glycerides are already now used for the synthesis of a range of products such as polymer building blocks, paints, coatings, surfactants and lubricants.^[2-5]

Biocatalytic transformations of the carboxylate group are very well established enabling (trans)esterification, amidation and reduction reactions (Scheme 2.1).^[6-9] The conversion of unsaturated, i.e. functionalised fatty acids is also straightforward comprising epoxidation^[3] and hydration^[10] of the C=C-double bond or allylic hydroperoxidation.^[11]

Less well-established are biocatalytic transformations of saturated, non-activated fatty acids. Obviously, this can be attributed to the challenging character of C-H activation chemistry.^[4] Nevertheless, adding functional groups to the alkane part of fatty acids would broaden their potential as starting material for bio-based chemistry. Recently, P450 enzymes exhibiting α -^[12] β -^[13] δ -^[14] or ω -selectivity^[15] have been reported.^[16] Also, fungal peroxygenases^[17] are capable of hydroxylating non-activated C-H-bonds in fatty acids. While peroxygenase-catalysed hydroxylations benefit from the intrinsically much simpler reaction mechanism compared to P450 monooxygenases, their practical usefulness is hampered by their generally low selectivity towards fatty acids.^[18-21]



Scheme 2.1. Established fatty acid valorisation approaches utilise existing functionalities such as the carboxylate group or pre-existing C=C-double bonds. In this contribution, we add functionality via selective, peroxygenase-catalysed hydroxylation enabling further transformations.

Very recently, we reported a protein engineering study on the prototype evolved peroxygenase from *Agroclybe aegerita* (*AaeUPO-PaDa-I*)^[22-24] to increase the regioselectivity of fatty acid hydroxylation.^[25] Due to a dramatically narrowed substrate access channel, the new mutant (referred to as *AaeUPO-Fett*) enabled higher regioselectivity (almost exclusively located at ω -1) as compared with its parent *AaeUPO-PaDa-I* mutant. Therefore, we reasoned that *AaeUPO-Fett* may be a useful biocatalyst for the valorisation of fatty acid (methyl esters) (FA(ME)s) into value-added chemical building blocks, such as esters, lactones, alcohols and amines.

2. Results and Discussion

In the first set of experiments, we systematically investigated the substrate scope of *AaeUPO-Fett* in comparison with its parent *AaeUPO-PaDa-I* (Figure 2.1). Both *AaeUPO* variants exhibited a more relaxed chain length spectrum when converting

Chapter 2

FAMES as compared to free FA. While in the last case, the C₁₄ fatty acid (myristic acid) was the best converted substrate, both variants oxidised a much broader range of FAMES ranging from C₅ to C₁₄.

As expected, *AaeUPO-Fett*-catalysed FA- or FAME-hydroxylations occurred with much higher regioselectivity when compared with the same reactions mediated by *AaeUPO-PaDa-I*. With the latter, the regioselectivity for ω -1 was generally lower than 60%, while for *AaeUPO-Fett* the ω -1 product was formed at least at 92% selectivity.

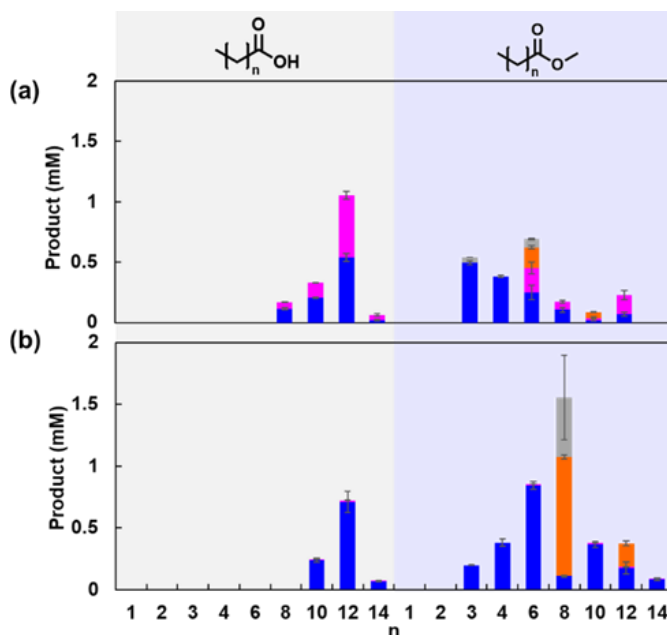


Figure 2.1. Comparison of fatty acid (ester) hydroxylations catalysed by *AaeUPO-PaDa-I* (a) and *AaeUPO-Fett* (b) by using different substrates. ω -1 hydroxylation products (■); ω -2 hydroxylation products (■); ω -1 ketone products (■); unknown products to be determined (■). Reaction conditions: [*AaeUPO*] = 1 μ M (for both *PaDa-I* and *Fett*), [substrate] = 5 mM, [MeCN] = 10% (v/v), [H_2O_2] = 2 mM \times h⁻¹, 50 mM KPi (pH 7.0), 600 rpm, 25 °C, reaction time = 4 h. Values represent the average of duplicates (n = 2). Error bars indicate the standard deviation.

Having a highly regioselective hydroxylation catalyst at hand, we further investigated the synthetic possibilities with *AaeUPO-Fett*. Selective ω -1 hydroxylation of medium-chain FAMES such as methyl hexanoate (**1a**) should yield a chiral, lactonisable product potentially useful as polymer building block or flavour and fragrance ingredient. The hydroxylation of **1a** itself went smoothly to approx. 90% conversion within the first 6 h and neither the undesired ω -2 hydroxylation product nor any overoxidation product (methyl 5-ketohexanoate) were observed (Figure 2.2). To our

surprise, the envisaged lactone was formed only in traces during the reaction. It could, however, be obtained quantitatively by subsequent acid treatment of the primary hydroxy ester in 77% ee (Figure S2.10).

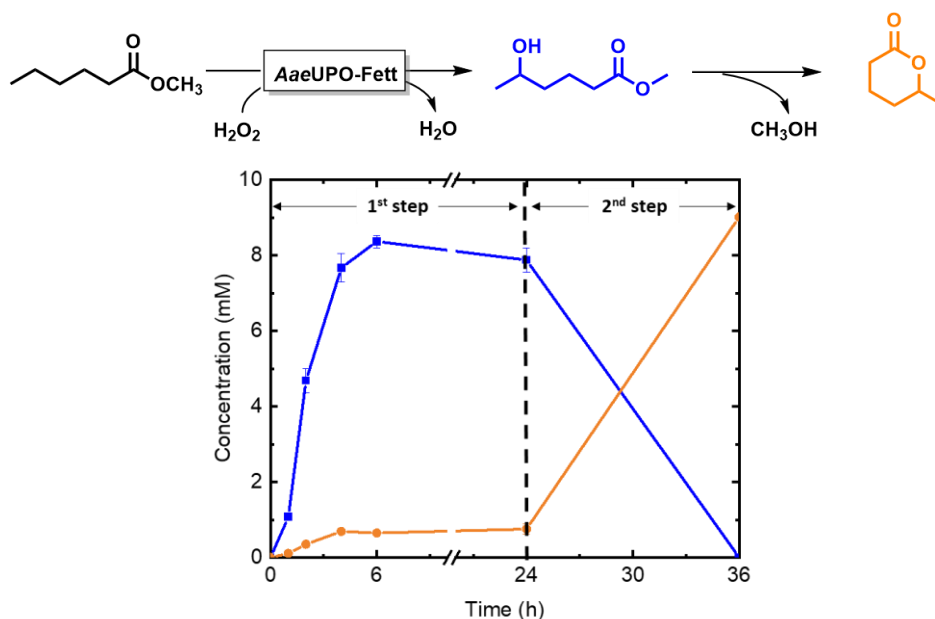
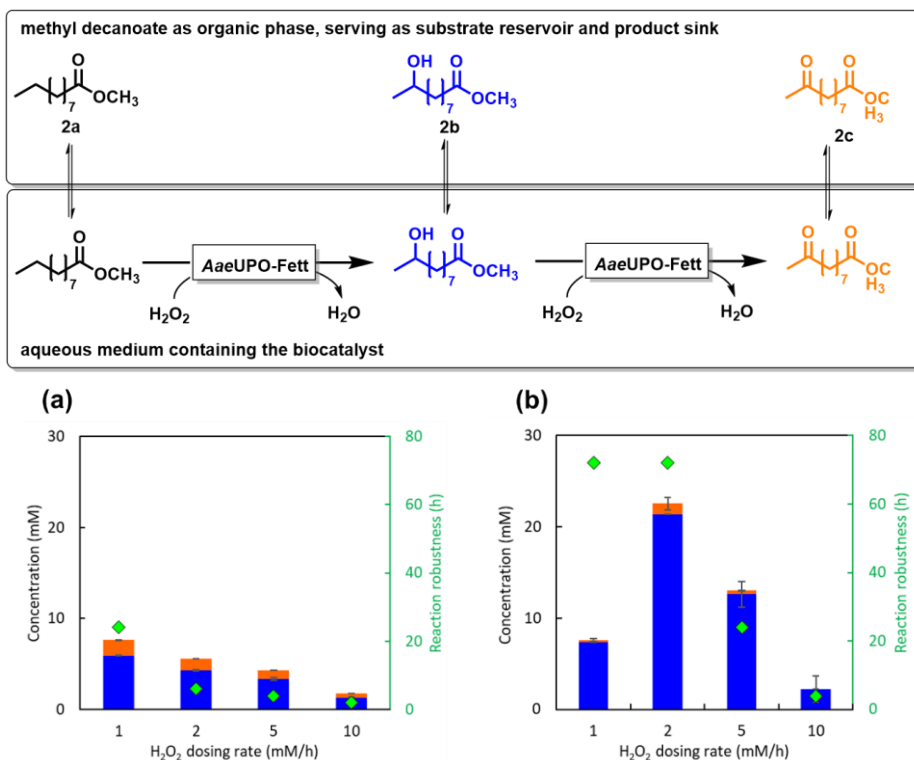


Figure 2.2. Hydroxylation reaction of methyl hexanoate catalysed by *AaeUPO-Fett* for the production of methyl 5-hydroxyhexanoate (■) and δ -hexalactone (●). Reaction conditions: First step: [*AaeUPO-Fett*] = 2.5 μ M, [methyl hexanoate] = 10 mM, [MeCN] = 10% (v/v), [H_2O_2] = 5 $\text{mM}\cdot\text{h}^{-1}$, 50 mM KPi (pH 7.0), 600 rpm, 25 $^\circ\text{C}$, 10 mL scale; second step: CH_2Cl_2 (5 $\text{mL}\cdot\text{g}^{-1}$ lactone), trifluoroacetic acid (0.04 $\text{mL}\cdot\text{g}^{-1}$ lactone), 300 rpm, 25 $^\circ\text{C}$. Values represent the average of duplicates ($n = 2$). Error bars indicate the standard deviation.

Next, we investigated the *AaeUPO-Fett*-catalysed hydroxylation longer-chain FAMES such as methyl decanoate (**2a**). Particularly, we were interested in the effect of different H_2O_2 addition rates on the robustness of the hydroxylation reaction (Figure 2.3). Under monophasic reaction conditions (i.e. the starting material being completely dissolved in the aqueous reaction medium) the robustness decreased with increasing feeding H_2O_2 rates with product accumulation ceasing after 2 to 24 h, depending on the H_2O_2 feed rate (Figure 2.3a). Furthermore, a pronounced overoxidation of the primary product to the corresponding ketone (**2c**) was observed accounting for up to 23% of the overall product. We reasoned that a two-liquid phase system (2LPS)^[26] with **2a** as water-insoluble organic phase serving as substrate reservoir and product sink (particularly for the desired **2b**) may circumvent these overoxidation issues and repeated the experiments in the presence of 20% (v/v) of

Chapter 2

2a (forming a second phase). Indeed, under 2LPS conditions the overoxidation was suppressed to less than 5% of the overall product formed (Figure 2.3b). Surprisingly, the reaction robustness was also increased significantly in the presence of **2a** as an organic phase. For example, dosing H_2O_2 at $2 \text{ mM}_{\text{final}} \times \text{h}^{-1}$ the product formation time increased from 6 h (under monophasic conditions) to 72 h in the 2LPS approach. As a result, the product concentration increased from 4.3 mM to more than 21 mM. 29 mg of **2b** were isolated from a 10-mL reaction with 79% isolation yield in more than 94% purity (Figure S2.3). *AaeUPO-Fett* performed respectable 22540 catalytic turnovers.



While hydroxy-FAMEs may be an interesting starting material for polyester synthesis we sought after further possible applications applying *Aae*UPO-Fett in different enzyme cascades.

Decarboxylation of the free hydroxy acids results in the corresponding (C₁-shortened) 2-alkanols. We tested a cascade with methyl decanoate (**2a**) combined with a lipase-catalysed hydrolysis and photoenzymatic decarboxylation (Figure 2.4). Particularly, the well-known lipase B from *Candida antarctica* (CalB)^[27] as well as the fatty acid photodecarboxylase from *Chlorella variabilis* (CvFAP) were used.^[28] To avoid undesired hydrolysis and photodecarboxylation of the starting material, the hydroxylation step was performed prior to the combined hydrolysis/photodecarboxylation. Pleasingly, the desired (*S*)-2-nonanol (**3**, 80% ee) as sole product was achieved.

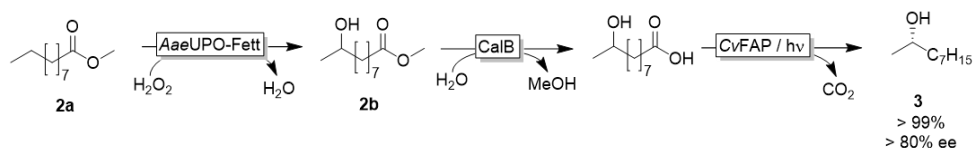


Figure 2.4. Multi-enzymatic cascade to convert methyl decanoate into (*S*)-2-nonanol. Reaction conditions: for the first step, [*Aae*UPO-Fett] = 1 μM , substrate/buffer = 1:4 (v/v), 50 mM KPi (pH 7.0), H₂O₂ dosing rate = 2 mM \times h⁻¹, 600 rpm, 25 $^{\circ}\text{C}$, 10 mL scale, 72 h. For the second and third steps, [methyl 9-hydroxydecanoate] = 5 mM, [CalB] = 25 U \times mL⁻¹, [MeOH] = 10 % (v/v), 100 mM Tris-HCl (pH 9.0), 25 $^{\circ}\text{C}$, 1 mL scale, overnight; then added [CvFAP] = 6 μM and switched on blue light (λ_{max} = 450 nm), light intensity of blue light = 14.5 $\mu\text{E}\times\text{L}^{-1}\times\text{s}^{-1}$.

Converting the peroxxygenase-introduced hydroxyl group itself also offers further possibilities for manipulation if further oxidised to the keto group. For example, reductive amination or Baeyer-Villiger oxidations come into reach in case a keto-group is present in the substrate. For this approach, we opted for an alcohol dehydrogenase-catalysed alternative (*vide infra*). We evaluated the alcohol dehydrogenase from *Shingobium yanoikuyae* (SyADH) for the oxidation of **2b** into the corresponding ketone (**2c**). SyADH was chosen because of its known low enantioselectivity and broad substrate scope.^[29-30] Indeed, already a preliminary test with SyADH gave near-full conversion of **2c** (Figure S2.16).

Next, we tested a cascade comprising *Aae*UPO-Fett, SyADH and the Baeyer-Villiger monooxygenase from *Aspergillus flavus* (BVMOAf1838)^[31-33] to convert FAMEs into the corresponding ω -hydroxy FAME acetate ester (**2d**) (Figure 2.5). The GCMS spectrum of the ester product showed a signal at $m/z=43$ characteristic of acetyl

Chapter 2

esters (Figure S2.15) indicating a preference for the “normal” migration product.^[31-33] As the ADH- and BVMO-catalysed oxidation steps were cofactor complementary, no additional cofactor regeneration system was necessary.

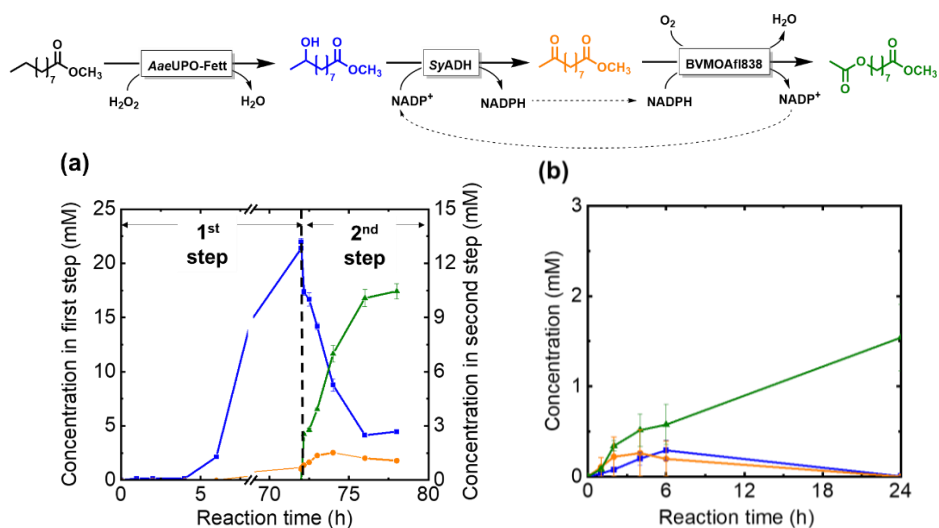


Figure 2.5. Proposed enzymatic cascade reaction to convert methyl decanoate into methyl 8-(acetyloxy)octanoate (▲), with the intermediate methyl 9-hydroxydecanoate (■) and methyl 9-oxo-decanoate (●) catalysed by the combination of AaeUPO-Fett, SyADH and BVMOAf1838. Representative time course of the (a) two-pot-two-step and (b) one-pot-one-step cascade reaction. Reaction conditions: (a) 0 h - 72 h, [AaeUPO-Fett] = 1 μM, methyl decanoate/buffer = 1:4 (v/v), 50 mM KPi buffer (pH 7.0), [H₂O₂] = 2 mM×h⁻¹, 1000 rpm, 25 °C, 1 mL scale. 72 h - 78 h: diluted organic phase from first step/ buffer = 1:4 (v/v), 100 mM Tris-HCl (pH 8.0), [SyADH cells] = 1 mg×mL⁻¹, [BVMOAf1838]=0.5 μM, [NADP⁺] = 1 mM, 1000 rpm, 25 °C, 1 mL scale. (b) [AaeUPO-Fett] = 1 μM, [SyADH cells] = 5 mg×mL⁻¹, [BVMOAf1838] = 0.5 μM, [NADP⁺] = 1 mM, methyl decanoate/ buffer= 1:4 (v/v), 100 mM Tris buffer (pH 8.0), [H₂O₂] = 2 mM×h⁻¹, 1000 rpm, 25 °C, 1 mL scale. For two-pot-two-step reaction, in the first step (0 h - 72 h), [AaeUPO-Fett] = 1 μM, methyl decanoate/50 mM KPi buffer (pH 7.0) = 1:4 (vol/vol), [H₂O₂] = 2 mM×h⁻¹, 1000 rpm, 25 °C, 1 mL scale. Values represent the average of duplicates (n = 2). Error bars indicate the standard deviation.

We then conducted the cascade as a two-pot-two-step reaction (Figure 2.5a) first performing the AaeUPO-Fett-catalysed hydroxylation for 72 h resulting in approx. 20 mM of the expected product **2b**. Afterwards, the organic phase was transferred to another aqueous reaction mixture comprising SyADH and BVMOAf1838. The conversion of **2b** into the final product (**2d**) was near complete after 5-6 h (>90% of **2d** based on the initially applied **2b**). Nevertheless, the conversion was not complete, which may be due to the unproductive decoupling reaction (i.e. direct, aerobic oxidation of NADPH)^[34] resulting in a NADP⁺ regeneration system and causing the

accumulation of 1.1 mM of the intermediate ketone. Interestingly, this uncoupling appeared to be less problematic when performing the reaction in a one-pot-one-step fashion (Figure 2.5b) as the intermediate products did not accumulate significantly. Finally, we pursued reductive amination of the intermediate ketone (**2c**) by replacing BVMOAf1838 with the reductive aminase from *Aspergillus oryzae* (*AspRedAm*), which accepts cyclopropylamine as amine donor.^[35] Thus, we obtained a moderate amount of the desired methyl 9-cyclopropylaminodecanoate (**2e**) (Figure 2.6).

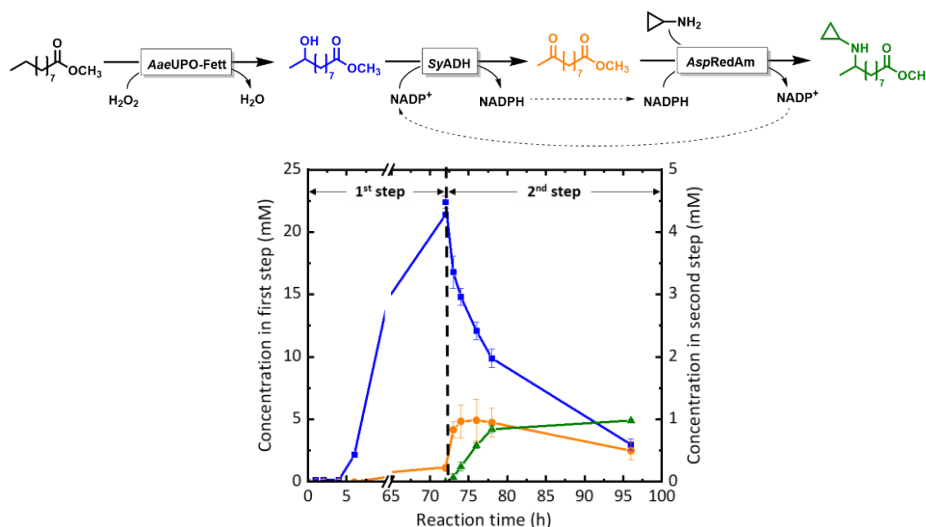


Figure 2.6. Proposed enzymatic cascade reaction to convert methyl decanoate into methyl 9-cyclopropylaminodecanoate (\blacktriangle), with the intermediate methyl 9-hydroxydecanoate (\blacksquare) and methyl 9-oxo-decanoate (\bullet) catalysed by *AaeUPO-Fett*, *SyADH* and *AspRedAm*. Reaction conditions: for the first step (0 - 72 h), [*AaeUPO-Fett*] = 1 μ M, methyl decanoate/ buffer= 1:4 (v/v), 50 mM KPi buffer (pH 7.0), [H_2O_2] = 2 mM \times h $^{-1}$, 1000 rpm, 25 $^\circ$ C, 1 mL scale. For the second step (72 h - 96 h), [methyl 9-hydroxydecanoate] = 5 mM, [*SyADH* cells] = 0.5 mg \times mL $^{-1}$, [*AspRedAm* purified enzyme] = 0.8 mg \times mL $^{-1}$, [DMSO] = 2 % (v/v), [NADP^+] = 1 mM, [cyclopropylamine] = 40 mM, 100 mM Tris-HCl (pH 9.0), 300 rpm, 25 $^\circ$ C, 1 mL scale. Values represent the average of duplicates (n = 2). Error bars indicate the standard deviation.

Interestingly, while the starting material for the second reaction (methyl 9-hydroxydecanoate) was continuously consumed, the final product did not accumulate to more than approx. 1 mM. Comparative experiments, however, demonstrated that the final product itself was not stable under the reaction conditions (Figure S2.20). Currently, we are lacking a fully plausible explanation for this observation. Possibly, polycondensation of the amino ester product to non-extractable oligomers may account for this.

3. Conclusion

In conclusion, with this contribution we have extended the synthetic potential of non-functionalised fatty acids as starting materials for value-added products and building blocks. Peroxygenases, especially if engineered for regioselectivity such as *AaeUPO-Fett*, are promising catalysts to add functionality to the alkyl chain. The primary products (i.e. hydroxy fatty acids) are interesting building blocks for lactone synthesis and for polyesters. If oxidised to the corresponding keto acids, further synthetic possibilities arise as demonstrated by the Baeyer-Villiger oxidation and the reductive amination reactions here.

4. Material and methods

4.1 Chemicals and materials

Ethylbenzene, alkanes, alkenes, 1-alcohols, 2-alcohols, fatty acids (FAs), fatty acid methyl esters (FAMES), monobasic dihydrogen phosphate (KH_2PO_4), dibasic monohydrogen phosphate (K_2HPO_4), hydrogen peroxide (H_2O_2), acetonitrile (MeCN), dimethyl sulfoxide (DMSO), methanol (MeOH), ethyl acetate, dichloromethane (CH_2Cl_2), trifluoroacetic acid (TFA), sodium bicarbonate (NaHCO_3), deuterated chloroform (CDCl_3), β -nicotinamide adenine dinucleotide phosphate (NADP^+) and its reduced form NADPH, acetone, Tris(hydroxymethyl)aminomethane (Tris), hydrogen chloride (HCl), cyclopropylamine, cyclohexanone, sodium dithionite, sodium dithionite ($\text{Na}_2\text{S}_2\text{SO}_4$), N,O-bis(trimethylsilyl)trifluoroacetamide (BSTFA), magnesium sulfate (MgSO_4), *Candida antarctica* lipase B, BVMOAfl838 purified enzyme and other commercial chemicals were purchased from Sigma-Aldrich, Fluka, Acros, Alfa-Aesar, or GECCO Biotech without any further purification. The water used was deionised.

4.2 Gene expression and protein purification

The genes encoding *AaeUPO-PaDa-I* and its mutant *AaeUPO-Fett* were heterologously expressed in *Pichia pastoris* and isolated following a previously described procedure.^[23] The concentrated supernatant of proteins were used in the experiments later.

E. coli C43 (DE3) cells expressing pET24b-*syadh* were cultivated in TB medium containing 50 $\mu\text{g mL}^{-1}$ kanamycin at 37 °C and 180 rpm until the optical density at 600 nm (OD_{600}) reached around 1.0. Gene expression was induced by adding 0.5 mM IPTG, the cultivation temperature was decreased to 20 °C and shaking frequency was reduced to 140 rpm. After cultivation for at least 20 h, cells were harvested by centrifugation (11000 $\times g$ at 4 °C for 10 min) and washed with buffer (50 mM KPi, pH 7.0). Cells stored in crystallization bowls at -80 °C were then lyophilised at 0.1 mbar and -28 °C, transferred to a 50 mL falcon tube and stored at -20 °C.^[36] If not stated otherwise, SyADH was used in the form of lyophilised *E. coli* cells.

E. coli BL21(DE3) cells expressing pET28a-*aspredam* were cultivated in 2 \times YT broth medium containing 30 $\mu\text{g mL}^{-1}$ kanamycin at 37 °C and 180 rpm until the optical density at 600 nm (OD_{600}) reached 0.6-0.8. Gene expression was induced by adding 0.5 mM IPTG and cultivation temperature was decreased to 20 °C. After cultivation for about 18 h, cells were harvested by centrifugation (11000 $\times g$ at 4 °C for 10 min) and washed twice with ice-cooled buffer A (100 mM Tris-HCl, 300 mM NaCl, 30 mM imidazole, pH 8.0). The cell pellet was resuspended in the same buffer and then cells were lysed by passing them through a Multi Shot Cell Disruption System at 1.5 kbar for 2 cycles. The crude cell lysate was obtained after centrifugation at 38000 $\times g$ at 4 °C for 40 min and then passed through a 0.45 μm filter. Purification was performed at 16 °C on a His Trap Ni-NTA FF column (5 mL, GE Healthcare) by a Biorad NGC system. After loading the lysate (20-120 mL), the column was washed with buffer A, and the target protein was eluted by a step gradient using 10-60% v/v buffer B (100 mM Tris-HCl, 300 mM NaCl, 300 mM imidazole, pH 8.0). The protein identity was visualised by SDS-PAGE and suitable fractions combined and concentrated by ultrafiltration (Amicon Ultra Centrifugal Filter 30 kDa cut-off). The concentrated purified protein was loaded on a 6 mL PD-10 desalting column (6 mL, PD-10) to remove the imidazole used during IMAC (immobilised affinity chromatography). The target protein was eluted by buffer C (100 mM Tris-HCl, 500 mM NaCl, pH 8.0), and the protein fractions were then collected and concentrated by ultrafiltration (30 kDa cut-off).^[35] The purified proteins were then frozen with liquid nitrogen and stored at -80 °C for later experiments.

Chapter 2

4.3 Enzyme concentrations

The extinction coefficient of ferrous carbon monoxide binding difference spectra (CO difference spectra) was utilised to determine the amount of correctly folded AaeUPO in the crude enzyme solution. 1 mL sample contained the UPO in an appropriate dilution, 50 mM Na₂S₂O₄ and buffer (20 mM Tris-HCl, pH 7.0). Before exposing the mixture to CO, a UV-Vis spectrum between 400 nm and 500 nm was recorded as baseline. After saturating the enzyme system with CO (bubbling for approx. 1 min), the spectrum between 400 nm and 500 nm was recorded again. The millimolar extinction coefficient at 445 nm $\epsilon = 107 \text{ mM}^{-1} \text{ cm}^{-1}$ was used to calculate the concentration of AaeUPO.^[37]

$$\text{AaeUPO conc. } (\mu\text{M}) = \frac{\Delta A_{445} - A_{490}}{\epsilon} \times \text{dilution time} \times 1000$$

The enzyme concentration of AspRedAm and CvFAP was determined by the BCA assay according to the conditions of the kit manufacturer (Uptima). Enzyme purity was assessed via SDS-PAGE analysis.

4.4 General procedure for substrate scope comparison

The 0.5 mL reaction was composed of 5 mM substrate, 10% v/v MeCN as co-solvent, 1 μM crude AaeUPO, 2 mM h⁻¹ H₂O₂ (2 mM H₂O₂ was added to the reaction system per hour manually), and buffer (50 mM KPi, pH 7.0), and was under 600 rpm shaking speed (Eppendorf ThermoMixer C) at 25 °C for 4 h in 2-mL clean Eppendorf tube. At the end of the reaction, samples were withdrawn and extracted with ethyl acetate (containing 5 mM 1-octanol as internal standard). The organic layer was dried over MgSO₄ for gas chromatography analysis. In order to estimate the concentration of different products, the following formula was used using 5 mM 1-octanol as internal standard.

$$\text{estimated product conc. (mM)} = \frac{\text{peak area of product}}{\text{peak area of internal standard}} \times \text{internal standard conc. (mM)}$$

4.5 Methyl hexanoate hydroxylation catalysed by AaeUPO-Fett

Mono-phasic system:

The 1-10 mL reaction was composed of 10 mM methyl hexanoate as substrate, 10% v/v MeCN as co-solvent, 1-10 μM AaeUPO-Fett mutant, 5 mM h⁻¹ H₂O₂ (continuously added with syringe pump), and buffer (50 mM KPi, pH 7.0), and was under 600 rpm

shaking speed at 25 °C for 24 h. Samples were withdrawn and extracted with ethyl acetate (containing 5 mM cyclooctane as internal standard). The organic layer was dried over MgSO₄ for gas chromatography analysis.

Bi-phasic system:

The 1 mL reaction was composed of buffer/methyl hexanoate (containing 5 mM cyclooctane)=4:1 (v/v), 1-10 μM *AaeUPO-Fett*, 5 mM h⁻¹ H₂O₂ (continuously added with syringe pump) and buffer (50 mM KPi, pH 7.0), and was under 1000 rpm shaking speed at 25 °C for 72 h. Samples from organic layer were withdrawn and diluted with ethyl acetate. It was then dried over MgSO₄ for gas chromatography analysis.

4.6 Synthesis of δ-hexalactone from methyl 5-hydroxyhexanoate

The reaction mixture from 10-mL mono-phasic system was extracted with ethyl acetate. The organic layer was dried over MgSO₄ and then evaporated under N₂ flow. After removing the solvent, liquid (57 mg) was dissolved in CH₂Cl₂ (5 mL g⁻¹ lactone) and TFA (0.04 mL g⁻¹ lactone). The lactonization reaction was performed at 300 rpm shaking speed at 25 °C for 12 h. Afterwards, the reaction was diluted with ethyl acetate and worked up with 100 mM NaHCO₃ solution. The organic layer was washed with water and dried with MgSO₄. After evaporation of the solvent, the residual fraction containing δ-hexalactone was resuspended in CDCl₃ and analysed by ¹H NMR (400 MHz) and ¹³C NMR (101 MHz). NMR spectra were recorded on an Agilent 400 spectrometer.

4.7 Methyl decanoate hydroxylation catalysed by *AaeUPO-Fett*

Mono-phasic system:

The 1-10 mL reaction mixture was composed of 10 mM methyl hexanoate as substrate, 10% v/v MeCN as co-solvent, 1 μM *AaeUPO-Fett*, 1-10 mM h⁻¹ H₂O₂ (continuously added with syringe pump) and buffer (50 mM KPi, pH 7.0), and was under 600 rpm shaking speed at 25 °C for 24 h. Samples were withdrawn and extracted with ethyl acetate (containing 5 mM cyclooctane as internal standard). The organic layer was dried over MgSO₄ and used for gas chromatography analysis.

Bi-phasic system:

The 1-10 mL reaction mixture was composed of buffer/methyl decanoate (containing 5 mM cyclooctane)=4:1 (v/v), 1 μM *AaeUPO-Fett*, 1-10 mM h⁻¹ H₂O₂ (continuously

Chapter 2

added with syringe pump) and buffer (50 mM KPi, pH 7.0), and was under 1000 rpm shaking speed at 25 °C for 72 h. Samples from the organic layer were withdrawn and diluted with ethyl acetate. After drying over MgSO₄, samples were analysed by gas chromatography.

4.8 Synthesis of 2-nonanol starting from methyl decanoate (cascade 2)

For the first step reaction (bi-phasic system):

The 1 mL reaction was composed of buffer/methyl decanoate (containing 5 mM cyclooctane as internal standard)=4:1 (v/v), 1 μM AaeUPO-Fett, 2 mM h⁻¹ H₂O₂ (continuously added with syringe pump) and buffer (50 mM KPi, pH 7.0), and was under 1000 rpm shaking speed at 25 °C for 72 h. Samples from the organic layer were withdrawn and diluted with ethyl acetate, then dried over MgSO₄ for gas chromatography analysis.

For second step reaction (mono-phasic system):

The 1 mL reaction was composed of 5 mM methyl 9-hydroxydecanoate synthesised from the first step, 10% v/v MeOH, 100 mM Tris-HCl (pH 9.0), 25 U mL⁻¹ CalB, 25 °C. Overnight, 6 μM CvFAP was added to the system and blue light ($\lambda_{\text{max}}=450$ nm) was switched on with light intensity of 14.5 μE L⁻¹ s⁻¹. Samples were withdrawn and extracted with ethyl acetate (containing 5 mM cyclooctane as internal standard). The organic layer was dried over MgSO₄ for gas chromatography analysis.

4.9 Light intensity measurement

The light intensity was determined by means of ferrioxalate actinometry. 0.5-1 mL ferrioxalate solution (37.5 mM in 50 mM H₂SO₄) in 4-mL transparent glass vial was illuminated under LED light. At defined intervals, 25 μL samples of the illuminated solution were taken and mixed with 175 μL of reactant solution (7.5 mL 50 mM H₂SO₄, 2 mL 0.1% 1,10-phenanthroline, 5 mL 1 M sodium acetate solution and 3 mL H₂O). The absorbance of the mixture was measured under 510 nm at room temperature. FeSO₄ was used as Fe(II) for the calibration curve. The light intensity was then calculated based on the Fe(II) generation rate in the irradiated ferrioxalate solution.

4.10 Synthesis of methyl 8-(acetyloxy)octanoate starting from methyl decanoate (cascade 3)

For one-pot one-step reaction:

The 1 mL reaction was composed of 1 μM AaeUPO-Fett, 5 mg mL^{-1} SyADH cells, 0.5 μM purified BVMOAfl838, 1 mM NADP^+ , buffer/methyl decanoate (containing 5 mM cyclooctane as internal standard)=4:1 (v/v), 2 mM h^{-1} H_2O_2 (continuously added with syringe pump) and buffer (100 mM Tris-HCl buffer, pH 8.0), and under 1000 rpm shaking speed at 25 °C for 24 h. Samples from the organic layer were withdrawn and diluted with ethyl acetate, then dried over MgSO_4 for gas chromatography analysis.

For two-pot two-step reaction:

The 1 mL reaction was composed of buffer/methyl decanoate (containing 5 mM cyclooctane as internal standard)=4:1 (v/v), 1 μM AaeUPO-Fett, 2 mM h^{-1} H_2O_2 (continuously with syringe pump) and buffer (50 mM KPi, pH 7.0), and was under 1000 rpm shaking speed at 25 °C for 72 h as first step. For the second step, the 1 mL reaction was composed of 1 mg mL^{-1} SyADH cells, 0.5 μM purified BVMOAfl838, 1 mM NADP^+ , diluted organic phase from first step/100 mM Tris-HCl (pH 8.0) = 1:4 (v/v) and under 1000 rpm shaking speed at 25 °C for another 6 h. (The organic phase here was diluted with methyl decanoate containing 5 mM cyclooctane as internal standard.) Samples from the organic layer were withdrawn and diluted with ethyl acetate, then dried over MgSO_4 for gas chromatography analysis.

4.11 Synthesis of methyl 9-cyclopropylaminodecanoate starting from methyl decanoate (cascade 4)

For the first step reaction (bi-phase):

The 1 mL reaction was composed of buffer/methyl decanoate (containing 5 mM cyclooctane as internal standard)=4:1 (v/v), 1 μM AaeUPO-Fett, 2 mM h^{-1} H_2O_2 (continuously added with syringe pump) and buffer (50 mM KPi, pH 7.0), and was under 1000 rpm shaking speed at 25 °C for 72 h as first step.

For the second step reaction (bi-phase):

The 0.5 mL reaction was composed of buffer/methyl decanoate (containing 5 mM cyclooctane as internal standard)=4:1 (v/v), 0.5-1 mg mL^{-1} SyADH cells, 320 μL AspRedAm lysate, 5-40 mM cyclopropylamine, 1 mM NADP^+ and buffer (50 mM KPi, pH 7.0), and under 300 rpm shaking speed at 25 °C for 24 h. Samples from the organic layer were withdrawn and diluted with ethyl acetate, then dried over MgSO_4 for gas chromatography analysis.

For second step reaction (mono-phase):

Chapter 2

The 1 mL reaction was composed of 5 mM methyl 9-hydroxydecanoate synthesised from first step as substrate, 2% v/v DMSO as co-solvent, 0.5 mg mL⁻¹ SyADH cells, 0.8 mg mL⁻¹ AspRedAm purified enzyme, 40 mM cyclopropylamine, 1 mM NADP⁺, 100 mM Tris-HCl (pH 9.0) and under 300 rpm shaking speed at 25 °C for 24 h. Samples were withdrawn and extracted with ethyl acetate (containing 5 mM cyclooctane as internal standard). The organic layer was dried over MgSO₄ for gas chromatography analysis.

4.12 Analysis using GS and GC-MS

All products obtained from ethyl benzene, alkanes, alkenes, alcohols, FAs and FAMES reactions were analysed by gas chromatography (model: SHIMADZU GC-2014) equipped with a flame ionization detector and a CP-Sil-5 column: (50 m × 0.53 mm × 1 μm). Nitrogen was used as carrier gas with a flow rate of 20 mL/min.

Different enantiomers of δ-hexalactone were separated by gas chromatography (model: SHIMADZU GC-2014) equipped with a flame ionization detector and a column HYDRODEX β-TBDAC (50 m × 0.25 mm × 0.25 μm). Helium was used as carrier gas with a flow rate of 30 mL/min.

Enantiomers of silylated 2-nonanol were separated by gas chromatography (model: SHIMADZU GC-2014) equipped with a flame ionization detector and a column HYDRODEX β-TBDAC (50 m × 0.25 mm × 0.25 μm). Helium was used as carrier gas with a flow rate of 63.5 mL/min.

In order to determine the structure of the hydroxylation product from FAs and FAMES, substrates and products were silylated. The reaction mixture was extracted with ethyl acetate (containing 5 mM 1-octanol as internal standard) dried over MgSO₄, which was then evaporated under N₂ flow. 50 μL of N,O-bis(trimethylsilyl)trifluoroacetamide (BSTFA) containing 1% v/v trimethylchlorosilane was used to dissolve the residual chemical(s) after 1 h incubation at 100 °C, the reaction mixture was cooled down to room temperature and diluted with 150 μL ethyl acetate. The derivatised samples were analysed by GC-MS (model: SHIMADZU GC-2014) equipped with a CP-Sil-5 column: (25 m × 0.25 mm × 0.4 μm). Helium was used as carrier gas with the flow rate of 50 mL/min.

4.13 Supporting Results

4.13.1 Supporting tables

Table S2.1. GC and GC-MS analysis method.

Entry	Column	Temperature profile	Compound and retention time
1	CP-Sil 5 CB (50 m × 0.53 mm × 1.0 μm)	100 °C hold 3 min, 25 °C/min to 155 °C hold 3 min, 25 °C/min to 278 °C hold 10 min, 30 °C/min to 345 °C hold 1 min	Table S2.2 ^a
2	CP-Sil 5 CB (50 m × 0.53 mm × 1.0 μm)	90 °C hold 3 min, 25 °C/min to 160 °C hold 4 min, 25 °C/min to 190 °C hold 2 min, 25 °C/min to 345 °C hold 1 min	methyl hexanoate: 5.97 min cyclooctane (IS): 6.29 min δ-hexalactone: 8.79 min methyl 5-hydroxyhexanoate: 8.84 min
3	HYDRODEX β-TBDAC (50 m × 0.25 mm × 0.25 μm)	90 °C hold 3 min, 10 °C/min to 245 °C hold 1 min	racemic δ-hexalactone: 15.01 min and 15.17 min
4	CP-Sil 5 CB (50 m × 0.53 mm × 1.0 μm)	90 °C hold 3 min, 25 °C/min to 160 °C hold 2 min, 25 °C/min to 190 °C hold 3 min, 25 °C/min to 250 °C hold 3 min, 25 °C/min to 345 °C hold 1 min	cyclooctane (IS): 6.21 min methyl decanoate: 11.74 min methyl 9-oxo-decanoate: 14.51 min methyl 9-hydroxydecanoate: 14.56 min 2-nonanol: 8.37 min 9-hydroxydecanic acid: 14.99 min silylated methyl 9-hydroxydecanoate: 15.62 min methyl 8-(acetyloxy)octanoate: 14.58 min methyl 9-cyclopropylaminodecanoate: 17.43 min
5	CP-Sil 5 CB (50 m × 0.53 mm × 1.0 μm)	110 °C hold 3 min, 25 °C/min to 190 °C hold 2.1 min, 25 °C/min to 230 °C hold 2.1 min,	silylated methyl 8-hydroxydecanoate: 9.62 min silylated methyl 9-hydroxydecanoate: 9.75 min

		30 °C/min to 325 °C hold 1 min	
6	HYDRODEX β-TBDAC (50 m × 0.25 mm × 0.25 μm)	90 °C hold 3 min, 25 °C/min to 250 °C hold 1 min	silylated (<i>R</i>)-2-nonanol: 28.22 min silylated (<i>S</i>)-2-nonanol: 28.79 min

(1) GC method for substrate screening; (2) optimised GC method for methyl hexanoate hydroxylation investigation; (3) chiral GC method for determination of δ-hexalactone two enantiomers; (4) optimised GC method for methyl decanoate hydroxylation and corresponding cascade reactions investigation; (5) GC-MS method for silylated compounds; (6) chiral GC method for determination of silylated 2-nonanol two enantiomers. ^a Retention time of different compounds could be found in Table S2.2.

Table S2.2. Retention time of different compounds for fatty acids (esters) screening^a

	n	Retention time of product (min)		
		P1	P2	P3
Fatty acids	1			
	2			
	3			
	4			
	6			
	8	10,938		
	10	12,104		
	12	13,134		
Fatty esters	14	14,155		
	1			
	2			
	3	6,453	6,693	
	4	7,944		
	6	9,568	9,606	9,836
	8	9,590	10,912	11,064
	10	11,998	12,456	
	12	11,509	13,134	
	14	14,157		

^a Compounds analysed by GC before silylation.

Table S3. Regioselectivity of AaeUPOs^a

	n	ω -1 / ω -2	
		Aae UPO-PaDa-I	Aae UPO-Fett
Fatty acids	8	68/32	-
	10	62/38	98/2
	12	51/49	98/2
	14	32/68	96/4
Fatty esters	3	99/1	99/1
	4	99/1	99/1
	6	55/45	99/1
	8	62/38	98/2
	10	57/43	97/3
	12	31/69	95/5
	14	-	92/8

^a Compounds analysed by GC after silylation.

4.13.2 Spectroscopic analysis of AaeUPO-PaDa-I and Fett

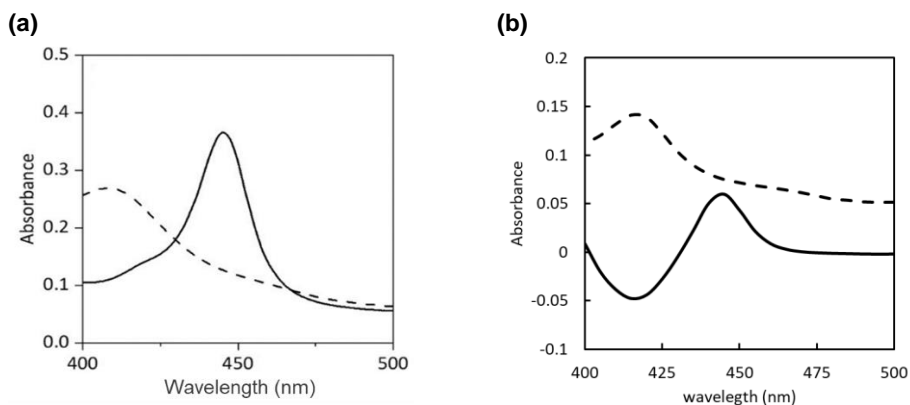


Figure S2.1. CO difference spectra of AaeUPO-PaDa-I (a)^[38], AaeUPO-Fett (b). Before (dashed line) and after (solid line) incubation with CO and Na₂S₂O₄ and after.

4.13.3 Optimisation of methyl hexanoate hydroxylation

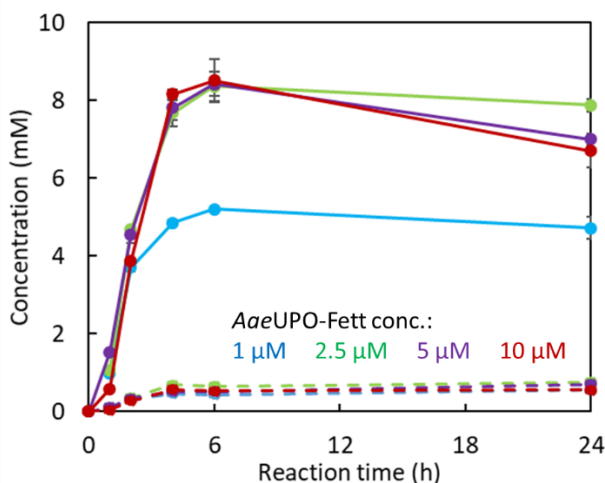
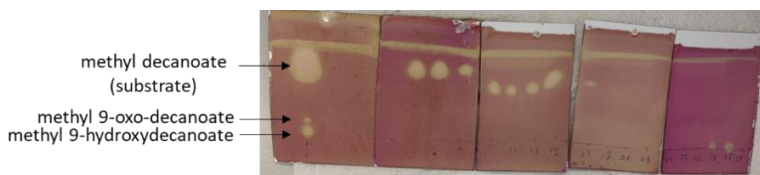


Figure S2.2. The effect of *AaeUPO-Fett* concentration on the formation of methyl 5-hydroxyhexanoate (solid lines) and δ -hexalactone (dashed lines). Reaction conditions: [*AaeUPO-Fett*] = 1–10 μM , [H_2O_2] = 5 mM h^{-1} , [methyl hexanoate] = 10 mM , [MeCN] = 10 vol%, 50 mM KPi buffer (pH 7.0), 600 rpm, 25 $^\circ\text{C}$, 10 mL scale. Values represent the average of duplicates ($n = 2$). Error bars indicate the standard deviation.

4.13.4 Isolation of methyl 9-hydroxydecanoate from 2LPS reaction system

(a)



(b)

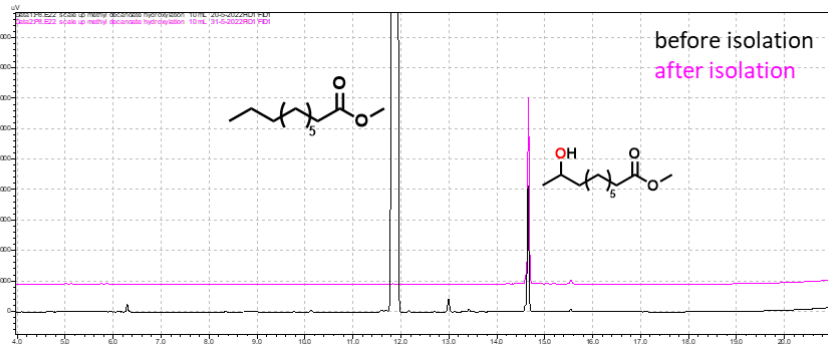


Figure S2.3. Isolation of methyl 9-hydroxydecanoate by flash column chromatography. (a) Thin layer chromatography (TLC) analysis of different fractions. (b) GC analysis before and after flash column chromatography. Elution conditions of TLC, fraction No. ≤ 17 , petroleum ether was used as elution solvent (6 CV); fraction No. 25: the mixture of 10 vol% ethyl acetate

and 90 vol% petroleum ether was used as elution solvent (1 CV); fraction No. 26-27: the mixture of 30 vol% ethyl acetate and 70 vol% petroleum ether was used as elution solvent (1 CV); fraction No. 28: the mixture of 50 vol% ethyl acetate and 50 vol% petroleum ether was used as elution solvent (1 CV); fraction No. 29-30: the mixture of 70 vol% ethyl acetate and 30 vol% petroleum ether was used as elution solvent (1 CV). Reagent used for revelation of spots: potassium permanganate (1.5 g of KMnO_4 , 10 g K_2CO_3 and 1.25 mL 10 wt% NaOH in 200 mL H_2O . A typical lifetime for this stain is approximately 3 months)

4.13.5 Optimisation of ADH/BVMOAfl838 two-pot two-step cascade reaction

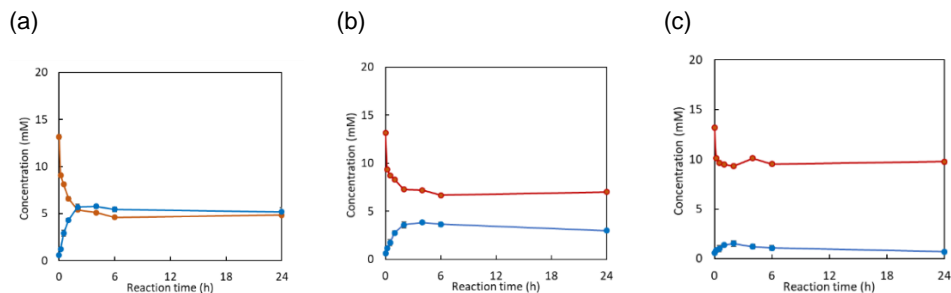
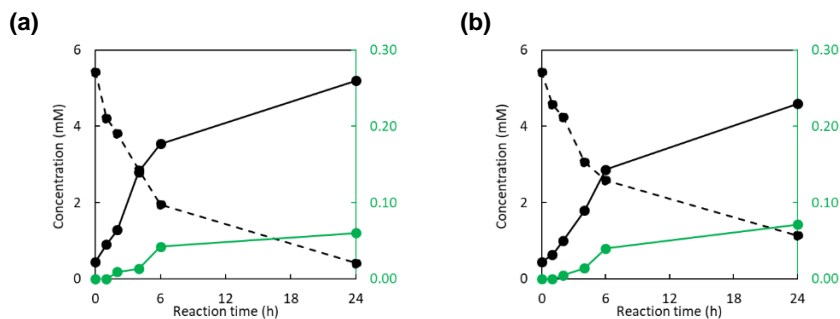


Figure S2.4. The effect of SyADH/BVMOAfl838 ratio on the concentration of methyl 9-oxo-decanoate (●) and the sum of methyl 8-(acetyloxy)octanoate and methyl 9-hydroxydecanoate (●) in the SyADH/BVMOAfl838 two-pot two-step cascade reaction starting from methyl 9-hydroxydecanoate. Reaction condition: diluted organic phase from first step (Fett-catalysed step)/100 mM Tris-HCl (pH 8.0) = 1:4 (v/v), [BVMOAfl838] = 0.5 μM , $[\text{NADP}^+] = 1 \text{ mM}$, 1000 rpm, 25 °C, 1 mL scale. (a), [SyADH cells] = 10 mg mL^{-1} ; (b), [SyADH cells] = 5 mg mL^{-1} ; (c) [SyADH cells] = 1 mg mL^{-1} . Values represent the average of duplicates ($n = 2$). Error bars indicate the standard deviation.

4.13.6 Optimisation of ADH/RedAm cascade reaction



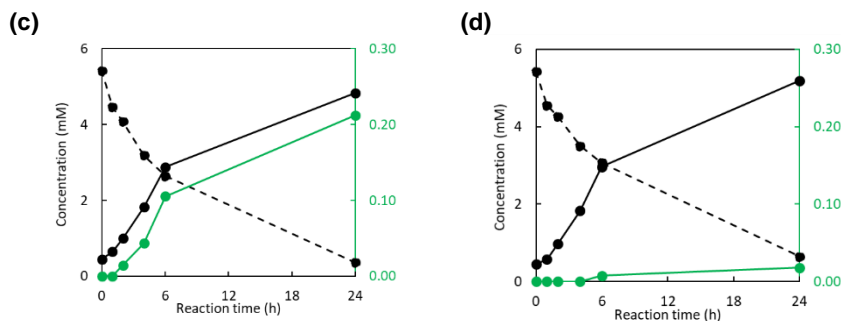


Figure S2.5. The effect of SyADH/AspRedAm ratio and cyclopropylamine concentration on the formation of methyl 9-cyclopropylaminodecanoate (●), methyl 9-hydroxydecanoate (black dashed line) and methyl 9-oxo-decanoate (black solid line) on the second step of cascade reaction. Reaction condition: [SyADH cells] = 0.5-1 mg mL⁻¹, [AspRedAm]=320 μL, [cyclopropylamine]=5-40 mM, [NADP⁺] = 1 mM, methyl decanoate/100 mM Tris buffer (pH 9.0) = 1:4 (v/v), 300 rpm, 25 °C, 0.5 mL scale. (a), [SyADH] = 1 mg mL⁻¹, [AspRedAm] = 320 μL, [cyclopropylamine] = 20 mM; (b), [SyADH] = 0.5 mg mL⁻¹, [AspRedAm] = 320 μL, [cyclopropylamine] = 20 mM; (c), [SyADH] = 0.5 mg mL⁻¹, [AspRedAm] = 320 μL, [cyclopropylamine] = 40 mM; (d), [SyADH] = 0.5 mg mL⁻¹, [AspRedAm] = 320 μL, [cyclopropylamine] = 5 mM. Values represent the average of duplicates (n = 2). Error bars indicate the standard deviation.

4.13.7 Purification of AspRedAm

After affinity purification via IMAC, approx. 600 μL purified enzyme with a protein concentration of 7.96 ± 0.07 mg mL⁻¹ and volumetric activity of 27.48 ± 0.27 U mL⁻¹ was obtained from 10 g wet cells.

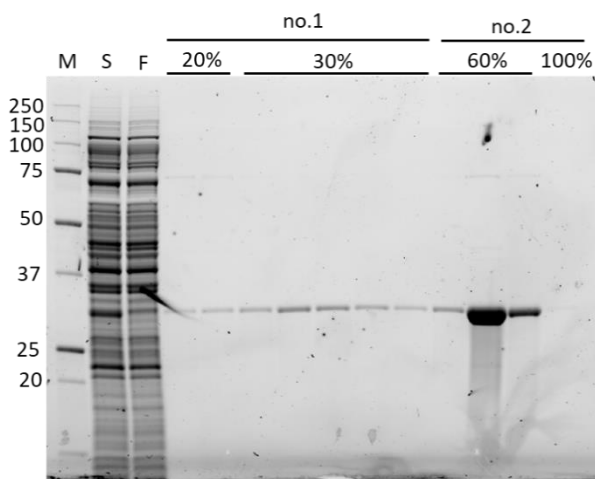


Figure S2.6. SDS-PAGE analysis of purified AspRedAm after Ni²⁺-affinity chromatography. Lanes no.1: 20 mL lysate was loaded on the 5-mL Ni-column; no.2: 120 mL lysate was loaded on the 5-mL Ni-column. 20%: 20% buffer B+80% buffer A was used as

elution buffer; 30%: 30% buffer B+70% buffer A was used as elution buffer; 60%: 60% buffer B+40% buffer A was used as elution buffer; 100%: 100% buffer B was used as elution buffer. M: precision plus protein all blue standard (Biorad); S: supernatant; F: flow-through. Buffer A: 100 mM Tris-HCl (pH 8.0), 300 mM NaCl, 30 mM imidazole; Buffer B: 100 mM Tris-HCl (pH 8.0), 300 mM NaCl, 300 mM imidazole. Buffer C: 100 mM Tris-HCl (pH 8.0), 500 mM NaCl.

4.13.8 GC analysis and GC-MS analysis

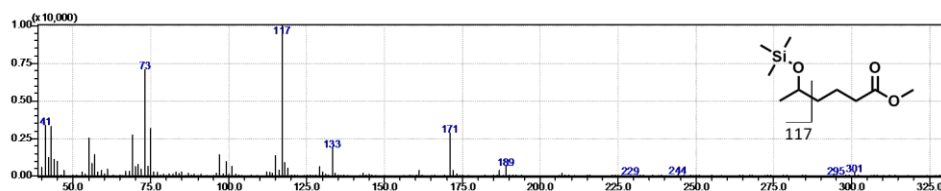


Figure S2.7. GC-MS analysis of silylated methyl 5-hydroxyhexanoate.

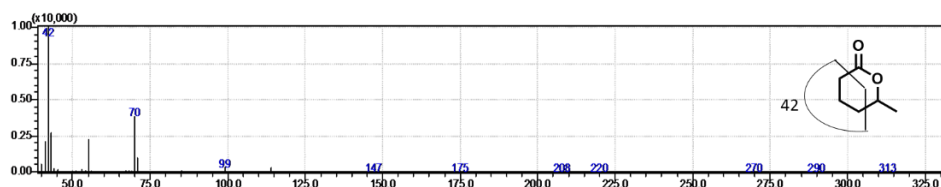


Figure S2.8. GC-MS analysis of δ -hexalactone.

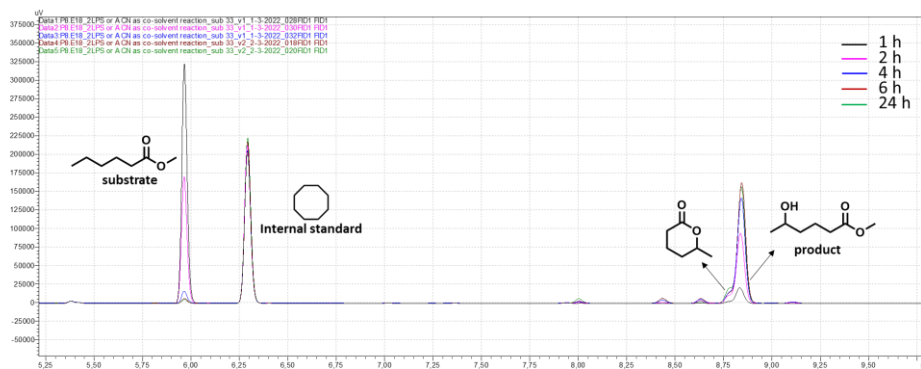


Figure S2.9. GC chromatogram of hydroxylation reaction from methyl hexanoate to methyl 5-hydroxyhexanoate.

Chapter 2

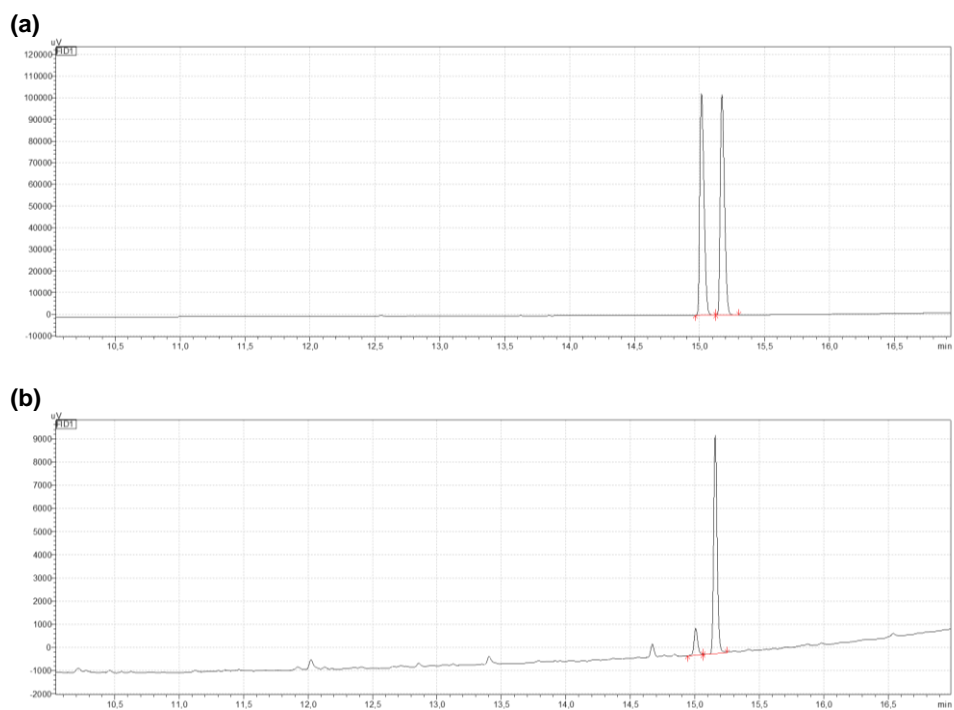


Figure S2.10. Chiral GC chromatogram of commercial racemic delta-hexalactone (a) and synthesised delta-hexalactone (b). The ee value of synthesised delta-hexalactone from enzymatic reaction is 77%.

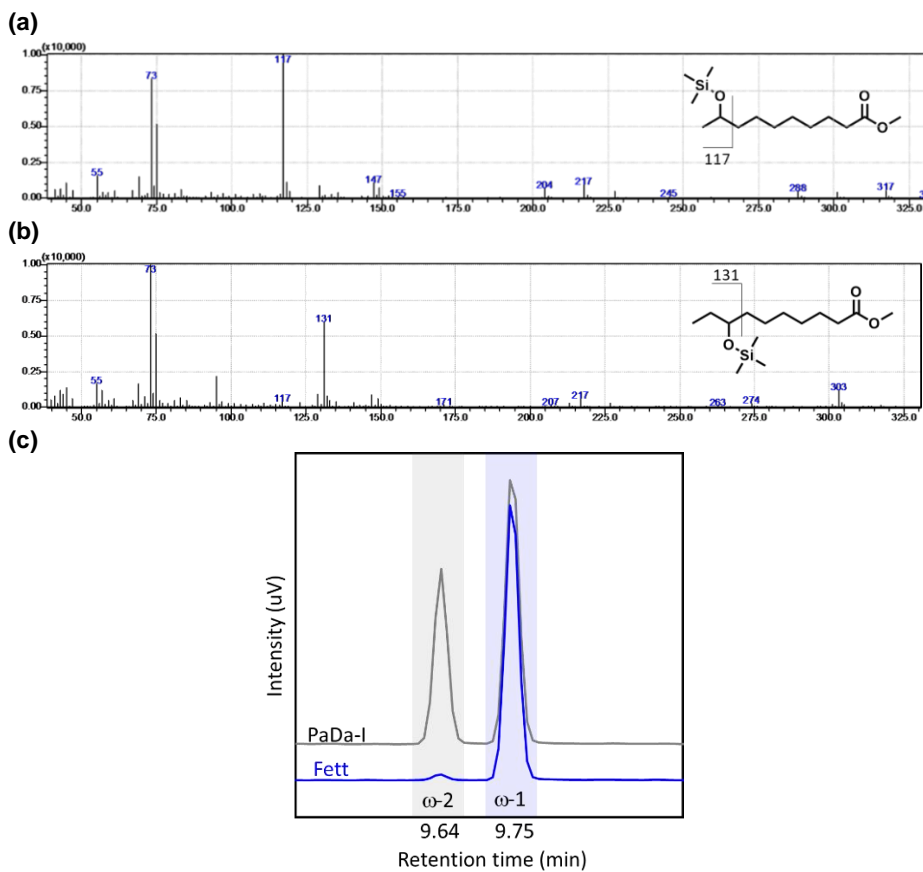


Figure S2.11. GC-MS analysis of silylated methyl 9-hydroxydecanoate (a) and methyl 8-hydroxydecanoate (b) and comparison of hydroxylation products in methyl decanoate hydroxylation catalysed by *AaeUPO*-PaDa-I and *AaeUPO*-Fett (c).

Chapter 2

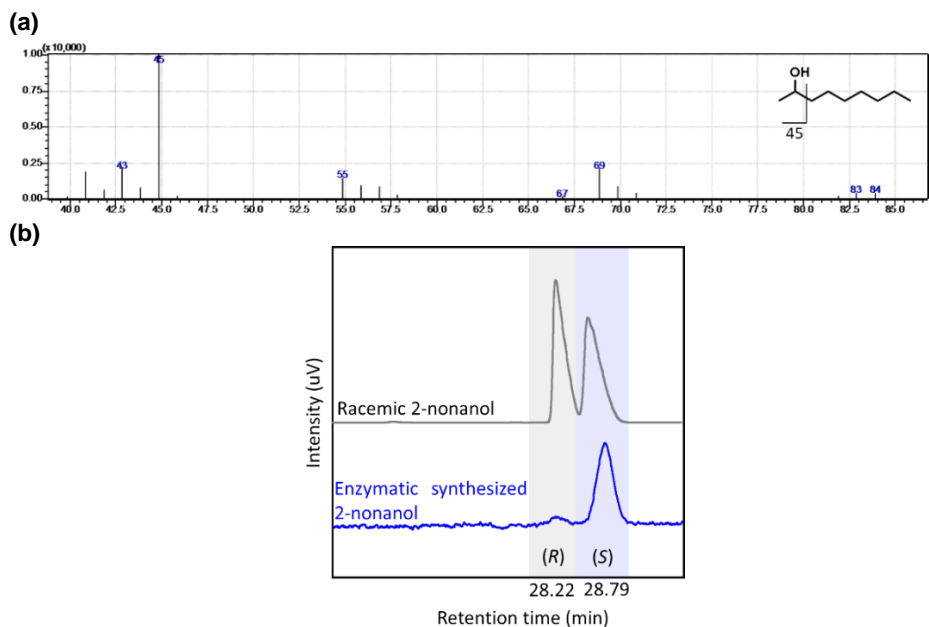


Figure S2.12. GC-MS (a) and chiral GC (b) analysis of 2-nonanol produced from methyl decanoate in the *Aae*UPO-*Fet*t/*Cal*B/*Cv*FAP two-pot-three-step cascade reaction.

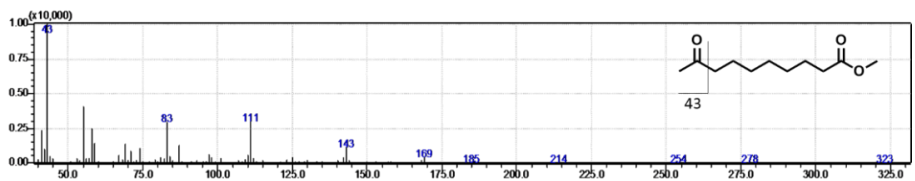


Figure S2.13. GC-MS analysis of methyl 9-oxo-decanoate.

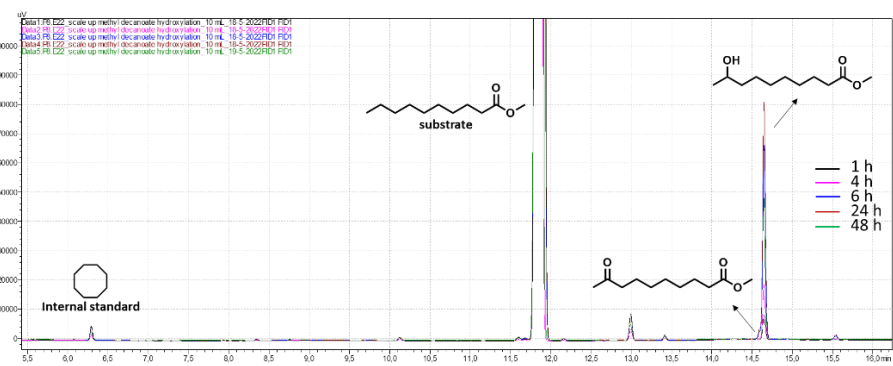


Figure S2.14. GC chromatogram of hydroxylation reaction from methyl decanoate to methyl 9-hydroxydecanoate.

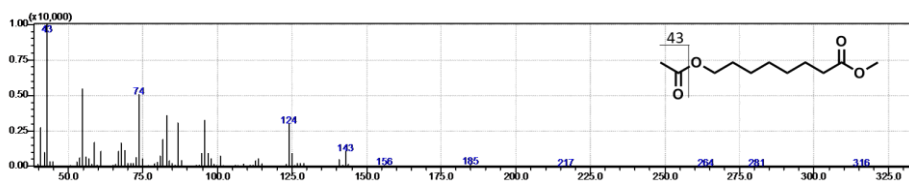


Figure S2.15. GC-MS analysis of methyl 8-(acetyloxy)octanoate.

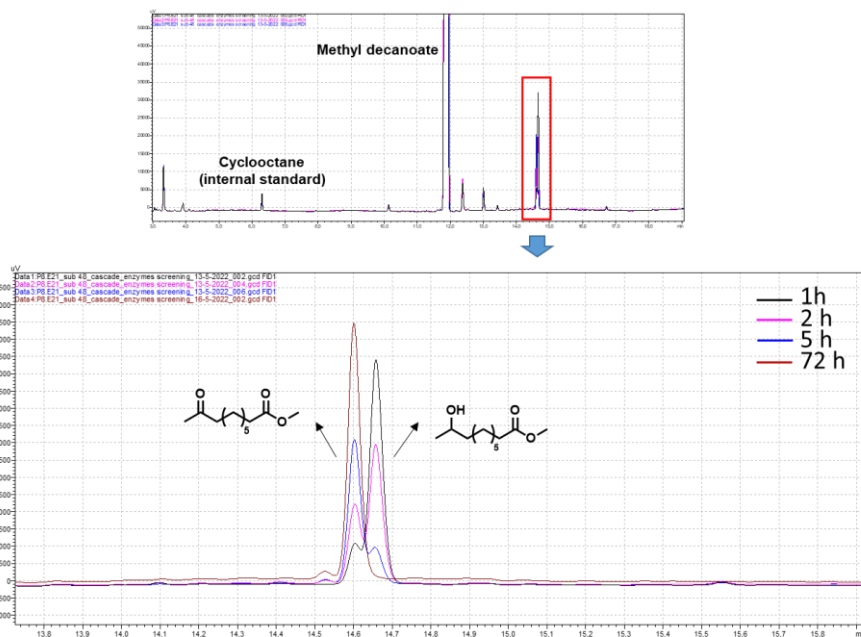


Figure S2.16. GC chromatogram of ADH-catalysed oxidation of methyl 9-hydroxydecanoate to methyl 9-oxo-decanoate.

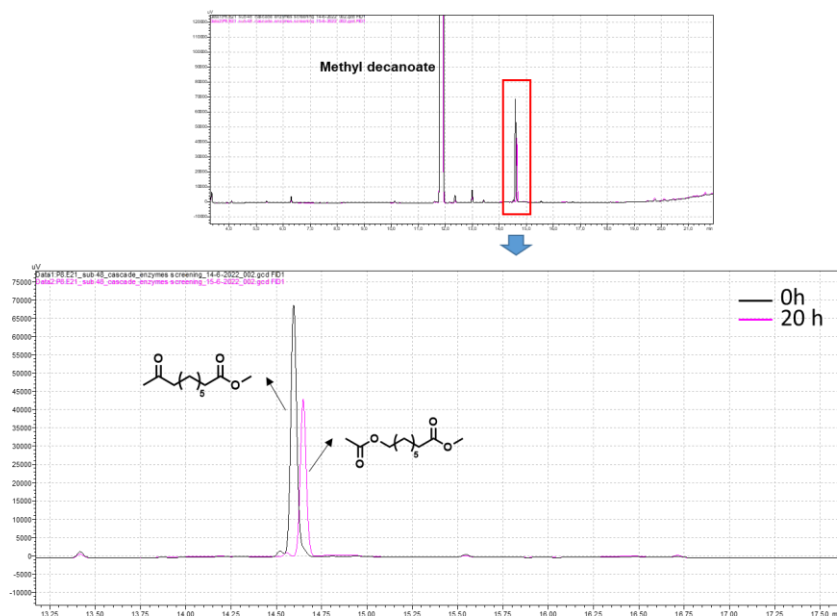


Figure S2.17. GC chromatogram of BVMO-catalysed oxidation of methyl 9-oxodecanoate to methyl 8-(acetyloxy)octanoate.

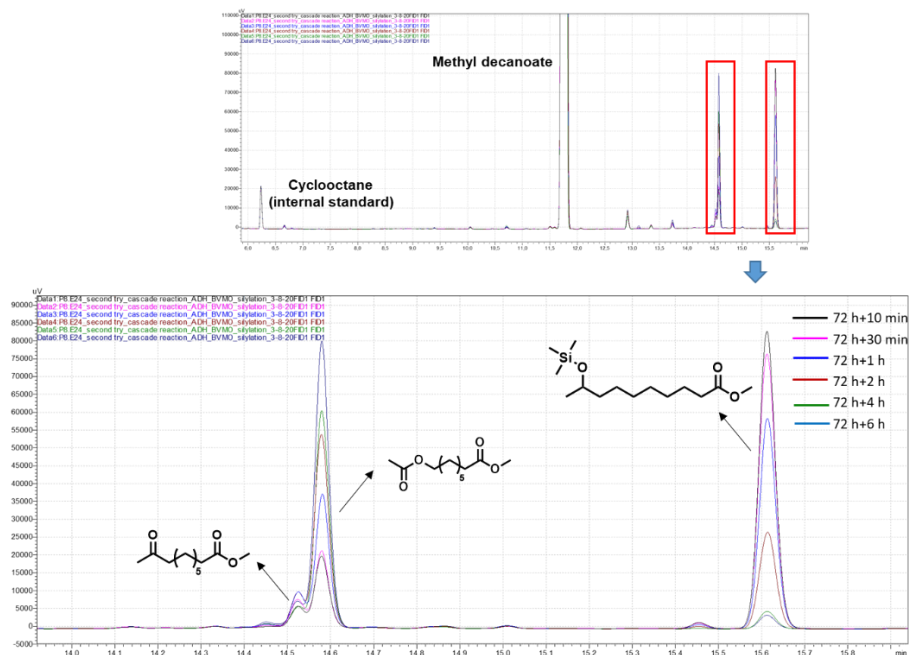


Figure S2.18. GC chromatogram of 2-pot 2-step of UPO/ADH/BVMO cascade reaction (after silylation), starting from methyl decanoate to methyl 8-(acetyloxy)octanoate. First step in first pot (0 - 72 h): UPO-catalysed hydroxylation of methyl decanoate; second step in second pot (72 h - 78 h): ADH/BVMO-catalysed reaction from methyl 9-hydroxyldecanoate to methyl 8-(acetyloxy)octanoate.

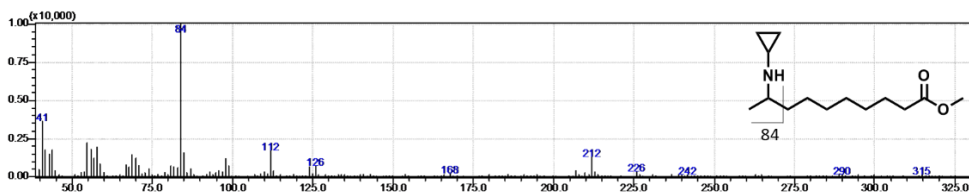


Figure S2.19. GC-MS analysis of methyl 9-cyclopropylaminodecanoate.

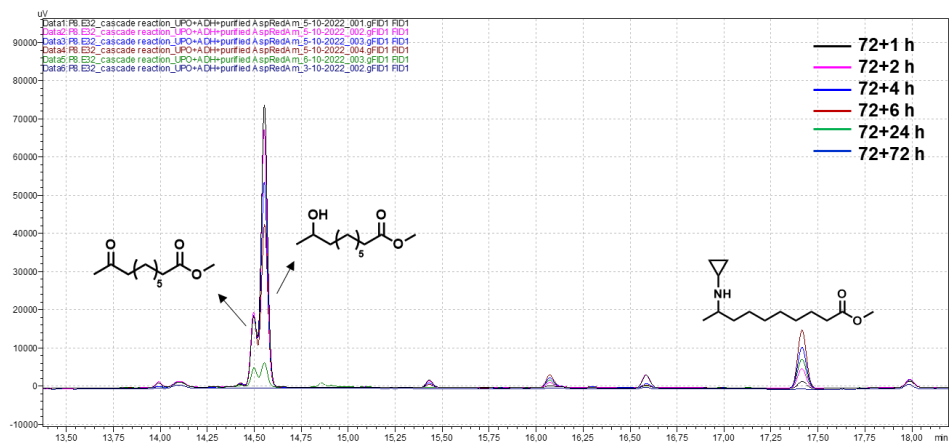


Figure S2.20. GC chromatogram of 2-pot 2-step of UPO/ADH/BVMO cascade reaction starting from methyl decanoate to methyl 9-cyclopropylaminodecanoate. First step in first pot (0-72 h): UPO-catalysed hydroxylation of methyl decanoate; second step in second pot (72 h - 144 h): ADH/RedAm-catalysed reaction from methyl 9-hydroxydecanoate to methyl 9-cyclopropylaminodecanoate.

Chapter 2

4.13.9 NMR analysis

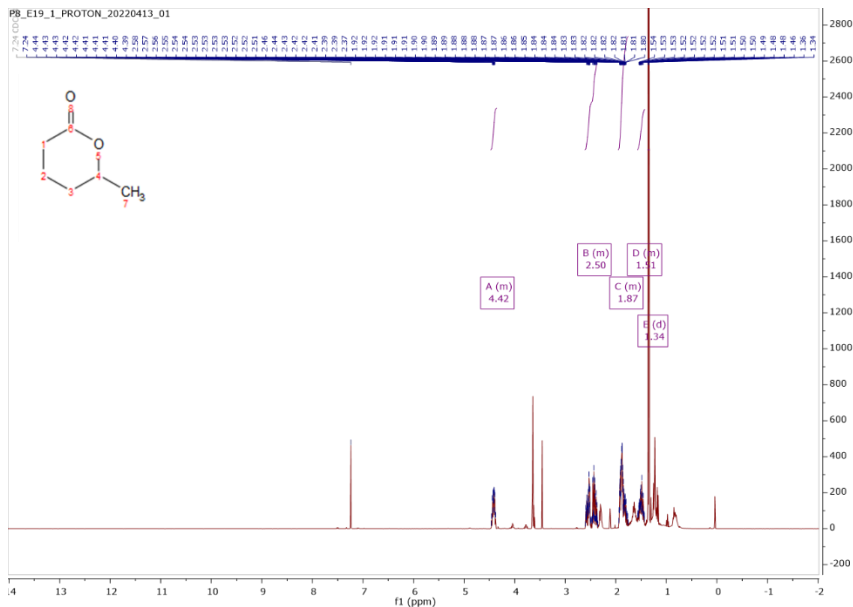


Figure S2.21. ^1H NMR of isolated δ -hexalactone. ^1H NMR (400 MHz, CDCl_3): δ 4.42 (m, 1H, 4-H), 2.50 (m, 1H, 1-H), 1.87 (m, 1H, 2-H), 1.51 (m, 1H, 3-H), 1.38 (d, 3H, 7-H).^[39]

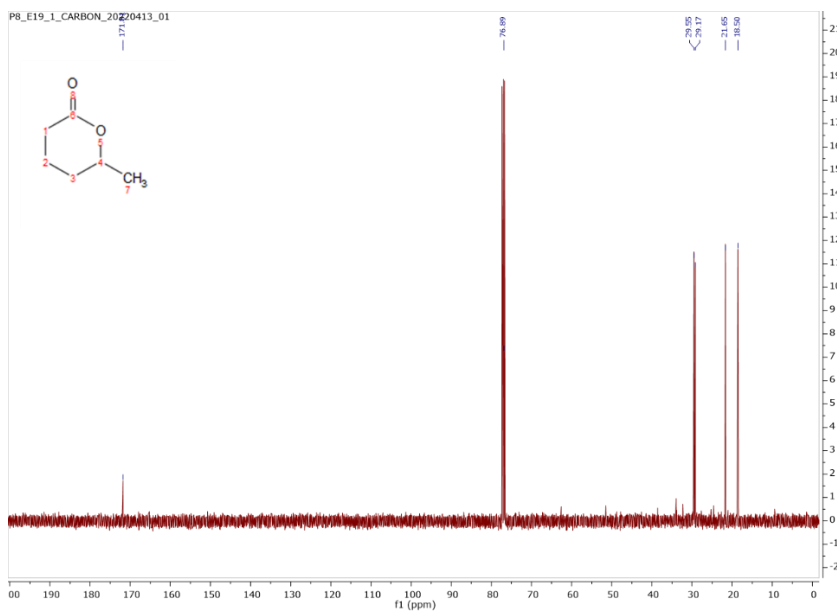


Figure S2.22. ^{13}C NMR of isolated δ -hexalactone. ^{13}C NMR (101 MHz, CDCl_3): δ 171.8 (6-C), 76.9 (4-C), 29.6 (1-C), 29.2 (2-C), 21.7 (3-C), 18.5 (7-C).^[39]

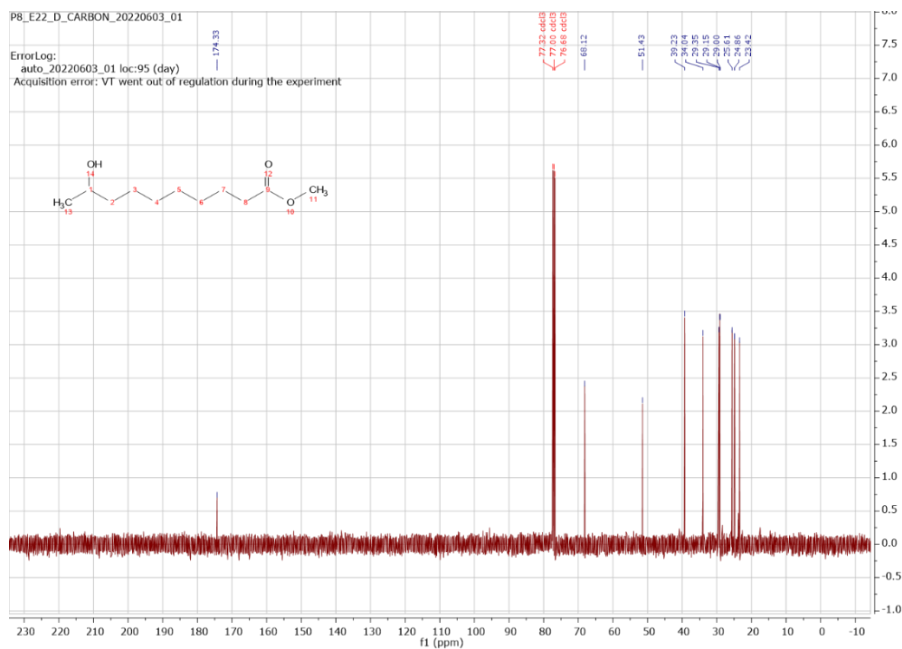


Figure S2.23. ^{13}C NMR of isolated methyl 9-hydroxydecanoate. ^{13}C MMR (101 MHz, CDCl_3): δ =174.3 (9-C), 68.1 (1-C), 51.4 (11-C), 39.2 (2-C), 34.0 (8-C), 29.4 (4-C), 29.2 (5-C), 29.0 (6-C), 25.6 (3-C), 24.9 (7-C), 23.4 (13-C).

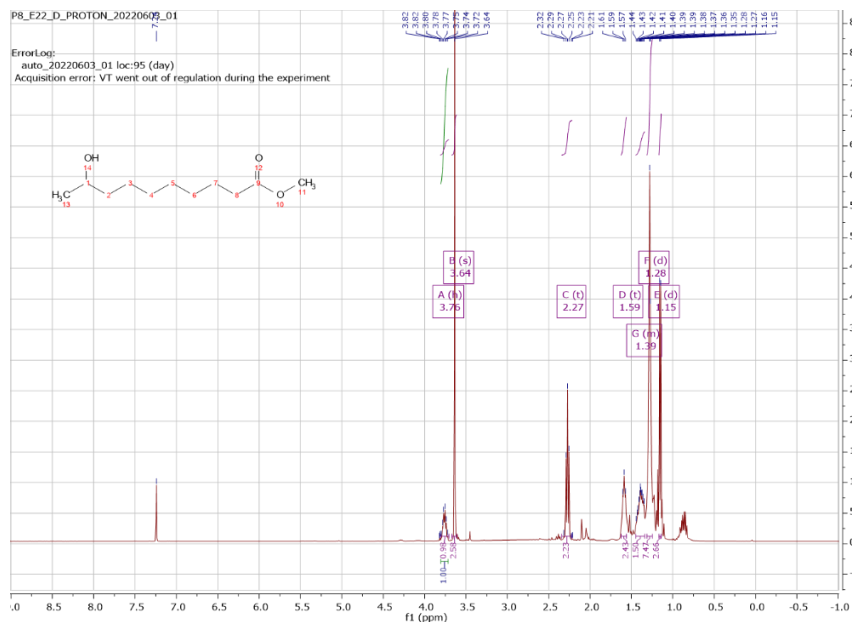


Figure S2.24. ^1H NMR of isolated methyl 9-hydroxydecanoate. ^1H NMR (400 MHz, CDCl_3): δ 3.76 (h, J = 6.2 Hz, 1H), 3.64 (s, 3H), 2.27 (t, J = 7.5 Hz, 2H), 1.59 (t, J = 7.2 Hz, 2H), 1.45 – 1.34 (m, 1H), 1.28 (d, J = 4.2 Hz, 7H), 1.15 (d, J = 6.2 Hz, 3H).

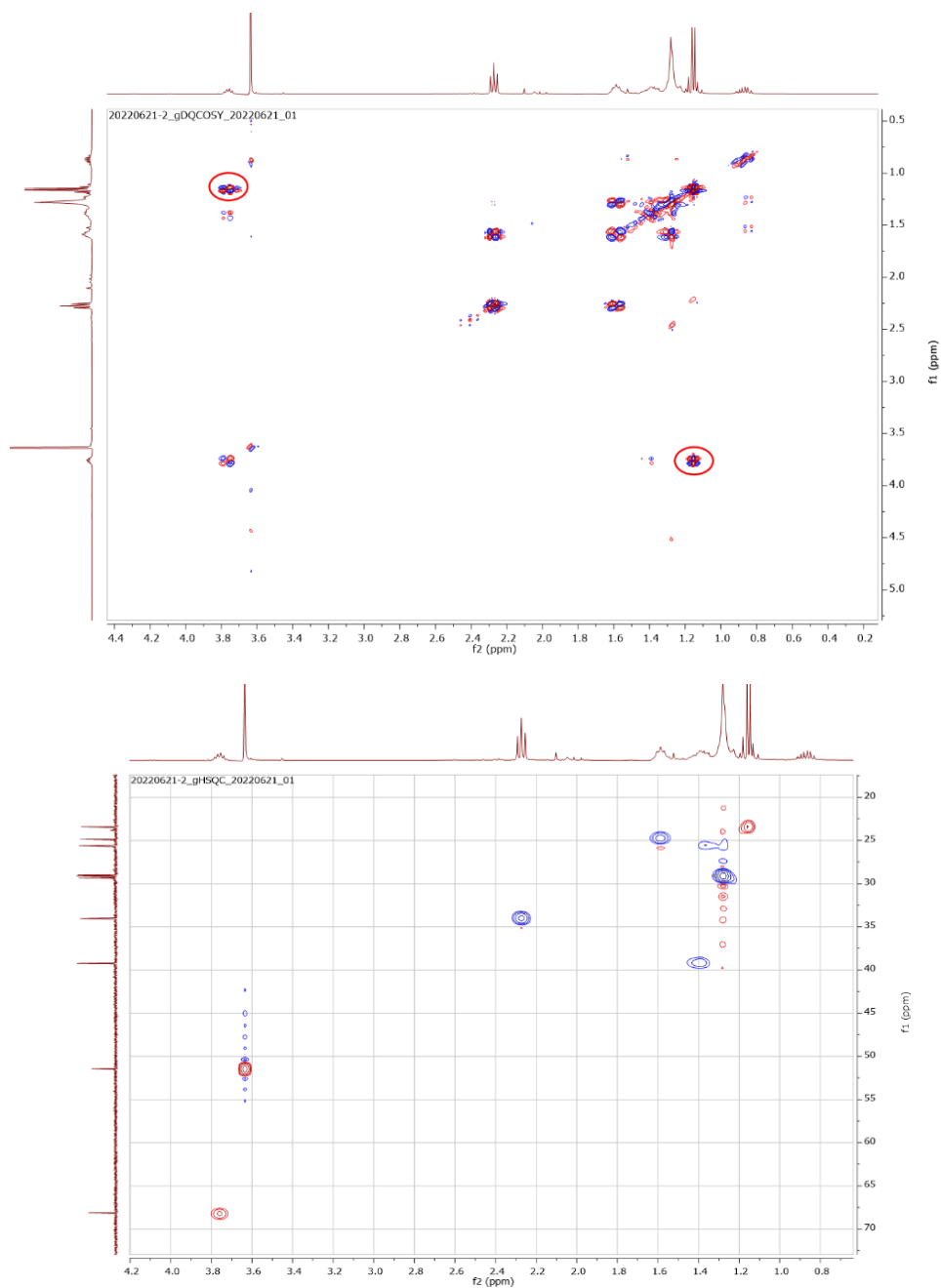


Figure S2.25. ^1H NMR, gDQCOSY and gHSQC of isolated methyl 9-hydroxydecanoate. In gDQCOSY, the shift at 3.76 ppm is corresponding to 1-H (top left circle, representing $-\text{CH}$ group next to $-\text{OH}$ group). The shift at 1.15 ppm is corresponding to 13-H (bottom right circle, representing $\omega-\text{CH}_3$ group) and there are no obvious signals next to it, indicating that the OH group is on $\omega-1$ position, which further confirms the GC-MS result.

4.13.10 Reaction setup



Figure S2.26. The setup employed for hydroxylation reaction catalysed by *AaeUPO-Fett* in this study.

All research data supporting the findings described in this chapter are available in 4TU.Centre for Research Data at <https://doi.org/10.4121/21164386.v1>

References

- [1] A. Pellis, M. Malinconico, A. Guarneri, L. J. N. B. Gardossi, *N Biotechnol* **2021**, *60*, 146-158.
- [2] R. I. Ma, L. Pérez, C. M. Ma, R. Pons, M. Mitjans, P. V. Ma, T. G. Ma, A. Pinazo, *Eur J Lipid Sci Technol* **2010**, *112*, 110-121.
- [3] C. Aouf, E. Durand, J. Lecomte, M.-C. Figueroa-Espinoza, E. Dubreucq, H. Fulcrand, P. Villeneuve, *Green Chem.* **2014**, *16*, 1740-1754.
- [4] U. Biermann, U. T. Bornscheuer, I. Feussner, M. A. Meier, J. O. Metzger, *Angew. Chem., Int. Ed.* **2021**, *60*, 20144-20165.
- [5] M. B. Ansorge-Schumacher, O. Thum, *Chem. Soc. Rev.* **2013**, *42*, 6475-6490.
- [6] U. Bornscheuer, R. Kazlauskas, *Hydrolases in Organic Synthesis*, 2nd ed., Wiley-VCH, Weinheim, **2006**.
- [7] A. Thomas, B. Matthäus, H.-J. Fiebig, in *Ullmann's Encyclopedia of Industrial Chemistry*, **2015**.
- [8] D. J. Anneken, S. Both, R. Christoph, G. Fieg, U. Steinberner, A. Westfechtel, in *Ullmann's Encyclopedia of Industrial Chemistry*, **2012**.
- [9] K. Noweck, W. Grafahrend, in *Ullmann's Encyclopedia of Industrial Chemistry*, **2012**.
- [10] P. L. Hagedoorn, F. Hollmann, U. J. A. M. Hanefeld, *Biotechnol.* **2021**, *105*, 6159-6172.
- [11] J.-W. Song, J.-H. Seo, D.-K. Oh, U. T. Bornscheuer, J.-B. Park, *Catal. Sci. Technol.* **2020**, *10*, 46-64.
- [12] L. Hammerer, M. Friess, J. Cerne, M. Fuchs, G. Steinkellner, K. Gruber, K. Vanhessche, T. Plocek, C. K. Winkler, W. J. C. Kroutil, *ChemCatChem* **2019**, *11*, 5642-5649.
- [13] K. Zhang, A. Yu, X. Chu, F. Li, J. Liu, L. Liu, W.-J. Bai, C. He, X. Wang, *Angew. Chem.*, **2022**, *61*, e202204290.
- [14] J. Manning, M. Tavanti, J. L. Porter, N. Kress, S. P. De Visser, N. J. Turner, S. L. J. A. C. I. E. Flitsch, *Angew. Chem., Int. Ed.* **2019**, *58*, 5668-5671.
- [15] W. Lu, J. E. Ness, W. Xie, X. Zhang, J. Minshull, R. A. Gross, *J. Am. Chem. Soc.* **2010**, *132*, 15451-15455
- [16] L. Hammerer, C. K. Winkler, W. Kroutil, *Catal Letters* **2018**, *148*, 787-812.

- [17] M. Hobisch, D. Holtmann, P. G. de Santos, M. Alcalde, F. Hollmann, S. Kara, *Biotechnol. Adv.* **2021**, *51*, 107615.
- [18] A. Olmedo, C. Aranda, J. C. Del Río, J. Kiebig, K. Scheibner, A. T. Martínez, A. Gutiérrez, *Angew. Chem.*, **2016**, *128*, 12436-12439.
- [19] A. Gutiérrez, E. D. Babot, R. Ullrich, M. Hofrichter, A. T. Martínez, C. José, *Arch. Biochem. Biophys.* **2011**, *514*, 33-43.
- [20] C. Aranda, J. Carro, A. González-Benjumea, E. D. Babot, A. Olmedo, D. Linde, A. T. Martínez, A. J. B. A. Gutiérrez, *Biotechnol. Adv.* **2021**, *51*, 107703.
- [21] E. D. Babot, J. C. del Río, L. Kalum, A. T. Martínez, A. Gutiérrez, *Biotechnol. Bioeng.* **2013**, *110*, 2323-2332.
- [22] R. Ullrich, J. r. Nüske, K. Scheibner, J. r. Spantzel, M. Hofrichter, *Appl. Environ. Microbiol.* **2004**, *70*, 4575-4581.
- [23] P. Molina-Espeja, S. Ma, D. M. Mate, R. Ludwig, M. Alcalde, *Enzyme Microb. Technol.* **2015**, *73*, 29-33.
- [24] P. Molina-Espeja, E. Garcia-Ruiz, D. Gonzalez-Perez, R. Ullrich, M. Hofrichter, M. Alcalde, *Appl. Environ. Microbiol.* **2014**, *80*, 3496-3507.
- [25] P. Gómez de Santos, A. González-Benjumea, Á. Fernández García, Y. Wu, A. But, P. Molina-Espeja, D. M. Maté, D. González-Pérez, W. Zhang, J. Kiebig, *Angew. Chem., Int. Ed.* **2023**, *62*, e20221737.
- [26] M. M. van Schie, J.-D. Spöring, M. Bocola, P. D. de María, D. Rother, *Green Chem.* **2021**, *23*, 3191-3206.
- [27] P. Chandra, R. Singh, P. K. J. M. C. F. Arora, *Microb. Cell Fact.* **2020**, *19*, 42.
- [28] D. Sorigue, B. Legeret, S. Cuine, S. Blangy, S. Moulin, E. Billon, P. Richaud, S. Brugiere, Y. Coute, D. Nurizzo, P. Mueller, K. Brettel, D. Pignol, P. Arnoux, Y. Li-Beisson, G. Peltier, F. Beisson, *Science* **2017**, *357*, 903-907.
- [29] I. Lavandera, A. Kern, V. Resch, B. Ferreira-Silva, A. Glieder, W. M. Fabian, S. de Wildeman, W. J. O. I. Kroutil, *Org. Lett.* **2008**, *10*, 2155-2158.
- [30] H. Man, K. Kędziora, J. Kulig, A. Frank, I. Lavandera, V. Gotor-Fernández, D. Rother, S. Hart, J. P. Turkenburg, G. J. T. i. c. Grogan, *Top. Catal.* **2014**, *57*, 356-365.
- [31] F. M. Ferroni, C. Tolmie, M. S. Smit, D. J. J. C. Opperman, *ChemBioChem* **2017**, *18*, 515-517.

Chapter 2

- [32] F. M. Ferroni, C. Tolmie, M. S. Smit, D. J. Opperman, *PLoS One* **2016**, *11*, e0160186.
- [33] F. Ferroni, M. Smit, D. J. J. o. M. C. B. E. Opperman, *J. Mol. Catal. B Enzym.* **2014**, *107*, 47-54.
- [34] A. Gran-Scheuch, L. Parra, M. W. J. A. S. C. Fraaije, *ACS Sustain. Chem. Eng.* **2021**, *11*, 4948-4959.
- [35] G. A. Aleku, S. P. France, H. Man, J. Mangas-Sanchez, S. L. Montgomery, M. Sharma, F. Leipold, S. Hussain, G. Grogan, N. J. Turner, *Nat. Chem.* **2017**, *9*, 961-969.
- [36] E. Puchľová, T. Hilberath, K. Vranková, F. Hollmann, *Front. Catal.* **2022**, *2*, 926316.
- [37] F. Tonin, F. Tieves, S. Willot, A. van Troost, R. van Oosten, S. Breestraat, S. van Pelt, M. Alcalde, F. Hollmann, *Org Process Res Dev* **2021**, *25*, 1414-1418.
- [38] F. E. Nintzel, Y. Wu, M. Planchestainer, M. Held, M. Alcalde, F. Hollmann, *ChemComm* **2021**, *57*, 5766-5769.
- [39] T. Chen, Z. Wang, J. Xiao, Z. Cao, C. Yi, Z. Xu, *Asian J. Org. Chem.* **2019**, *8*, 1321-1324.

Chapter 3: An alginate-confined peroxygenase-CLEA for styrene epoxidation

Friederike E. H. Nintzel, Yinqi Wu, Matteo Planchestainer,
Martin Held, Miguel Alcalde, and Frank Hollmann

Based on *Chem. Commun.* 2021, 57, 5766.

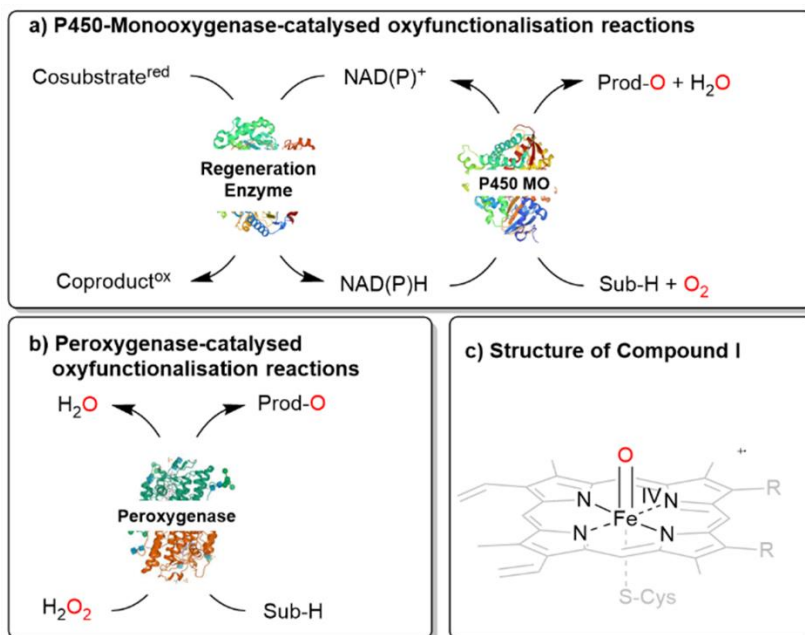
Summary

Oxyfunctionalisation reactions in neat substrate still pose a challenge for biocatalysis. Here, we report an alginate-confined peroxygenase-CLEA to catalyse the enantioselective epoxidation of *cis*- β -methylstyrene in a solvent-free reaction system achieving turnover numbers of 96 000 for the biocatalyst and epoxide concentrations of 48 mM.

1. Introduction

Biocatalytic oxyfunctionalisation reactions are enjoying an increasing interest in organic chemistry.^[1] Especially the often very high regio- and enantioselectivity of enzymatic oxyfunctionalisation reactions such as hydroxylations or epoxidations offers synthetic chemists straightforward access to chiral building blocks, which with traditional chemical means are difficult to prepare.

Next to the well-known P450 monooxygenases,^[2] in recent years also peroxygenases^[3] have been in the centre of attention. P450 monooxygenases reductively activate molecular oxygen to form the catalytically active oxyferryl-heme species. Peroxygenases form this species directly from partially reduced oxygen species (peroxides) and thereby circumvent the complex molecular architectures of P450 monooxygenases (Scheme 3.1).



Scheme 3.1. Comparison of (a) P450 monooxygenase-catalysed and (b) peroxygenase-catalysed oxyfunctionalisation reactions. (c) Both enzyme classes utilise Compound I as the oxygenating agent.

The synthetic application of both enzyme classes, however, still suffers from the poor water solubility of the majority of starting materials, resulting in rather dilute reaction mixtures with an enormous water footprint. Therefore, increasing the starting material

(and product) concentration is of utmost importance to increase the economic viability and environmental friendliness of such biocatalytic reactions.^[4]

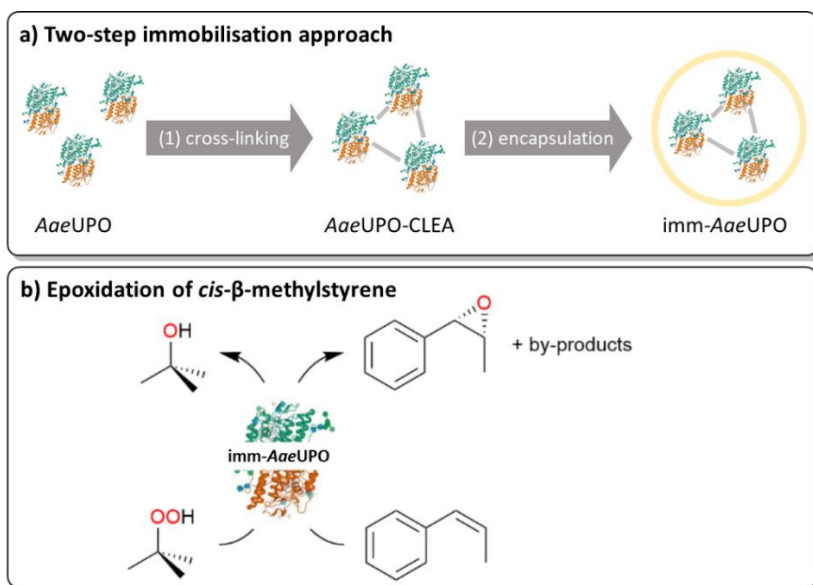
One common approach to increase the substrate loading is to use the so-called two liquid phase approach^[5] in which an aqueous, biocatalyst-containing layer is contacted with a hydrophobic, organic layer serving as substrate reservoir and product sink. To alleviate possible phase transfer rate limitations of this system, intensive mechanical stirring is needed, which however, also may impair the stability of the biocatalyst.^[6]

The latter issue can be addressed by immobilising the biocatalyst to a heterogeneous carrier material and thereby physically protecting the enzyme. While a limited number of studies report immobilisation of peroxygenases, this technique is not fully explored yet for this enzyme class.^[7-12] In previous works, we could demonstrate that immobilised peroxygenases in principle can even be applied in neat (i.e. almost water-free) reaction media.^[9] A drawback of this approach, however, was the very poor specific activity of the immobilised enzyme, possibly due to a combination of activity losses of the enzyme during immobilisation and further activity losses originating from dehydration of the enzyme surface.

Encapsulating enzymes in alginate matrices may represent an elegant compromise. The so-confined enzymes are mechanically stabilised while still situated in a micro-aqueous environment.^[8, 11, 13]

2. Results and Discussion

We therefore set out to immobilise a peroxygenase in an alginate matrix and evaluate its catalytic activity under non aqueous reaction conditions. As model enzyme we chose the recombinantly expressed, evolved peroxygenase from *Agrocybe aegerita* (*AaeUPO*)^[14-16] as catalyst for the epoxidation of styrene and *cis*- β -methylstyrene (Scheme 3.2). The biocatalyst was obtained from the supernatant of the fermentation broth of recombinant *Pichia pastoris* and used without further purification.



Scheme 3.2. (a) Overview of the utilised immobilisation approach consisting of CLEA formation and alginate confinement. (b) Epoxidation of *cis*- β -methylstyrene by immobilised AaeUPO with *tert*-butyl hydroperoxide (t-BuOOH) as oxidant.

Confining AaeUPO in Ca²⁺-hardened alginates proved to be feasible. To our surprise, however, the resulting immobilisate showed low, and somewhat irreproducible catalytic activity (Fig. 4.1a), which most likely was due to leaching of the enzyme from the beads during the immobilisation procedure and storage. To improve the retention of the biocatalyst in the alginate beads, we decided to increase its molecular mass by covalent cross-linking (CLEA formation).^[17-19]

Indeed, CLEA formation more than doubled the catalytic activity of the immobilised peroxygenase (Fig. 4.1a). Further improvements were achieved by using chitosan as coagulant^[20-23] and by increasing the enzyme load (Fig. 4.1a). Additional optimisation steps are reported in the 4.7. It is important to note that the size of the beads had a significant influence on the activity of the immobilised peroxygenase. The larger the beads, the lower the catalytic activity under otherwise identical conditions (Fig. 4.1b). Overall, approximately 19% of the enzyme was immobilised (as determined via quantification of the amount of active heme sites using CO-differential spectra) and 11.4% of the peroxidase activity, as judged by the ABTS oxidation activity, was found back in the immobilisates. It is worth mentioning here that AaeUPO immobilisation also increased its storage stability. While the free enzyme completely lost its catalytic

activity after 12 days storage at room temperature, the immobilised version exhibited at least 80% of its initial activity even after two weeks (Fig. S4.10).

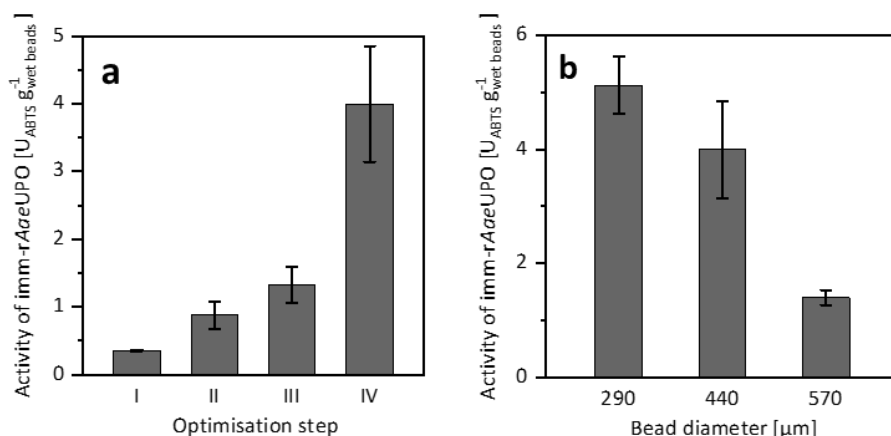


Figure 3.1. (a) Activity of imm-AaeUPO during optimisation of the immobilisation procedure, determined by ABTS-activity assay in aqueous environment. (b) Activity of imm-AaeUPO immobilisates with different diameters, determined by ABTS-activity assay in aqueous environment. Reference (I) is the encapsulation of free AaeUPO. The catalytic activity of imm-AaeUPO was improved by CLEA formation (II), by application of chitosan as coagulant (III), and by maximising the enzyme load (IV). Data represents the average of duplicates.

Having the immobilised AaeUPO preparation at hand, we decided to compare its catalytic performance in the epoxidation of *cis*-β-methylstyrene with the free enzyme in a two liquid phase approach (Fig. 4.2) using *t*BuOOH as oxidant.

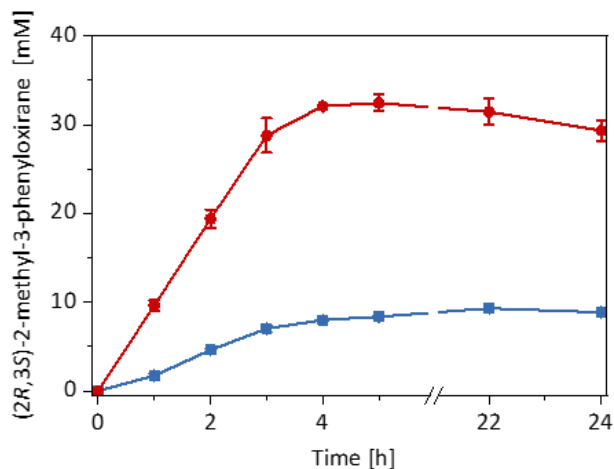


Figure 3.2. Product formation over time for the epoxidation of *cis*-β-methylstyrene in different reaction systems. imm-AaeUPO in neat substrate (180 mg immobilisate in 570 mL *cis*-β-methylstyrene) (red circles), and free AaeUPO in a two-liquid phase system (180 mL

Chapter 3

TRIS-HCl buffer (20 mM, pH 7): 570 mL *cis*- β -methylstyrene) (blue squares). General reaction conditions: [AaeUPO] = 0.5 μ M, t BuOOH feeding rate = 10 mM h⁻¹, room temperature, shaking at 99 rpm with 60° angle in an overhead rotator. Data represents the average of duplicates.

Very much to our surprise the immobilised enzyme outperformed the free enzyme under otherwise identical conditions (such as volumetric ratio of aqueous or alginate volume to the organic phase and enzyme concentrations). With the immobilised enzyme the product accumulation rate was approx. 10 mM h⁻¹ (corresponding to the t BuOOH feed rate) while with the free enzyme it was only 3 mM h⁻¹. A plausible explanation for this may be the higher surface area of the reactions using alginate-immobilised AaeUPO, largely eliminating the diffusion rate limitation of t BuOOH and/or *cis*- β -methylstyrene into the aqueous reaction phase (Fig. S4.13).

Overall, in this experiment, approx. 30 mM of enantiomerically pure (2*R*,3*S*)-2-methyl-3-phenyloxirane has been synthesised within 4 h corresponding to a turnover number (TN = mol_{Product} \times mol_{AaeUPO}⁻¹) for the enzyme of 60 000 and an average (over 4 h) turnover frequency of 4.1 s⁻¹. It should be mentioned here, that under these reaction conditions several side products such as benzaldehyde and phenylacetone were observed (*vide infra*).

Despite the promising results, the reactions stopped after approximately 5 h. We suspected the irreversible, oxidative inactivation of the heme-containing biocatalyst by the hydroperoxide to account for the low robustness of the reaction.

Therefore, we performed a series of experiments varying the t BuOOH addition rate (Fig. 4.3). While the initial product formation rate decreased with decreasing t BuOOH feeding rates, the long-term robustness of the reaction increased: at a t BuOOH feeding rate of 20 mM h⁻¹, product formation rates of 9 mM h⁻¹ were observed but the product accumulation ceased after 4 h. Applying a t BuOOH feeding rate of 1 mM h⁻¹ approximately the same product formation rate was observed, albeit for at least 72 h. Also the formation of the undesired side products decreased considerably with lower t BuOOH feeding rates (Fig. S4.17). Both observations are most likely related to each other. At high t BuOOH feeding rates, the peroxide availability exceeds the enzyme's epoxidation capacity resulting in oxidative inactivation of the heme prosthetic group and release of iron ions. The latter catalyse Fenton-like transformations resulting in non-selective oxidation of the *cis*- β -methylstyrene starting material and formation of the undesired side-products.

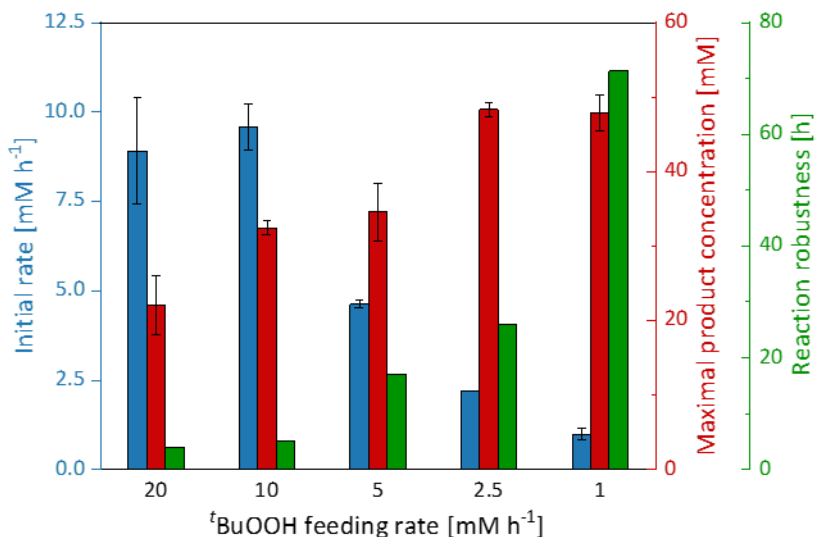


Figure 3.3. Initial rate, maximal product concentration and reaction robustness of the epoxidation of *cis*- β -methylstyrene catalysed by imm-*AaeUPO* at different *t*BuOOH feeding rates. Reaction set-up: 570 mL *cis*- β -methylstyrene, supplemented with 180 mg immobilisate and continuously fed with the indicated *t*BuOOH rate. General reaction conditions: [*AaeUPO*] = 0.5 μ M, room temperature, shaking at 99 rpm with 60° angle in an overhead rotator. Data represents the average of duplicates.

In any case, lowering the *t*BuOOH feeding rate not only increased the robustness of the reaction but also reduced the side-product formation. Under these conditions, 48 mM (6.4 g L⁻¹) of enantiomerically pure (2*R*,3*S*)-2-methyl-3-phenyloxirane have been synthesised within 72 h. This corresponds to excellent TN of 96 000 for the biocatalyst. This catalytic performance also favourably compares to other enzyme systems such as flavin-dependent monooxygenases.^[24-27] Admittedly, the current substrate scope of the proposed immobilised *AaeUPO* preparation is rather limited, preliminary experiments on styrene epoxidation indicate a similar catalytic potential for this substrate (Fig. S4.19). Future experiments will broaden the synthetic scope of the proposed *AaeUPO* preparation.

To obtain a first overview over the environmental impact of the reaction system established in this study, we used Sheldon's E-factor^[28-29] to estimate the wastes generated in the formation of (2*R*,3*S*)-2-methyl-3-phenyloxirane. As shown in Table 3.1, a total of 153.3 kg of waste was generated per kg of the desired product. 70% of the E-factor contribution stems from non-reacted starting material, which in a putative preparative-scale reaction can be recovered via distillation. The second-largest

Chapter 3

contributor (24%) is the enzyme preparation. The latter is mostly comprised of the alginate beads and buffer (making 99% of the total mass of the immobilised enzyme).

Table 3.1. E-Factor analysis of the epoxidation of *cis*- β -methylstyrene to (2*R*,3*S*)-2-methyl-3-phenyloxirane.

Products	(2 <i>R</i> ,3 <i>S</i>)-2-methyl-3-phenyloxirane	4.8
	^t BuOH ^a	41.0
	Various side products ^b	0.9
Reactants	<i>cis</i> - β -Methylstyrene ^c	515.9
	^t BuOOH ^a	0.0
Catalyst	<i>Aae</i> UPO	180.0
E-factor	SUM (waste)	737.9
	SUM (epoxide product)	4.8
	E-factor	153.3

^a It is assumed that all added ^tBuOOH converted into ^tBuOH. The indicated ^tBuOH mass includes decane which was used for dilution of ^tBuOOH. ^b Concentrations and masses of side products were estimated based on the GC calibration line and response factor of (2*R*,3*S*)-2-methyl-3-phenyloxirane. ^c Mass of *cis*- β -methylstyrene after reaction stop is estimated based on formation of epoxide and side products. ^d *Aae*UPO includes imm-*Aae*UPO beads.

3. Conclusion

We are convinced that further optimisation of the immobilisation protocol will improve the *Aae*UPO loading in the alginate beads. For example using alginate-in-oil emulsions for the bead preparation will certainly improve the *Aae*UPO loading.^[30] Also the E-factor contribution of the oxidant and its by-product ^tBuOH, respectively, can be reduced significantly when co-immobilising the formate oxidase from *Aspegillus oryzae* (*Ao*FOX) to use methanol as sacrificial electron donor for the *in situ* generation of H₂O₂.^[31-34] Implementing this system will eliminate the ^tBuOH contribution to E-factor (8.5 kg kg⁻¹) and reduce it to approx. 0.11 kgCO₂ kg_{Product}⁻¹. Overall, in this contribution we have established alginate-confined peroxygenase-CLEAs as practical enzyme preparations for the selective epoxidation of styrene derivatives such as *cis*- β -methylstyrene to synthesise enantiomerically pure epoxides. In terms of catalyst efficiency (more than 90 000 catalytic cycles observed), the current system outperforms comparable reaction systems using chemical catalysts,^[35] P450 monooxygenases^[36] or other established enzymatic systems,^[26-27, 37] also compared to our previous efforts using immobilised *Aae*UPO.^[9] We are convinced that further optimisation will bring this approach to maturity and will establish an economically and environmentally feasible reaction system.

4. Material and methods

4.1 Chemicals and materials

Alginate sodium salt (from brown algae, low viscosity), chitosan (low viscosity), iso-propanol, acetonitrile, ethanol, ammonium sulphate, glutaraldehyde (50% aq. solution), 2,2'-azino-bis(3-ethylbenzothiazoline-6-sulphonic acid) diammonium salt (ABTS), hydrogen peroxide (30% aq. solution), calcium chloride dihydrate, barium chloride, strontium chloride, sodium hydroxide, sodium dithionite, carbon monoxide gas, terephthalaldehyde, formaldehyde, iminodiacetic acid, bovine serum albumin (BSA), super folder green-fluorescent protein (sfGFP), Bradford dye reagent, SDS loading dye, SDS protein ladder, n-heptane, ethyl acetate, triethylamine, silica TLC plate, benzaldehyde, *cis*- β -methylstyrene, decane, tetradecane, phenylacetone, styrene, styrene oxide, phenylacetaldehyde, magnesium sulphate, methyl *tert*-butyl ether, *tert*-butyl hydroperoxide, and further commercial chemicals were purchased from Sigma-Aldrich, Fluka, Alfa-Aesar, Roche, Emsure, Messer and TCI Europe without any further purification. Ultrapure water from Milli-Q was used for all experiments.

4.2 Production of AaeUPO

4.2.1 Enzyme expression and purification

The laboratory-evolved expression variant PaDa-1 of the peroxygenase from *Agrocybe aegerita* (AaeUPO) was heterologously expressed in *Pichia pastoris* and isolated following a previously described procedure.^[15]

4.2.2 SDS-PAGE analysis

AaeUPO (5 μ g) in Tris/HCl buffer (20 mM, pH 7.0) was mixed with 6x SDS loading buffer. Samples were boiled for 10 min at 99 °C and centrifuged for 5 min at 13 000 g. A SDS-PAGE was loaded with 5 μ L AaeUPO and 5 μ L protein ladder. The page was run for 20 min at 80 V and for 1 h at 150 V. Proteins were detected via Coomassie staining.

4.2.3 Bradford assay

General protein concentrations were determined by Bradford assay in 1 mL cuvettes with 20 μ L protein solution in Tris/HCl buffer (20 mM, pH 7.0) and 980 μ L Bradford

Chapter 3

dye reagent. Absorbance was detected at 595 nm in a UV-Vis spectrophotometer. Concentrations were quantified based on a standard curve of horseradish peroxidase.

4.2.4 Determination of *Aae*UPO concentration

Absorbance at 420 nm

As previously described,^[10] the millimolar extinction coefficient $115 \text{ mM}^{-1} \text{ cm}^{-1}$ at 420 nm was used to determine the concentration of purified *Aae*UPO. Herein, the UV-Vis spectrum between 350 nm and 500 nm of different dilutions of purified *Aae*UPO in 1 mL Tris/HCl buffer (20 mM, pH 7.0) was recorded, normalised and evaluated accordingly.

CO difference spectra

To determine the amount of active *Aae*UPO, the extinction coefficient of *Aae*UPO from the ferrous carbon monoxide binding difference spectra (CO difference spectra) was utilised. Purified *Aae*UPO was prepared in 1 mL Tris/HCl buffer (20 mM, pH 7.0) at different dilutions. $\text{Na}_2\text{S}_2\text{O}_4$ was added in a final concentration of 10 mM to reduce the heme-thiolate enzyme. Subsequently, the UV-Vis spectrum between 400 nm and 500 nm was recorded in a UV-Vis spectrophotometer. After saturating the enzyme solution with CO, the spectrum between 400 nm and 500 nm was measured again to record the absorbance shift which occurs due to heme-CO adduct formation in active *Aae*UPO. The millimolar extinction coefficient $107 \text{ mM}^{-1} \text{ cm}^{-1}$ at 445 nm^[38-39] was utilised to calculate the concentration and mass of active imm-*Aae*UPO after normalisation.

4.2.5 ABTS activity assay

Activity of *Aae*UPO and *Aae*UPO-CLEAs

Activity of *Aae*UPO and *Aae*UPO-CLEAs was determined by ABTS assay as describes earlier.^[39] Measurements were performed in 1 mL of 150 mM sodium phosphate citrate buffer at pH 4.4 with 0.3 mM ABTS and 1 mM H_2O_2 . Absorbance

was determined every 6 sec over 60 sec at 420 nm in an UV-Vis spectrophotometer Genesys 150 from Thermo Scientific.

The activities were calculated in U_{ABTS} ($1 U_{ABTS} = 1 \mu\text{mol}_{ABTS} \text{ min}^{-1}$) with the millimolar extinction coefficient of ABTS ($\epsilon_{\lambda} = 36.8 \text{ mM}^{-1} \text{ cm}^{-1}$).

Activity of imm-AaeUPO

Activity of imm-AaeUPO was assayed in 10 mL of 100 mM MES buffer at pH 5 with 0.3 mM ABTS and 1 mM H_2O_2 . Absorbance was measured every 30 sec over 90 sec at 420 nm in UV-Vis spectrophotometer Genesys 150 from Thermo Scientific. The activities were calculated in U_{ABTS} ($1 U_{ABTS} = 1 \mu\text{mol}_{ABTS} \text{ min}^{-1}$) with the millimolar extinction coefficient of ABTS ($\epsilon_{\lambda} = 36.8 \text{ mM}^{-1} \text{ cm}^{-1}$).

Recovered activities

Recovered activities of agg-AaeUPO and imm-AaeUPO were calculated with use of the starting AaeUPO mass in mg and expressed in percentage:

$$\text{Recovered activity of agg-AaeUPO [\%]} = \frac{\text{agg-AaeUPO activity [} U_{ABTS} \text{ mg}_{AaeUPO}^{-1} \text{]}}{\text{AaeUPO starting activity [} U_{ABTS} \text{ mg}_{AaeUPO}^{-1} \text{]}} \times 100$$

$$\text{Recovered activity of imm-AaeUPO [\%]} = \frac{\text{imm-AaeUPO activity [} U_{ABTS} \text{ mg}_{AaeUPO}^{-1} \text{]}}{\text{AaeUPO starting activity [} U_{ABTS} \text{ mg}_{AaeUPO}^{-1} \text{]}} \times 100$$

4.3 Optimisation of the enzyme immobilisation process

4.3.1 Optimised protocol for the preparation of imm-AaeUPO

5 mg AaeUPO (112.6 nmol) were diluted in a volume of 2.5 mL Tris/HCl buffer (20 mM, pH 7) containing 10 mg low-viscosity chitosan. The solution was precipitated with 9 times the volume iso-propanol (22.5 mL) and cross-linked with 5000 molar protein equivalents of glutaraldehyde (563 μmol).

After 2 h of incubation, the samples of AaeUPO-CLEAs were centrifuged for 5 min at 4000 rpm, 4 °C and the supernatant was discarded. The pellet was washed with 5 mL Tris/HCl buffer (20 mM, pH 7) and resuspended in 500 μl Tris/HCl buffer (20 mM, pH 7). The resuspended AaeUPO-CLEAs were clarified with a 40 μm sieve. A solution of 2.5% (w/v) low viscosity alginate in MilliQ water was prepared and purified by filtration through a 5 μm membrane filter. The 500 μl AaeUPO-CLEAs were mixed with 9.5 mL of alginate solution.

Chapter 3

For preparation of the imm-*AaeUPO* alginate beads, a semi-automated encapsulator (Encapsulation Unit VAR-J30 from Nisco Engineering Inc.) was used with the following parameters: frequency 3.35 kHz, amplitude 0%, 21 hPa, 4.34 mA. The prepared alginate-enzyme suspension was transferred into a 20 mL syringe and extruded through a 150 μm diameter nozzle with 3.3 mL min^{-1} speed. The droplets were captured in 100 mL of 100 mM CaCl_2 hardening solution under constant agitation. After 30 min of hardening, the imm-*AaeUPO* alginate beads were collected with a 40 μm sieve and washed with 10 mL of 5 mM CaCl_2 washing solution. imm-*AaeUPO* was stored in Tris/HCl buffer (20 mM, pH 7) containing 5 mM CaCl_2 at 4°C.

4.3.2 Optimisation of the precipitation reagent

To determine the optimal precipitation reagent, 1 mg *AaeUPO* (22.5 nmol) was diluted in a volume of 500 μL Tris/HCl buffer (20 mM, pH 7). The solution was precipitated with 9 volumes of iso-propanol, acetonitrile, ethanol, or saturated ammonium sulphate solution. Afterwards, 5000 times molar excess (112.6 μmol) of glutaraldehyde was added. In addition, the same experiment was conducted without any precipitation reagent.

After 2 h of incubation, the samples of *AaeUPO*-CLEAs were treated as described in the optimised protocol. After clarification, activity of the *AaeUPO*-CLEAs was determined by ABTS assay and expressed as recovered activity relative to free *AaeUPO*.

4.3.3 Optimisation of the aggregation reagent

In order to determine the optimal cross-linking protocol, five different aggregation reagents were tested. 1 mg *AaeUPO* (22.5 nmol) was diluted in a volume of 500 μL Tris/HCl buffer (20 mM, pH 7). The solution was precipitated with 9 volumes of iso-propanol (4.5 mL) and aggregated with glutaraldehyde, terephthalaldehyde, starch oxide/ polyaldehyde starch, formaldehyde, or iminodiacetic acid. All aggregation reagents were applied in 5000 times molar excess (112.6 μmol) compared to *AaeUPO*.

In addition, the same experiment was conducted without adding any aggregation reagent. All subsequent steps follow the optimised protocol. Activity of the resulting immobilisates was tested by ABTS assay and expressed in $U_{\text{ABTS}} \text{g}^{-1} \text{wet beads}$.

The starch oxide/ polyaldehyde starch was freshly prepared as the following:^[40-41] 5 mL of a 0.7 M solution of NaIO₄ was brought to pH 4.0 by addition of sulfuric acid. Starch was added to reach a 1:1 molar ratio with NaIO₄ (568 mg of starch). The solution was constantly stirred at 37°C – 40°C during the addition. After stirring for 3 – 4 h at 37°C – 40°C, acetone was added to the solution. The precipitate was washed with solvent and water, and subsequently dried to recover a white powder of oxidized starch.

4.3.4 Optimisation of the co-aggregator

1 mg AaeUPO (22.5 nmol) was diluted in a volume of 500 µL Tris/HCl buffer (20 mM, pH 7). Bovine serum albumin (BSA) and chitosan were tested separately and in combination as co-aggregators. The compounds were used in double the quantity (2 mg) of AaeUPO and added to the prepared solution. In addition, the same experiment was performed without addition of a co-aggregator. The mixture was precipitated with 9 times the volume iso-propanol (4.5 mL) and aggregated with 5000 molar protein equivalents of glutaraldehyde (112.6 µmol / 22.5 µL of a 50% stock). All subsequent steps follow the optimised protocol. Activity of the resulting immobilisates was tested by ABTS assay and expressed in U_{ABTS} g⁻¹_{wet beads}.

4.3.5 Optimisation of the glutaraldehyde concentration

1 mg AaeUPO (22.5 nmol) and 2 mg chitosan were diluted in a volume of 500 µL Tris/HCl buffer (20 mM, pH 7). The mixture was precipitated with 9 times the volume iso-propanol (4.5 mL). To test different concentrations of the aggregation reagent glutaraldehyde, 500 molar AaeUPO equivalents, 5000 molar AaeUPO equivalents, and 50 000 molar AaeUPO equivalents were used for aggregation of the protein-chitosan mix. All subsequent steps follow the optimised protocol. Activity of the resulting immobilisates was tested by ABTS assay and expressed in U_{ABTS} g⁻¹_{wet beads}.

4.3.6 Optimisation of the catalyst loading

In order to determine the optimal catalyst loading, the immobilisation of 1 mg, 2 mg, 5 mg and 10 mg AaeUPO was analysed. 1 mg / 2 mg / 5 mg / 10 mg AaeUPO and 2 mg / 4 mg / 10 mg / 20 mg chitosan were diluted in a volume of 500 µL / 1 mL / 2.5 mL / 5 mL Tris-HCl buffer (20 mM, pH 7). The mixture was precipitated with 9 times the volume iso-propanol and aggregated with 5000 molar protein equivalents of

Chapter 3

glutaraldehyde. All subsequent steps follow the optimised protocol. Activity of the resulting immobilisates was tested by ABTS assay and expressed in $U_{ABTS} \text{ g}^{-1}_{\text{wet beads}}$. Moreover, recovered activity relative to free *AaeUPO* was determined.

4.3.7 Optimisation of the alginate concentration

Resuspended *AaeUPO*-CLEAs were prepared as given in the optimised protocol and clarified with a 40 μm sieve. Solutions of 2.5%, 3%, 3.5%, and 4% low viscosity alginate in MilliQ water were prepared and purified by filtration through a 5 μm membrane filter. The 500 μL *AaeUPO*-CLEAs were mixed with 9.5 mL of the alginate solutions. All subsequent steps follow the optimised protocol. Activity of the resulting immobilisates was tested by ABTS assay and expressed in $U_{ABTS} \text{ g}^{-1}_{\text{wet beads}}$.

4.3.8 Optimisation of the counterions

An alginate-enzyme suspension was prepared as described in the optimised protocol. It was transferred into a 20 mL syringe and extruded through a 150 μm diameter nozzle with 3.3 mL min^{-1} speed using a semi-automated encapsulator set-up as outlined in the optimised protocol. In order to test the effect of counterions used for hardening of the alginate beads, 50 mM CaCl_2 , 100 mM CaCl_2 , 200mM CaCl_2 , 100mM BaCl_2 , and 100 mM SrCl_2 were examined as hardening solutions. The alginate-enzyme droplets were captured in 100 mL of these solutions under constant agitation. After 30 min of hardening, the imm-*AaeUPO* alginate beads were collected with a 40 μm sieve and washed with 10 mL of 5 mM CaCl_2 , 5mM BaCl_2 , or 5 mM SrCl_2 washing solution. imm-*AaeUPO* was stored in 20 mM Tris/HCl buffer (pH 7) containing 5 mM CaCl_2 , 5mM BaCl_2 , or 5 mM SrCl_2 at 4°C. Activity of the resulting immobilisates was tested by ABTS assay and expressed in $U_{ABTS} \text{ g}^{-1}_{\text{wet beads}}$.

4.3.9 Optimisation of the alginate bead diameter

The immobilisation was performed as described in the optimised protocol. Next to using a 150 μm diameter nozzle in the semi-automated encapsulation unit, nozzles of 50 μm , 100 μm , 200 μm , and 400 μm diameter were utilised to examine the effect of beads size on the immobilisation efficiency.

For manual preparation of imm-*AaeUPO*, an alginate-enzyme suspension was prepared as described in the optimised protocol and was transferred into a 20 mL syringe connected to a 0.5 mm x 16 mm cannula. With use of a syringe pump, the

alginate-enzyme suspension was extruded at a constant speed of 3.3 mL min⁻¹. The droplets were captured in 100 mL of 100 mM CaCl₂ hardening solution under constant agitation. Hardening, washing, and storage were performed as in the optimised protocol. Activity of all resulting immobilisates was tested by ABTS assay and expressed in U_{ABTS} g⁻¹_{wet beads}.

4.4 Determination of immobilisation efficiency

4.4.1 Determination of the immobilisation yield

The immobilisation yield was obtained by using two different approaches. First, the general AaeUPO concentration within the immobilisates was quantified with use of the millimolar extinction coefficient at 420 nm. Moreover, the concentration of active heme-sites inside imm-AaeUPO was determined by CO difference spectra.

Herein, 200 mg of dry imm-AaeUPO beads were dissolved in 5 mL of 150 mM sodium phosphate citrate buffer at pH 4.4 and incubated for 30 min. The solution was neutralised with NaOH and the concentration of AaeUPO inside the solution was determined with use of the millimolar extinction coefficient at 420 nm. Afterwards, the solution was concentrated to a volume of 1 mL using a centrifugal filter unit Ultra-4 with 10 kDa molecular weight cut-off from Amicon. The AaeUPO concentration inside the resulting solution was quantified by CO difference spectra. The immobilisation yield was determined relative to the starting mass of AaeUPO of 5 mg:

$$\text{Immobilisation yield [\%]} = \frac{\text{Mass of imm-AaeUPO [mg]}}{\text{Starting mass of AaeUPO [mg]}} \times 100$$

4.4.2 Analysis of storage stability

A sample of imm-AaeUPO alginate beads as well as AaeUPO enzyme stock was stored at 4°C and at room temperature and activity over time was tracked by ABTS assay. The stability was calculated in percentage:

$$\text{Stability [\%]} = \frac{\text{Activity at sample timepoint [U mg}_{\text{AaeUPO}}^{-1}\text{]}}{\text{Starting activity [U mg}_{\text{AaeUPO}}^{-1}\text{]}}$$

4.4.3 Light and fluorescence microscopy

Samples analysed by light microscopy were prepared following the optimized immobilisation protocol. Samples for fluorescence microscopy were prepared respectively with the following deviations from the protocol: 1 mg sfGFP^[42] was

Chapter 3

diluted in a volume of 300 μL Tris/HCl buffer (20 mM, pH 7). The suspension was clarified with a 40 μm sieve. A solution of 2.5% low viscosity alginate in MilliQ water was prepared and purified by filtration through a 5 μm membrane filter. The 300 μL GFP was mixed with 4.7 mL of alginate solution.

Light microscopy pictures were taken with use of the white light channel of Microscope Axio Observer A1 from ZEISS. Fluorescence microscopy pictures were taken as overlay of the white light channel and GFP channel. Size measurement was performed with the inbuilt ZEISS software.

4.5 Gas chromatography (GC)

4.5.1 Chemical synthesis of GC standard 2-methyl-3-phenyloxirane

In order to serve as standard chemical for analytics, racemic 2-methyl-3-phenyloxirane was synthesised as previously described.^[9] After synthesis, qualitative analysis of the product purity was performed with Thin-Layer-Chromatography (TLC). Herein, silica TLC plate was used as solid phase. A 98:2 mixture of n-heptane and ethyl acetate including 1% triethylamine for basification of the silica TLC plate was used as mobile phase.

Purification of the product mixture was undertaken with an automated Reveleris X2 flash purification system. A 4 g Reveleris silica column was used as solid phase and a 98:2 mixture of n-heptane and ethyl acetate including 1% triethylamine was used as single mobile phase at 15 mL min⁻¹ flow rate. Product fractions were collected within the first 3 minutes and analysed by TLC and gas chromatography. Fractions with high purity were pooled and remaining solvent was evaporated using a rotary vacuum evaporator.

4.5.2 GC for *cis*- β -methylstyrene epoxidation

Product mixtures of *cis*- β -methylstyrene epoxidation were analysed using a Shimadzu GC-2014 gas chromatograph with a flame ionization detector and a CP Sil 5 CB column (dimensions: 50.0 m x 0.53 mm x 1.00 μm nominal). Carrier gas: Nitrogen; Column flow: 20 mL/min. The utilised temperature profile and retention times of all analysed compounds are given in the following (Table S3.1).

Concentrations of 2-methyl-3-phenyloxirane, benzaldehyde and phenylacetone were quantified based on calibration lines and with use of an internal standard tetradecane. Calibration lines were set up in duplicates by preparing respective concentrations

including 100 mM tetradecane in styrene as solvent. 5 μL of this mixture was diluted in 1 mL of methyl *tert*-butyl ether and dried with MgSO_4 before GC analysis. Commercially available standard chemicals were used for the calibration lines of benzaldehyde and phenylacetone. For 2-methyl-3-phenyloxirane, a self-synthesised standard was used. In all cases, standard purities based on peak area ratios were taken into account by only using the peak area at expected retention times for the calibration lines.

Table S3.1. Overview on the standard method for GC analysis of the *cis*- β -methylstyrene epoxidation reactions.

Rate ($^{\circ}\text{C min}^{-1}$)	Temp ($^{\circ}\text{C}$)	Hold (min)
-	70	5
30	80	3
30	106	4
30	160	2
30	340	1
Compound	Retention time (min)	
Benzaldehyde (by-product)	6.32	
<i>cis</i> - β -Methylstyrene (substrate)	7.37	
Decane (solvent of $t\text{BuOOH}$)	7.92	
By-product A	8.71	
2-methyl-3-phenyloxirane (product)	10.51	
By-product B	10.82	
Phenylacetone (by-product)	11.15	
By-product C	14.16	
By-product D	14.82	
By-product E	15.23	
By-product F	15.46	
Tetradecane (internal standard)	16.38	

4.5.3 Chiral GC for *cis*- β -methylstyrene epoxidation

To determine enantiomeric excess (ee), product mixtures of *cis*- β -methylstyrene epoxidation were analysed as previously described[9] by chiral GC (Shimadzu GC-2010) with a flame ionization detector and a Lipodex E 1b (Macherey-Nagel) column (dimensions: 50.0 m \times 0.25 mm \times 0.25 μm). Carrier gas: Helium; Column flow:

Chapter 3

2.16 mL/min; Split ratio: 100; Linear velocity: 38 cm/s. The utilised temperature profile and retention times of all analysed compounds are given in the following (Table S3.2). Enantiomers were quantified by peak area integration and the *ee* was calculated as:

$$ee = \frac{\text{peak area (R)} - \text{peak area (S)}}{\text{peak area (R)} + \text{peak area (S)}} \times 100\%$$

Table S3.2. Overview on the method for chiral GC analysis of the *cis*- β -methylstyrene epoxidation reactions.

Rate (°C min ⁻¹)	Temp (°C)	Hold (min)
-	100	15
20	220	1
Compound	Retention time (min)	
Styrene (solvent of epoxide)	4.00	
<i>cis</i> - β -Methylstyrene (substrate)	5.20	
(2 <i>R</i> ,3 <i>S</i>)-2-methyl-3-phenyloxirane (product)	10.31	
(2 <i>S</i> ,3 <i>R</i>)-2-methyl-3-phenyloxirane (product)	13.24	
Tetradecane (internal standard)	18.21	

4.5.4 GC for styrene epoxidation

Product mixtures of styrene epoxidation were analysed by chiral GC (Gas chromatography GC System 6890 Series from Agilent) with a flame ionization detector and a CP-Chiasil-Dex-CB column from Agilent (dimensions: 25.0 m x 250 μ m x 0.25 μ m nominal). Helium served as carrier gas and the injection volume was 5 μ L. Product formation was determined as GC conversion, obtained with peak area integrations of the product mixture. The utilised temperature profile and retention times of all analysed compounds are given in the following (Table S3.3).

Table S3.3. Overview on the standard method for GC analysis of the styrene epoxidation reactions.

Rate (°C min ⁻¹)	Temp (°C)	Hold (min)
-	70	1
20	200	1
Compound	Retention time (min)	
Styrene (substrate)	3.10	

Styrene oxide and phenylacetaldehyde (products)	approx. 4.83
Tetradecane (internal standard)	6.21

4.6 Enzymatic epoxidation reactions

4.6.1 Epoxidation of *cis*- β -methylstyrene

The reaction was performed in small GC vials at room temperature, shaking at 99 rpm with 60° angle in an overhead rotator (Figure S3.1). *tert*-Butyl hydroperoxide (t BuOOH) was fed continuously with use of a syringe pump and 1 mL syringes which were connected with tubes to the reaction vials.

Before start of the reaction, *cis*- β -methylstyrene was supplemented with 100 mM tetradecane as internal standard and saturated with Tris/HCl buffer (20 mM, pH 7). Moreover, a 5 M stock of t BuOOH in decane was supplemented with 100 mM internal standard tetradecane. If further dilution of t BuOOH was required, decane was used as solvent.

A GC vial was prepared with 0.5 μ M *Aae*UPO. For the case of imm-*Aae*UPO, 180 mg of carefully dried immobilisates were utilised. For the case of free *Aae*UPO in a two liquid phase system, 0.5 μ M enzyme was prepared in an aqueous phase of 180 μ L Tris/HCl buffer (20 mM, pH 7). For the case of free *Aae*UPO in a micro-aqueous system, 0.5 μ M enzyme was prepared in an aqueous phase of 6.6 μ L Tris/HCl buffer (20 mM, pH 7).



Figure S3.1. Reaction set-up for the enzymatic epoxidation of *cis*- β -methylstyrene. On the left, syringe pumps for continuous t BuOOH supply. Syringes are connected to tubes which lead to the reaction mixture inside GC vials on the right.

Chapter 3

An overhead rotator is used for shaking of the reaction at 99 rpm, 60° at room temperature.

To start the reaction, the prepared *cis*- β -methylstyrene was added to the GC vial to reach a final volume of 750 μ L. Subsequently, the vials were connected to the continuous $^4\text{BuOOH}$ feed. The utilised feed rate is indicated in the caption of the respective figures. 5 μ L samples were taken at indicated time points, diluted in 1 mL methyl *tert*-butyl ether, and dried with MgSO_4 . Product mixtures were analysed by gas chromatography. Turnover frequencies (TOF) and turnover numbers (TN) were calculated as the following:

$$\text{TOF [s}^{-1}] = \frac{\text{Concentration of product [mM]}}{\text{Concentration of enzyme [mM]} \times \text{time [s]}}$$

$$\text{TN} = \frac{\text{Concentration of product [mM]}}{\text{Concentration of enzyme [mM]}}$$

4.6.2 Epoxidation of styrene

Continuous $^4\text{BuOOH}$ feed

The same set-up as for the epoxidation of *cis*- β -methylstyrene was used. Styrene was prepared with 2% internal standard tetradecane and saturated with Tris/HCl buffer (20 mM, pH 7). If required, dilution of $^4\text{BuOOH}$ was performed with decane as solvent. A GC vial was prepared with 0.8 μM carefully dried imm-*AaeUPO* beads. 1 mL of styrene was added into the vial. The reaction was started with a pulse of $^4\text{BuOOH}$ of 1 mM final concentration. Subsequently, the vials were connected to the continuous $^4\text{BuOOH}$ feed. The feed rate during the biotransformation is indicated in the caption of the respective figures. Samples were taken at indicated time points, diluted in 1 mL methyl *tert*-butyl ether, dried with MgSO_4 , and analysed by gas chromatography.

$^4\text{BuOOH}$ pulse feeding

Styrene and $^4\text{BuOOH}$ were prepared as for the reactions with continuous feed. 0.2 μM *AaeUPO* were provided in a GC vial as carefully dried imm-*AaeUPO* or in a micro-aqueous system with 2 μL phase of Tris/HCl buffer (20 mM, pH 7). 500 μL of styrene

were added and the reaction was started with the addition of $t\text{BuOOH}$ in pulses of 1.25 mM final concentration every 15 min. Samples were taken at indicated time points, diluted in 1 mL methyl *tert*-butyl ether, dried with MgSO_4 , and analysed by gas chromatography.

4.6.3 E-factor analysis

The E-factors were calculated according to literature[10]. All waste that was produced during a reaction was taken into account, including water:

$$\text{E-factor} = \frac{\sum m_{\text{wastes}} [\text{kg}]}{m_{\text{product}} [\text{kg}]}$$

4.7 Supporting Results

4.7.1 Production of *AaeUPO*

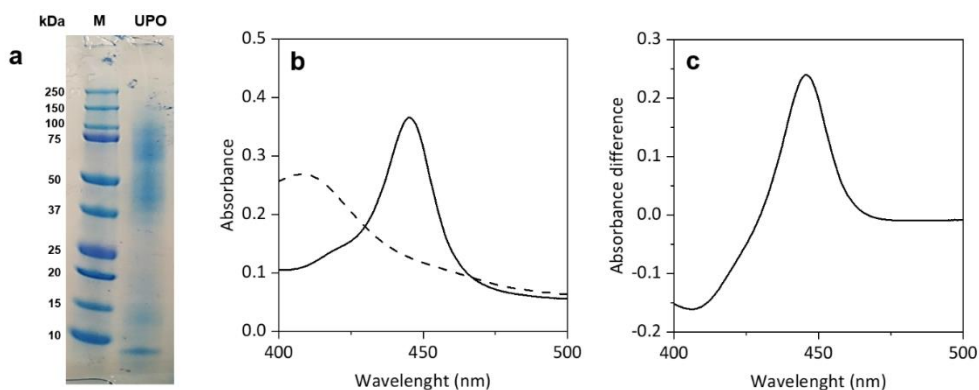


Figure S3.2. General characterisation of *AaeUPO*. (a) SDS-PAGE analysis of purified *AaeUPO*. M = molecular weight marker; UPO = *AaeUPO*. Expected molecular weight of *AaeUPO* is 44.4 kDa.[1] [11] (b) Spectra of purified *AaeUPO* after reduction with $\text{Na}_2\text{S}_2\text{O}_4$ (dashed line) and after incubation with carbon monoxide (solid line). (c) CO difference spectra of purified *AaeUPO*.

4.7.2 Immobilisation of *AaeUPO*

Optimisation of CLEA formation: precipitation

Iso-propanol was selected as optimal precipitation reagent due to a high recovered activity, its easy handling, and its low hazardousness.

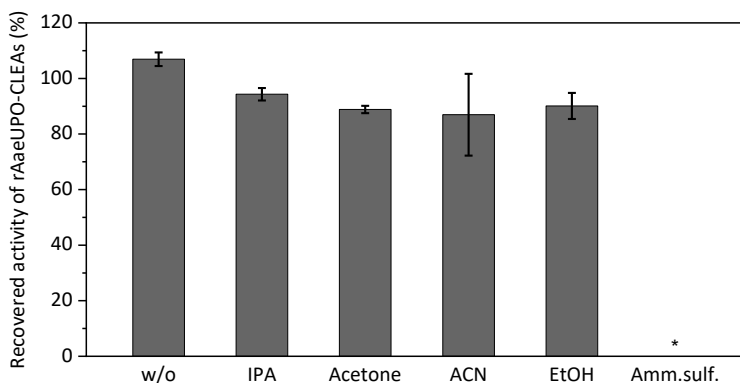


Figure S3.3. Selection of the optimal precipitation reagent, used for precipitation prior to CLEA formation. Recovered activity of *AaeUPO*-CLEAs after precipitation with different precipitation reagents was determined relative to free *AaeUPO* by ABTS-activity assay in aqueous environment. w/o = no precipitation reagent; IPA = iso-propanol; ACN = acetonitrile; EtOH = ethanol; Amm.sulf. = saturated ammonium sulphate solution. At conditions, indicated with asterisk (*), no enzyme precipitation was observed. Data represents an average of duplicates.

Optimisation of CLEA formation: cross-linking

5000 molar equivalents of glutaraldehyde were chosen for cross-linking and chitosan was selected as co-aggregator since respective immobilisates yielded highest ABTS oxidation activities.

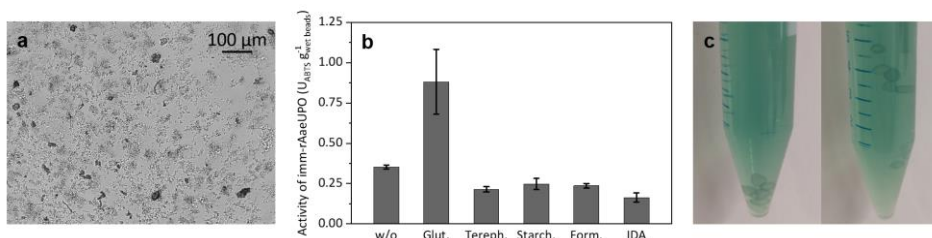


Figure S3.4. Formation of *AaeUPO*-CLEAs. (a) Resuspended and clarified *AaeUPO* CLEAs, prepared with glutaraldehyde. (b) Absolute activity of imm-*AaeUPO* prepared with different aggregation reagents, determined by ABTS-activity assay in aqueous environment. Glut. = glutaraldehyde; Tereph. = Terephthalaldehyde; Starch. = starch oxide/ polyaldehyde starch; Form. = formaldehyde; IDA = iminodiacetic acid; w/o = no aggregation reagent as control. Data represents an average of duplicates. (c) ABTS oxidation product accumulates at the outer layer of the imm-*AaeUPO* beads. Here, beads with 2 mm diameter were used.

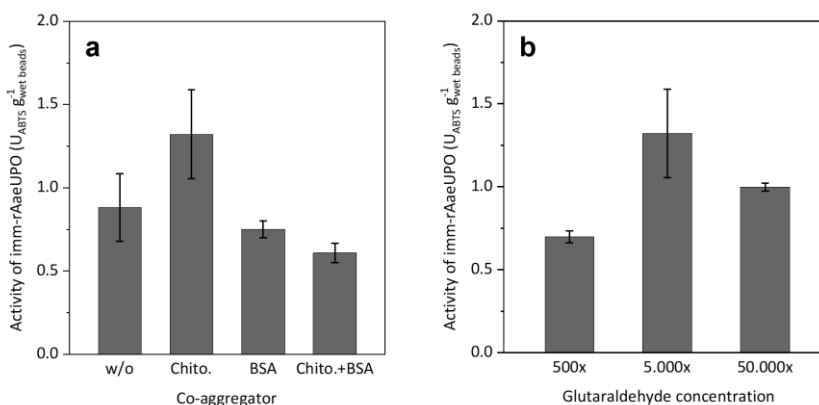


Figure S3.5. Optimisation of AaeUPO cross-linking. Activity of imm-AaeUPO at different immobilisation conditions, determined by ABTS-activity assay in aqueous environment. Data represents an average of duplicates. (a) Selection of the optimal co-aggregator. w/o = no co-aggregator as control; Chito. = chitosan. (b) Optimisation of glutaraldehyde concentration. 'x' indicates molar equivalents of enzyme.

Optimisation of alginate confinement: catalyst loading

An enzyme loading of $0.5 \text{ mg}_{\text{Protein}} \text{ g}_{\text{beads}}^{-1}$ was used in the optimised immobilisation protocol.

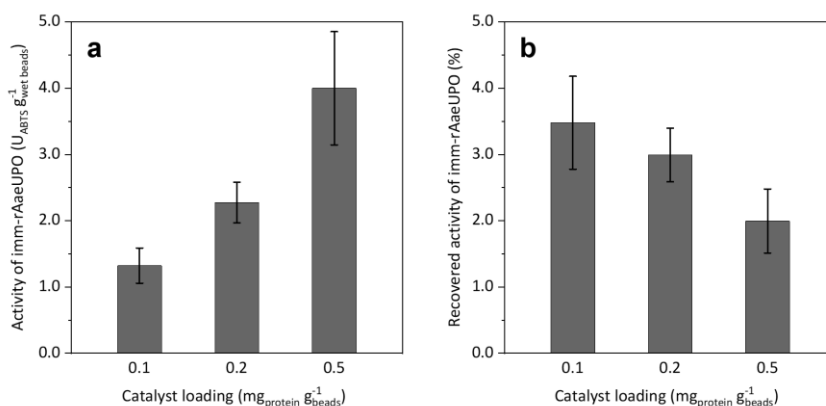


Figure S3.6. Optimisation of imm-AaeUPO enzyme loading. Activities of imm-AaeUPO at different loadings of AaeUPO were determined by ABTS-activity assay in aqueous environment. Data represents an average of duplicates. Catalyst loading of $1 \text{ mg}_{\text{Protein}} \text{ g}_{\text{beads}}^{-1}$ did not yield functional catalyst beads. (a) Absolute activity of imm-AaeUPO. (b) Recovered activity of imm-AaeUPO, determined relative to free AaeUPO.

Chapter 3

Optimisation of alginate confinement: alginate concentration and counter ions

In the final immobilisation protocol, 2.5% alginate was utilised and 100 mM CaCl₂ was used for hardening of the immobilisates.

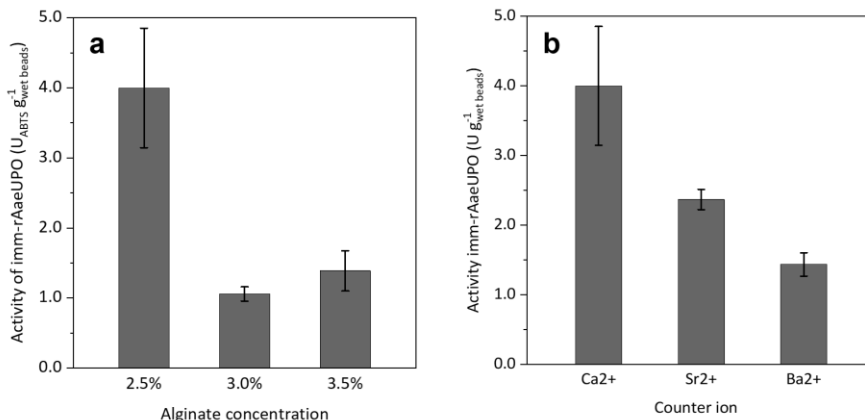


Figure S3.7. Influence of alginate concentration and counter ions on alginate confinement. Activity of imm-AaeUPO at different immobilisation conditions, determined by ABTS-activity assay in aqueous environment. Data represents an average of duplicates. (a) Selection of the optimal alginate concentration. 4% alginate concentration did not yield functional catalyst beads. (b) Determination of the most suited counter ion.

Diameter of the immobilisate

In the final immobilisation protocol, imm-AaeUPO beads of 440 μm diameter were prepared as they were most homogeneous in size and shape. Moreover, an even distribution of protein inside the alginate beads was observed after encapsulating non-cross linked GFP.

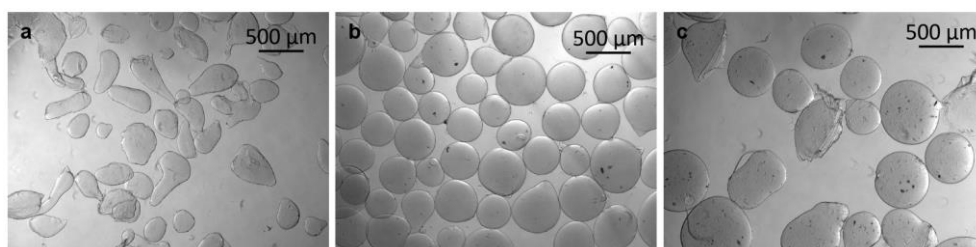


Figure S3.8. Shape and size of imm-AaeUPO beads of different diameters. Since a semi-automated encapsulation unit was used for the preparation of the enzyme alginate beads, the beads size could be controlled by the choice of the nozzle diameter. (a) 100 μm nozzle diameter yielded 290 μm diameter beads; (b) 150 μm nozzle diameter yielded 440 μm diameter beads; (c) 200 μm nozzle diameter yielded 570 μm diameter beads. For 50 μm and 400 μm nozzle diameter, the formation of alginate beads was not possible.

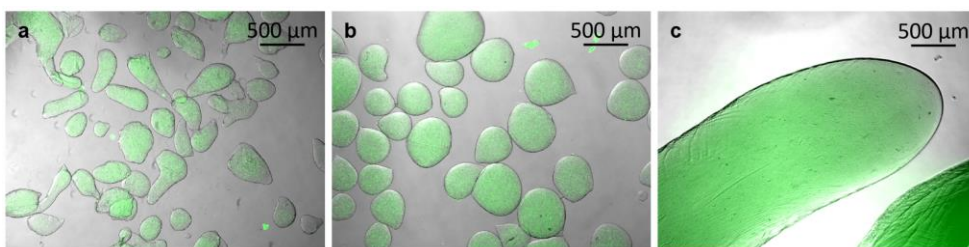


Figure S3.9. Encapsulation of GFP visualised by fluorescence microscopy. Free GFP was confined in calcium alginate beads of different diameters. (a) 290 μm diameter beads; (b) 440 μm diameter beads; (c) 2 mm diameter beads.

4.7.3 Immobilisation efficiency

Table S3.4. Key values of the immobilisation efficiency. Data represented an average of duplicates.

	Key value [%]
Immobilisation yield of imm-AaeUPO ^[a]	18.5 \pm 4.0
Immobilisation yield of imm-AaeUPO ^[b]	18.7 \pm 3.1
Relative specific activity of imm-AaeUPO ^[c]	11.4 \pm 2.2
Recovered activity of AaeUPO-CLEAs	47.8 \pm 3.8
Recovered activity of imm-AaeUPO	2.1 \pm 0.4

^[a] Yield determined leveraging the absorbance peak of AaeUPO at 420 nm for the total concentration of AaeUPO.

^[b] Yield determined as active heme sites inside imm-AaeUPO by CO-differential spectra.

^[c] Specific activity for ABTS oxidation in aqueous environment was 44.4 $\text{U}_{\text{ABTS}} \text{mg}^{-1} \text{protein}$. Here, expressed relative to free AaeUPO.

Chapter 3

4.7.4 Storage stability of imm-AaeUPO

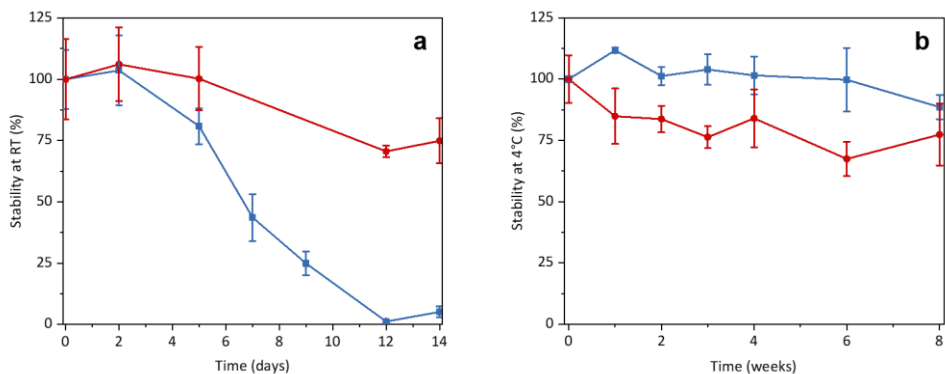


Figure S3.10. Storage stability of imm-AaeUPO. The stability during storage of immobilisate (red circles) was analysed in comparison to the storage stability of free AaeUPO (blue squares). Data was obtained by ABTS-activity assay in aqueous environment and represents an average of triplicates. (a) Storage at room temperature for 14 days. (b) Storage at 4 °C for 8 weeks.

4.7.5 Epoxidation of *cis*- β -methylstyrene

Synthesis of epoxide standard

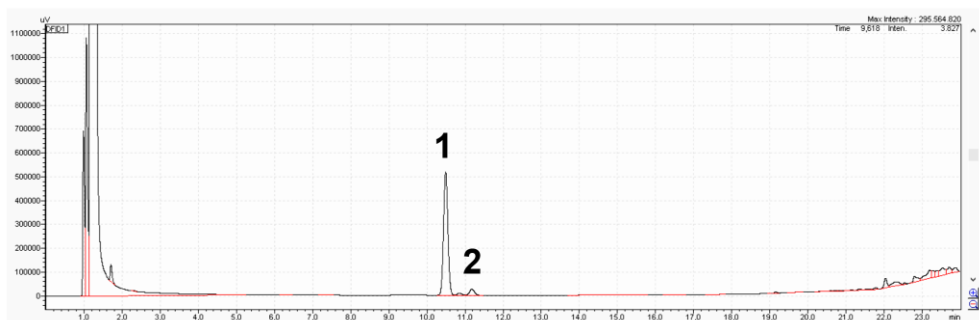


Figure S3.11. GC chromatogram of the synthesised standard chemical 2-methyl-3-phenyloxirane (racemic) after purification. 1 = 2-methyl-3-phenyloxirane; 2 = phenylacetone. Final purity of about 90% was estimated based on peak area ratio.

Enzymatic epoxidation of *cis*- β -methylstyrene

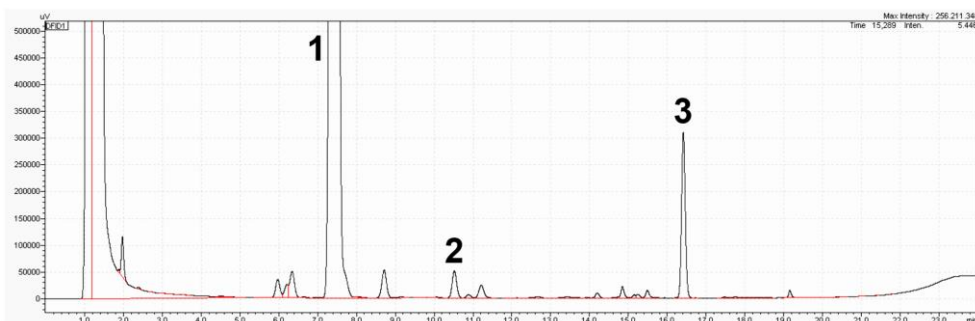


Figure S3.12. Example GC chromatogram for the epoxidation of *cis*- β -methylstyrene. Here, the reaction catalysed by imm-*AaeUPO* with 10 mM h^{-1} t BuOOH feed is shown. 1 = *cis*- β -Methylstyrene; 2 = (2*R*,3*S*)-2-methyl-3-phenyloxirane; 3 = Tetradecane (internal standard).

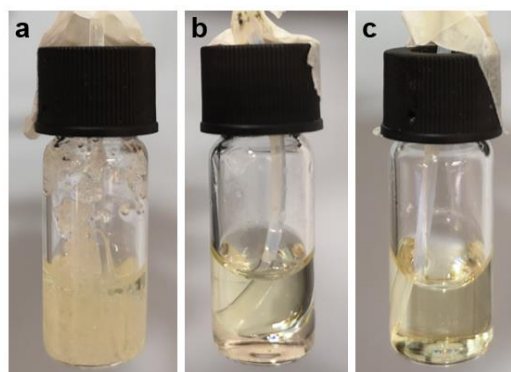


Figure S3.13. Visual comparison of the three reaction systems. (a) 180 mg imm-*AaeUPO* immobilisates dispersed in 570 μ L *cis*- β -methylstyrene. (b) Two liquid phase system with free *AaeUPO* in 180 μ L buffer (bottom phase) and 570 μ L *cis*- β -methylstyrene (top phase). (c) Micro-aqueous system with free *AaeUPO* in 6.6 μ L buffer (small droplets on the bottom of the flask) and 743.4 μ L *cis*- β -methylstyrene.

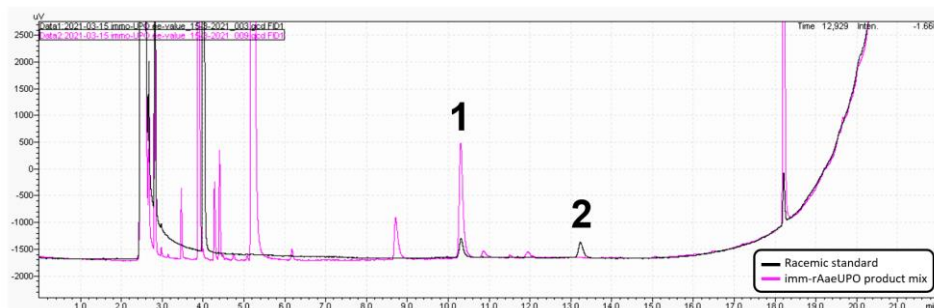


Figure S3.14. Chromatogram of the chiral GC analysis of an imm-*AaeUPO* product mixture. The epoxidation of *cis*- β -methylstyrene with 1 mM h^{-1} t BuOOH feed was analysed

Chapter 3

after 72 h. Black = Chemically synthesised racemic standard; Pink = imm-AaeUPO product mix; 1 = (2*R*,3*S*)-2-methyl-3-phenyloxirane; 2 = (2*S*,3*R*)-2-methyl-3-phenyloxirane.

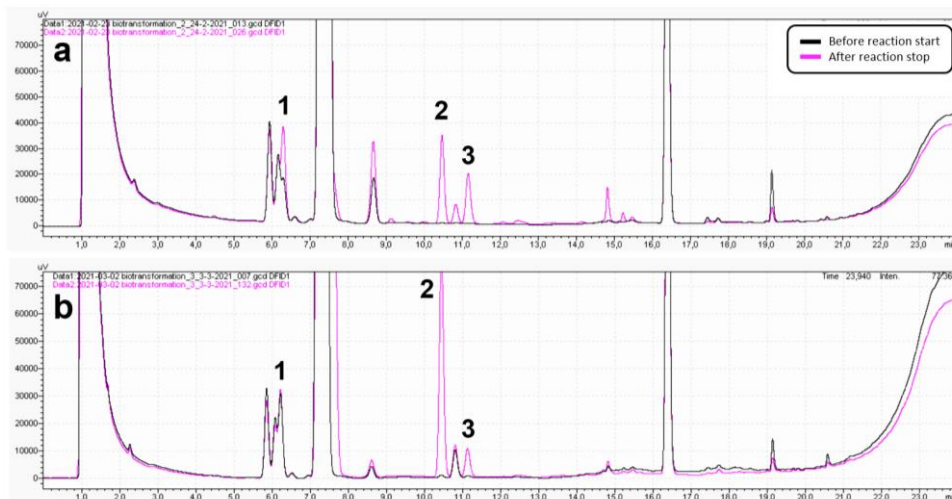


Figure S3.15. GC chromatograms of side product formation in the epoxidation of *cis*- β -methylstyrene catalysed by imm-AaeUPO. 1 = Benzaldehyde; 2 = (2*R*,3*S*)-2-methyl-3-phenyloxirane; 3 = Phenylacetone. (a) Using 20 mM h⁻¹ tBuOOH as oxidant. The reaction mixture was analysed before start of the reaction (black) and after its stop at 4 h (pink). (b) Using 1 mM h⁻¹ tBuOOH as oxidant. The reaction mixture was analysed before start of the reaction (black) and after its stop at 72 h (pink).

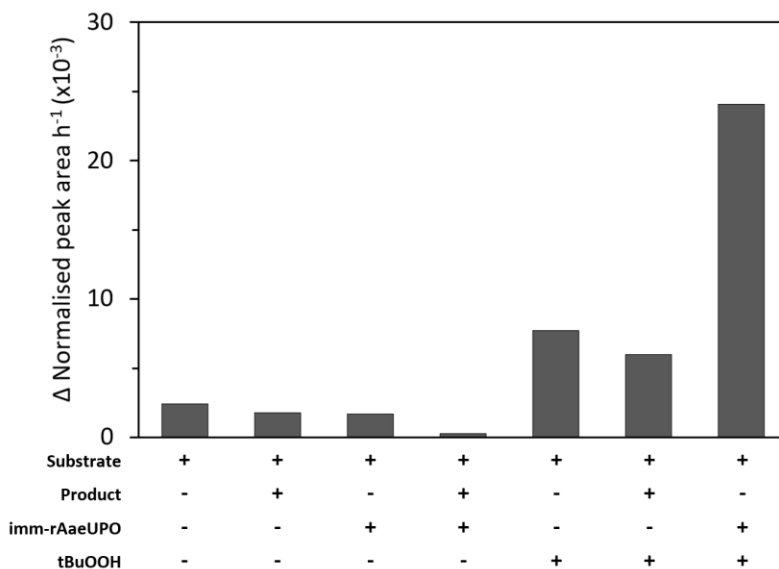


Figure S3.16. Control experiments to determine influencing factors of side product formation. Different components of the reaction mixture were incubated for 24 h and the change of normalised peak area h⁻¹ of all observed side products was determined. Each bar

represents side product(s) formation rate. Substrate = *cis*- β -methylstyrene; Product = (2*R*,3*S*)-2-methyl-3-phenyloxirane (10 mM); [imm-*Aae*UPO] = 0.5 μ M; [*t*BuOOH] = 10 mM h⁻¹.

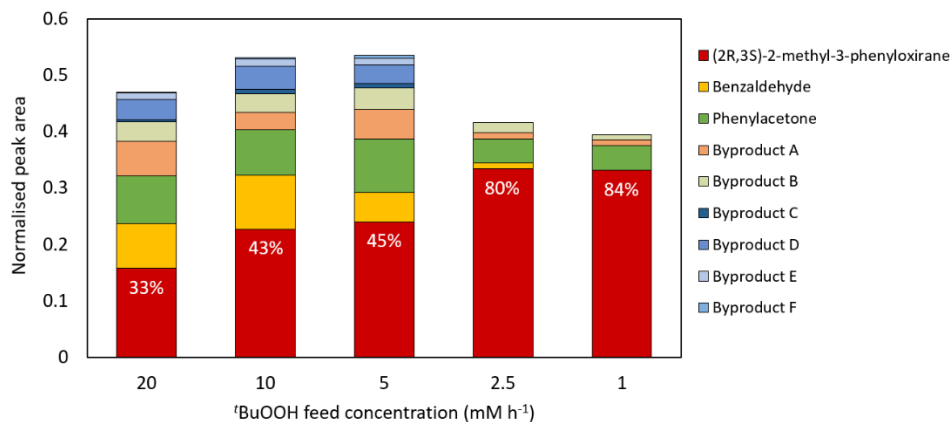
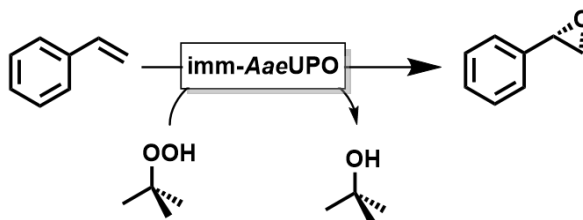


Figure S3.17. Product spectrum based on normalised peak area after reaction stop of the epoxidation of *cis*- β -methylstyrene by imm-*Aae*UPO at different *t*BuOOH feed concentrations. The share of epoxide product is indicated in white letters. Reactions were analysed at the following time points: after 4h (20 mM h⁻¹), after 5h (10 mM h⁻¹), after 22h (5 mM h⁻¹) after 26h (2.5 mM h⁻¹), after 72h (1 mM h⁻¹).

4.7.6 Epoxidation of styrene



Scheme S3.1. Reaction equation for the epoxidation of styrene by imm-*Aae*UPO with *tert*-butyl hydroperoxide as oxidant.

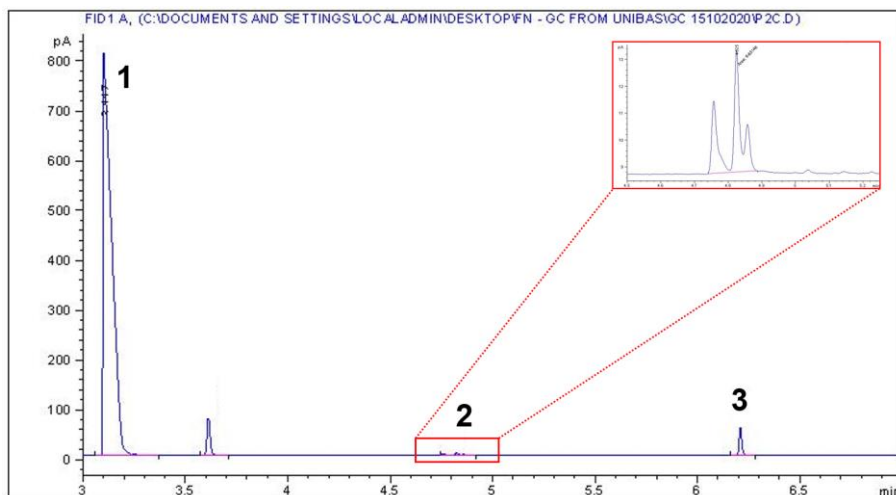


Figure S3.18. Example GC chromatogram for the epoxidation of styrene. 1 = Styrene; 2 = Product mix; 3 = Tetradecane (internal standard).

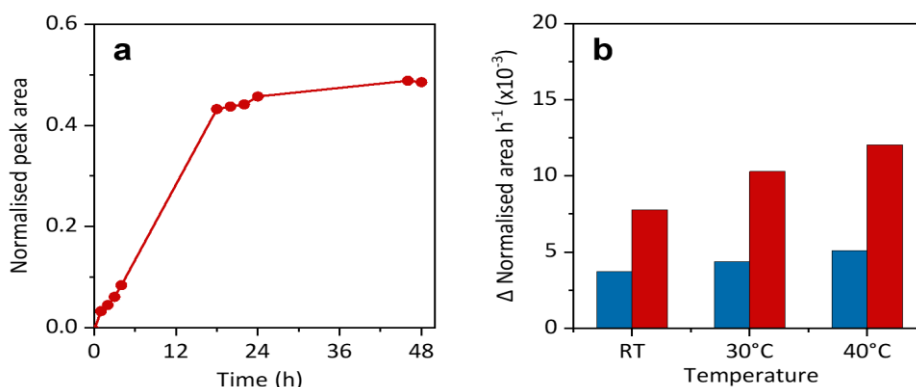


Figure S3.19. (a) Product formation over 48 h during epoxidation of styrene by imm-AaeUPO with continuous ^tBuOOH feed; (b) Product formation rates over 1.5 h of free AaeUPO (blue) and imm-AaeUPO (red) for the epoxidation of styrene. General reaction conditions (a): [AaeUPO] = 0.8 μM, ^tBuOOH feeding rate = 8.5 mM h⁻¹, room temperature, shaking at 99 rpm with 60° angle in an overhead rotator. (b): [AaeUPO] = 0.2 μM; ^tBuOOH pulse feeding of 1.25 mM every 15 min; temperatures were room temperature (RT), 30 °C, and 40 °C; shaking at 99 rpm with 60° angle in an overhead rotator. Data represented an average of duplicates.

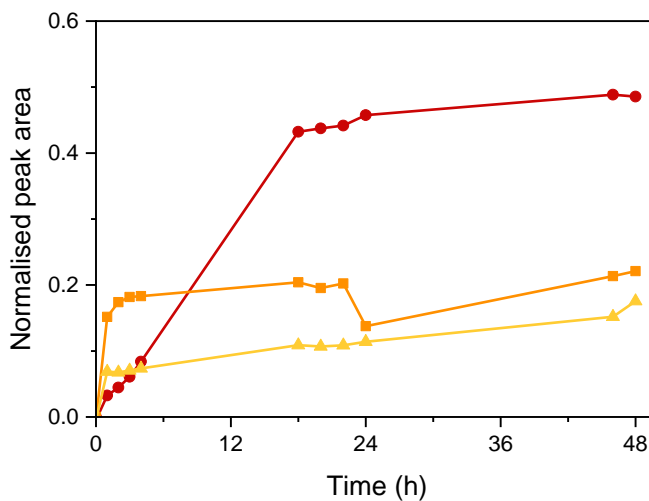


Figure S3.20. Impact of $t\text{BuOOH}$ feed rate. Product formation over time for the epoxidation of styrene with different $t\text{BuOOH}$ feed rates. Red circles = continuous $t\text{BuOOH}$ feed at 8.5 mM h^{-1} , orange squares = $205 \text{ mM } t\text{BuOOH}$ supply every 24 h, yellow triangles = $2.2 \text{ M } t\text{BuOOH}$ (the equimolar amount of used styrene) at the beginning of the reaction. General reaction conditions: $[\text{AaeUPO}] = 0.8 \text{ }\mu\text{M}$, room temperature, shaking at 99 rpm with 60° angle in an overhead rotator.

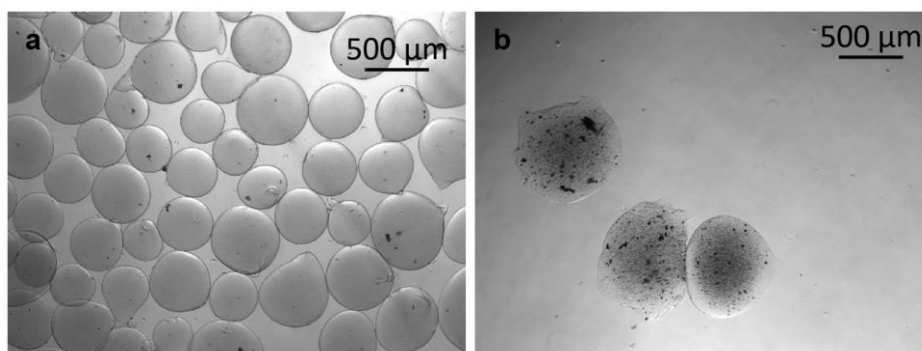


Figure S3.21. Appearance of imm-AaeUPO before and after the epoxidation reaction. (a) Freshly prepared imm-AaeUPO alginate beads. (b) imm-AaeUPO after 72 h incubation in the reaction mixture containing neat styrene, $t\text{BuOOH}$ and epoxidation products.

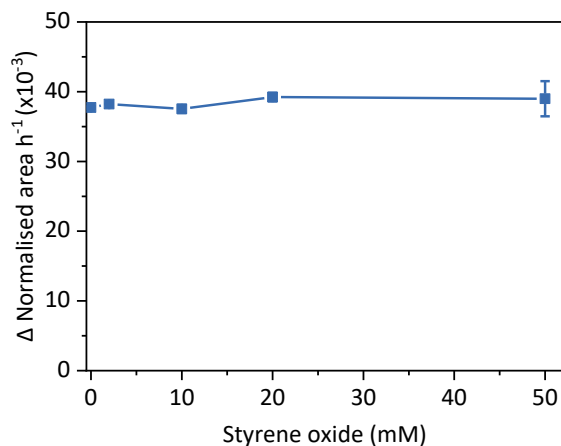


Figure S3.22. Influence of increasing product concentrations. Epoxidation of styrene with free *AaeUPO* in the presence of styrene oxide. General reaction conditions: $V = 500 \mu\text{L}$ styrene, $[\text{AaeUPO}] = 2.5 \mu\text{M}$, $[\text{tBuOOH}] = 2.5 \text{ mM}$ every 15 min, $[\text{styrene oxide}] = 0 - 50 \text{ mM}$. Data represents an average of duplicates.

Table S3.5 Catalytic rates of imm-*AaeUPO* at different bead diameters. Data represents an average of duplicates.

Bead diameter (μm)	Immobilisation yield (%)	ABTS activity [$U_{\text{ABTS}} \text{ g}_{\text{wet}} \text{ beads}^{-1}$]	Styrene activity ^[a] [Δ norm. area $\text{h}^{-1} \text{ g}_{\text{wet}} \text{ beads}^{-1}$]
2000	23.2 ± 2.4	1.4 ± 0.1	0.16 ± 0.00
440	18.7 ± 3.1	4.0 ± 0.9	0.22 ± 0.03
290	11.5 ± 0.0	5.1 ± 0.5	0.12 ± 0.04

[a] General reaction conditions: $V(\text{styrene}) = 500 \mu\text{L}$, $m(\text{beads}) = 25 \text{ mg}$ or 50 mg , $c(\text{tBuOOH}) = 1.25 \text{ mM}$ every 15 min.

All research data supporting the findings described in this thesis are available in 4TU.Centre for Research Data at <https://doi.org/10.4121/22193554.v1>

References

- [1] J. Dong, E. Fernández-Fueyo, F. Hollmann, C. E. Paul, M. Pesic, S. Schmidt, Y. Wang, S. Younes, W. Zhang, *Angew. Chem., Int. Ed.*, **2018**, *57*, 9238-9261.
- [2] V. B. Urlacher, M. Girhard, *Trends Biotechnol.* **2019**, *37*, 882-897.
- [3] M. Hobisch, D. Holtmann, P. G. de Santos, M. Alcalde, F. Hollmann, S. Kara, *Biotechnol. Adv.* **2021**, *51*, 107615.
- [4] Y. Ni, D. Holtmann, F. Hollmann, *ChemCatChem* **2014**, *6*, 930-943.
- [5] M. M. van Schie, J.-D. Spöring, M. Bocola, P. D. de María, D. Rother, *Green Chem.* **2021**, *23*, 3191-3206.
- [6] E. Churakova, I. W. Arends, F. Hollmann, *ChemCatChem* **2013**, *5*, 565-568.
- [7] A. Yayci, T. Dirks, F. Kogelheide, M. Alcalde, F. Hollmann, P. Awakowicz, J. E. Bandow, *J. Phys. D: Appl. Phys.* **2020**, *54*, 035204.
- [8] M. Hobisch, M. M. C. H. van Schie, J. Kim, K. Røjkjær Andersen, M. Alcalde, R. Kourist, C. B. Park, F. Hollmann, S. J. C. Kara, *ChemCatChem* **2020**, *12*, 4009-4013.
- [9] M. C. Rauch, F. Tieves, C. E. Paul, I. W. Arends, M. Alcalde, F. Hollmann, *ChemCatChem* **2019**, *11*, 4519-4523.
- [10] E. Fernández-Fueyo, Y. Ni, A. G. Baraibar, M. Alcalde, L. M. van Langen, F. Hollmann, *J. Mol. Catal. B: Enzym.* **2016**, *134*, 347-352.
- [11] M. Poraj-Kobielska, S. Peter, S. Leonhardt, R. Ullrich, K. Scheibner, M. Hofrichter, *Biochem. Eng. J.* **2015**, *98*, 144-150.
- [12] P. Molina-Espeja, P. Santos-Moriano, E. García-Ruiz, A. Ballesteros, F. J. Plou, M. Alcalde, *Int. J. Mol. Sci.* **2019**, *20*, 1627.
- [13] L. Fernandez-Arrojo, B. Rodriguez-Colinas, P. Gutierrez-Alonso, M. Fernandez-Lobato, M. Alcalde, A. O. Ballesteros, F. J. Plou, *Process Biochem.* **2013**, *48*, 677-682.
- [14] R. Ullrich, J. r. Nüske, K. Scheibner, J. r. Spantzel, M. Hofrichter, *Appl. Environ. Microbiol.* **2004**, *70*, 4575-4581.
- [15] P. Molina-Espeja, S. Ma, D. M. Mate, R. Ludwig, M. Alcalde, *Enzyme Microb. Technol.* **2015**, *73*, 29-33.
- [16] P. Molina-Espeja, E. Garcia-Ruiz, D. Gonzalez-Perez, R. Ullrich, M. Hofrichter, M. Alcalde, *Appl. Environ. Microbiol.* **2014**, *80*, 3496-3507.

Chapter 3

- [17] R. A. Sheldon, S. van Pelt, *Chem. Soc. Rev.* **2013**, *42*, 6223-6235.
- [18] C. Mateo, J. M. Palomo, L. M. Van Langen, F. Van Rantwijk, R. A. Sheldon, *Biotechnol. Bioeng.* **2004**, *86*, 273-276.
- [19] L. Cao, F. van Rantwijk, R. A. Sheldon, *Org. Lett.* **2000**, *2*, 1361-1364.
- [20] M.-Q. Xu, S.-S. Wang, L.-N. Li, J. Gao, Y.-W. Zhang, *Catalysts* **2018**, *8*, 460.
- [21] S. Velasco-Lozano, F. López-Gallego, J. C. Mateos-Díaz, E. Favela-Torres, *Biocatalysis* **2016**, *1*, 166-177.
- [22] S. Talekar, A. Joshi, G. Joshi, P. Kamat, R. Haripurkar, S. Kambale, *RSC Adv.* **2013**, *3*, 12485-12511.
- [23] D. Grajales-Hernández, M. Armendáriz-Ruiz, S. Velasco-Lozano, F. López-Gallego, J. C. Mateos-Díaz, *Appl. Microbiol. Biotechnol.* **2020**, *104*, 10033-10045.
- [24] C. Paul, D. Tischler, A. Riedel, T. Heine, N. Itoh, F. Hollmann, *ACS Catal.* **2015**, *5*, 2961-2965.
- [25] H. Toda, R. Imae, T. Komio, N. Itoh, *Appl. Microbiol. Biotechnol.* **2012**, *96*, 407-418.
- [26] K. Hofstetter, J. Lutz, I. Lang, B. Witholt, A. Schmid, *Angew. Chem., Int. Ed.* **2004**, *43*, 2163-2166.
- [27] A. Schmid, K. Hofstetter, H. J. Feiten, F. Hollmann, B. Witholt, *Angew. Chem., Int. Ed.* **2001**, *343*, 732-737.
- [28] R. A. Sheldon, *Green Chem.* **2017**, *19*, 18-43.
- [29] R. A. Sheldon, *Chem. Commun.* **2008**, 3352-3365.
- [30] L. Mazutis, R. Vasilias, D. A. Weitz, *Macromol. Biosci.* **2015**, *15*, 1641-1646.
- [31] S. J. P. Willot, M. D. Hoang, C. E. Paul, M. Alcalde, I. W. Arends, A. S. Bommarius, B. Bommarius, F. Hollmann, *ChemCatChem* **2020**, *12*, 2713-2716.
- [32] F. Tieves, S. J. P. Willot, M. M. C. H. van Schie, M. C. R. Rauch, S. H. H. Younes, W. Zhang, J. Dong, P. Gomez de Santos, J. M. Robbins, B. Bommarius, *Angew. Chem., Int. Ed.* **2019**, *58*, 7873-7877.
- [33] J. M. Robbins, A. S. Bommarius, G. Gadda, *Arch. Biochem. Biophys.* **2018**, *643*, 24-31.
- [34] J. M. Robbins, M. G. Souffrant, D. Hamelberg, G. Gadda, A. S. Bommarius, *Biochemistry* **2017**, *56*, 3800-3807.

- [35] D. Banerjee, R. V. Jagadeesh, K. Junge, M. M. Pohl, J. Radnik, A. Brückner, M. Beller, *Angew. Chem., Int. Ed.* **2014**, *53*, 4359-4363.
- [36] M. R. Sarkar, J. H. Lee, S. G. Bell, *ChemBioChem* **2017**, *18*, 2119-2128.
- [37] H. Toda, R. Imae, N. Itoh, *Tetrahedron: Asymmetry* **2012**, *23*, 1542-1549.
- [38] T. Hilberath, A. van Troost, M. Alcalde, F. Hollmann, *Front. Catal.* **2022**, *2*, 882992.
- [39] F. Tieves, F. Tonin, E. Fernández-Fueyo, J. M. Robbins, B. Bommarius, A. S. Bommarius, M. Alcalde, F. Hollmann, *Tetrahedron* **2019**, *75*, 1311-1314.
- [40] W. Lu, Y. Shen, A. Xie, W. Zhang, *J. Phys. Chem. B* **2013**, *117*, 3720-3725.
- [41] J. Yu, P. R. Chang, X. Ma, *Carbohydr. Polym.* **2010**, *79*, 296-300.
- [42] J.-D. Pédelacq, S. Cabantous, T. Tran, T. C. Terwilliger, G. S. Waldo, *Nat. Biotechnol.* **2006**, *24*, 79-88.

Chapter 4: Intensification of photobiocatalytic decarboxylation of fatty acids for the production of biodiesel

Hong T. Duong, Yinqi Wu, Jisk van der Meer, Alexander Sutor, Bastien O. Burek, Frank Hollmann, and Jonathan Z. Bloh

Based on *ChemSusChem* 2021, 14, 1053-1056 and master end project thesis of Jisk van der Meer.

Summary

Light-driven biocatalytic processes are notoriously hampered by poor penetration of light into the turbid reaction media. In this study, wirelessly powered light-emitting diodes are found to represent an efficient and scalable approach for process intensification of the photobiosynthetic production of diesel alkanes from renewable fatty acids.

1. Introduction

Biodiesel is an important pillar of the ongoing global transition from fossil energy carriers to renewable alternatives.^[1] Most widespread are fatty acid methyl esters (FAMEs) derived from natural fatty acids. FAMEs, however, exhibit some intrinsic disadvantages, which limit their application as drop-in-substitute for established fossil diesel. Due to their chemical nature as esters, the caloric value of FAMEs (ca. 32.6 MJ L⁻¹) is significantly lower (by approx. 11%) compared to fossil diesel (being essentially alkanes).^[2] Another drawback of FAMEs lies in their production by transesterification of natural fats and oils. Base or acid-catalysed transesterification with methanol is an equilibrium reaction and therefore necessitates considerable molar surpluses of methanol to shift the equilibrium in the desired direction. Furthermore, free fatty acids present in natural feedstock have to be dealt with in order to minimize catalyst inactivation.

A very promising solution circumventing the above-mentioned challenges is to simply decarboxylate fatty acids into the corresponding (C1-shortened) alkanes (Scheme 4.1). The resulting biodiesel product chemically resembles fossil diesel and can be obtained from the starting material without further reagents in an irreversible reaction. Chemical catalysts facilitating the decarboxylation of (fatty)acids require relatively harsh reaction conditions^[3] thereby negatively influencing the energy consumption for biodiesel production and also leading to undesired side reactions.

Therefore, we became very interested in the recently reported photoactivated fatty acid decarboxylase from *Chlorella variabilis* NC64A (CvFAP).^[4] Upon illumination with visible light ($\lambda=450$ nm) CvFAP catalyses the decarboxylation of a broad range of fatty acids.^[4-15] However, photochemical processes are severely limited by current reactor designs involving external illumination. Particularly with heterogeneous, optically non-transparent, and highly reflective reaction mixtures, the poor penetration depth of photons into the reactor leaves the majority of the contained catalysts unilluminated and therefore idle. This is particularly pronounced when scaling to larger reactor dimensions. As a result, the productivities of the photoenzymatic decarboxylation reactions generally lie in the range of a few mmol L⁻¹ h⁻¹ and therefore are orders of magnitude too low to be of industrial relevance.

a) state-of-the-art technology



- Equilibrium reaction necessitating surplus of MeOH
- FAMEs with low caloric value

b) photobiocatalytic decarboxylation



- + Irreversible reaction
- + Production of *real* (Bio)Diesel

Scheme 4.1. Comparison of traditional biodiesel synthesis by (trans) esterification (a) and the proposed photobiocatalytic decarboxylation (b).

2. Results and discussion

To alleviate this shortcoming, we have recently established a new photoreactor concept comprising internal illumination by means of wirelessly powered light emitters (WLEs).^[16] This concept allows for high specific light intensities and is readily scalable. The WLEs are small (1 cm diameter) spherical polymer shells containing an LED and a receiving circuit for their electromagnetic energy supply (Figure 4.1). They can move freely inside the reaction medium and can be fluidized by gas flow or stirring. The power transfer is realized contactless by resonant inductive coupling (RIC) from coils mounted on the outside of the reactor (for more details, see 4.3).^[17-19]

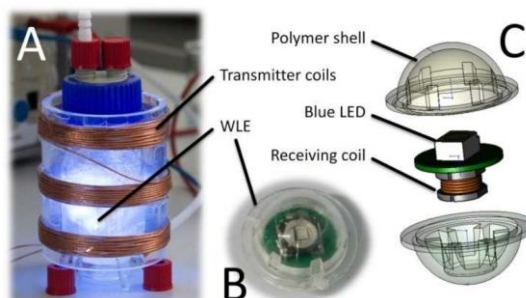


Figure 4.1. A photograph of the reactor setup employed in this study (A) as well as the individual wireless light emitters (WLE; B) and an explosion scheme of their makeup^[20] (C).

Chapter 4

RIC-powered LEDs have previously been used for algae cultivation and water purification,^[21-23] but with much lower specific light intensities. Compared to earlier studies^[16] we have succeeded in improving the system resulting in much higher (ca. 27-fold) specific light intensities. Therefore, we decided to apply the WLE concept to the photocatalytic decarboxylation of fatty acids to show that this technique is a step towards industrial application of photon-driven biodiesel production.

To establish the proof-of-concept, we used the CvFAP-catalysed decarboxylation of hexadecanoic acid (palmitic acid) into pentadecane. As the biocatalyst, we chose CvFAP heterologously expressed in *Escherichia coli*. The whole cells harvested from the fermentation were used as the biocatalyst. It should be noted that *E. coli* cells not containing the expression vector for CvFAP (under otherwise identical conditions) exhibited no detectable formation of pentadecane.

By using the conventional external illumination setup with conventional LEDs, palmitic acid was converted into pentadecane in approximately 90% yield within 8 h (Figure 4.2). However, performing the same experiment using the proposed internal illumination resulted in full conversion in less than 20 min (Figure 4.2), corresponding to a more than 22-fold acceleration of the product formation rate.

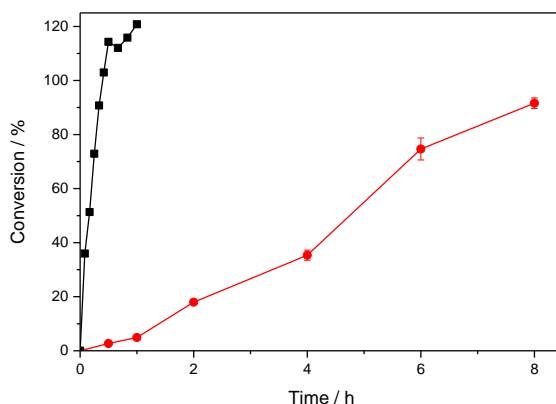


Figure 4.2. Photoenzymatic conversion of palmitic acid into pentadecane using external illumination (●) and internal illumination using WLEs (■). Conditions: [palmitic acid]₀=13 mM; [rec. *E. coli*]=50 g L⁻¹ ([CvFAP]=6 μM); buffer: 100 mM Tris-HCl (pH 8.5), 30 vol% DMSO, volume=50 mL; T=20°C; photon flux of external illumination: 27 mmol L⁻¹ h⁻¹ and of internal illumination: 390 mmol L⁻¹ h⁻¹ (40 WLEs).

Admittedly, most of this rate acceleration is due to the higher light intensity enabled by the internal illumination technique. However, even a direct comparison of internal and external illumination at the same incident photon flux density revealed a clear

advantage of the former with about 1.8-fold higher observed reaction rates (see below).

Using whole recombinant *E. coli* cells generally resulted in the accumulation of approximately 15-16 mmol L⁻¹ of pentadecane (ca. 120% yield). Control experiments in the absence of palmitic acid revealed that the additional product originated from conversion of cell membrane components of the whole cell catalyst, thereby explaining the higher conversion (Figure 4.2).

Encouraged by the impressive rate-acceleration, we next systematically investigated the influence of catalyst loading and light intensity on the productivity of the photoenzymatic decarboxylation reaction. At a fixed light intensity, the product formation rate steadily increased with increasing catalyst concentration (Figure 4.3). At low enzyme concentration, the product formation rate increased approximately linearly just like for an ordinary enzyme. Here, the enzyme appears to be oversaturated by photons and is only limited by its own, intrinsic catalytic activity. Indeed, the maximum TOF ($\text{TOF} = \text{mol}_{\text{product}} \times \text{t}^{-1} \times \text{mol}_{\text{CvFAP}}^{-1}$) observed in these experiments was 4.0 s⁻¹, which is an order of magnitude higher than previously reported.^[4, 15] At higher enzyme concentration, this was no longer the case and gradually, photon limitation manifested resulting in a plateau where the rate no longer increases.

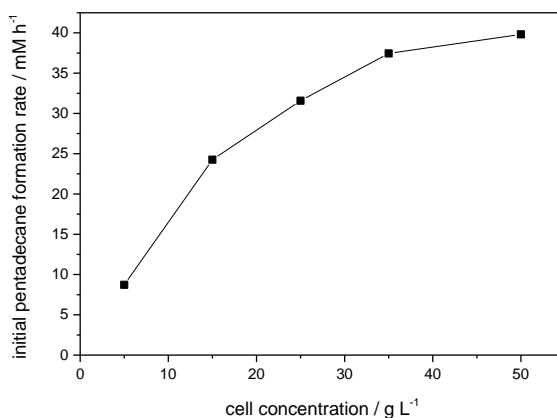


Figure 4.3. Biocatalyst-concentration dependency of the photoenzymatic decarboxylation of palmitic acid to pentadecane. Conditions: [palmitic acid]₀=13 mM; [rec. *E. coli*]=50 g L⁻¹ ([CvFAP]=6 μM); buffer: 100 mM Tris-HCl (pH 8.5), 30% v/v DMSO, volume=50 mL; T=20°C; internal illumination with a photon flux of 390 mmol L⁻¹ h⁻¹ (40 WLEs).

Similarly, also the light intensity directly influenced the overall reaction rate (Figure 4.4). After an initial almost linear increase, mild light saturation effects became

Chapter 4

apparent at higher photon flux density resulting in a slightly diminished response. This is a typical behaviour also often observed for heterogeneous photocatalytic reactions.^[24] It is an inevitable consequence of the exponential light intensity decay as at higher light intensity, the areas near the light source will start to show symptoms of photon saturation while farther away, this is still far from happening. As mentioned above, the external illumination experiments show the same trend, albeit with systematically lower rates. It also appears that in this case, the reaction rate levels off at the lower maximum value, although this could not be experimentally verified yet as no light source strong enough was available.

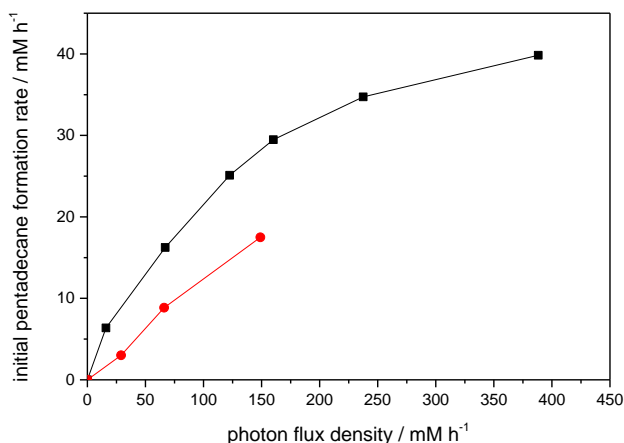


Figure 4.4. Comparison of the initial pentadecane formation rate using WLEs for internal illumination (■) and a LED for external illumination (●) at different light intensities. Conditions: [palmitic acid]₀=13 mM; [rec. *E. coli*]= 50 g L⁻¹ ([CvFAP]=6 μM); buffer: 100 mM Tris-HCl (pH 8.5), 30 vol% DMSO, volume=50 mL; T=20°C. The variation of the internal illumination light intensity was achieved by addition of different numbers of WLEs while for external illumination this was realized by changing the driver current.

The advantage of the internal illumination can be attributed to two effects. First of all, it is less affected by reflection losses resulting from the strongly turbid reaction suspension, as more light is productively scattered back into the medium rather than out of the reactor. Additionally, the light is also more evenly distributed throughout the reactor, avoiding “bright” spots and the associated local photon oversaturation.^[24] We expect that the latter effect and with it the advantage of internal illumination will become even more pronounced when scaled to larger reactor volumes due to the then reduced (illuminated) surface-to-volume ratio in case of external illumination. To the best of our knowledge, this is the first time that such a significant advantage of internal illumination has been experimentally demonstrated.

In line with earlier estimations, the observed apparent quantum yield (AQY) of the reaction is remarkably high with up to 39.8% (for details, see 4.7.4).^[4] Interestingly, the decarboxylation reaction is endothermic with a heat of reaction of +71.1 kJ mol⁻¹ (calculated from heat of combustion; see 4.7.4). The thermodynamic driving force stems from the photons used with an energy of 265.9 kJ mol⁻¹ (for $\lambda=450$ nm). This also means that the reaction is actually photosynthetic, i.e., part of the photon energy is found in the product, making the high AQY even more remarkable as such reactions typically suffer from poor efficiency.^[25]

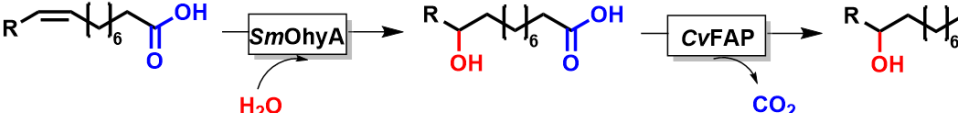
At perfect quantum efficiency and assuming loss-free photon generation, the maximum theoretical energy efficiency of the reaction $[\Delta_c H^0_{\text{products}} \times (\Delta_c H^0_{\text{educts}} + E_{\text{photons}})^{-1}]$ would be as high as 98.1%. Even though the actually achieved energy efficiency in this non-optimized lab setup was 32.1%, already 89.8% appears possible with the AQY reached here by optimising the setup to match state-of-the-art efficiencies for the electronic parts and the inductively coupled energy transfer^[26] as well as the LEDs (see the 4.7.5).^[27-28] This is remarkable considering that established processes for the synthesis of renewable fuels such as Power-to-Liquids reach energy efficiencies around or below 50%.^[29]

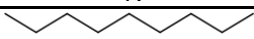
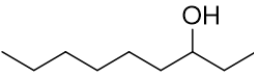

Using homogeneously dissolved fatty acids does not represent a scalable approach for the large-scale transformation of fatty acids into alkanes due to the low product titers. We therefore also investigated a two liquid phase approach to increase the overall payload of the fatty acids in the reactor system. For this, we chose triolein as the organic phase (representing future oil phases) to form a 200 mM solution of palmitic acid. More than 50% conversion was achieved within 2 h with a rate similar to the one achieved in the monophasic system. However, at this point the product formation abruptly ceased (Figure S4.6). Further addition of fresh catalyst resulted in further product formation. This experiment highlights the current limitation of the proposed photobiocatalytic alkane production system being the comparably poor long-term stability of the enzyme catalyst under process conditions. In our experiments the turnover numbers for CvFAP ($\text{TON} = \text{mol}_{\text{product}} \times \text{mol}_{\text{CvFAP}}^{-1}$) never exceeded 9000. These turnover numbers are well in the range of TONs previously observed for CvFAP^[10-15] indicating that the light intensity itself is not the main parameter for CvFAP inactivation. This supports the CvFAP inactivation mechanism proposed by Scrutton and co-workers, assuming that intermediate radical species occurring in the catalytic mechanism may cause inactivation of the biocatalyst.^[6]

Advances have also been made in the valorisation of fatty acids,^[30-31] among which transformation from natural fatty acids to long-chain secondary alcohols are particularly interesting in cosmetic formulations or building blocks.^[32-33] A preparative-scale of photoenzymatic cascade combining an oleate hydratase from *Stenotrophomonas maltophilia* (*SmOhyA*) and CvFAP has been performed by using the photocatalytic set-up we established (Table 4.1). For first-step hydration, co-solvent and substrate loadings were optimised for higher productivity when oleic acid was used as substrate (see 4.7.7). In the second-step of decarboxylation, 84% conversion was achieved within 5 h (Figure S4.9).

To explore the photocascade scope, ricinoleic acid and linoleic acid were converted to the corresponding alcohols following the one-pot two-step procedure. For both reactions, approx. 87% conversion was obtained after overnight hydration and nearly full conversion was achieved within 1-3 h for decarboxylation reactions starting from hydroxylated intermediates to secondary alcohols.

Table 4.1. Preparative-scale of photoenzymatic cascade reactions starting from unsaturated fatty acids to secondary alcohols.



-R	Conversion (%) ^a	Conversion (%) ^b
	> 95	84
	87	> 99
	87	> 99

^a Conversion of the hydration reaction. Reaction condition: [unsaturated fatty acid] = 20 mM, [*SmOhyA* cells] = 20 g L⁻¹, 50 mM Tris-HCl buffer (pH 6.5), volume = 250 mL

^b Conversion of decarboxylation reaction. After 20.5 h of hydration reaction, decarboxylation was initiated under reaction condition: [hydrated fatty acid] = 10 mM, [CvFAP cells] = 30 g L⁻¹, internal illumination λ_{\max} = 450 nm, light intensity = 98 mmol L⁻¹ h⁻¹, 50 mM Tris-HCl buffer (pH 6.5), volume = 50 mL.

3. Conclusion

In the present study, we have demonstrated that the rate of photobiocatalytic reactions, such as the decarboxylation of fatty acids, can be dramatically increased by using intensified internal illumination. The same technique also allows to seamlessly scale-up the production volume to industrially relevant dimensions. The

conditions presented herein seem to approach the limit for wild type CvFAP. Already, (photon) saturation effects become apparent which probably make further intensification challenging. Nevertheless, at the productivity achieved in this study, the process could produce 264 mL of pentadecane per liter of reaction volume each day, clearly pointing towards larger scale implementation. This study, however, also revealed a current shortcoming of the proposed photosynthetic fuel generation being the rather low operational stability of CvFAP, which needs further improvement. The low turnover numbers mean that the enzyme needs to be continuously replenished, resulting in a high cost contribution of the biocatalyst.^[34] On one hand, current expression levels of CvFAP (ca. 10% of the total protein) are still comparably low, necessitating relatively high loadings of *E. coli* cells in the reaction. Optimisation of the expression conditions will alleviate this issue. On the other hand, we are convinced that further improvements can be expected from fermentation optimisation and protein engineering resulting in more robust enzyme variants to render the envisioned photosynthetic production of alkanes economically feasible.

4. Material and methods

4.1 Chemicals and materials

Palmitic acid, dimethyl sulfoxide (DMSO), tris(hydroxymethyl)aminomethane (Tris), hydrogen chloride (HCl), kanamycin, Isopropyl β -D-1-thiogalactopyranoside (IPTG), sulfuric acid (H₂SO₄), 1,10-phenantroline, sodium acetate and other commercial chemicals were purchased from Sigma-Aldrich, Fluka, Acros or Alfa-Aesar, without any further purification. The water used was distilled.

4.2 Protein expression

The *Escherichia coli* (*E. coli*) BL21(DE3) cells containing the plasmid pET-28a(+) expressing CvFAP were cultivated in terrific broth (TB) medium containing 50 μ g mL⁻¹ kanamycin at 37 °C and 180 rpm. When the optical density at 600 nm (OD₆₀₀) reached 0.7-0.8, protein induction was initiated by adding 0.5 mM IPTG and cultivation temperature was decreased to 17 °C. After cultivation for about 20 h, cells were harvested by centrifugation (11000 \times *g* at 4 °C for 10 min), washed twice with ice-cooled 100 mM Tris-HCl (pH 8.5).

Chapter 4

Oleate hydratase from *Stenotrophomonas maltophilia* (*SmOhyA*) was produced using recombinant expression in *E. coli* BL21(DE3) containing pACYC-*SmOhyA*. The pre-cultures were grown overnight in terrific broth (TB) medium, containing 34 $\mu\text{g mL}^{-1}$ chloramphenicol. The pre-cultures were used to inoculate 1 L cultures (TB + 50 $\mu\text{g mL}^{-1}$ chloramphenicol, in 5 L shake flasks). The cells were grown at 37 °C, 180 rpm until an OD_{600} of roughly 0.9 was reached. To induce the production of protein, isopropyl- β -D-thiogalactopyranoside (IPTG) was added to a final concentration of 0.5 mM. The cultures were then left overnight (20 h) at 20 °C, 180 rpm. The cells were harvested using centrifugation at 10 000 g for 10 min at 10 °C, washed twice with ice-cooled 100 mM Tris-HCl (pH 8.5). The cell pellet was subsequently collected and stored at -80°C.

4.3 Photocatalytic set-ups

The reactions were performed in a cylindrical glass reactor (100 mL, 56 mm diameter, 105 mm height). For internal illumination wireless light emitters (WLE) were used which consist of a ferrite core inductor (WE-PD2 4532 10 μH , Würth), a capacitor (82 nF) and a blue LED (XPGDRY-L1-0000-00401, 451 nm peak emission, Cree Inc.), connected all in parallel. These elements form an oscillating circuit with a certain resonance frequency and are encapsulated in a SiO_2 coated cyclic olefin polymer hollow with a diameter of 10 mm. To power them, the reactor was surrounded with three copper wire coils (18 turns each) in series with a distance of 20 mm, mounted on a PMMA tube (75 mm diameter, 105 mm height). The coil was connected to a capacitor with an appropriate capacitance to generate a series resonant circuit with a resonance frequency of 178 kHz. This circuit was connected in parallel to an oscillator amplifier circuit with the same resonant frequency of 178 kHz. The reaction mixture was stirred with a PEEK stirrer with a PTFE 4-blade radial flow impeller. Further details of the reactor have been described earlier by us.^[16] For external illumination a collimated blue LED (M450LP1, 450 nm peak emission, Thorlabs) has been used.

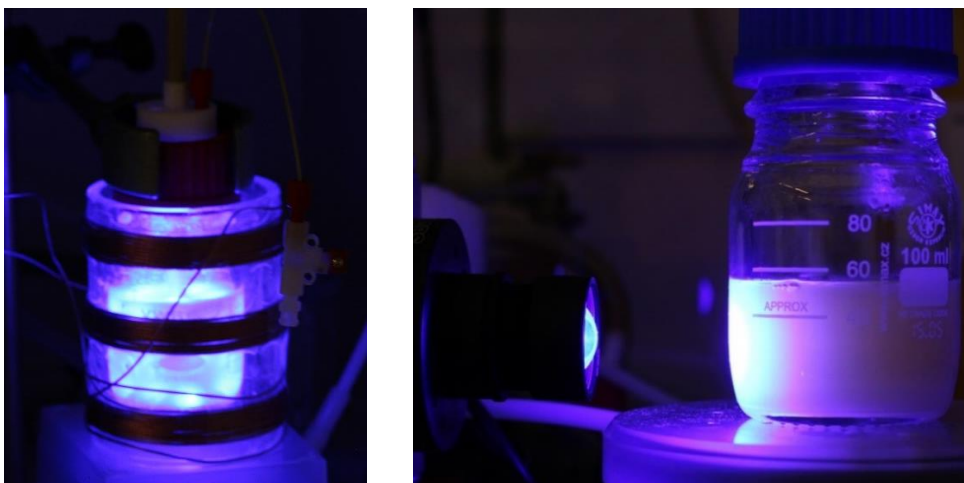


Figure S4.12. Pictures of the internal (left) and external (right) illuminated reactors under operating conditions.

4.4 Chemical actinometry

The volumetric photon flux density (q_p) was determined by means of ferrioxalate actinometry according to Hatchard and Parker.^[35] 50 mL of a freshly prepared ferrioxalate solution (37.5 mM in 0.05 M H_2SO_4 (98% Merck)) was added to the reactor and irradiated either with a varying amount of WLE or the external blue LED. At defined intervals, 25 μ L samples of the irradiated ferrioxalate solution were taken and mixed with 175 μ L of a solution consisting of 7.5 mL H_2SO_4 (0.05 M), 2 mL 0.1% 1,10-phenantroline (Carl Roth) solution, 5 mL sodium acetate solution (1M (Carl Roth)) and 3 mL deionized water. The absorbance of the resulting ferroin complex was measured at the maximum absorption of 510 nm using a UV-Vis microplate reader (PowerWave HT, BioTek). The respective iron(II) concentration has been determined using iron(II)sulfate as an authentic standard. The photon flux was calculated subsequently using the iron(II) generation rate as well as the quantum yield and transmission of the ferrioxalate solution. The power consumption was measured at the wall plug using a commercial power meter (KD-302, profitec).

4.5 Photocatalytic pentadecane production with *CvFAP@E.coli*

CvFAP@E.coli were added to 35 mL of TRIS-HCl buffer (100 mM, pH= 8.5) and properly mixed. The mixture was added to the photoreactor and filled up to 50 mL

Chapter 4

total volume with palmitic acid (43.3 mM, Sigma Aldrich) dissolved in DMSO (> 99.7 %, Sigma Aldrich).

4.6 Analysis methods

4.6.1 Extraction

For palmitic acid decarboxylation reaction

400 μL samples were taken from the suspension at defined intervals and mixed with 100 μL of HCl (37%, Carl Roth) in an ultrasonic bath for 10 minutes. Afterwards the samples were extracted with 250 μL ethyl acetate (>99.5%, Roth). The organic phase was dried with Mg_2SO_4 (VWR) for later analysis.

For photoenzymatic cascade reactions

In preparation of analysis on GC, an equal part (1:1 v/v) of ethyl acetate (containing 5 mM 1-octanol) was added to samples taken from a reaction mixture. The organic phase was collected after centrifugation and dried with Mg_2SO_4 (VWR) for later analysis.

4.6.2 Silylation

An extraction was performed as described above. After drying, the organic phase was evaporated under nitrogen flow. To this, 50 μL of the silylating agent N,O-Bis(trimethylsilyl)trifluoroacetamide (BSTFA), containing 1 vol% trimethylsilane (TMS) was added. The vial was heated for 1 h at 100°C. After cooling down to room temperature, 150 μL of ethyl acetate (containing 5 mM of 1-octanol) was added to allow for injection in GC.

4.6.3 Esterification

To a 200 μL sample, 800 μL of methanol, containing 10 vol% sulfuric acid, was added and heated for 1 h at 80°C. After returning to room temperature, 500 μL of n-heptane, containing 5 mM 1-octanol, was added to extract the esters. The organic phase was washed with 200 μL H_2O and dried with Mg_2SO_4 (VWR) for later analysis.

4.6.4 Gas chromatography

For palmitic acid decarboxylation reaction

The reactions were analysed *via* GC-MS (GCMS-QP5050, SHIMADZU, column: Rxi-5HT, Restek GmbH, 30 m × 0.25 mm × 0.1 µm, max. temperature 400°C, method: He carrier, 30 kPa constant pressure, split (split ratio: 21), start: 70 °C for 2 min, with a heating rate of 25 °C min⁻¹ up to 300°C, total time: 13 min).

For hydrations and photoenzymatic cascade reactions

The reactions were analyzed on a Shimadzu GC-2010 Plus system using, AOC-20i autosampler & AOC-20s carousel, FID-2010 Plus detector with N₂ as the carrier gas. Column: Cpsil 5 CB: 50 m × 0.53 mm × 1.0 µm.

4.6.5 High pressure liquid chromatography

The reactions were analyzed on a Shimadzu Prominence modular system consisting of a LC-20AT pump, CBM-20A system controller, SIL-20A autosampler, CTO-20A column oven and SPD-M20A detector. Samples were separated using a Osaka Soda (Shiseido) CAPCELL PAK C8 DD (150 × 3.0mm) using HPLC grade solvents.

4.6.6 Nuclear magnetic resonance

NMR measurements were performed on a Agilent 400-MR DD2 NMR spectrometer using a 5 mm ONE NMR Probe, operating at 25 °C. Deuterated DMSO and chloroform were used as solvents.

Chapter 4

4.7 Supporting results

4.7.1 Determination of the photon flux density with chemical actinometry

External illumination

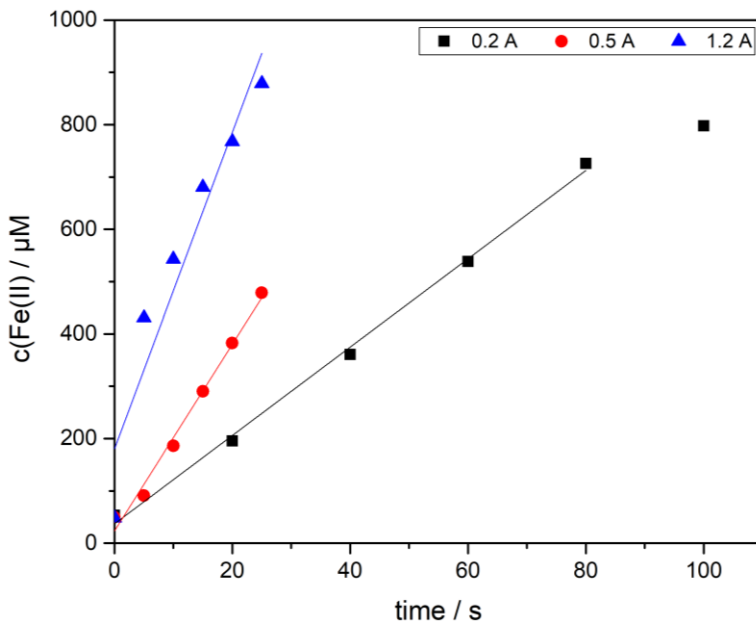


Figure S4.13. Concentration -time-curves of the iron(II) generation under illumination of the ferrioxalate solution. Reaction conditions: 50 mL ferrioxalate solution, varying the applied current to the LED from 0.2 to 1.2 A, under Ar atmosphere.

Table S4.5. Determined volumetric photon flux (q_p) in dependence of the applied LED current using external illumination.

LED current / A	q_p / mM h^{-1}
0.2	29.1
0.5	66.2
1.2	149.0

Internal illumination

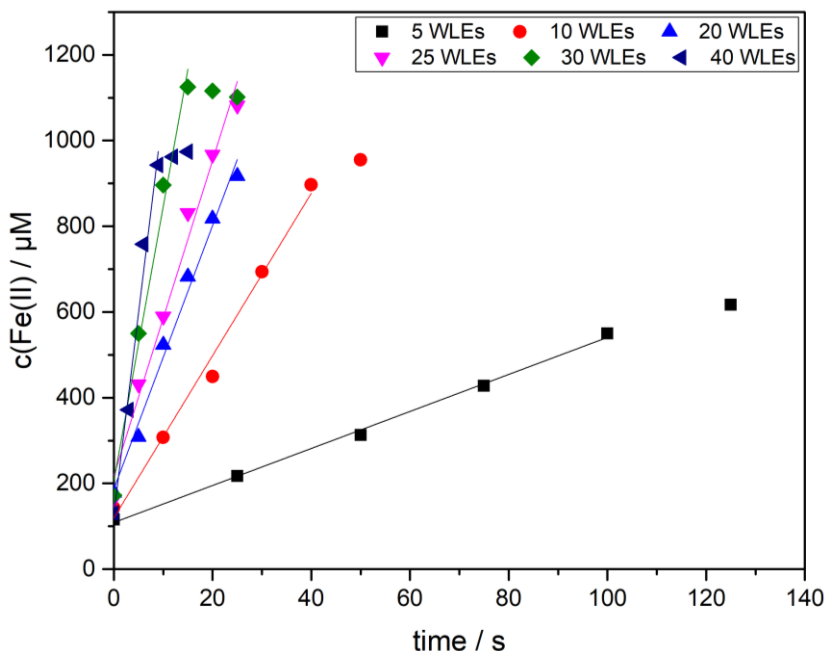


Figure S4.14. Concentration -time-curves of the iron(II) generation under illumination of the ferrioxalate solution. Reaction conditions: 50 mL ferrioxalate solution, 5-40 WLE under Ar atmosphere.

The radiant flux in the reactor (P_{light}) can be calculated by multiplying the respective photon flux density (q_p) with the reaction volume (50 mL) and the molar energy of the photons (see eq. 1). The wall plug efficiency is the quotient of the light power and the electrical power consumption (P_{el}) at the wall plug (see eq. 2).

$$P_{\text{light}} = q_p \times V \times \frac{h \times c}{\lambda} \times N_A \quad (\text{eq.1})$$

$$\text{WPE} = \frac{P_{\text{light}}}{P_{\text{el}}} \quad (\text{eq.2})$$

Table S4.6. Determined photon flux (q_p) with the respective electrical power consumption at the wall plug (P_{el}) as well as light output (P_{light}) and the resulting wall plug efficiency (WPE) of the internal illumination.

N_{WLE}	Volume / mL	$q_p / \text{mE L}^{-1} \text{h}^{-1}$	P_{el} / W	$P_{\text{light}} / \text{mW}$	WPE / %
5	50	16.6	6.0	60	1.0
10	50	67.0	7.6	245	3.2
20	50	122.6	9.4	450	4.8

25	50	160.1	9.9	590	6.0
30	50	237.5	10.7	875	8.2
40	50	388.3	11.8	1430	12.1

4.7.2 Pentadecane production with different cell concentrations

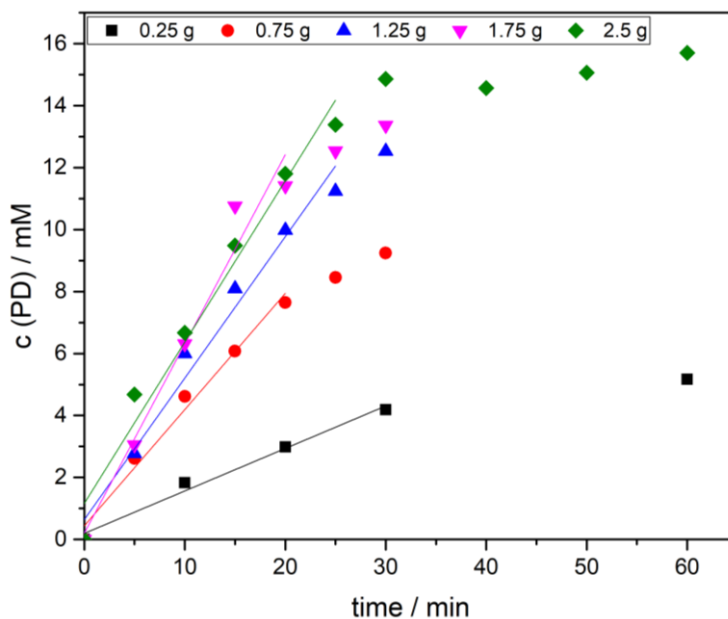


Figure S4.15. Concentration-time-profiles for the pentadecane production with different cell concentrations. Reaction conditions were as follows: 13.1 mM palmitic acid, 50 mL total volume, 70 mM TRIS-HCl buffer, varying the $C_{vFAP@E.Coli}$ concentration from 0.25 to 2.5 g corresponding to respective enzyme concentrations of 0.6 to 6 μ M, 40 WLE, 20 V amplifier voltage.

4.7.3 Pentadecane production as a function of the number of WLEs

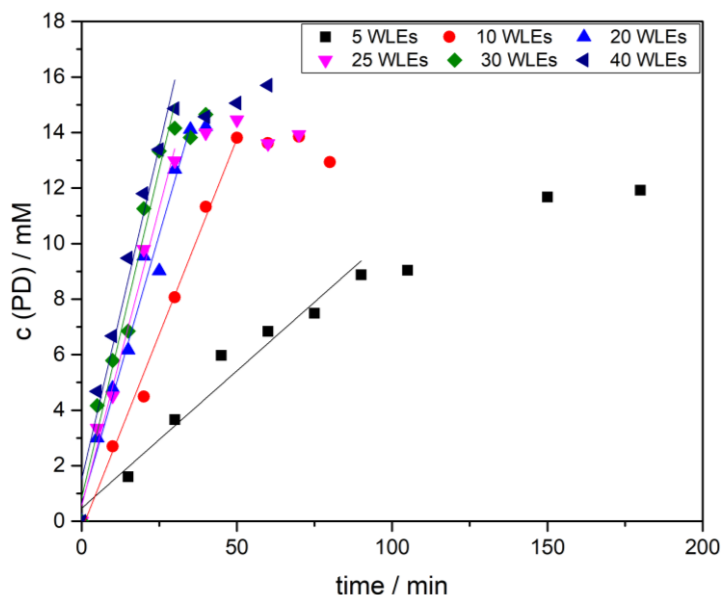


Figure S4.16. Concentration-time-profiles for the pentadecane production with different numbers of WLEs. Reaction conditions were as follows: 13.1 mM palmitic acid, 50 mL total volume, 70 mM TRIS-HCl buffer, 2.5 g CvFAP@*E.Coli*, varying the number of WLEs from 5 to 40, 20 V amplifier voltage.

4.7.4 Efficiency calculations

The apparent quantum yield (AQY) can be calculated by dividing the rate of pentadecane production (k_{PD}) by the photon flux density (q_P , see eq. 3).

$$AQY = \frac{k_{PD}}{q_P} \quad (\text{eq.3})$$

The overall energy efficiency (EE) can be calculated by dividing the combustion energy of the product pentadecane ($\Delta_c H_{PD}^0 = -10048.7 \text{ kJ mol}^{-1}$)^[36] by the combustion energy of the educt palmitic acid ($\Delta_c H_{PA}^0 = -9977.6 \text{ kJ mol}^{-1}$)^[37] plus the energy necessary to generate the photons (eq. 4). The former can be calculated according to eq. 5 from the molar photon energy divided by the efficiency of generating the photons (WPE) and the efficiency of converting a photon into the product (AQY).

$$EE = \frac{\Delta_c H_{PD}^0}{\Delta_c H_{PA}^0 + E_{photons}} \quad (\text{eq.4})$$

$$E_{photons} = \frac{\frac{h \times c}{\lambda} \times N_A}{WPE \times AQY} \quad (\text{eq.5})$$

Table S4.3. Kinetic and efficiency data for Pentadecane production as a function of different number of WLEs.

N WLE	$q_P / \text{mE L}^{-1} \text{h}^{-1}$	$k(\text{PD}) / \text{mM h}^{-1}$	AQY / %	EE / %
5	16.0	6.4	39.8	12.9
10	67.0	16.2	24.2	23.0
20	122.6	25.1	20.5	27.2
25	160.1	29.5	18.4	29.4
30	237.5	34.7	14.7	31.2
40	388.3	39.8	10.3	32.1

4.7.5 Theoretical energy efficiency

The presented system is non-optimized in terms of efficiency of amplifier, LED and resonant inductive coupling (RIC). Assuming literature known values of 91 % for the amplifier and 84 % for RIC, 80 % for a blue LED^[27-28] and a transmission of 90 % through the polymer shell^[16] of the WLE, the WPE of a state-of-the-art system could be as high as 55 %. With this WPE and the maximum AQY of 39.8 % observed in this work, a theoretical energy efficiency of 89.8 % for the conversion of palmitic acid into pentadecane can be realized.

4.7.6 Two liquid phase reaction

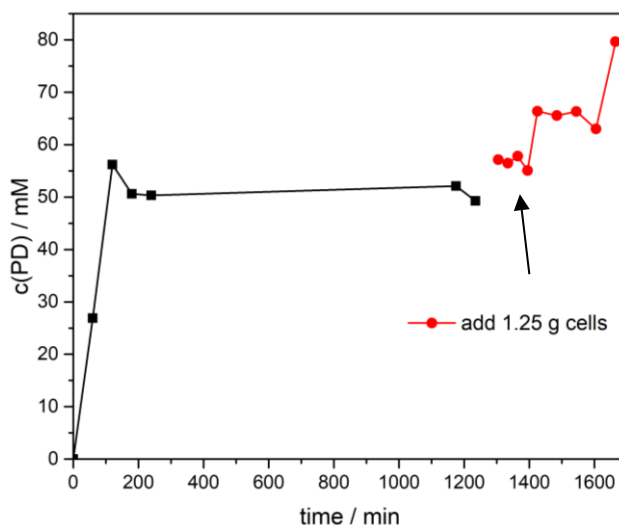


Figure S4.17. Concentration-time-profiles for the pentadecane production in a two liquid phase system using triolein as organic phase. Reaction conditions were as follows: 25 mL of 200 mM palmitic acid in triolein, 25 mL of a 100 mM TRIS-HCl buffer containing 2.5 g CvFAP@*E.Coli*, after 1305 min 1.25 g of cells were added, 40 WLE, 20 V amplifier voltage.

4.7.7 Optimisation of hydration reaction

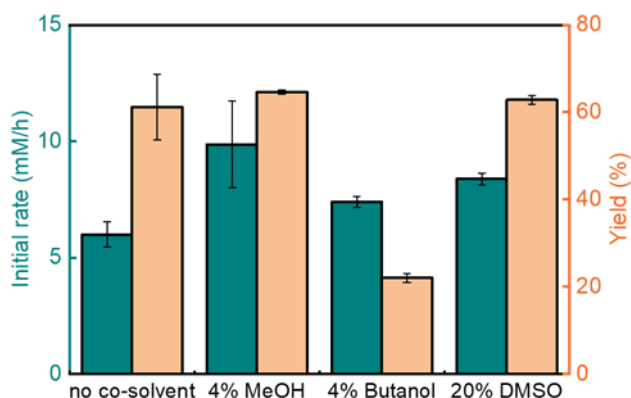


Figure S4.7. Comparison of initial rate (■) and yield (■) of oleic acid hydration under conditions containing different co-solvents. Reaction conditions: [oleic acid] = 30 mM, [*SmOhyA* cells] = 50 g \times L $^{-1}$, 50 mM Tris-HCl buffer (pH = 6.5), with or without co-solvent, reaction volume = 20 mL, 30 °C, magnetic stirring, reaction time = 19.5 h.

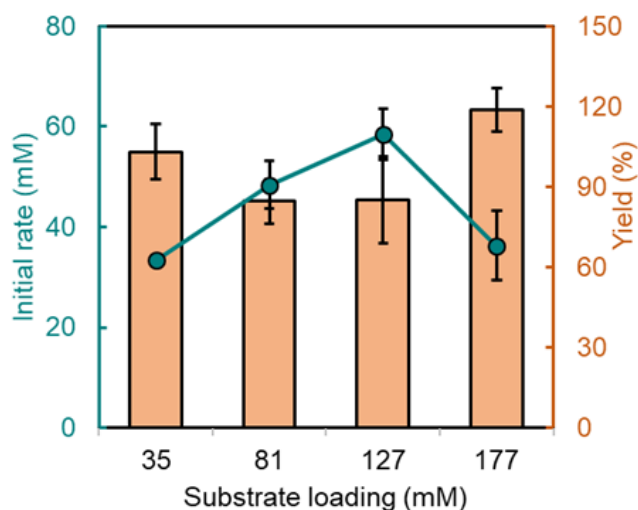


Figure S4.8. Comparison of oleic acid hydration yield (●) and initial rate (●) under different substrate loadings. Reaction conditions: [oleic acid] = 35-177 mM, [*SmOhyA* cells] = 50 g \times L $^{-1}$, 50 mM Tris-HCl buffer (pH = 6.5), reaction volume = 20 mL, 30 °C, 400 rpm, reaction time = 1 h ([oleic acid] = 35 mM) or 5 h ([oleic acid] = 81-177 mM).

4.7.8 Photoenzymatic cascade reaction

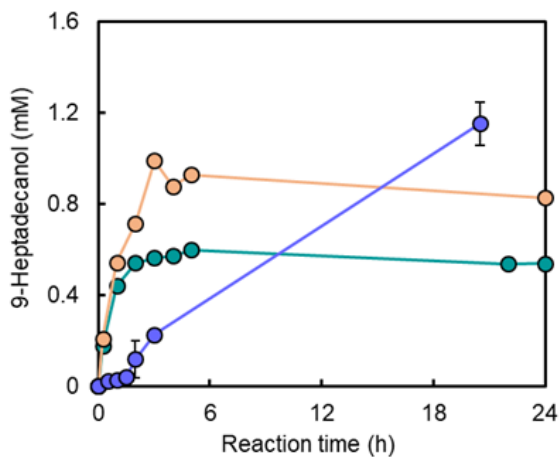


Figure S4.9. Time course of conversion of (*R*)-10-hydroxystearic acid to 9-heptadecanol catalysed by CvFAP under illumination with different light intensity. Reaction conditions: [(*R*)-10-hydroxystearic acid] = 16-30 mM, [CvFAP cells] = 30 g x L⁻¹, 50 mM Tris-HCl buffer (pH = 8.0), room temperature, internal illumination λ_{\max} = 450 nm, light intensity = 52 mmol x L⁻¹ x h⁻¹ (●), 98 mmol x L⁻¹ x h⁻¹ (●) or 390 mmol x L⁻¹ x h⁻¹ (●).

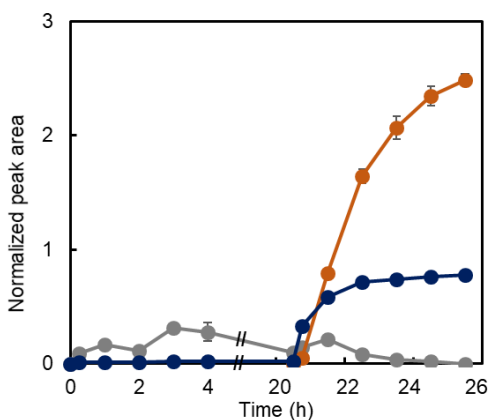
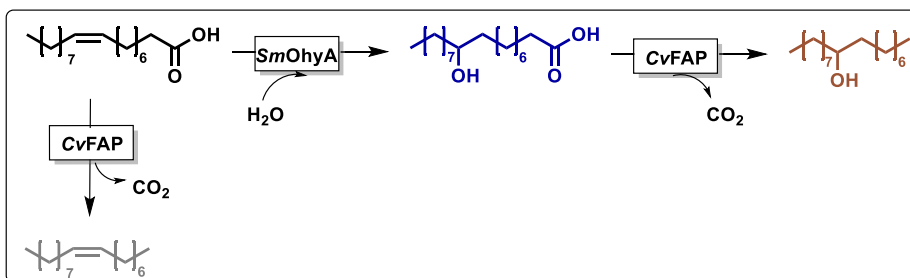


Figure S4.10. Time course of the photoenzymatic cascade starting from oleic acid. Reaction condition: [oleic acid]=10 mM, [CvFAP cells] = 30 g L⁻¹, [SmOhyA cells] = 20 g L⁻¹,

photon flux = $98 \text{ mmol L}^{-1} \text{ h}^{-1}$, 50 mM Tris-HCl buffer (pH 6.5), volume=50 mL, light on after 20.5 h. 10-hydroxystearic acid (●), 9-heptadecanol (●), 9-heptadecene (●).

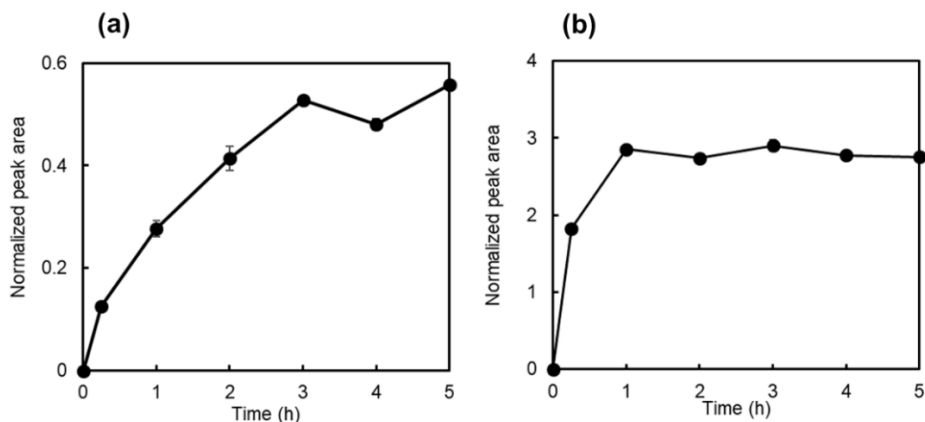


Figure S4.11. Time course of the decarboxylation reaction for the formation of heptadec-7,9-diol (a) and heptadec-6-en-9-ol (b) catalysed by CvFAP. Reaction conditions: [10,12-dihydroxyoctadecanoic acid or 10-hydroxyoctadec-12-enoic acid]=10 mM, [CvFAP cells] = 30 g L^{-1} , photon flux = $98 \text{ mmol L}^{-1} \text{ h}^{-1}$, 50 mM Tris-HCl buffer (pH 6.5), volume=50 mL.

All research data supporting the findings described in this chapter are available in 4TU.Centre for Research Data at DOI: 10.4121/22194004, which is going to be released.

References

- [1] E. F. Aransiola, T. V. Ojumu, O. Oyekola, T. Madzimbamuto, D. Ikhu-Omoregbe, *Biomass Bioenergy* **2014**, *61*, 276-297.
- [2] M. Balat, H. Balat, *Energy Convers. Manage.* **2008**, *49*, 2727-2741.
- [3] G. J. S. Dawes, E. L. Scott, J. Le Nôtre, J. P. Sanders, J. H. Bitter, *Green Chem.* **2015**, *17*, 3231-3250.
- [4] D. Sorigue, B. Legeret, S. Cuine, S. Blangy, S. Moulin, E. Billon, P. Richaud, S. Brugiere, Y. Coute, D. Nurizzo, P. Mueller, K. Brettel, D. Pignol, P. Arnoux, Y. Li-Beisson, G. Peltier, F. Beisson, *Science* **2017**, *357*, 903-907.
- [5] F. Yang, J. A. DeLuca, R. Menon, E. Garcia-Vilarato, E. Callaway, K. K. Landrock, K. Lee, S. H. Safe, R. S. Chapkin, C. D. Allred, *Microb. Cell Fact.* **2020**, *19*, 219.
- [6] B. Lakavath, T. M. Hedison, D. J. Heyes, M. Shanmugam, M. Sakuma, R. Hoeven, V. Tilakaratna, N. S. Scrutton, *Anal. Biochem.* **2020**, 113749.
- [7] D. J. Heyes, B. Lakavath, S. J. Hardman, M. Sakuma, T. M. Hedison, N. S. Scrutton, *ACS Catal.* **2020**, *10*, 6691-6696.
- [8] M. Amer, E. Z. Wojcik, C. Sun, R. Hoeven, J. M. Hughes, M. Faulkner, I. S. Yunus, S. Tait, L. O. Johannissen, S. J. Hardman, *Energy Environ. Sci.* **2020**, *13*, 1818-1831.
- [9] J. Xu, Y. Hu, J. Fan, M. Arkin, D. Li, Y. Peng, W. Xu, X. Lin, Q. Wu, *Angew. Chem., Int. Ed.* **2019**, *58*, 8474-8478.
- [10] W. Zhang, J.-H. Lee, S. H. Younes, F. Tonin, P.-L. Hagedoorn, H. Pichler, Y. Baeg, J.-B. Park, R. Kourist, F. Hollmann, *Nat. Commun.* **2020**, *11*, 2258.
- [11] Y. Ma, X. Zhang, W. Zhang, P. Li, Y. Li, F. Hollmann, Y. Wang, *ChemPhotoChem* **2019**, *4*, 39-44.
- [12] Y. Ma, X. Zhang, Y. Li, P. Li, F. Hollmann, Y. Wang, *Sustain. Energ. Fuels* **2020**, *4*, 4232-4237.
- [13] H. J. Cha, S. Y. Hwang, D. S. Lee, A. R. Kumar, Y. U. Kwon, M. Voß, E. Schuiten, U. T. Bornscheuer, F. Hollmann, D. K. Oh, *Angew. Chem., Int. Ed.* **2020**, *59*, 7024-7028.
- [14] W. Zhang, M. Ma, M. M. Huijbers, G. A. Filonenko, E. A. Pidko, M. van Schie, S. de Boer, B. O. Burek, J. Z. Bloh, W. J. van Berkel, *J. Am. Chem. Soc.* **2019**, *141*, 3116-3120.

- [15] M. M. Huijbers, W. Zhang, F. Tonin, F. Hollmann, *Angew. Chem. Int. Ed.* **2018**, *57*, 13648-13651.
- [16] B. Burek, A. Sutor, D. W. Bahnemann, J. Z. Bloh, *Catal. Sci. Technol.* **2017**, *7*, 4977-4983.
- [17] A. Sutor, M. Heining, C. Lindenberger, R. Buchholz, *IEEE Trans. Magn.* **2014**, *50*, 8700204..
- [18] M. Heining, A. Sutor, S. Stute, C. Lindenberger, R. Buchholz, *J. Appl. Physiol.* **2015**, *27*, 59-66.
- [19] M. Heining, R. Buchholz, *Biotechnol. J.* **2015**, *10*, 1131-1137.
- [20] M. Heining, Dissertation, Erlangen, Friedrich-Alexander-Universität Erlangen-Nürnberg (Germany), **2016**.
- [21] J. Kuipers, H. Bruning, D. Yntema, H. Rijnaarts, *J. Photochem. Photobiol. A* **2015**, *299*, 25-30.
- [22] J. Kuipers, H. Bruning, S. Bakker, H. Rijnaarts, *Sens. Actuators A* **2012**, *178*, 217-222.
- [23] J. Kuipers, H. Bruning, D. Yntema, S. Bakker, H. Rijnaarts, *IEEE Trans. Ind. Electron.* **2013**, *61*, 2356-2361.
- [24] J. Z. Bloh, *Front. Chem.* **2019**, *7*, 128-140.
- [25] F. E. Osterloh, *ACS Energy Lett.* **2017**, *2*, 445-453.
- [26] A. Sutor, M. Heining, R. Buchholz, *Energies* **2019**, *12*, 1165.
- [27] L. Y. Kuritzky, A. C. Espenlaub, B. P. Yonkee, C. D. Pynn, S. P. DenBaars, S. Nakamura, C. Weisbuch, J. S. Speck, *Opt. Express* **2017**, *25*, 30696-30707.
- [28] M. A. Der Maur, A. Pecchia, G. Penazzi, W. Rodrigues, A. Di Carlo, *Phys. Rev. Lett.* **2016**, *116*, 027401.
- [29] D. H. König, N. Baucks, R.-U. Dietrich, A. Wörner, *Energy* **2015**, *91*, 833-841.
- [30] P. Tufvesson, J. Lima-Ramos, M. Nordblad, J. M. Woodley, *Org. Process Res. Dev.* **2010**, *15*, 266–274.
- [31] Y. Zhang, Y.-Q. Wu, N. Xu, Q. Zhao, H.-L. Yu, J.-H. Xu, *ACS Sustainable Chem. Eng.* **2019**, *7*, 7218-7226.
- [32] C. B. Davis, R. D. Hartnell, P. D. Madge, D. J. Owen, R. J. Thomson, A. K. Chong, R. L. Coppel, M. von Itzstein, *Carbohydr. Res.* **2007**, *342*, 1773-1780.

Chapter 4

- [33] E. W. Sugandhi, J. O. Falkinham III, R. D. Gandour, *Bioorg. Med. Chem.* **2007**, *15*, 3842-3853.
- [34] P. Tufvesson, J. Lima-Ramos, M. Nordblad, J. M. Woodley, *Org. Process Res. Dev.* **2011**, *15*, 266-274.
- [35] C. Hatchard, C. A. Parker, *Proc. Math. Phys. Eng. Sci. PROY SOC A-MATH PHY* **1956**, *235*, 518-536.
- [36] E. J. Prosen, F. D. Rossini, *J. Res. Natl. Bur. Stand.* **1945**, *34*, 263-269.
- [37] H. A. Swain, L. S. Silbert, J. G. Miller, *J. Am. Chem. Soc.* **1964**, *86*, 2562-2566.

Chapter 5: Stabilisation of the fatty acid decarboxylase from *Chlorella variabilis* by caprylic acid

Yinqi Wu, Caroline Paul, and Frank Hollmann

Based on *ChemBioChem* 2021, 22, 2420-2423.

Summary

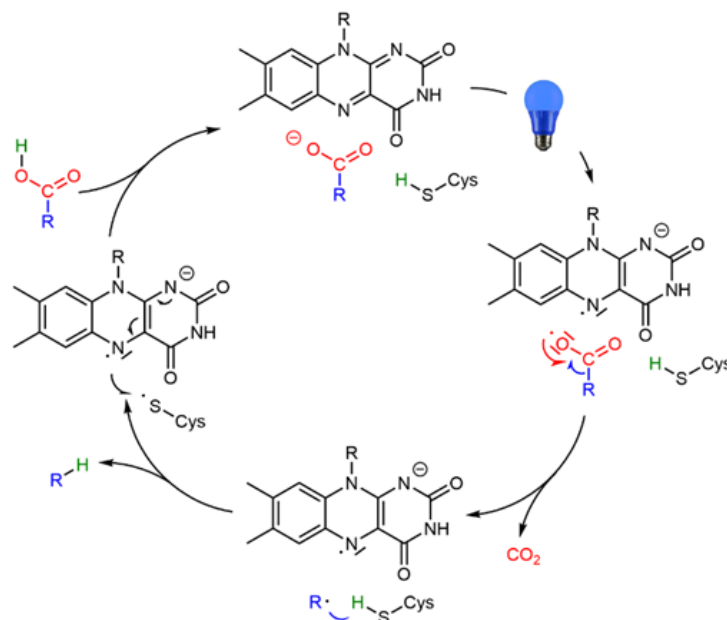
The fatty acid photodecarboxylase from *Chlorella variabilis* NC64A (CvFAP) catalyses the light-dependent decarboxylation of fatty acids. Photoinactivation of CvFAP still represents one of the major limitations of this interesting enzyme en route to practical application. In this study we demonstrate that the photostability of CvFAP can easily be improved by the administration of medium-chain length carboxylic acids such as caprylic acid indicating that the best way of maintaining CvFAP stability is 'to keep the enzyme busy'.

1. Introduction

The recently discovered fatty acid photodecarboxylase from *Chlorella variabilis* NC64A (CvFAP) catalyses the light-driven decarboxylation of fatty acids into their corresponding (C1-shortened) alkanes.^[1-2] CvFAP-catalysed transformations may play a role in the synthesis of fuel alkanes^[3-8] or value-added fine chemicals.^[9-10] Next to DNA photolyase^[11-12] and protochlorophyllide oxidoreductase,^[13] the flavin adenine dinucleotide (FAD)-containing CvFAP so far represents the only known example of a photoenzyme.

Upon illumination, the photoexcited FAD cofactor ($^1\text{FAD}^*$) inside the enzyme abstracts a single electron from the active site-bound carboxylate substrate resulting in the FAD semiquinone radical ($\text{FAD}^{\bullet-}$) and carboxyl radical. The latter rapidly decarboxylates yielding a short-lived alkyl radical (R^{\bullet}) which abstracts a H-atom from conserved cysteine or asparagine active site residues. The catalytic cycle is closed by an electron transfer from $\text{FAD}^{\bullet-}$ to the amino acid radical (Scheme 5.1).^[2, 14]

Similar to other flavin-containing enzymes,^[15-17] CvFAP is prone to photochemical inactivation.^[18] Scrutton and co-workers therefore suggested keeping CvFAP as much as possible under dark (or red light) conditions to minimise its inactivation.^[18] The same authors also reasoned that the photoinactivation may originate from a CvFAP malfunction upon photoactivation in the absence of a carboxylate substrate. In this situation, the photoexcited, high redox-potential flavin is assumed to oxidise nearby active site amino acid residues leading to irreversible inactivation of the enzyme.



Scheme 5.1. Catalytic cycle of the photoenzymatic decarboxylation of carboxylic acids catalysed by the photodecarboxylase from *Chlorella variabilis* NC64A (CvFAP).

2. Results and Discussion

We therefore set out to investigate whether the light-dependent inactivation of CvFAP may simply be alleviated by incubating the enzyme with carboxylic acids.

Prior to investigating the effect of irradiation on the stability of CvFAP, we first tested the thermal stability of the enzyme to rule out possible effect of thermal inactivation on the photoinactivation experiments. CvFAP rapidly lost its catalytic activity upon incubation at temperatures higher than 30°C ($t_{1/2}(40^{\circ}\text{C})\sim 2.7$ h; $t_{1/2}(50^{\circ}\text{C})<1$ h; after 24 h incubation at the temperatures, the catalytic activity was completely lost), whereas at 30°C, more than 90% of its initial activity was retained for at least 22 h (Figure 5.1 and Figure S5.2). We therefore continued our investigations under conditions at 30°C.

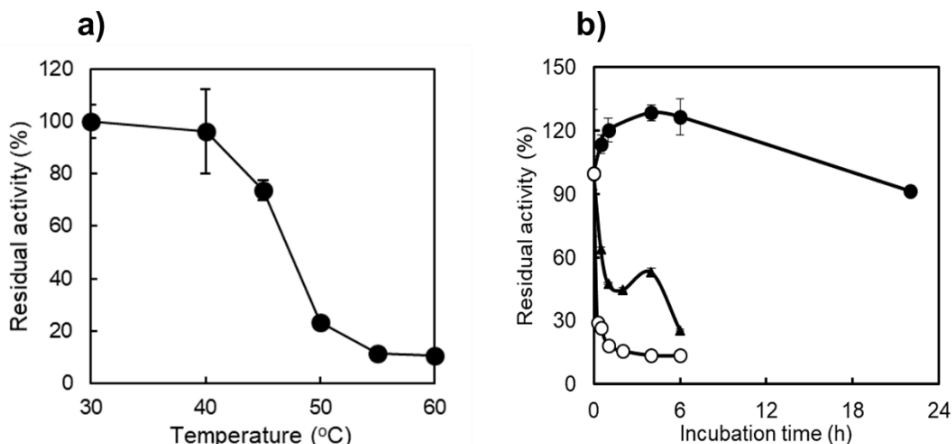


Figure 5.1. Thermal stability of CvFAP under dark conditions. (a) Residual activity of CvFAP after 15 min incubation at the temperature indicated, (b) Time course of CvFAP activity upon incubation at 30°C (●), 40°C (▲), 50°C (○). Incubation conditions: [CvFAP]=18 μM , buffer: 100 mM Tris-HCl (pH 8.5), protected from light. Activity assay conditions: [palmitic acid]₀=13 mM, [DMSO]=30 vol%, buffer: 100 mM Tris-HCl (pH 8.5), [CvFAP]=3–6 μM , light intensity of blue light=14.5 $\mu\text{E L}^{-1} \text{s}^{-1}$, $T=37^\circ\text{C}$, reaction time=30 min. Data represent the mean \pm SD of two independent experiments.

Next, we compared the photochemical inactivation of CvFAP as purified enzyme and as crude cell extract preparation (Figure 5.2). In previous studies we had already observed a significant difference in CvFAP performance in purified form and as crude cell extract.^[5] Under blue light illumination, the crude cell extract preparation of CvFAP was significantly more stable exhibiting a half-life time of approx. 19 h. Under the same conditions, the purified enzyme was almost completely inactivated within 2 h ($t_{1/2}$ ~1 h). Under dark conditions, both enzyme preparations exhibited comparable robustness.

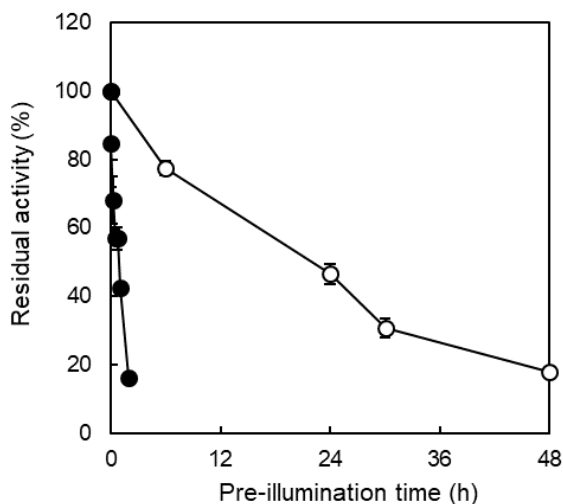


Figure 5.2. Comparison of photochemical inactivation of CvFAP as purified enzyme (●) and crude cell extract preparation (○). Incubation conditions: [CvFAP]=18 μM , buffer: 100 mM Tris-HCl (pH 8.5), light intensity of blue light=14.5 $\mu\text{E L}^{-1} \text{s}^{-1}$, $T=30\text{ }^\circ\text{C}$. Activity assay conditions: [palmitic acid]₀= 13 mM, [DMSO]=30 vol%, buffer: 100 mM Tris-HCl (pH 8.5), [CvFAP]=3-6 μM , light intensity of blue light=14.5 $\mu\text{E L}^{-1} \text{s}^{-1}$, $T=37\text{ }^\circ\text{C}$, reaction time=30 min. Data represent the mean \pm SD of two independent experiments.

It is worth mentioning here that the inactivation of the purified enzyme also depended on the wavelength of the light applied during incubation. Blue light ($\lambda_{\text{max}}=450\text{ nm}$) had the most pronounced inactivating effect, followed by green light ($\lambda_{\text{max}}=550\text{ nm}$) whereas red light ($\lambda_{\text{max}}=650\text{ nm}$) slightly influenced the stability of purified CvFAP (Figure 5.3). This corresponds well with the UV/Vis spectrum of CvFAP-bound FAD and supports the assumption of photoexcited FAD being the main cause of photoinactivation.

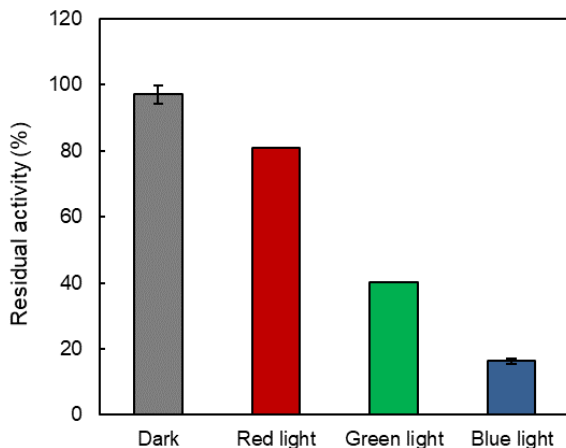


Figure 5.3. Residual activity of purified CvFAP illuminated under different wavelength of LEDs. Incubation conditions: [CvFAP]=18 μM , buffer: 100 mM Tris-HCl (pH 8.5), protected from light or illuminated by different color of light, T= 30 $^{\circ}\text{C}$, pre-illumination time=2 h. Activity assay conditions: [palmitic acid]₀= 13 mM, [DMSO]=30 vol%, buffer: 100 mM Tris-HCl (pH 8.5), [CvFAP]=3-6 μM , light intensity of blue light=14.5 $\mu\text{E L}^{-1} \text{s}^{-1}$, T=37 $^{\circ}\text{C}$, reaction time=30 min. Data represent the mean \pm SD of two independent experiments.

The strikingly higher photostability of CvFAP in crude cell extracts (Figure 5.2) may be attributed to the presence of *E. coli* borne carboxylic acids in these preparations. We therefore examined the influence of various carboxylic acids on the photostability of purified CvFAP (Figure 5.4).

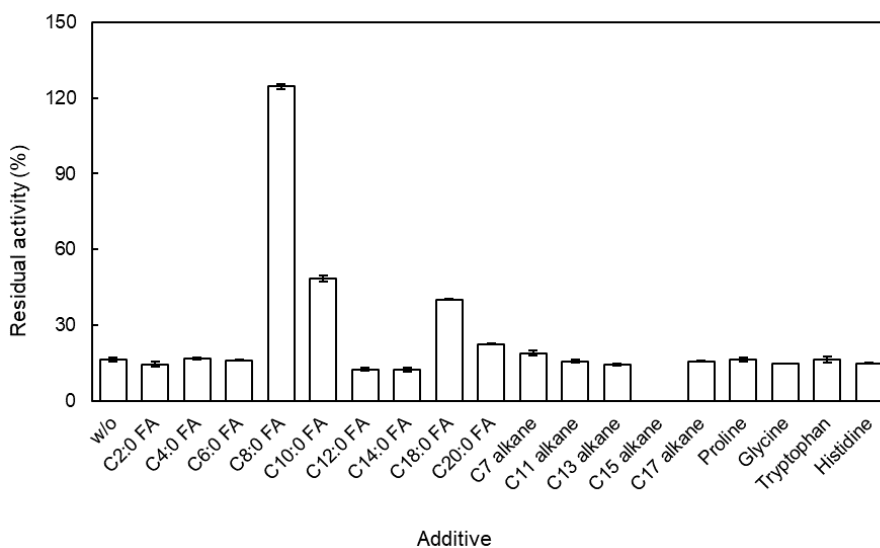


Figure 5.4. Influence of additive on the photostability of purified CvFAP. Incubation condition: [CvFAP]=18 μM , buffer: 100 mM Tris-HCl (pH 8.5), [DMSO]=5 vol %, light intensity

of blue light= $14.5 \mu\text{E L}^{-1} \text{s}^{-1}$, $T= 30 \text{ }^\circ\text{C}$, pre-illumination time=2 h, [additive]=10 mM. Activity assay conditions: [palmitic acid]₀= 13 mM, [DMSO]=30 vol%, buffer: 100 mM Tris-HCl (pH 8.5), [CvFAP]=3-6 μM , light intensity of blue light= $14.5 \mu\text{E L}^{-1} \text{s}^{-1}$, $T=37 \text{ }^\circ\text{C}$, reaction time=30 min. Data represent the mean \pm SD of two independent experiments.

Alkanes (as reaction products) did not exceed a significant stabilising effect on illuminated CvFAP, whereas several fatty acids stabilised the illuminated enzyme. This indicates that the photostability of CvFAP is linked to its decarboxylation reaction. Interestingly, caprylic acid had the most pronounced stabilising effect. This was somewhat unexpected as according to the previously determined substrate scope of CvFAP,^[1] caprylic acid should be a much poorer substrate compared to C₁₆-C₁₈ carboxylic acids. Currently, we are lacking a plausible explanation for why octadecanoic/eicosanoic acid were less efficient than caprylic acid, possibly the concentration of free octadecanoic/eicosanoic acid (more hydrophobic and hence exhibiting a lower critical micelle concentration) was lower than the one of caprylic acid. Possibly, the stabilising effect of caprylic acid may also be associated to the 'decoy effect' of the C₇ alkane product.^[3]

We further investigated the concentration-dependency of the stabilising effect of caprylic acid (Figure 5.5). Increasing the concentration of caprylic acid up to 10 mM steadily increased the stabilising effect, which may well be explained with increasing saturation of the active site of CvFAP. Further increase of the caprylic acid concentration apparently gradually decreased the stabilising effect. Most likely, this, however, is an artefact from the activity assay based on the accumulation of pentadecane. At high caprylic acid concentrations, its decarboxylation competes with the decarboxylation of palmitic acid and thereby reduce the pentadecane formation rate. In fact, caprylic acid could be converted during the pre-illumination process catalysed by CvFAP. After 24 h pre-illumination, little caprylic acid was detected and CvFAP exhibited little residual activity, compared with 46% residual activity of that incubated in dark for 24 h (Figure 5.2 and Figure S5.3).

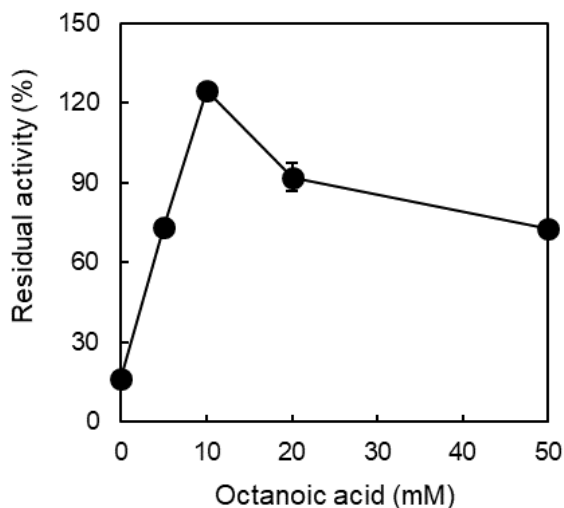
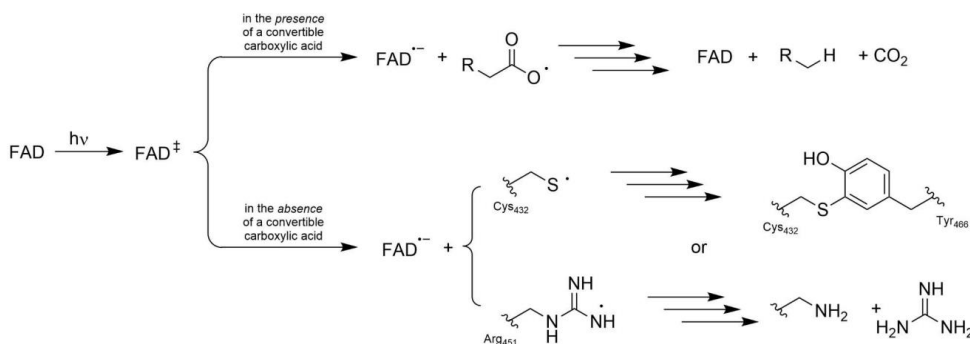


Figure 5.5. Influence of additive on the photostability of purified CvFAP. Incubation condition: [CvFAP]=18 μM , buffer: 100 mM Tris-HCl (pH 8.5), [DMSO]=5 vol %, light intensity of blue light=14.5 $\mu\text{E L}^{-1} \text{s}^{-1}$, T= 30 $^{\circ}\text{C}$, incubation time=2 h, [octanoic acid]=0-50 mM. Activity assay conditions: [palmitic acid]₀= 13 mM, [DMSO]=30 vol%, buffer: 100 mM Tris-HCl (pH 8.5), [CvFAP]=3-6 μM , light intensity of blue light=14.5 $\mu\text{E L}^{-1} \text{s}^{-1}$, T=37 $^{\circ}\text{C}$, reaction time=30 min. Data represent the mean \pm SD of two independent experiments.

Finally, we confirmed the stabilising effect of caprylic acid on purified, pre-illuminated CvFAP used in semi-preparative transformation of palmitic acid. Figure 5.5 impressively demonstrates the positive effect of simple caprylic acid in the pre-illumination reaction. While in the absence of caprylic acid, very low concentration of pentadecane was detected, the product accumulation rate of the caprylic acid protected CvFAP was comparable to activities previously observed (without pre-illumination).

Photoinactivation of CvFAP remains a major limitation to preparative application of this promising catalyst. In accordance with the CvFAP inactivation mechanism proposed by Scrutton and co-workers,^[18] our results indicate that photoexcitation of CvFAP in the absence of a convertible substrate (carboxylic acid) represents the main cause for CvFAP photoinactivation. In this situation, the photoexcited flavin oxidises active-site borne amino acids, which in light of the recent mechanistic studies by Beisson and co-workers,^[2] may be the catalytically active cysteine or arginine (Scheme 5.2).



Scheme 5.2. Possible mechanisms of CvFAP inactivation. In the presence of a carboxylic acid substrate the photoexcited flavin prosthetic group catalysed the radical decarboxylation reaction (see also Scheme 5.1). In the absence of a carboxylic acid, the photoexcited flavin may interact with amino acid residues such as Cys432 or Arg451 (and/or others) to resulting in chemically modified active site amino acid residues.

In the case of cysteine, it may be argued that the thiyl radical (lacking suitable reaction partners) may react with further amino acids such as tyrosine 466. It is also conceivable that arginine 451 undergoes deguanidination. These inactivation reactions may be expected to be dependent on the protonation stage of the amino acids and that pH-dependent inactivation experiments may shed a light on this. Moreover, digestion of the photoinactivated enzyme and mass-spectroscopic analysis of the fragments will shed a light on the inactivation mechanism and possibly serve as guiding principle for future CvFAP engineering to increase its photorobustness. Evidently, the generally observed ‘simple’ photobleaching of the flavin prosthetic group may also considerably contribute to the photoinactivation of CvFAP.

3. Conclusion

In the present study we have shown that the photostability issue of CvFAP, at least under illumination conditions, can significantly be alleviated by the addition of caprylic acid (and possibly some other carboxylic acids not tested yet). In line with previous suggestions by Scrutton and co-workers, these results point towards ‘keeping CvFAP catalytically busy’ as the most promising strategy to minimise photoinactivation of the enzyme.

4. Material and methods

4.1 Chemicals and materials

Eicosanoic acid (C20:0 FA), octadecanoic acid (C18:0 FA), hexadecanoic acid (C16:0 FA), myristic acid (C14:0 FA), lauric acid (C12:0 FA), decanoic acid (C10:0 FA), caprylic acid (C8:0 FA), hexanoic acid (C6:0 FA), butyric acid (C4:0 FA), acetic acid (C2:0 FA), proline, glycine, tryptophan, histidine, DMSO, heptane (C7 alkene), undecane (C11 alkene), tridecane (C13 alkene), pentadecane (C15 alkene), heptadecane (C17 alkene), bovine serum albumin (BSA) and other commercial chemicals were purchased from Sigma-Aldrich, Fluka, Acros or Alfa-Aesar, without any further purification. The water used was distilled.

4.2 Protein expression and purification

The *E. coli* BL21(DE3) cells containing the plasmid pET-28a(+) expressing CvFAP were cultivated in terrific broth (TB) medium containing 50 $\mu\text{g mL}^{-1}$ kanamycin at 37 °C and 180 rpm. When the optical density at 600 nm (OD600) reached 0.7-0.8, protein induction was initiated by adding 0.5 mM IPTG and cultivation temperature was decreased to 17 °C. After cultivation for about 20 h, cells were harvested by centrifugation (11000 $\times g$ at 4 °C for 10 min), washed twice with ice-cooled buffer A (50 mM Tris-HCl, 300 mM NaCl, 10 mM imidazole, 10% glycerol, pH 8.0). The cell pellet was resuspended in the same buffer containing 1 mM PMSF and 1 mM MgCl_2 and then cells were lysed by passing them through a Multi Shot Cell Disruption System at 1.5 kbar. The lysates were centrifuged at 38000 $\times g$ at 4 °C for 1 h and then passed through a filter of 0.45 μm to remove the particulate fraction. The purification was made on a His Trap Ni-NTA FF column (5 mL, GE Healthcare). After loading the lysate, the column was washed by 20 vol% buffer B (50 mM Tris-HCl, 300 mM NaCl, 200 mM imidazole, 10% glycerol, pH 8.0) and protein was then eluted by a step gradient using 40 vol% buffer B. The fractions were determined by SDS-PAGE and concentrated by ultrafiltration (50 kDa filters). The Ni-NTA column purification was performed by NGC system in the 10 °C fridge covered by aluminum foil. The concentrated purified protein was loaded on the desalting column (6 mL, PD10) to remove imidazole. Protein was eluted by buffer (100 mM Tris-HCl, pH 8.5). The yellow fractions were collected and protein concentration used for activity assay corresponded the protein containing FAD. FAD was quantified by measuring

absorbance at 450 nm on the protein which was previously heated at 95 °C for 5 min in the addition of 1 w/w % SDS.

4.3 Activity assay

The activity of enzyme CvFAP was assayed at 37 °C by monitoring the increase of pentadecane in a 1-mL reaction by using the gas chromatography (Shimadzu GC-2014) equipped with the column CP Sil 5 CB (50 m × 0.53 mm × 1.0 μm), using flame ionization detection (FID), and N₂ as the carrier gas. The standard assay mixture was composed of 13 mM palmitic acid as substrate, 30 vol% DMSO as cosolvent, buffer (100 mM Tris-HCl, pH 8.5), and CvFAP with an appropriate concentration and was under gentle magnetic stirring at 37 °C under the illumination of blue light (light intensity=14.5 μE L⁻¹ s⁻¹) for 30 min.

4.4 Thermal stability assay

The residual activity of CFE CvFAP and purified CvFAP were determined by incubating the enzyme (18 μM) in buffer (100 mM Tris-HCl, pH 8.5) at different temperature protected from light for a proper time and then performed the activity assay. The activity of CvFAP without any incubation before the activity assay was defined as 100% residual activity.

4.5 Photostability assay

The residual activity of CFE CvFAP and purified CvFAP were determined by incubating the enzyme CvFAP (18 μM) in buffer (100 mM Tris-HCl, pH 8.5) at 30 °C under the illumination of LEDs for a proper time and then performed the activity assay. The activity of CvFAP without any incubation or pre-illumination before the activity assay was defined as 100% residual activity. The half-lives($t_{1/2}$) of enzyme under corresponding conditions were calculated according to the deactivation function: $\ln(\text{residual activity}) = -kD/t$; $t_{1/2} = \ln 2/kD$. kD here represents the deactivation rate constant.

4.6 Photoenzymatic decarboxylation of palmitic acid to pentadecane

The 1 mL reaction was composed of 13 mM palmitic acid as substrate, 30 vol% DMSO as cosolvent, 3 μM purified CvFAP, and buffer (100 mM Tris-HCl, pH 8.5) and

Chapter 5

was under gentle magnetic stirring at 30°C under the illumination of blue light (light intensity=14.5 $\mu\text{E L}^{-1} \text{s}^{-1}$). Samples were withdrawn and extracted with ethyl acetate (containing 5 mM 1-octanol) for gas chromatography analysis.

4.7 Light intensity measurement

The light intensity was determined by means of ferrioxalate actinometry. 1 mL ferrioxalate solution (37.5 mM in 50 mM H_2SO_4) in a 4-mL transparent glass vial was illuminated under LED light. At defined intervals, 25 μL samples of the illuminated solution were taken and mixed with 175 μL of another solution (7.5 mL 50 mM H_2SO_4 , 2 mL 0.1% 1,10-phenantroline, 5 mL 1 M sodium acetate solution and 3 mL H_2O). The absorbance of the mixture was measured under 510 nm at room temperature. FeSO_4 was used as Fe(II) for the calibration curve. The light intensity was then calculated based on the Fe(II) generation rate in the irradiated ferrioxalate solution.

4.8 Gas Chromatography (GC)

The enzyme activity and time course of decarboxylation reaction catalysed by CvFAP were measured by monitoring the production of pentadecane by using the gas chromatography (Shimadzu GC-2014) with FID, equipped with column CP Sil 5 CB (50 m \times 0.53 mm \times 1.0 μm), 20 mL/min N_2 as the carrier gas. The injection temperature was 340 °C.

Table S5.1. Details of GC analysis.

Compound	Retention time (min)	Temperature profile
Palmitic acid (substrate)	10.76	110 °C hold 3 min, 25 °C/min to 190 °C hold 2.1 min, 25 °C/min to 230 °C
1-Octanol (internal standard)	3.23	hold 2.1 min, 30 °C/min to 325 °C
Pentadecane (product)	6.79	hold 1 min

4.9 Supporting results

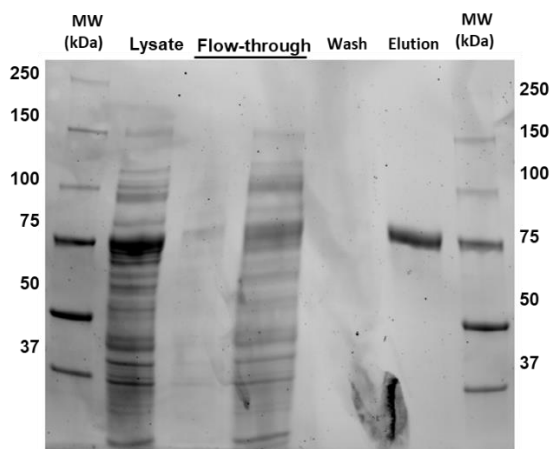


Figure S5.1. SDS-PAGE analysis of the cell-free extract and purified samples of CvFAP during the protein purification process. From left to right: (1) Molecular weight marker; (2) CFE CvFAP; (3) Flow-through from the Ni-column; (4) Wash fractions; (5) Elution fractions; (6) Molecular weight marker. Molecular weight marker of CvFAP is 77 kDa.

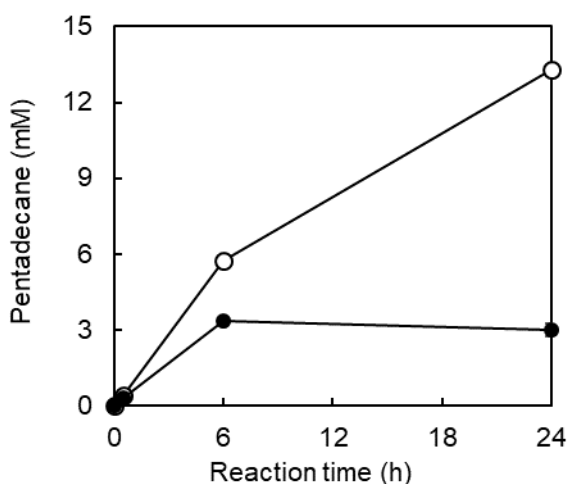
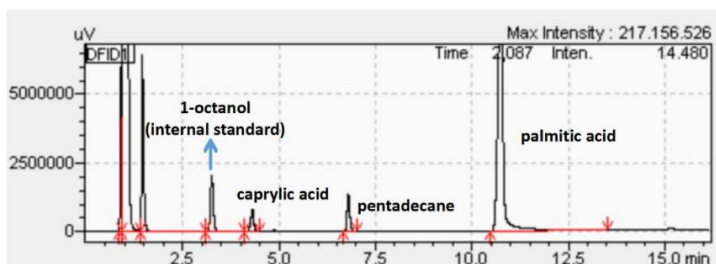


Figure S5.2. Decarboxylation of palmitic acid to pentadecane catalysed by purified CvFAP at 30 °C (O) or 37 °C (●) under blue light illumination. Reaction condition: [CvFAP]=3 μ M, [palmitic acid]₀=13 mM, [DMSO]=30 vol %, buffer: 100 mM Tris-HCl (pH 8.5), light intensity of blue light=14.5 μ E L⁻¹ s⁻¹, T=30 °C or 37 °C. Data represent the mean \pm SD of two independent experiments.

(A)



(B)

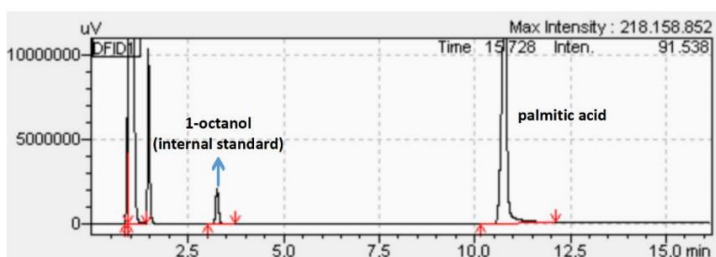


Figure S5.3. GC chromatograms of the palmitic acid decarboxylation catalysed by purified CvFAP for 0.5 h which has been pre-illuminated under blue light with 10 mM caprylic acid for 2 h (A) and 24 h (B).

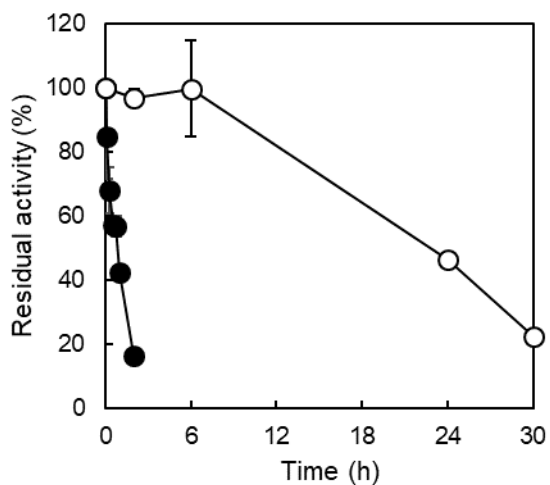


Figure S5.4. Time course of activity of purified CvFAP illuminated under blue light (●) or protected from light source (○). Incubation condition: [CvFAP]=18 μ M, buffer: 100 mM Tris-HCl (pH 8.5), light intensity of blue light=0 or 14.5 μ E L⁻¹ s⁻¹, T=30 °C, incubation time=0-48 h. Data represent the mean \pm SD of two independent experiments.

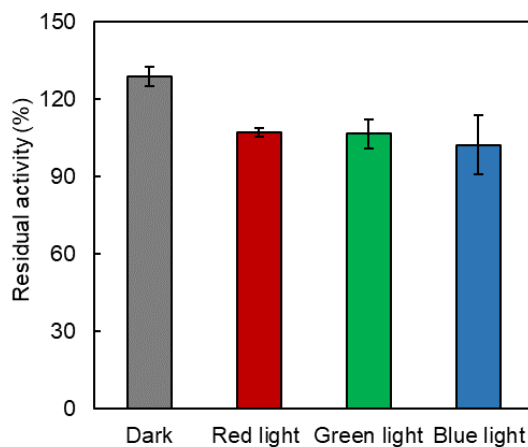


Figure S5.5. Photostability of CvFAP crude cell extract preparation illuminated under different wavelength of LEDs. Incubation condition: [CvFAP]=18 μ M, buffer: 100 mM Tris-HCl (pH 8.5), under illumination of different wavelength of light, T= 30 $^{\circ}$ C, incubation time=4 h. Data represent the mean \pm SD of two independent experiments.

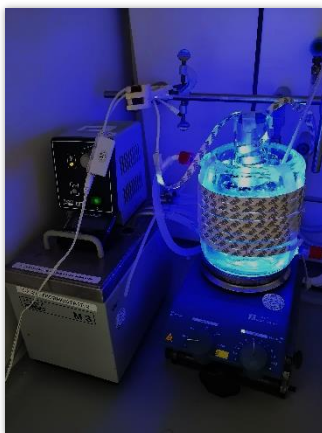


Figure S5.6. The homemade setup employed in this study.

All research data supporting the findings described in this chapter are available in 4TU.Centre for Research Data at <https://doi.org/10.4121/22193944.v1>

References

- [1] D. Sorigue, B. Legeret, S. Cuine, S. Blangy, S. Moulin, E. Billon, P. Richaud, S. Brugiere, Y. Coute, D. Nurizzo, P. Mueller, K. Brettel, D. Pignol, P. Arnoux, Y. Li-Beisson, G. Peltier, F. Beisson, *Science* **2017**, *357*, 903-907.
- [2] D. Sorigué, K. Hadjidemetriou, S. Blangy, G. Gotthard, A. Bonvalet, N. Coquelle, P. Samire, A. Aleksandrov, L. Antonucci, A. Benachir, *Science* **2021**, *372*, eabd5687.
- [3] R. Lin, C. Deng, W. Zhang, F. Hollmann, J. D. Murphy, *Trends Biotechnol* **2021**, *39*, 370-380.
- [4] W. Zhang, M. Ma, M. M. Huijbers, G. A. Filonenko, E. A. Pidko, M. van Schie, S. de Boer, B. O. Burek, J. Z. Bloh, W. J. van Berkel, *J. Am. Chem. Soc.* **2019**, *141*, 3116-3120.
- [5] M. M. Huijbers, W. Zhang, F. Tonin, F. Hollmann, *Angew. Chem., Int. Ed.* **2018**, *57*, 13648-13651.
- [6] Y. Ma, X. Zhang, Y. Li, P. Li, F. Hollmann, Y. Wang, *Sust. Energy Fuels* **2020**, *4*, 4232-4237.
- [7] S. Bruder, E. J. Moldenhauer, R. D. Lemke, R. Ledesma-Amaro, J. Kabisch, *Biotechnol. Biofuels* **2019**, *12*, 1-13.
- [8] H. T. Duong, Y. Wu, A. Sutor, B. O. Burek, F. Hollmann, J. Z. Bloh, *ChemSusChem* **2021**, *14*, 1053–1056.
- [9] W. Zhang, J.-H. Lee, S. H. Younes, F. Tonin, P.-L. Hagedoorn, H. Pichler, Y. Baeg, J.-B. Park, R. Kourist, F. Hollmann, *Nat. Commun.* **2020**, *11*, 2258.
- [10] H. J. Cha, S. Y. Hwang, D. S. Lee, A. R. Kumar, Y. U. Kwon, M. Voß, E. Schuiten, U. T. Bornscheuer, F. Hollmann, D. K. Oh, *Angew. Chem., Int. Ed.* **2020**, *59*, 7024-7028.
- [11] K. Brettel, M. Byrdin, *Curr. Opin. Struct. Biol.* **2010**, *20*, 693-701.
- [12] D. Zhong, *Ann. Rev. Phys. Chem.* **2015**, *66*, 691-715.
- [13] M. Gabruk, B. Mysliwa-Kurdziel, *Biochem.* **2015**, *54*, 5255-5262.
- [14] D. J. Heyes, B. Lakavath, S. J. Hardman, M. Sakuma, T. M. Hedison, N. S. Scrutton, *ACS Catal.* **2020**, *10*, 6691-6696.
- [15] M. Rauch, M. Huijbers, M. Pabst, C. Paul, M. Pešić, I. Arends, F. Hollmann, *BBA-Prot. Proteom.* **2020**, *1868*, 140303.

- [16] R. J. Kutta, N. Archipowa, N. S. Scrutton, *Phys. Chem. Chem. Phys.* **2018**, *20*, 28767-28776.
- [17] N. Skjoldager, M. Blanner Bang, M. Rykær, O. Björnberg, M. J. Davies, B. Svensson, P. Harris, P. Hägglund, *Sci. Rep.* **2017**, *7*, 1-10.
- [18] B. Lakavath, T. M. Hedison, D. J. Heyes, M. Shanmugam, M. Sakuma, R. Hoeven, V. Tilakaratna, N. S. Scrutton, *Anal. Biochem.* **2020**, *600*, 113749.

Chapter 6: Conclusion and Outlook

Chapter 6

Biocatalysts are enzymes or microorganisms that can catalyse chemical reactions with high selectivity under mild conditions, making them ideal candidates for sustainable chemical synthesis. By utilising biocatalysts, we can provide alternatives to traditional chemical methods, which often require harsh conditions, toxic solvents and generate waste. Nowadays, biocatalysis exhibits great application potential in pharmaceuticals, fine chemicals and biofuels. To fully exploit the potential of biocatalysis and create a more sustainable and environmentally friendly future, we still need to continue research to improve the efficiency, stability and specificity of biocatalysts, as well as to develop new biocatalytic reactions and explore novel applications.

In this thesis, we explored a variety of possibilities to apply unspecific peroxygenase from *Agrocybe aegerita* (AaeUPO) and fatty acid photodecarboxylase from *Chlorella variabilis* (CvFAP). The main goal was to use biocatalysts for the challenging chemical reactions, i.e. oxyfunctionalisation and decarboxylation. The investigation was meant to explore the alternatives to chemocatalysis. The approaches presented could be divided into four sections, as shown below.

Oxyfunctionalisation reactions:

- **Chapter 2:** Peroxygenase-promoted enzymatic cascades for the valorisation of fatty acids
- **Chapter 3:** An alginate-confined peroxygenase-CLEA for styrene epoxidation

Decarboxylation reactions:

- **Chapter 4:** Intensification of photobiocatalytic decarboxylation of fatty acids for the production of biodiesel
- **Chapter 5:** Stabilisation of the fatty acid decarboxylase from *Chlorella variabilis* by caprylic acid

1. Peroxygenase-promoted enzymatic cascades for the valorisation of fatty acids

Derivatization of fatty acids generally relies on pre-existing functional groups such as the carboxylate group or C=C-double bonds. Biocatalytic transformations of saturated, non-activated fatty acids enable the addition of functional groups to the alkane part of fatty acids, attributing the challenging character of C-H activation

chemistry.^[1-4] The oxyfunctionalisation reactions are reported to be catalysed by cytochrome P450 monooxygenases (P450s) and fungal peroxygenases.^[5-8] Compared with well-known P450s, peroxygenases excel in the much simpler reaction mechanism, while their synthesis application is hampered by their generally low selectivity.^[9-12]

In our recent work, a new mutant (*AaeUPO-Fett*) was obtained enabling higher regioselectivity (almost exclusively located at ω -1).^[13] We further explore the substrate scope of fatty acids (esters) and extend the synthetic potential of non-functionalised fatty acids (esters) as starting materials for value-added products and building blocks, such as lactones and polyesters. Under the optimised reaction condition, respectable 22540 catalytic turnovers are achieved when methyl decanoate is used as substrate. In the combination of *AaeUPO-Fett* with lipase B from *Candida antarctica* (*CalB*)^[14] and fatty acid photodecarboxylase from *Chlorella variabilis* (*CvFAP*)^[15] fatty alcohol synthesis is expected. Further synthesis possibilities arise in the enzymatic cascade reactions by the Baeyer-Villiger oxidation and the reductive amination reactions after the oxidation of hydroxy acids (esters) to keto acids (esters) (Figure 6.1).

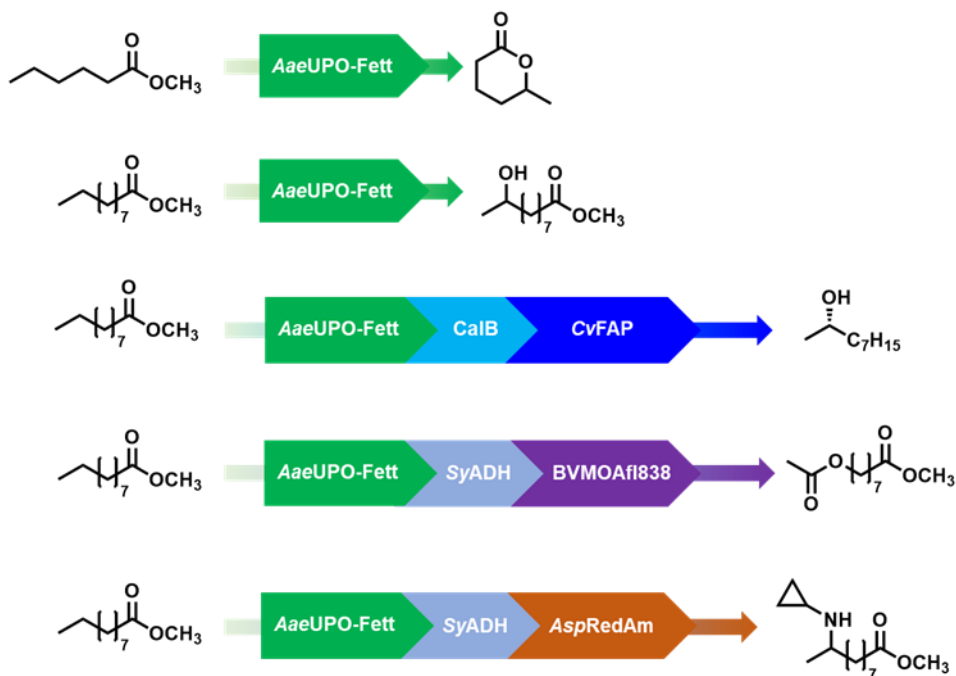


Figure 6.1. Peroxygenase-promoted (cascade) reactions.

Chapter 6

Despite various possibilities for fatty acids valorisation promoted by peroxygenase, we cannot deny that it is still far from industrial requirements. First of all, the stereoselectivity of *Aae*UPO-Fett towards fatty esters is eager to improve, where it is 77% for methyl hexanoate and 80% for methyl decanoate. Further protein rational design at the enzyme binding pocket could be performed to regulate the orientation of substrate binding for higher stereoselectivity. Alternatively, it is also possible to oxidise the hydroxy fatty esters to keto fatty esters and then perform the selective reduction to produce chiral products via multi-enzyme cascade reactions.^[16] Secondly, overoxidation was also observed when methyl decanoate was used as substrate. We simply circumvent it by applying a two-liquid-phase system (2LPS), while it is also worth mentioning other strategies, including protein engineering to regulate substrate specificity between fatty esters and hydroxy fatty esters, utilising flow reactor with immobilised enzyme to control the product concentration in a low range, combining other enzymes to catalyse the reduction of keto fatty esters. Thirdly, oxidative inactivation is not an uncommon issue for UPOs in oxyfunctionalisation reactions. Even under a relatively low H_2O_2 dosing rate ($2 \text{ mM}\times\text{h}^{-1}$), *Aae*UPO-Fett completely lost activity after 72 h in methyl decanoate hydroxylation. Future research on the mechanism of oxidative inactivation is required to obtain robust UPOs via protein engineering and/or enzyme immobilisation, in which case biocatalysis could be comparable with chemocatalysis. Besides, it has been demonstrated by several enzymatic cascade reactions, but there is still some space for improvement. For instance, *Cv*FAP and *Asp*RedAm show limited activity towards the intermediate (*S*)-methyl 9-hydroxydecanoic acid and methyl 9-oxo-decanoate, respectively, whereas longer reaction time and higher enzyme loading were required. We therefore believe that gene mining for biocatalysts with specific substrate preference and reaction engineering would greatly increase the turnover numbers of cascade reactions, making it more efficient and economical.

2. An alginate-confined peroxygenase-CLEA for styrene epoxidation

Unspecific peroxygenases, as a promising alternative for the oxyfunctionalisation reactions, are enjoying an increasing interest.^[9] Selective epoxidation occurring on C=C bonds makes contributions to chiral building block synthesis.^[17] To increase the

economic viability and environmental friendliness of the biocatalytic reactions, a non-aqueous reaction condition was established to avoid the high water footprint. The difference between the hydrophobic organic phase and hydrophilic enzyme often result in enzyme activity losses or mass transfer issue.

After the optimisation of immobilisation steps, *AaeUPO* was encapsulated in alginate matrices after the CLEA formation. The imm-*AaeUPO* exhibited better thermal stability, remaining 80% residual activity after incubation at room temperature for two weeks, while free *AaeUPO* lost all activity after 8 days. When imm-*AaeUPO* was used as catalyst for *cis*- β -methylstyrene epoxidation in the neat substrate reaction medium, the productivity (1.25 mM h⁻¹) was three times higher than that of free *AaeUPO*, mainly due to the elimination of ^tBuOOH and/or *cis*- β -methylstyrene diffusion rate limitation. Further investigation of ^tBuOOH feeding rate led to an excellent TN of 96 000 for the biocatalyst, with 48 mM enantiomerically pure (2*R*,3*S*)-2-methyl-3-phenyloxirane formed within 72 h, outperforming comparable reaction systems (Table 6.1).

Table 6.1. Comparison of the catalytic performance of the proposed system with some methods reported.

Catalyst	Oxidant	TN (Cat) ^[a]	Ref.
Co _{1,3} O _{1,4} -N/C	^t BuOOH	25 (150 after several recycles)	[18]
CYP101B1	NADPH/O ₂ ^[b]	~3080 ^[b]	[19]
StyAB ^[b]	NADPH/O ₂ ^[c]	2867	[20]
Imm- <i>AaeUPO</i>	^t BuOOH	96 000	Chapter 3

^[a] TN = moles_{product} × moles_{catalyst}⁻¹;

^[b] Recombinant cells (*E. coli* overexpressing the P450 monooxygenase CYP101B1, from a *Novosphingobium* strain) were used as catalyst; the enzyme concentration was estimated to be 650 nM; O₂ was reductively activate by the P450 monooxygenase;

^[c] StyAB: Styrene monooxygenase from *Pseudomonas* sp. VLB120 (recombinantly expressed in *E. coli*).

This catalytic performance of imm-*AaeUPO* favourably compares to chemical catalysts,^[18] P450 monooxygenases^[19] or other established enzymatic systems,^[21-24] However, only *cis*- β -methylstyrene and styrene were used as neat substrate reaction medium, the applicability of the biocatalyst needs to be further investigated. In addition, imm-*AaeUPO* was sensitive toward oxidants, which also remains a key

issue for other UPOs. *In situ* generation of oxidant, protein engineering and/or gene mining for high oxidant tolerant enzymes could be doable options. It is also worth mentioning that the largest contributors to E-factor were non-reacted starting material and enzyme preparation. It indicates that the relatively low activity recovery led to the limited specific activity of imm-UPOs,^[21, 25] remaining the bottleneck of the oxyfunctionalisation reactions catalysed by imm-UPOs. We are convinced that further optimising the immobilisation procedure to increase the enzyme immobilisation yield could make the reaction system more economical and environmentally feasible. Therefore, the UPO system would be a promising alternative to chemocatalysis in oxyfunctionalisation reactions.

3. Intensification of photobiocatalytic decarboxylation of fatty acids for the production of biodiesel

Conversion of natural fatty acids to alkanes as biodiesel exhibits the advantage of higher caloric value and avoiding the considerable molar surpluses of methanol, compared with the most widespread transesterification.^[26] Light-dependent fatty acid decarboxylation catalysed by CvFAP represents a simple and direct system for the production of biodiesel. However, the heterogeneous, optically non-transparent, and highly reflective reaction mixtures result in the poor penetration depth of photons into the reactor. Therefore, a major of catalysts is unilluminated and idle, limiting the productivity of photoenzymatic decarboxylation.^[27-33]

A new photoreactor concept comprising internal illumination by means of wirelessly powered light emitters (WLEs) has been recently established to alleviate this above shortcoming.^[34] By utilising the WLEs technique, we have demonstrated that the rate of photoenzymatic reactions could be dramatically increased (22-fold rate acceleration), allowing to seamlessly scale-up the production volume to industrially relevant dimensions.

This study, however, also revealed current shortcomings of the proposed photosynthetic fuel generation (Table 6.2). On the one hand, the cost of pentadecane synthesised in the photodecarboxylation is $631 \text{ €} \times L_{\text{pentadecane}}^{-1}$, which is much higher than the market price of pentadecane. The major contributions are the catalyst preparation (62.8%) and co-solvent (36.9%).

Table 6.2. Cost of pentadecane produced from CvFAP-catalysed decarboxylation of palmitic acid

	Raw materials	Cost (€×L _{pentadecane} ⁻¹)
Substrate	Palmitic acid	1.67
Catalyst	CvFAP@ <i>E.coli</i>	395.96
Buffer	Tris	0.03
	HCl	0.23
	H ₂ O	0.23
Co-solvent	DMSO	232.88
Sum		631.00

To reduce the cost of enzyme, the optimisation of gene expression system and the fermentation process is required. Furthermore, in our experiments, the turnover numbers for CvFAP ($\text{TON} = \text{mol}_{\text{product}} \times \text{mol}_{\text{CvFAP}}^{-1}$) never exceeded 9000, resulting in high enzyme loadings in photodecarboxylation reactions. To our surprise, under illumination with high light intensity, catalysts would completely lose activity within a short time (approx. 2 h), leading to poor operational stability. We believe that enzyme usage could be significantly decreased when a more efficient and robust reaction is established through reaction engineering. Performing the photoenzymatic reaction under anaerobic environment is proposed to solve this issue.^[35] Alternatively, we are convinced that further improvements can be expected from increasing the substrate affinity of enzyme resulting in more stable enzyme variants to render the envisioned photosynthetic production of alkanes economically feasible.

Besides, reaction optimisation is required to get rid of the current co-solvent dimethyl sulfoxide (DMSO), which is not only expensive but also makes downstream processing difficult. Other co-solvents, i.e. methanol, could be alternatively used in photodecarboxylation, towards which CvFAP showed modest organic tolerance.^[36] In addition, compared with DMSO, methanol exhibits strength in low price and ease of downstream processing. Furthermore, applying 2LPS or MARS by utilising cheap alkanes as water insoluble solvent might be another doable option. In this case, no co-solvent is required and the organic phase could be recycled or directly used as biodiesel without further isolation. Apart from it, alkanes could also serve as decoy molecule to increase the enzyme activity (and stability) when shorter fatty acids are used as substrate.^[37]

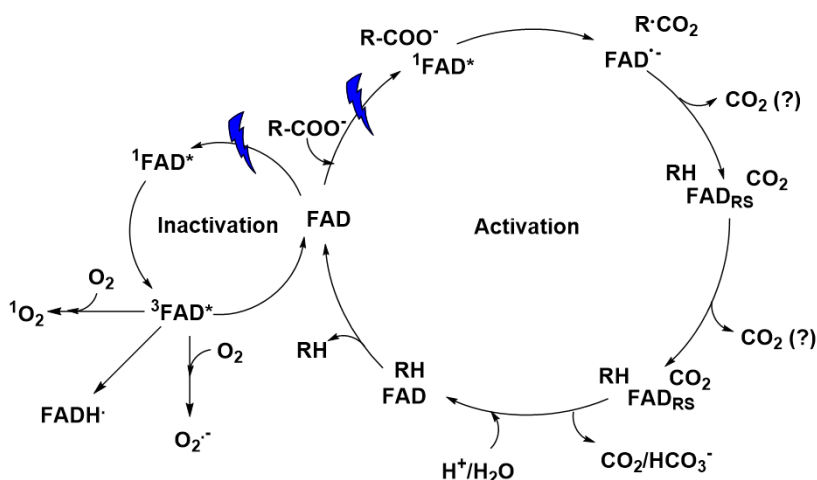
On the other hand, more efforts should be spent on high-valued products instead of bulk chemicals to make the biocatalysis more economical. For instance, the advantage of biocatalysis would dominate when CvFAP exhibits great activity and

selectivity towards some pharmaceutical chemicals. In this case, the cost of enzyme preparation and solvent would not be a problem.

4. Stabilisation of the fatty acid decarboxylase from *Chlorella variabilis* by caprylic acid

Decarboxylation of fatty acids to their corresponding (C_1 -shortened) alkanes plays a role in the synthesis of biofuels^[15, 30, 38] and other value-added fine chemicals.^[29, 33] The recently discovered FAD-contained photoenzyme CvFAP so far represents the only known biocatalyst for non-oxidative decarboxylation of fatty acids.^[39] On the one hand, the light-dependent enzyme catalyse the decarboxylation reaction under blue light illumination. On the other hand, the illumination also cause photo inactivation to CvFAP (Scheme 6.1).^[35, 40]

There is a significant difference in photostability between purified enzyme ($t_{1/2} < 1$ h) and crude cell extraction ($t_{1/2} \sim 19$ h). Further investigation on the effect of various *E. coli*-borne carboxylic acids (C_2 - C_{20} fatty acids) on photostability indicates that the photostability of CvFAP is linked to its decarboxylation reaction. Among, caprylic acid had the most pronounced stabilising effect, although, towards which enzyme does not show substrate preference. However, it is worth mentioning that the stabilisation became ineffective when caprylic acid was completely converted. The addition of high concentration of caprylic acid will lead to the competition for the enzyme active site with the target substrate.



Scheme 6.1. Catalytic mechanism and photoinactivation of CvFAP.^[35, 40-42]

Photoinactivation of CvFAP remains a major limitation to preparative application of this promising catalyst. For synthesis applications, cell-free extract or whole cells would be recommended to use as catalyst for decarboxylation reactions due to their higher photostability. Besides, a radical-based inactivation mechanism has been proposed^[40] and it has been demonstrated that the poor photostability resulted from the superoxide radical and singlet oxygen formed in CvFAP in the absence of substrate under aerobic environment.^[35] To alleviate the light-dependent inactivation, avoiding the light illumination or keeping enzyme under dim red light during enzyme preparation and performing photodecarboxylation under anaerobic environment could be a promising approach. In addition, rational designing the enzyme active site to improve the substrate binding is one of the promising strategies to regulate the enzyme photostability. Alternatively, the flavin-tag labeling method allowing the covalent attachment of FAD to CvFAP using a short flavinylation peptide-tag, in which case, cofactor FAD could be exposed at the protein surface,^[43] might help substrate binding and production releasing. Therefore, the formation of superoxide radical and singlet oxygen formed could be circumvented.

5. Final conclusion

This thesis is dedicated to demonstrate the application possibilities of biocatalysts (UPO and FAP) in oxyfunctionalisation and decarboxylation reactions. Enzymatic cascade reactions, enzyme immobilisation for non-aqueous reaction condition, photobiocatalytic reaction intensification and enzyme stabilisation have been investigated to exploit the potential of biocatalysis. The continuous research of these techniques will help to develop more efficient, robust and economical biocatalytic approaches, providing more suitable and environmentally friendly options for chemical reactions.

References

- [1] U. Biermann, U. T. Bornscheuer, I. Feussner, M. A. Meier, J. O. Metzger, *Angew. Chem., Int. Ed.* **2021**, *60*, 20144-20165.
- [2] R. I. Ma, L. Pérez, C. M. Ma, R. Pons, M. Mitjans, P. V. Ma, T. G. Ma, A. Pinazo, *Eur. J. Lipid Sci. Technol.* **2010**, *112*, 110–121.
- [3] C. Aouf, E. Durand, J. Lecomte, M.-C. Figueroa-Espinoza, E. Dubreucq, H. Fulcrand, P. Villeneuve, *Green Chem.* **2014**, *16*, 1740-1754.
- [4] M. B. Ansorge-Schumacher, O. Thum, *Chem. Soc. Rev.* **2013**, *42*, 6475-6490.
- [5] M. Hobisch, P. De Santis, S. Serban, A. Basso, E. Byström, S. Kara, *Org. Process Res. Dev.* **2022**, *26*, 2761-2765.
- [6] L. Schäfer, R. Karande, B. Bühler, *Front. Bioeng. Biotechnol.* **2020**, *8*, 140.
- [7] J. Chen, F. Kong, N. Ma, P. Zhao, C. Liu, X. Wang, Z. Cong, *ACS Catal.* **2019**, *9*, 7350-7355.
- [8] F. Tonin, F. Tieves, S. Willot, A. van Troost, R. van Oosten, S. Breestraat, S. van Pelt, M. Alcalde, F. Hollmann, *Org. Process Res. Dev.* **2021**, *25*, 1414-1418.
- [9] M. Hobisch, D. Holtmann, P. G. de Santos, M. Alcalde, F. Hollmann, S. Kara, *Biotechnol. Adv.* **2021**, *51*, 107615.
- [10] S. Peter, M. Kinne, X. Wang, R. Ullrich, G. Kayser, J. T. Groves, M. Hofrichter, *FEBS J.* **2011**, *278*, 3667-3675.
- [11] C. E. Paul, E. Churakova, E. Maurits, M. Girhard, V. B. Urlacher, F. Hollmann, *Bioorg. Med. Chem.* **2014**, *22*, 5692-5696.
- [12] A. Olmedo, C. Aranda, J. C. Del Río, J. Kiebist, K. Scheibner, A. T. Martínez, A. Gutiérrez, *Angew. Chem.* **2016**, *128*, 12436-12439.
- [13] P. Gómez de Santos, A. González-Benjumea, Á. Fernández García, Y. Wu, A. But, P. Molina-Espeja, D. M. Maté, D. González-Pérez, W. Zhang, J. Kiebist, *Angew. Chem., Int. Ed.* **2022**, *62*, e2022173.
- [14] P. Chandra, R. Singh, P. K. Arora, *Microb. Cell Factories* **2020**, *19*, 169.
- [15] M. M. Huijbers, W. Zhang, F. Tonin, F. Hollmann, *Angew. Chem., Int. Ed.* **2018**, *57*, 13648-13651.
- [16] X. Xu, H. Brasselet, E. Jongkind, M. Alcalde, C. Paul, F. Hollmann, *ChemBioChem* **2022**, *23*, e202200017.

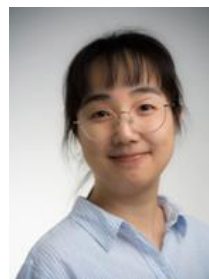
- [17] Z. A. Morrison, M. Nitz, *Org. Lett.* **2020**, *22*, 1453-1457.
- [18] D. Banerjee, R. V. Jagadeesh, K. Junge, M. M. Pohl, J. Radnik, A. Brückner, M. Beller, *Angew. Chem.* **2014**, *126*, 4448-4452.
- [19] M. R. Sarkar, J. H. Lee, S. G. Bell, *ChemBioChem* **2017**, *18*, 2119-2128.
- [20] K. Hofstetter, J. Lutz, I. Lang, B. Witholt, A. Schmid, *Angew. Chem., Int. Ed.* **2004**, *43*, 2163-2166.
- [21] M. C. Rauch, F. Tieves, C. E. Paul, I. W. Arends, M. Alcalde, F. Hollmann, *ChemCatChem* **2019**, *11*, 4519-4523.
- [22] C. Mateo, J. M. Palomo, L. M. Van Langen, F. Van Rantwijk, R. A. Sheldon, *Biotechnol. Bioeng.* **2004**, *86*, 273-276.
- [23] A. Schmid, K. Hofstetter, H. J. Feiten, F. Hollmann, B. Witholt, *Adv. Synth. Catal.* **2001**, *343*, 732-737.
- [24] H. Toda, R. Imae, N. Itoh, *Tetrahedron: Asymmetry* **2012**, *23*, 1542-1549.
- [25] L.-E. Meyer, B. F. Hauge, T. M. Kvorning, P. De Santis, S. Kara, *Catal. Sci. Technol.* **2022**, *12*, 6473-6485.
- [26] M. Balat, H. Balat, *Energy Convers. Manag.* **2008**, *49*, 2727-2741.
- [27] M. M. E. Huijbers, W. Zhang, F. Tonin, F. Hollmann, *Angew. Chem., Int. Ed.* **2018**, *57*, 13648-13651.
- [28] M. Amer, E. Z. Wojcik, C. Sun, R. Hoeven, J. M. Hughes, M. Faulkner, I. S. Yunus, S. Tait, L. O. Johannissen, S. J. Hardman, *Energy Environ. Sci.* **2020**, *13*, 1818-1831.
- [29] H. J. Cha, S. Y. Hwang, D. S. Lee, A. R. Kumar, Y. U. Kwon, M. Voß, E. Schuiten, U. T. Bornscheuer, F. Hollmann, D. K. Oh, *Angew. Chem.* **2020**, *132*, 7090-7094.
- [30] Y. Ma, X. Zhang, Y. Li, P. Li, F. Hollmann, Y. Wang, *Sustain. Energy Fuels* **2020**, *4*, 4232-4237.
- [31] J. Xu, Y. Hu, J. Fan, M. Arkin, D. Li, Y. Peng, W. Xu, X. Lin, Q. Wu, *Angew. Chem.* **2019**, *131*, 8562-8566.
- [32] Y. Ma, X. Zhang, W. Zhang, P. Li, Y. Li, F. Hollmann, Y. Wang, *ChemPhotoChem* **2019**, *4*, 39-44.
- [33] W. Zhang, J.-H. Lee, S. H. Younes, F. Tonin, P.-L. Hagedoorn, H. Pichler, Y. Baeg, J.-B. Park, R. Kourist, F. Hollmann, *Nat. Commun.* **2020**, *11*, 2258.
- [34] B. Burek, A. Sutor, D. W. Bahnemann, J. Z. Bloh, *Catal. Sci. Technol.* **2017**, *7*, 4977-4983.

Chapter 6

- [35] X. Guo, A. Xia, W. Zhang, F. Li, Y. Huang, X. Zhu, X. Zhu, Q. Liao, *Chin Chem Lett.* **2023**, *34*, 107875.
- [36] Q. Wu, D. Li, T. Han, J. Xue, W. Xu, J. Xu, *Angew. Chem.* **2021**, *133*, 20863-20867.
- [37] W. Zhang, M. Ma, M. M. Huijbers, G. A. Filonenko, E. A. Pidko, M. van Schie, S. de Boer, B. O. Burek, J. Z. Bloh, W. J. van Berkel, *J. Am. Chem. Soc.* **2019**, *141*, 3116-3120.
- [38] R. Lin, C. Deng, W. Zhang, F. Hollmann, J. D. Murphy, *Trends Biotechnol.* **2021**, *39*, 370-380.
- [39] D. Sorigué, B. Legeret, S. Cuiné, S. Blangy, S. Moulin, E. Billon, P. Richaud, S. Brugière, Y. Couté, D. Nurizzo, *Science* **2017**, *357*, 903-907.
- [40] B. Lakavath, T. M. Hedison, D. J. Heyes, M. Shanmugam, M. Sakuma, R. Hoeven, V. Tilakaratna, N. S. Scrutton, *Anal. Biochem.* **2020**, *600*, 113749.
- [41] D. J. Heyes, B. Lakavath, S. J. Hardman, M. Sakuma, T. M. Hedison, N. S. Scrutton, *ACS Catal.* **2020**, *10*, 6691-6696.
- [42] D. Sorigué, K. Hadjidemetriou, S. Blangy, G. Gotthard, A. Bonvalet, N. Coquelle, P. Samire, A. Aleksandrov, L. Antonucci, A. Benachir, *Science* **2021**, *372*, eabd5687.
- [43] Y. Tong, M. Lee, J. Drenth, M. W. J. B. C. Fraaije, **2021**, *32*, 1559-1563.

Curriculum Vitae

Name: Yinqi Wu
Date of Birth: 21.04.1994
Place of Birth: Wuxi, Jiangsu, China



Education

09.2012 – 06.2016 **Bachelor in Bioengineering**
Changzhou University, China
09.2016 – 06.2019 **Master in Light Industry Technology and Engineering**
East China University of Science and Technology, China
10.2019 – 09.2023 **PhD candidate in Biotechnology**
Delft University of Technology, The Netherlands

List of publications

- [1] Duong, H. T.,⁺ **Wu, Y.**,⁺ Sutor, A., Burek, B. O.,^{*} Hollmann, F.^{*} and Bloh, J. Z.^{*} Intensification of photobiocatalytic decarboxylation of fatty acids for the production of biodiesel. *ChemSusChem*, **2021**, 14(4), 1053-1056.
- [2] **Wu, Y.**, Paul, C. E. and Hollmann, F.^{*} Stabilisation of the fatty acid decarboxylase from *Chlorella variabilis* by caprylic acid. *ChemBioChem*, **2021**, 22(14), 2420-2423.
- [3] Nintzel, F. E.,⁺ **Wu, Y.**,⁺ Planchestainer, M., Held, M., Alcalde, M. and Hollmann, F.^{*} An alginate-confined peroxygenase-CLEA for styrene epoxidation. *Chem Commun*, **2021**, 57(47), 5766-5769.
- [4] de Santos, P. G.,⁺ González-Benjumea, A.,⁺ Fernandez-Garcia, A.,⁺ Aranda, C., **Wu, Y.**, But, A., Molina-Espeja, P., Maté, D. M., Gonzalez-Perez, D., Zhang, W., Kiebist, J., Scheibner, K., Hofrichter, M., Świderek, K., Moliner, V., Sanz-Aparicio, J., Hollmann, F., Gutiérrez, A. and Alcalde, M.^{*} Engineering a highly regioselective

fungal peroxygenase for the synthesis of hydroxy fatty acids. *Angew. Chem., Int. Ed.*, **2023**, *62*, e2022173.

[5] Domestici, C., **Wu, Y.**, Hilberath, T., Alcalde, M., Hollmann, F.* and Macchioni, A.* Hybrid organometallic and enzymatic tandem catalysis for oxyfunctionalisation. *ChemCatChem*, **2023**, *15*, e202201623.

[6] **Wu, Y.**, Paul, C. E., Hilberath, T., Jongkind, E. P.J., Zhang, W., Alcalde, M. and Hollmann, F.* Peroxygenase-promoted enzymatic cascades for the valorisation of fatty acids. *ChemCatChem*, **2023**, *15*, e202300411.

[7] **Wu, Y.**,⁺ Chen, Q.,⁺ Chen, Q.,⁺ Geng, Q., Zheng, Y., Zhao, C., Zhang, Y., Zhou, J., Wang, B.,* Xu, J.* and Yu, H.* Precise regulation of the substrate selectivity of Baeyer-Villiger monooxygenase to minimize overoxidation of prazole sulfoxides. *Chinese J. Catal. (Accepted)*

[8] **Wu, Y.**, Paul, C. E. and Hollmann, F.* Mirror, mirror on the wall who is the greenest of them all? A critical comparison of chemo- and biocatalytic oxyfunctionalisation reactions. (*Manuscript in preparation*)

[9] **Wu, Y.**, Brasselet, H., van der Meer, J. and Hollmann, F.* Preparative production of cosmetic alcohols using a photoenzymatic cascade. (*Manuscript in preparation*)

Patent

[1] Hollmann, F., **Wu, Y.**, Duong, H. T., Burek, B. O., & Bloh, J. Z. Photobiocatalytic decarboxylation of fatty acids. 2020. NL2027059B1.

[2] Hollmann, F., Brasselet, H., **Wu, Y.**, Alcalde, M., Opperman, D. Oxidative lactonization reaction transforming fatty acids into lactones catalysed by a peptide with peroxygenase activity. Ref. G160764NL00, OCT-22-044. *Patent pending*.

+ authors contributed equally

* Corresponding author

Acknowledgements

Time flies. Before writing acknowledgements, I did not realise I am at the end of my PhD journey. Within four years, we experienced the terrible COVID-19 pandemic together, which made my PhD study a little bit different from my expectation. Fortunately, I have been surrounded by many nice people and working in a very nice and friendly group. Without their help and support, this thesis could not have been finished.

The first person I would like to thank greatly is Frank. Without him, I would not be able to have the opportunity to do my PhD at TU Delft. As a supervisor, he provided an endless flow of project ideas, some of which are quite creative and cool. More important, he has given us a lot of academic freedom and he is always open for discussion and encouraging all “crazy” ideas to promote our enthusiasm. For me, Frank is not only a supervisor but also a mentor. I would never forget the first practice I had with him “Say no”. Many thanks for letting me have the brave and strategy to stand up for myself while keeping a good relationship.

Secondly, many thanks to my co-promotor Caroline. She has provided me with a lot of practical supervision. In our regular bi-weekly meeting, she was always very willing to help me with the experimental questions and writing stuff. Also, many thanks for the discussion and suggestions regarding my future career. I appreciate a lot for the academic world she showed me.

Thirdly, I would like to thank my officemate, Thomas. It is my pleasure to share the office room with him for three years. As a biochemist, he gave a lot of helps and discussions on my project, providing many different perspectives. Apart from lab work, the activities we had together with others in Leeuwenhorst (NCCC), Hamburg (Biocat), Düsseldorf (Christmas market), Keukenhof, and Delft are very impressive. Also, thanks to Hugo. We had a very good collaboration on a master project supervision and patent application. I would not forget the “shitty jokes” he made. It is he who brought laughter and happiness to our lab and office. Many thanks to another skilful scientist, Jacob. He helped me a lot in organic chemistry and NMR analysis.

Then, I would like to thank Allison, Aster, Ewald, Christian, Chiara, Yutong, Sam and Keiko for many interesting discussions about science, culture and daily life. Many thanks to colleagues who have already left BOC group, Andrada, Fabio, José, Eva,

Sabry, Eman, Georg, Morten, Albert, Luuk and Stefan. They gave me a lot of help when I started my PhD study. Many thanks to my friend Jianan, Ying, Zejia, Yixuan and Qi. We had very nice holiday time in Maastricht, Paris, Berlin and Rome. I look forward to meeting you again.

Special thanks to our secretaries Mieke and Irma. Mieke helped me a lot with my visa application and accommodation. I felt very warm when I received her email on Chinese New Year. Irma organises fruit box every Monday afternoon as a regular social event for BOC group. She also helped me a lot with paperwork.

Next, my sincere thanks to other professors in BOC group, Ulf, Peter-Leon, Duncan, Kristina and Fred. I learned a lot from their suggestions, questions and discussions every Friday at BOC seminar.

Also, special thanks to technicians: Marc, Remco, Lloyd, Laura, Stephen and Linda. Without their technical support, I do not think I could finish my PhD study.

Furthermore, special thanks to all my students: Friederike, Jisk and Anna-Lena. I had the privilege of supervising their master projects. They also taught me a lot about communication and supervision unconsciously when I was helping them. I hope I showed them the beauty of science and research.

Last but not least, I would like to thank my family. My parents are always encouraging me to chase my dream at any age. They have been supporting me without a doubt. Special thanks to my ex-boyfriend, who accompanied me via online chat during this four-year adventure.